**ALMA MATER STUDIORUM - UNIVERSITÀ DI BOLOGNA**

**SCUOLA DI INGEGNERIA E ARCHITETTURA**

DIPARTIMENTO DI INGEGNERIA CIVILE, AMBIENTALE E DEI MATERIALI

*CORSO DI LAUREA IN INGEGNERIA EDILE-ARCHITETTURA*

**TESI DI LAUREA**

in
Costruzioni in Zona Sismica

# Mechanical behaviour of composite spandrels in unreinforced masonry buildings

CANDIDATO

Salvatore Marino

RELATORE
Chiar.mo Prof. Ing. Pier Paolo Diotallevi

CORRELATORI

Prof. Katrin Beyer
Dott. Ing. Luca Landi

Sessione II

Anno Accademico 2012/2013

*ai miei nonni*
*(to my grandparents)*

# Contents

# Abstract

The object of this thesis is to study the mechanical behaviour of composite spandrels. With piers, spandrels constitute the load-bearing elements of masonry walls. Composite spandrels are a subset of the spandrel. That term, in fact, refers to spandrels with a RC element underneath (as ring beam or slabs).
In case of seismic analysis of a masonry building the effect supplied by those elements is often neglected. This is due to the lack of knowledge on their mechanical behaviour. For this reason, several research groups are still involved in this study. In particular, the work of this thesis belongs to the research project carried out by professor Katrin Beyer, director of the Earthquake Engineering and Structural Dynamic Laboratory (EESD) of the Swiss Federal Institute of Technology in Lausanne (EPFL), Switzerland.

In the first chapter of this thesis there is a brief introduction of the state of art of design/assessment of masonry buildings. It starts with a description of the response of a masonry building under a seismic action. Subsequently the analysis procedures proposed in the codes are shown focusing on the one used in this thesis, the pushover analysis. The chapter ends with a brief description of the methods for design/assessment of masonry buildings proposed by researchers and defining the validity range and the limits of this thesis.
In the second chapter the experimental campaign, carried out by professor Katrin Beyer, on a series of composite spandrels is described. These experiments constitute the experimental background that is the starting point of the study. In fact, with those results it is possible to calibrate a numerical model useful to carry on further analysis.

*ABSTRACT*

That numerical model is developed with the numerical software ATENA and it is described in the third chapter.
In the fourth chapter the failure modalities of the composite spandrels, recorded during the experiments, are described. From this study equations are proposed, in order to predict the shear strength and the stiffness of the composite spandrels.
In the fifth chapter the parametric analyses carried out, with the numerical model developed in ATENA, are detailed. In these analyses, starting from the initial model, the following characteristics have been changed: axial load in the piers, height of the RC beam, length and height of the spandrel and geometry of the bricks. This in order to study how those parameters influence the mechanical response of the composite spandrels. The results obtained are then compared with the equations proposed in the fourth chapter.

# Riassunto

La presente tesi tratta il comportamento meccanico delle fasce di piano in muratura composite. Assieme ai maschi murari, le fasce di piano costituiscono gli elementi portanti di una parete in muratura. Una particolare sottoclasse delle fasce di piano è costituita proprio dalle fasce di piano composite. Con tale termine ci si riferisce alle fasce di piano che hanno al di sotto un elemento portante in conglomerato cementizio armato, come ad esempio cordoli o solai.
Spesso, in caso di analisi sismica di un edificio in muratura, l'effetto fornito da tali elementi è trascurato e si considera solamente il contributo dei maschi murari. Ciò è dovuto anche alla scarsa conoscenza che ancora oggi si possiede sul loro comportamento meccanico. Per questo motivo diversi gruppi di ricerca tutt'ora sono impegnati in tale studio. In particolare, il lavoro di questa tesi, s'inserisce nel più ampio progetto di ricerca condotto dalla professoressa Katrin Beyer, direttrice del Laboratorio di Ingegneria Sismica e Dinamica Strutturale del Politecnico di Losanna (Svizzera).

Il primo capitolo è dedicato ad una breve introduzione sullo stato dell'arte nella progettazione e valutazione sismica di edifici in muratura, inizia quindi con una descrizione della risposta strutturale di un edificio in muratura sottoposto ad azione sismica. Successivamente si pone l'attenzione sui metodi di analisi presenti nelle norme italiane ed europee, soffermandosi in particolare su quello usato in questa tesi, ossia l'analisi di pushover. Il capitolo si chiude con una breve descrizione dei metodi di studio per gli edifici in muratura proposti da alcuni ricercatori e definendo il campo di studio e dei limiti di applicabilità della tesi.
Nel secondo capitolo sono descritti gli esperimenti condotti dalla profesoressa

*RIASSUNTO*

Beyer su una serie di fasce di piano composite. Tali prove costituiscono il necessario background sperimentale che rappresenta il punto di partenza dello studio. Grazie a quei risultati è infatti possibile calibrare un modello numerico con il quale si possono effettuare ulteriori analisi.
Il modello numerico in questione, sviluppato con il software di calcolo ATENA, è descritto nel terzo capitolo.
Il quarto capitolo si incentra sullo studio delle modalità di crisi delle fasce di piano riscontrate nel corso degli esperimenti. Da tale studio sono state proposte delle equazioni per determinare la capacità tagliante e la rigidezza delle fasce di piano.
Nel quinto capitolo sono descritte le analisi parametriche condotte con il modello numerico sviluppato in ATENA. In tali analisi, a partire dal modello iniziale, sono state cambiate, una per volta, le seguenti caratteristiche: sforzo assiale nei maschi murari, altezza della trave in cemento armato, lunghezza e altezza della fascia di piano e geometria dei mattoni. Questo con lo scopo di studiare come questi parametri possano influenzare la risposta delle fasce di piano. I risultati ottenuti sono poi confrontati con le equazioni proposte nel quarto capitolo.

# Introduction

Apart from wood, masonry is probably the oldest building material used for constructions that still finds wide use in today's building industries. Nonetheless its mechanical behaviour is still object of several ongoing researches. For years, in fact, the research has been focused more on construction materials as reinforced concrete and steel, whereas for masonry were still used traditional methods and rules-of-thumb.

Masonry buildings constitute a significant part of existing constructions. In Italy, for instance, most of the city centres are formed by ancient masonry dwellings (figure 1a). However, masonry is still used for new constructions (figure 1b). This is for its characteristics as durability and low maintenance, therefore it ensures good physical properties (for instance a good thermal insulation), which make living in masonry buildings rather comfortable.


Figure 1: a) View of the centre of Bologna, Italy (from www.viagginews.com), b) Masonry building under construction (from www.poroton.it)

A considerable amount of masonry buildings are built in seismic prone areas, as in Italy.
Masonry behaves radically different from reinforced concrete and steel. In fact, for buildings made up with the former materials it is usually possible to identify which are the load-bearing elements (as pillars and beams) and the infill. In masonry buildings, instead, this is not always possible. With the exception of very thin or slender walls, in fact, almost all elements have a static function and have an influence in the global mechanical behaviour of the construction.
Currently, however, not all elements that constitute a masonry building are taken into account in seismic analyses. In fact, considering the external walls, usually only the vertical elements (piers) are considered. The effects of the horizontal element that bridge the openings such as windows and doors are neglected. The coupling effect of those elements, called spandrels, is usually not considered although they are often subjected to damage during an earthquake (figure 2).

Figure 2: Finale Emilia hospital, after the earthquake that stroke Emilia-Romagna region (Italy) in May 2012. Wide cracks opened in the spandrels (from http://www.eqclearinghouse.org)

The main reason why spandrel elements are not considered in the design of URM structures is the lack of experimental evidence for the behaviour of masonry spandrels under seismic loading [BAD10]. For this reason, research groups are still carrying on studies in order to obtain a major understanding of spandrels mechanical behaviour.
First of all, it is necessary to do a classification of the type of spandrels that exist. Several spandrel configuration exist but, roughly, it is possible to distinguish between composite and masonry spandrel. This latter category refers to spandrel supported by masonry arches or lintels. The composite spandrels present, instead, a reinforced concrete element (ring beam or slab) underneath. This type of spandrel is more common in new constructions.
The purpose of this thesis is exactly to study the mechanical behaviour of composite spandrel.
It belongs to a wider research project carried on by professor Katrin Beyer at the Swiss Federal Institue in Lausanne (Switzerland). In 2009 she carried out a series of experiments with the aim to study composite and masonry spandrel (figure 3).

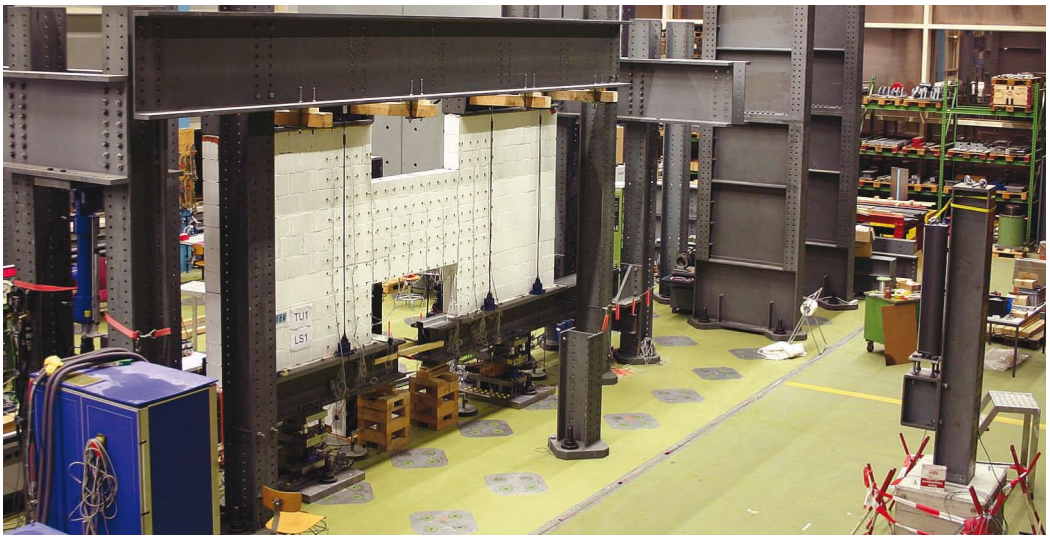


Figure 3: Test setup of the experiments on composite and masonry spandrels (from [BAD10] p.43)

These experiments are described in the second chapter of this thesis and they constitute the starting point of this thesis. In fact, with the results obtained from those experiments, it is possible to develop a numerical model with the aim to reproduce them.
In the third chapter, the numerical model, which is developed with the numerical software ATENA, is described. In this model, non-linear behaviours of the materials are taken into account. This, in order to create a model as close as possible to the experimental specimens.
This model, developed with a simplified micro-modelling approach, captures well the main characteristics of the mechanical response of the spandrels as: the shear capacity, the stiffness and the deformed shape. However, it is not suitable for engineering purpose. In fact, to carry on analysis on a single spandrel, few hours are required. Days are required for the analysis of a single wall. This model is therefore not suitable for the design/assessment of a whole masonry building.

For this reason, several simplified approaches exist to study the behaviour of masonry buildings. Some methods that consider the inelastic properties of the materials are described in section 1.3. One of these methods is the equivalent frame idealization of masonry walls (figure 4).

Within this method, a masonry wall is represented by a frame where the pillars represent the piers and the beams the spandrels. As already said, the knowledge on spandrel mechanical behaviour is not comparable with piers one. Therefore, currently, in the equivalent frame models approaches, for the spandrel are used the same properties as for the piers.

With the availability of experimental ad numerical data, it is possible to study in depth the mechanical behaviour of composite spandrels. This with the aim to develop analytical models that could be implemented in the equivalent frame model approaches. For this reason, features as the shear capacity, the stiffness and the displacement capacity of composite spandrels need to be known.

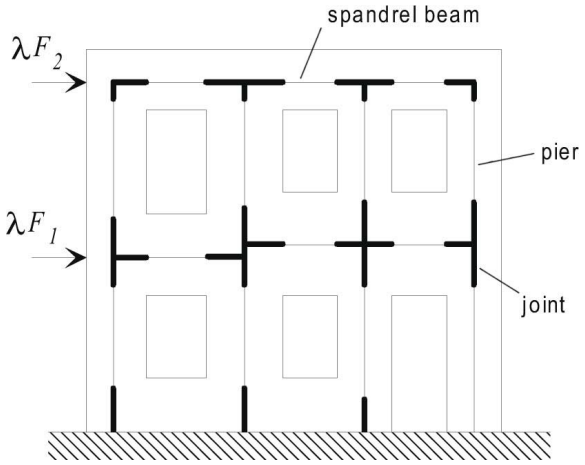


Figure 4: Example of an equivalent frame idealization of a masonry wall (from [Mag00] p.2)

Therefore, the main objectives of this thesis are here summarized:

- To calibrate a numerical model able to predict the main features of composite spandrel response under a seismic loading;
- To carry on parametric analysis with the numerical model which was developed. This, in order to study how some geometrical or mechanical parameters influence composite spandrel behaviour;
- To propose equations in order to use them for the development of an analytical model for composite spandrels.

The applicability domain and the limitation of this work are outlined in section 1.5.

# Chapter 1

# State of the art in unreinforced masonry design

In this chapter there is a brief overview of the current techniques and methods used for the seismic design of masonry buildings.
First of all, there is a description of the main characteristics of masonry buildings loaded with horizontal actions, such as the difference in the in-plane or out-of-plane behaviour and the coupling effect provided by spandrels in masonry walls.
After a brief description of current structural analyses for design/assessment of buildings in seismic zones (section 1.2), the focus is pointed out on one of these analyses (section 1.3), the static non-linear analysis. This is the one used for the study carried out in this thesis, which topic is the mechanical behaviour of composite spandrels (in section 1.1.1 there is an explanation of the terminology used in this thesis). For this reason, some methods that use this kind of analysis, already developed by researchers, are described. Since they are mainly numerical models, in section 1.4 the recent techniques which are studied to create numerical models of masonry building are briefly described. With these models it is possible to carry on numerical analysis useful for the design/assessment of masonry buildings. In this thesis, however, both numerical and analytical models are used, each with its domain of application. Therefore, the chapter ends outlining the validity range and the limitations of this thesis.

## 1.1 URM buildings seismic behaviour

In this section it is briefly described the seismic behaviour of buildings made of unreinforced masonry (URM).
Despite masonry is probably the oldest building material, its mechanical behaviour is still subject of several studies. The reasons are manifold. There is, in fact, still a lack of knowledge both in the mechanical properties and above all in masonry building general behaviour under a seismic input. For centuries these dwellings were built without any formal regulation. In Italy, for instance, the first code for masonry buildings was introduced in 1987 (and for reinforced masonry only in 1996).
Before, masonry buildings were built with the experience drawn by constructions already built and with the so called "rule of art". Those rules are fairly important, in fact also the current Italian and European codes, [NTC08] [CEN04b] introduce the concept of the "simple building", i.e. a regular building in which some requirements are satisfied and no other structural analysis or safety verification are required.
However, those requirements are rather binding, there are limitations, for instance: in the number of storeys, in the minimum total cross-sectional area of walls in two orthogonal directions, in the plan configuration of the building, in the slenderness of the walls and so on.

### 1.1.1 Local and global effects, terminology

Experiences of past earthquakes show that in masonry building is very important how the load bearing elements are linked, failure in fact can occur in two main different modes.
The first mechanism, called "first damage mode" usually involves the out of plane response of the walls, whereas the "second damage mode" mechanisms is associated to the in-plane behaviour. In figure 1.1 examples of these two mechanism are shown.

Usually the "first damage mode" does not involve the totality of the building but only parts or elements, for this reason it is often called as local damage. During an earthquake both out-of-plane and in-plane response are

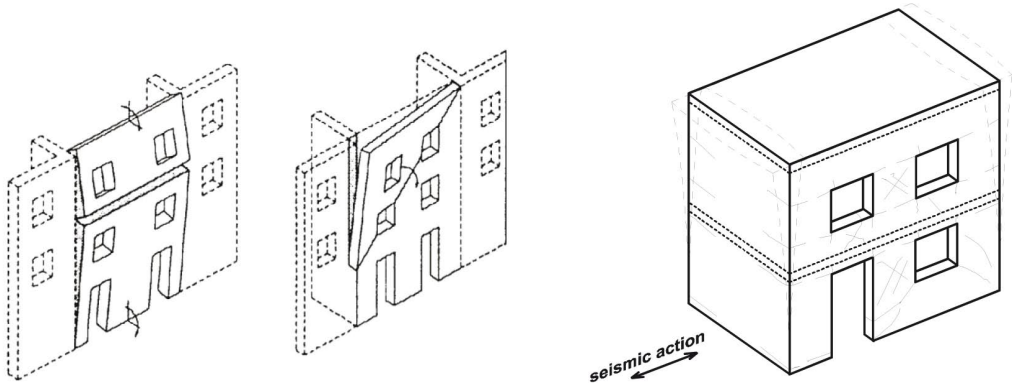


Figure 1.1: Examples of "local" damage and global response mechanism (from [Mag06] p.5)

simultaneously mobilized, but it is generally recognized that a satisfactory seismic behaviour is attained only if out-of-plane collapse is prevented and in-plane strength and deformation capacity of walls can be fully exploited [Mag06].

For this reason in the codes there are restrictions on the general building design and in the details, in order to avoid the trigger of the "first damage mode".

The in-plane strength of the walls can be fully exploited and the out-of-plane collapse avoided if, for instance, the floor diaphragms effect and a proper connection between floor and walls are present. The presence of ring beams is another recommendation of both European and Italian codes to avoid local damages.

In figure 1.2 is shown an example of damages caused by a "first damage mode" mechanism in an old building. It is possible to see that there were not enough connection elements between the walls in the two directions. That is probably because the building is rather old, there are not reinforced concrete floors and there are not ring beams either.

In figure 1.3 a more recent building is shown. In the last floor is still possible to see a local mechanism, but most of the damages are in the ground floor, where there are big cracks in the piers due to shear.

In section 1.1.2 there is a brief description of the typical failure modes of masonry piers (see terminology) subjected to in-plane seismic load.

Figure 1.2: Example of "first damage mode" mechanism (from [BP09] p.171)

Figure 1.3: Example of "second damage mode" mechanism (from http://ww2.unime.it/ingegneria/new/materiale)

As said, the study of masonry buildings requires the knowledge of the mechanical behaviour of the components that constitute masonry and also how the different load bearing elements work under a given load.
The in-plane response of a masonry wall, in fact, strongly depends on the response of its main components: piers and spandrels.
For the sake of clarity, in figure 1.4 it is shown the terminology used in this thesis, where:

- A pier is a masonry element that starts from the foundation of the building and it extends up to the roof. Piers are delimited by opening. $L_{pier}$ refers to the length of the piers.
- The spandrels are the elements that lie on an opening between two piers, they are in grey in figure 1.4. These are elements with length $L_{SP}$ and height $H_{SP}$. In this thesis only composite spandrels are studied, that are the sum of masonry spandrel and RC beam.
- The words "RC beam" are not referred only to reinforced concrete beams, but also to reinforced concrete slabs or ring beams.
- With the words "masonry spandrel", it is referred in literature to spandrel without RC beams or slabs underneath. In this thesis, instead, the words "masonry spandrel" or "masonry of the spandrel", refers to the masonry that lies on the RC beam between two openings.
- A masonry wall is formed by piers and spandrels.
- Piers are usually loaded with an axial load that is the sum of their self weight and the weight that comes from the floors. The spandrel are unloaded. In case of earthquake both piers and spandrels are subjected to shear and bending moment.

Concerning the mechanical behaviours of the piers many studies were already carried out and several articles were published. Instead, spandrels mechanical behaviour and their failure modalities were less known and studied.

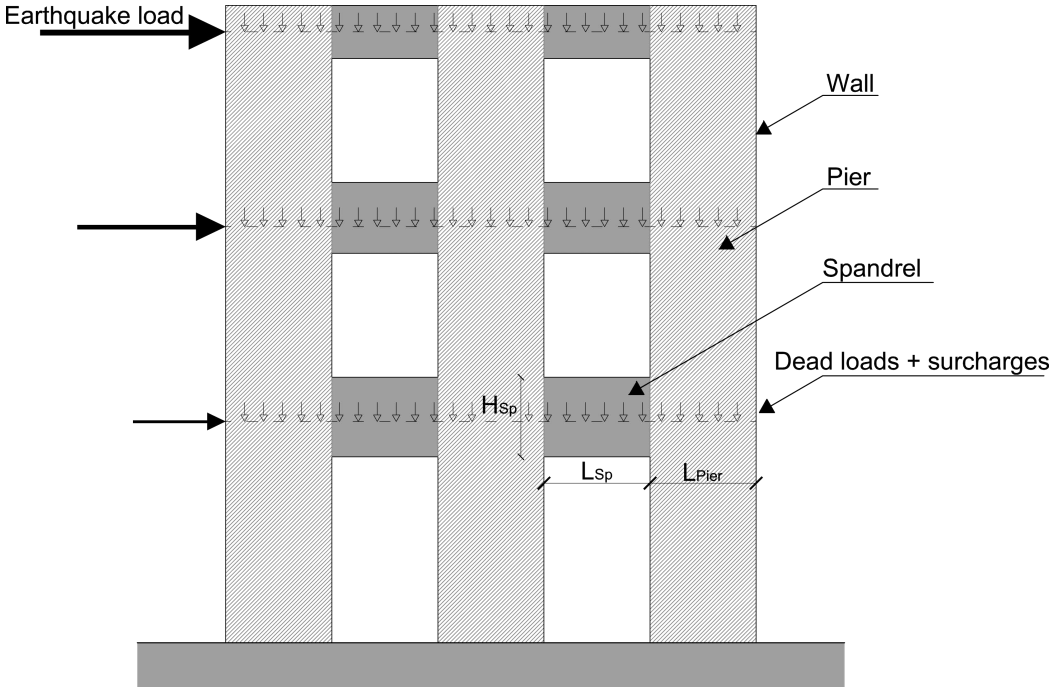


Figure 1.4: Terminology used

Even considering only bricks masonry (and so neglecting other type of masonry such as stone masonry), it is possible to identify different classes of spandrels. In old buildings is rather common to find masonry spandrels with a masonry arch or with lintels (usually made with stone or timber) that bride the opening. In more recent dwellings is possible to find lintels made of steel or RC. These spandrels are called simply masonry spandrels, whereas spandrels with a RC beam or a RC slab underneath are called "composite spandrels".

In this thesis only the mechanical behaviour of composite spandrels are studied. Masonry spandrel will not be studied. The aim of this study is to obtain a better understanding of composite spandrel mechanical behaviour. Knowledge that could be useful to develop an equivalent frame model for a static non-linear analysis (pushover analysis) of masonry buildings.
The pushover analysis is one of the four analysis that codes allow to use for earthquake design of buildings. All these procedures are briefly described in section 1.2.

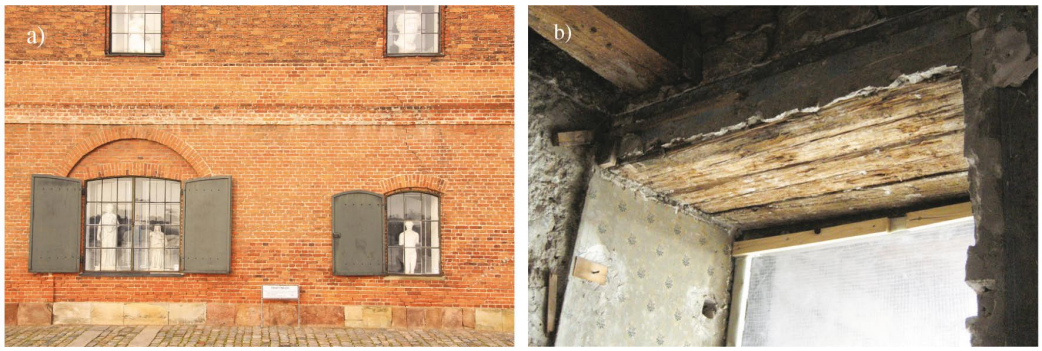


Figure 1.5: Examples of spandrels made with a) masonry arches b) timber lintel (from [BAD10] p.5)

### 1.1.2 Coupling effect and cracks pattern in URM buildings

The non-linear behaviour of a masonry building (i.e. when the load bearing elements of a building start cracking and do not work in the elastic field anymore) does not depend only on the plastic deformation capacity of the material, piers and spandrels that compose a masonry wall, but also on the coupling effect and the consequent failure mechanism.
In fact, since piers are joined by floors and spandrels, a coupling effect is produced, and depending on the extent of the spandrels, this coupling effect will be bigger or smaller.
In a general way, every wall plane can be regarded as a system of coupled piers, the case of interacting cantilever piers being a "limit case" where the stiffness of the spandrels becomes negligible with respect to the stiffness of the piers and hence the coupling effect reduces to zero [Lan02].

In the figure 1.6 taken from [Lan02] three kinds of coupling effects are taken into account. In 1.6 a) there is the case of interacting cantilever piers, where the total overturning moment due to the applied horizontal forces is carried by the piers alone, proportional to their stiffness, resulting a very high bending moments at the base of them. The opposite case is in 1.6 c) where there are strongly coupled piers, and the total overturning moment due to

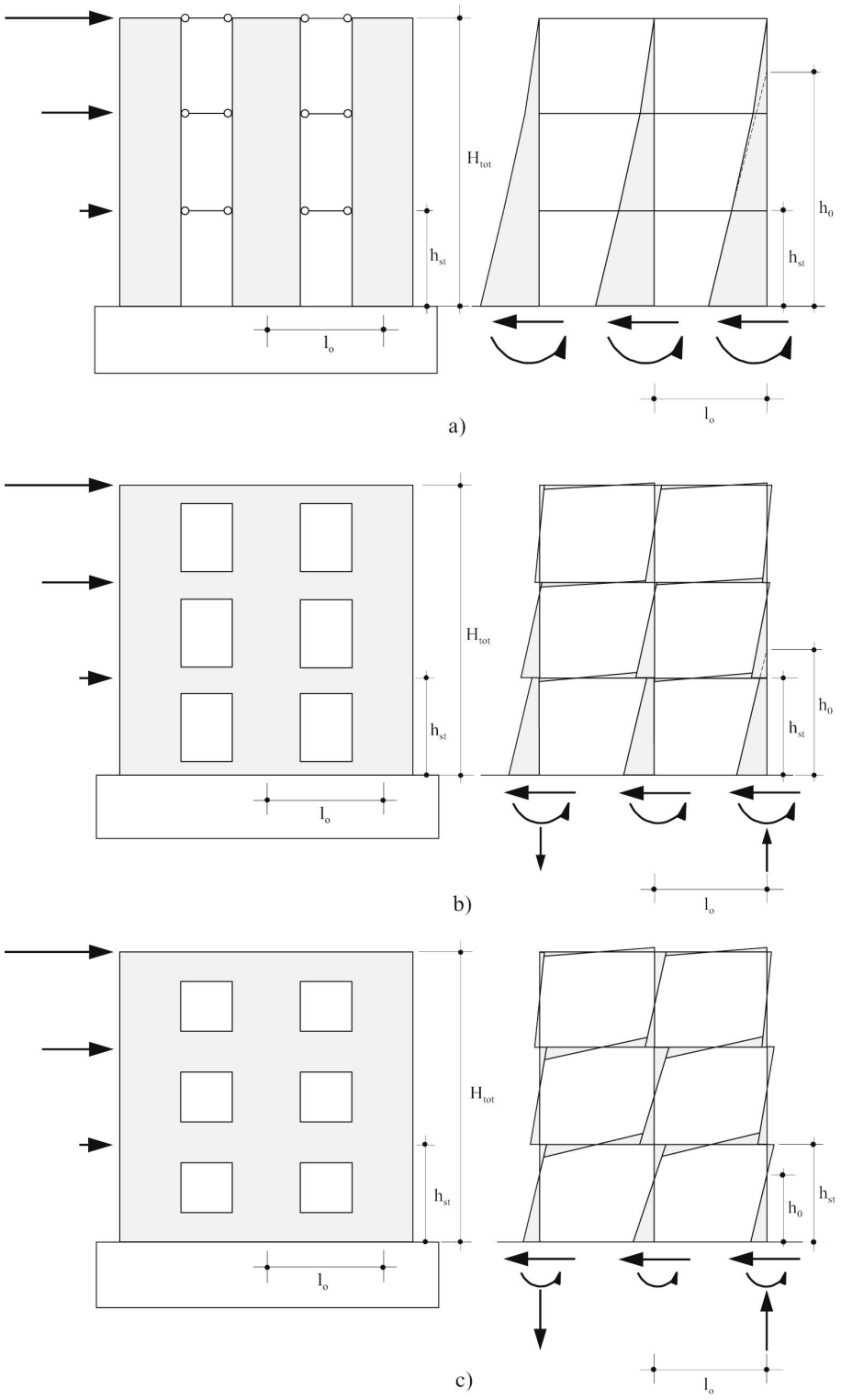


Figure 1.6: Bending moment distribution for three cases of coupled walls a) negligible coupling effect (interacting cantilever walls), b) intermediate coupling effect and c) strong coupling effect due to horizontally acting earthquake forces and corresponding reactions (from [Lan02] p.24)

the applied horizontal forces is mainly carried by high normal forces in the outer piers resulting from the vertical shear forces transmitted by the spandrels. The bending moments at the base of the piers are therefore rather small compared to those of a cantilever wall. In the intermediate case is shown in 1.6 b) where the frame action is less and hence that part of the total overturning moment carried by the piers is increased whereas the normal forces are reduced [Lan02]. In figure 1.7 the deformed shape for each case is shown.

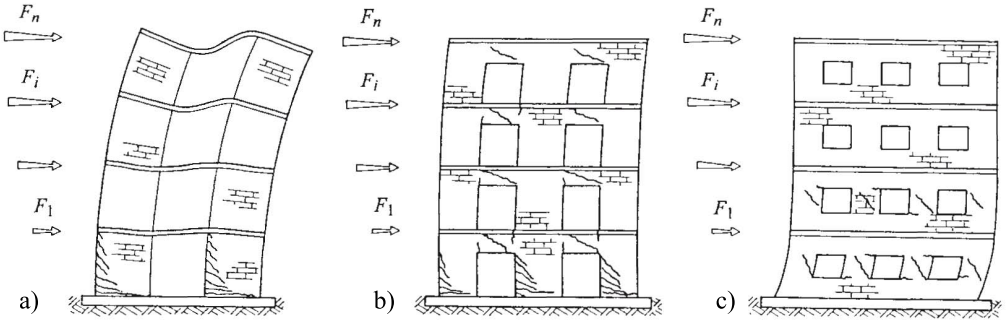


Figure 1.7: Deformation and crack pattern for three cases of coupled walls a) cantilever walls linked by flexible floor and slabs , b) coupled shear wall with weak spandrels and c) coupled shear wall with weak piers (from [Tom99] p.183)

As it is possible to see in figure 1.7, the frame action reflects also on the cracks pattern of a wall after the seismic load. If there are strong spandrels, cracks appear in the piers and vice versa. If there is no coupling effect supplied by spandrels cracks are expected at the base of the piers. It has been studied that for masonry piers three typical failure modes exist that are shown in figure 1.8. Several articles and publications have been written to describe the characteristics of these failure modes, and, for a complete explanation of the problem, elements as the height of zero moment should be introduced. However, it is possible to say, very roughly, that a rocking behaviour is expected when the coupling effect is rather low, whereas shear

failures are more frequent in case of strong coupling effect. The sliding failure usually manifests when the axial load in the piers is low.
After an earthquake, in many masonry buildings shear cracks usually open, that could be an indication that there is not the case of interacting cantilever walls, but there is probably a coupling effect. Also for this reason spandrels effect should be taken into account.

With these failure modalities, however, it is not possible to describe the failure modalities of composite spandrels properly. There are, in fact, deep differences between spandrel and piers as: (i) the absence of a relevant axial load in the spandrel (ii) the different orientation of the bedjoints respect to the direction of the shear load; furthermore in the composite spandrel there is also the presence of an RC beam.
For all the reasons above-mentioned, it is necessary to study different failure modalities suitable for composite spandrels. The starting point of this study is the experimental campaign carried out by professor Katrin Beyer, described in the second chapter of this thesis.

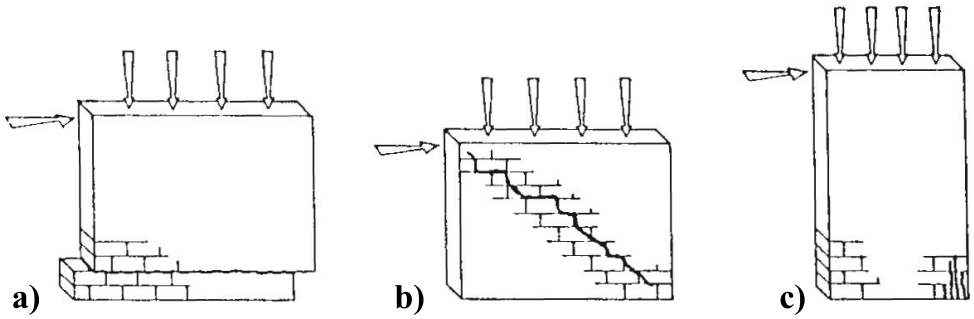


Figure 1.8: Typical failure modes of masonry piers a) Sliding b) Shear c) Rocking (from [Tom99] p.110)

## 1.2 Analysis methods for seismic design

For the seismic design of buildings, the Italian code [NTC08], imposes to use models that are able to predict the three-dimensional behaviour of the building during the action of an earthquake. It is therefore necessary to pay attention to model the building mass distribution, stiffness and strength properly. Several analysis methods are available, and they are briefly described in this section. They vary from very simple analysis that consider the earthquake action as horizontal forces that are applied over the height of the building to very complex ones that solve time-history analysis. It is possible to use these analysis for all kind of buildings, but, especially for buildings built with brittle materials, it is very important take into account the presence of cracks. Cracks, in fact, cause a reduction of stiffness and of the active part of the cross section of the load bearing elements. For this reason the Italian and European codes suggest a rough reduction of initial stiffness by 50%. According to the code [NTC08], [CEN04b], the analysis methods for the earthquake design of building can be divided into linear or non-linear, as shown in figure 1.9.

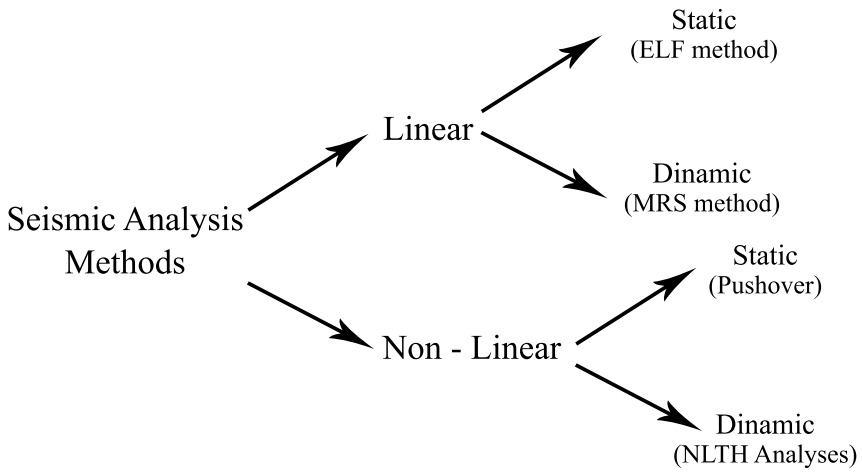


Figure 1.9: Seismic analysis methods according to European and Italian codes

### 1.2.1 Linear analyses

With the words "linear analyses" are described all the methods which models do not include materials non-linear characteristics. There are two kinds of analyses available: a static and a dynamic method. The static analyses consider the seismic action as static forces proportional to the mass of the building, whereas the dynamic analyses consider the modal response of a building.

#### Linear static analyses

The equivalent lateral force method (ELF) is the simplest approach available with the Italian code [NTC08]. It is allowed to use this method only if the building is rather regular so that the first mode of vibration is predominant. The code supplies the equations with which is possible to calculate the first fundamental frequency of the construction and the equivalent static forces to apply. These forces are applied over the height of the building and the corresponding internal forces are determined with a linear elastic analysis. In fact, materials non-linearities are not described, therefore the stiffness is linear and elastic and an equivalent viscous damping is imposed.

#### Linear dynamic analyses

The linear dynamic analyses are commonly used for the seismic design of buildings. These analyses are called "Modal analyses with response spectrum" (MRS) and are mainly used with a force-based design approach. The aim of the method is to simplify the complex dynamic response of a building studying the independent response of each natural mode of vibration. The first limitation of this method is that inelastic behaviours are not considered. The building is therefore modelled as a multi-degree-of-freedom system with a linear elastic stiffness matrix.
Determining the modal frequencies for each degree-of-freedom, and considering an equivalent viscous damping, it is possible to find out the acceleration that acts on the building. This comes from the acceleration spectra detailed by the code. However not all the modes need to be considered, but only the modes that give enough contribution to the response (the code also define

which modes need to be considered). The modal responses are then combined using method as the square-root-sum-of-squares.
This approach is now very used because it is rather simple to use with a FEM software. There are some aspects however that cause doubts. First, since the material are modelled as elastic, their plastic behaviour is derived from the elastic one using reduction coefficients. In [FMMC09], for instance a behaviour factor q, is deeply studied. That coefficient is used to evaluate masonry non linear behaviour in linear elastic analyses, for seismic design of unreinforced clay masonry building. The q factor is used to reduce the elastic response to take into account the post-elastic effects.
Then, as already described, in masonry building there are different kinds of failure (rocking, shear and sliding) that cannot be caught by an elastic model.

### 1.2.2 Non-linear analyses

In the non-linear analyses there are equations and constitutive laws that describe the post-elastic behaviour of the materials. These laws describe the loss in strength and the residual capacity of materials and load bearing elements.
Even for these kind of analyses is possible to distinguish methods where force are applied statically and others that consider the dynamic nature of the earthquake.

#### Non-linear static analyses

In the non-linear static analysis the dead load are applied to the building model and then horizontal loads are applied proportionally to the inertia forces. Those loads are scaled and increased until a global or local failure mechanism is reached. For this reason these kind of analyses are called "pushover" analyses.
These analyses can be in force or displacement control. Usually for the earthquake design the displacement control is preferred. This is because with a displacement control is possible to study the post-peak behaviour and possibles softening behaviours. However, the choice of a displacement control

is not without disadvantages. These methods do not consider in fact the dynamic response such as the natural modes of vibration. So, imposing a displacement pattern, there is the risk to "force" the deformed shape of the structure and consequently there could be the risk to modify the failure mode. Therefore, since these methods do not consider the dynamic behaviours, they are not suitable for irregular buildings for which higher modes become important [Lan02].
However, the great advantage of these analyses, with respect to the linear ones, is that they take into account directly the effects of non-linear material response and hence the calculated internal forces and deformations will be more reasonably approximated. Therefore they would be closer to those expected during an earthquake [Lan02].
Several method exist, and they all have in common that the non-linear force-deformation relationship of the building is represented by a pushover curve. The static non-linear analysis is used in this thesis for the study of composite spandrels. For this reason, in section 1.3, there is a description of some methods already developed by researchers.

**Non-linear dynamic analyses**

The Non-Linear Time History analysis (NLTH) is the most complex analysis for predicting forces and displacements in a building under a seismic action. The building model has to describe the materials non-linear mechanical characteristics and the seismic input is modelled using time-history analyses. It is required to use different ground motion records because this kind of analysis is rather sensitive of that, although the characteristics of the ground motion used are detailed by the codes.
Since the use of this kind of method is still rather difficult it is not much widespread in earthquake design yet. Its use is mandatory for the Italian code [NTC08] only for building with a base isolation system that cannot be modelled with an equivalent linear model.

### 1.2.3 Summary of EC8/NTC08 analysis methods

In table 1.1 the peculiar characteristics for each method are summarized, underlining for each positive and negative attributes.
As already said, there is not a better or worse method, it depends on the scope of the analysis. Currently the linear methods are more used for design purposes. The non-linear methods, instead, are used mainly for verification and assessment [Sul13].

| | **Good attributes** | **Bad attributes** |
|---|---|---|
| ELF method | Fast and simple. | Cannot be used for vertically irregular or tall building. |
| | Few modelling decisions necessary. | Does not consider non-linear effects of the response. |
| MRS method | A simple and fast method (when in possession of a suitable commercial analysis software). | Does not consider non-linear effects of the response. |
| | | Sensitive to modelling decisions. |
| Pushover analysis | Considers non-linear response. | Does not consider dynamic effects well. |
| | Is fast compared to NLTH analysis. | Currently limited to systems dominated by $1^{st}$ mode response. |
| NLTH analysis | Very powerful method that can provide accurate indications of the response. | Requires significant expertise: it is difficult and slow. |
| | Can be used for all structural types. | Sensitive to modelling decisions. |

Table 1.1: Summary of seismic analysis methods

## 1.3 Static non-linear analysis methods for masonry buildings

Since the study of masonry spandrel in this thesis has been carried out with a static non-linear analysis it is worth to focus more on some methods already developed by researchers.

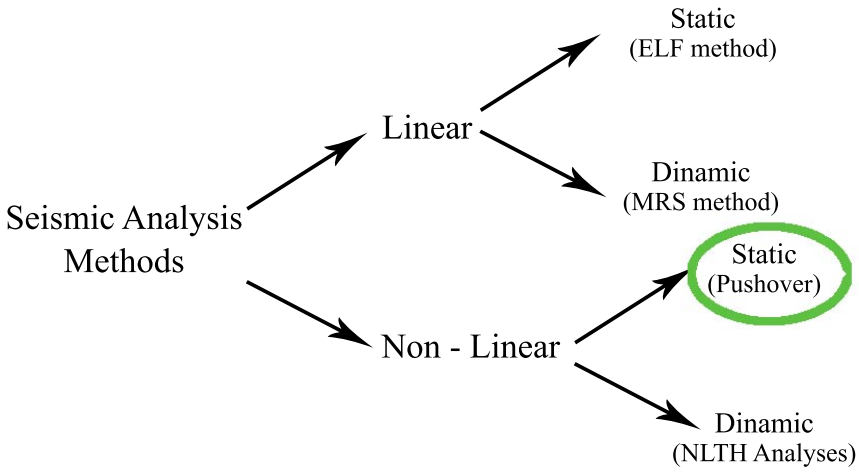


The need for non-linear analyses had been recognized in Italy and Slovenia as early as in the late 1970s, after the 1976 Friuli earthquake. Already in [DM:81], recommendations on seismic assessment, repair and strengthening of masonry buildings were issued in Italy, suggesting the use of an equivalent static, simplified non-linear assessment method which had been proposed and developed in Slovenia by Tomaževic in 1978 [Mag06]. This method that has undergone several refinements in the subsequent years, is called the "storey-mechanism" and is probably the oldest method developed for masonry building.
It is a rather simple method, that could be solved also with manual calculations. It consists of a separate non-linear interstorey shear-displacement analyses for each storey, where each masonry pier is characterized by an ide-

alized non-linear shear-displacement curve (typically elastic-perfectly plastic with limited ductility) [Mag06]. Therefore, in this method, all the deformations are concentrated in the piers and the sum of slab and spandrels are considered as stiff. This is probably more suitable for traditional unreinforced masonry construction where piers are weaker than spandrels and damage will occur in piers first [Tom99]. In this case, spandrel are rigid and strong, whereas the flexural capacity of the walls is low due to their little height between two slabs; the consequence of this is that a predominant shear behaviour of piers is expected and the frame analogy may be simplified. In figure 1.10 an example of force distribution in the piers, with the hypothesis above-mentioned, is shown.

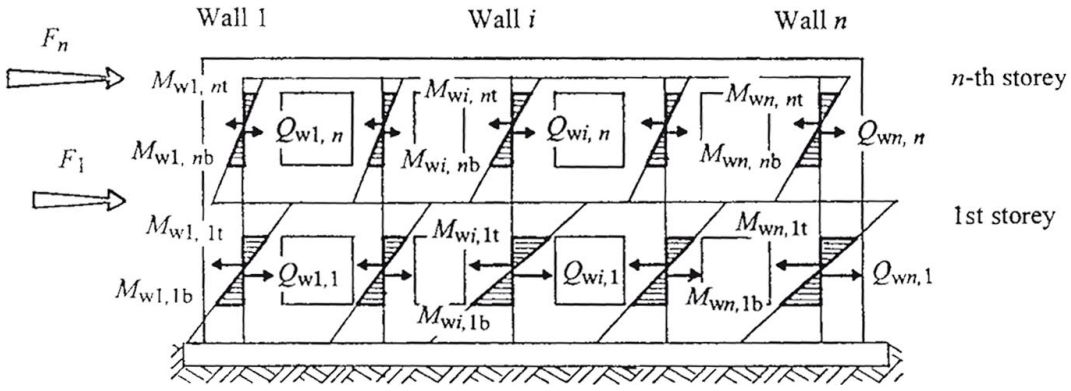


Figure 1.10: Distribution of action effects in a shear wall with rigid spandrels and unreinforced masonry piers: bending moments (M), and shear forces (Q) (from [Tom99] p.187)

A detailed description of the method is in [Tom99], here are summarized the main steps. After having chosen the shape of distribution of displacements along the height of the building, the shear walls are deformed according to the assumed structural model. Then the calculation is repeated step by step increasing the imposed displacements. Once the walls enter into the non-linear range, the structural system of the building and and stiffness matrices are modified.
As result of calculation, the resistance envelope is obtained. An example of this is shown in figure 1.11.

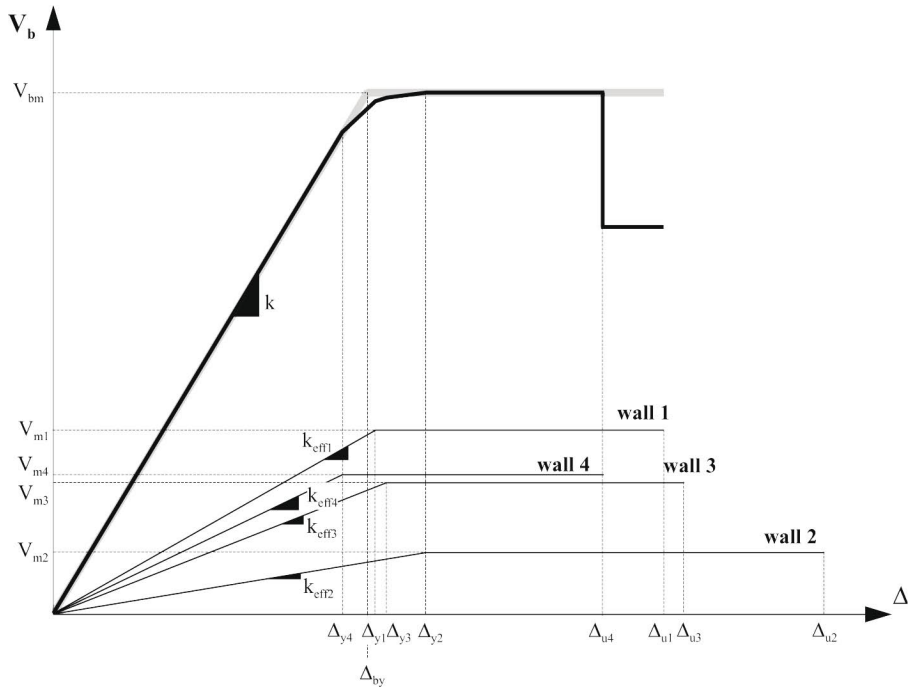


Figure 1.11: Example of capacity curve that could be obtained with the "storey method" (from [Lan02] p.28)

The simplicity of the storey-mechanism approach, however, is paid with a series of limitations which may restrict its application only to some classes of buildings not exceeding two, arguably three storeys [Mag06], and with a series of drawbacks as:

1. It is not possible to have deformation or cracks in the spandrels.
2. Only shear failures are allowed in piers.
3. The stiffness is overestimated, whereas the ductility is underestimated.
4. Since the method studies each storey separately (i.e. no global analyses are carried out):
    - it is not assured that the conditions of equilibrium are globally and locally always respected,
    - it is not possible to determine the variation of the axial load in the piers due to the seismic action.

Therefore, the need for more general methods of analysis led to the development of more refined methods as equivalent frame idealization models or numerical models (FEM models). Both methods present advantages and disadvantages, that will be briefly described in the next sections, where two methods are described: the SAM model, developed and implemented at the University of Pavia by professors Magenes and Della Fontana, and the macroelement approach developed by professors Brencich, Gambarotta and Lagomarsino at the University of Genoa.

### 1.3.1 Equivalent frame idealization models

With an equivalent frame idealization model the structure is idealized as an assemblage of vertical (piers) and horizontal (spandrels) elements. Piers and spandrels are connected by rigid offsets and each element is modelled by proper constitutive laws [SR11]. This kind of approaches are a step forward the "storey mechanism", but still introduce strong simplifications, and thus their accuracy depend on the consistency between the adopted hypotheses and the actual structural problem. It is required, for instance, that the geometry of the walls and the distribution of the openings are rather regular. In that case, in fact, it is possible to define which parts of the walls could be modelled as spandrels and which ones as piers.

The SAM (Simplified Analysis of Masonry building) method, developed by professors Magenes and Della Fontana at the University of Pavia, is an equivalent frame model approach. A detailed description of the method is in [Mag00], here the main features of the method are pointed out.
In figure 1.12 an example of an equivalent frame idealization model of a masonry wall is shown. The pier element and the spandrel element are modelled as beam-column elements with shear deformation, while the joint elements are supposed infinitely resistant and stiff, and are modelled by means of rigid offsets at the ends of the pier and spandrel elements. The pier element is supposed to have an elasto-plastic behaviour with limited deformation. The element displays a linear elastic behaviour until one of the possible failure criteria is met [Mag00]. This is a step forward the "storey method", in fact

not only the shear failure is allowed, but also rocking or sliding failures are taken into account. The theoretical background used in this method is described in [MC97].

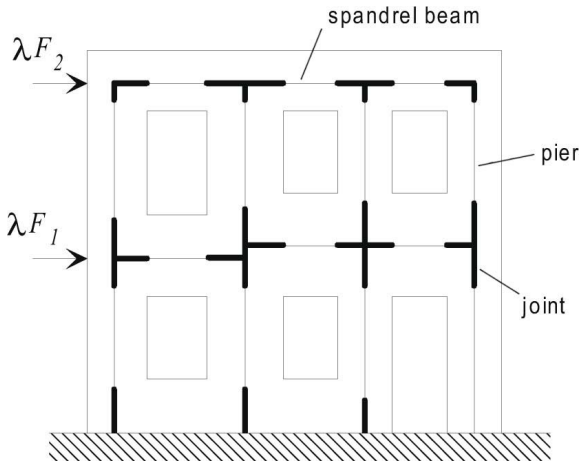


Figure 1.12: Equivalent frame idealization of a masonry wall (from [Mag00] p.2)

In figure 1.13 the idealized non-linear behaviour for piers and spandrel is shown. For the piers is supposed a elastic-perfectly plastic with limited ductility behaviour. For these elements a large amount of experimental data is available. From this data is, for instance, possible to see that shear failures occur in piers for a drift value of about 0.4%. Therefore, the main task is manage to evaluate the shear capacity of the piers, in fact, known the drift limit and the shear capacity, little errors in the valuation of the initial stiffness do not change significantly the general mechanical behaviour of the piers.
The spandrel beam element is formulated similarly to the pier element, taking into account the different orientation of bedjoints with respect to the axial force. The possible failure mechanisms are flexure and shear. For flexural failure the formulation is identical to the pier element. For shear strength it is considered that, because of the openings above and below the spandrel element, the bedjoints have almost zero normal stress, and shear strength is therefore provided by cohesion only [Mag00].

In figure 1.13 the non-linear behaviour of spandrels failing in shear is shown. For spandrels elements there is not the same availability of theories and experiments as for piers, but there are, for instance, deep differences in the post-peak behaviour between composite or masonry spandrels. An experimental campaign to study spandrels mechanical behaviour were carried out by professor Katrin Beyer at the Swiss Federal Institute of Technology of Zurich. A detailed description of this work is in [BAD10].
In SAM method, by means of the parameters $\alpha$, $\gamma_1$, $\gamma_2$ (shown in figure 1.13) it is possible to take into account the different possible behaviours of the spandrel post-peak behaviour, from elastic-brittle to elastic perfectly-plastic. As already said the main drawbacks of this method are that a rather regular geometry of the walls and the distribution of the openings is required and therefore this method does not consider any out-of-plane response.

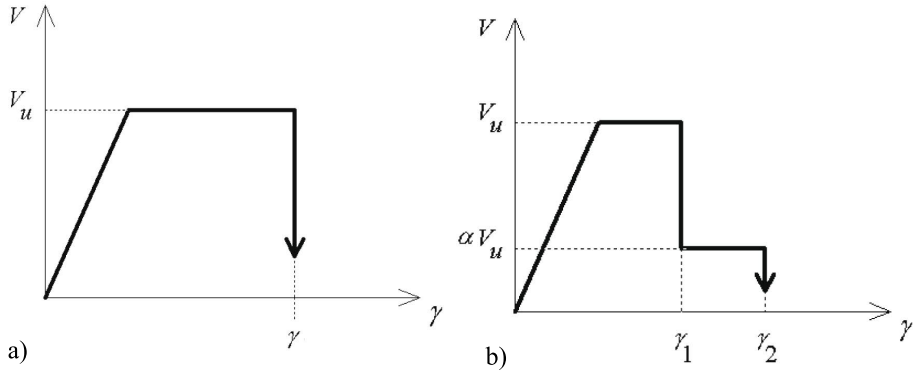


Figure 1.13: Idealized non-linear behaviour of a)piers and b)spandrels elements (from [Mag00] p.2)

### 1.3.2 Macro-elements approaches

The macro-elements approaches are located in the middle between the equivalent frame models and two-dimensional elements models. In the models made of 2-dimensional elements a greater effort is placed to describe elements that constitute masonry. Those are usually finite elements models and they could have different levels of detail. They span from simpler models where in continuous elements all the main features of the masonry are described to

detailed micro-models where each element with all its mechanical properties is described. In the next section there is a brief overview of these methods.
In the macro-elements approaches, instead, the entire structure is obtained by assembly of macro-elements each of which has its own failure modalities. A macro-elements model has been developed by professors Brencich, Gambarotta and Lagomarsino at the University of Genoa.
That model is based on an assemblage of two-dimensional shear walls connected to each other and to flexible floor diaphragms. In order to reduce the number of d.o.f. of the model, there are simplified assumptions on the kinematics of each shear walls. Each shear wall is assumed as consisting of deformable panels, named macro-elements, representative of piers and spandrels, and by rigid elements that connect the piers and the spandrels themselves. This scheme comes out from the observation that, in most cases, the inelastic and damaging mechanisms in the masonry can be localised in piers and spandrels, while the areas where they are connected seldom experience any kind of damage [BGL98].
An example of the macro-element is depicted in figure 1.14. Those elements can be considered as made up of three sub-structures: the bottom and top layers (1 and 3) in which the extensional and bending effects are thought to be concentrated but where no shear deformation is allowed,and the central part (2) undergoing shear deformations and which, on the other hand, does not exhibit axial and bending deformation [BGL98].
In the same figure is therefore possible to see the kinematics (nodal displacement and rotations) and the statics (axial and shear forces, bending) variables used in that model. A more detailed description of that method is in [BGL98].

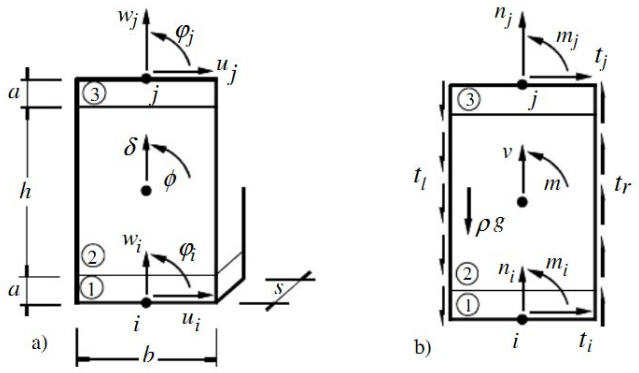


Figure 1.14: Kinematic a) and static b) variables of the macroelement (from [BGL98] p.2)

## 1.4 Micro and macro modelling for masonry buildings

To create a FEM model is probably the most detailed way for the design/assessment of a masonry building. Also, with FEM models is possible to carry on non-linear dynamic analysis. In these approaches, masonry constitutive elements (units, mortar) are discretized into a number of finite elements; proper constitutive laws are adopted for bricks and mortar, taking into account, all the non-linearities involved in the problem [SR11]. The effort is to observe the structural behaviour of masonry panels, highlighting the damage mechanisms occurred during the loading process. Several techniques exist to create a FEM model, there is not a better or a worse one, it depends on the aim of the analysis, if it is more important to study global or local behaviours. In this section the recent studied techniques to model masonry building are briefly described.

Masonry is a very non-homogeneous material, it is formed by rigid elements as bricks or stones and mortar. The mortar has the purpose to link the rigid elements and to give the possibility to resist to horizontal actions, but this is often also the weakest part of a masonry wall. Mortar, in fact, usually has a lower compression strength than bricks and furthermore since it has also a different Poisson's ratio of bricks it causes vertical cracks in them when

are subjected to a compression load. That is because the Poisson's ratio of mortar is smaller than bricks one, so it tends to a bigger strain than bricks. As a consequence, at the interface between mortar and bricks there is a local tensile stress and therefore cracks open in the bricks.

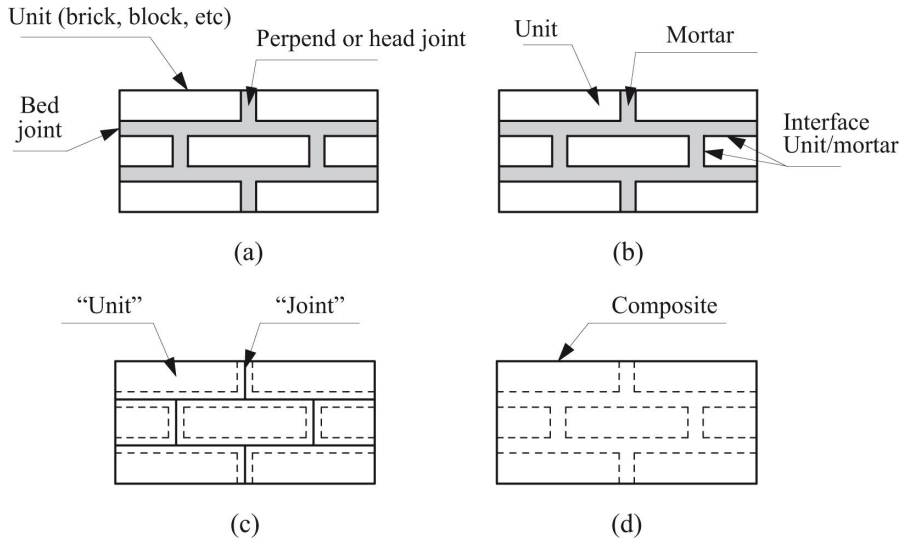


Figure 1.15: Modeling strategies for masonry structures: (a) masonry sample; (b) detailed micro-modeling; (c) simplified micro-modeling; (d) macromodeling. (from [Lou96] p.12)

A description of the available kinds of model is in [Lou96], see figure 1.15:

- Detailed micro-modeling - units and mortar in the joints are represented by continuum elements whereas the unit-mortar interface is represented by discontinuous elements;
- Simplified micro-modeling - expanded units are represented by continuum elements whereas the behaviour of the mortar joints and unit-mortar interface is lumped in discontinuous elements;
- Macro-modeling - units, mortar and unit-mortar interface are smeared out in the continuum.

In the first approach, Young's modulus, Poisson's ratio and, optionally, inelastic properties of both unit and mortar are taken into account. In the

second approach, each joint, consisting of mortar and the two unit-mortar interfaces, is lumped into an "average" interface while the units are expanded in order to keep the geometry unchanged. Thus masonry is considered as a set of elastic blocks bonded by potential fracture/slip lines at the joints. Accuracy is lost since Poisson's effect of the mortar is not included. The third approach does not make a distinction between individual units and joints but treats masonry as a homogeneous anisotropic continuum [Lou96].

There is not a modelling strategy better or worse, because they can be used for different applications. The micro-model approach is suitable for analysis of detail of masonry structures, where it is important the local behaviour, whereas the macro-models are more useful for analysis of whole buildings or where it is not influential the knowledge of the local variations of the stresses.

However also these methods present drawbacks as an high computational effort required to obtain accurate models, which can make their adoption unsustainable for professional practice. Therefore, FEM models suffer from some issues like the potential mesh-dependency and the large number of input parameters required [SR11].
Masonry, in fact, is a construction material whose properties are influenced by a large number of factors: material properties of the units and mortar, arrangement of bed and head joints, anisotropy of units, dimension of units, joint width, quality of workmanship, degree of curing, environment and age [Lou96]. Of course the quality of workmanship cannot be computed, but to develop a good model for a masonry building it is necessary a very good knowledge of mechanical properties of masonry components (which are not always available). For this reason, during experimental campaigns, tests on bricks, mortar and so on are usually carried out. In the next chapter the experimental campaign which had the aim to study spandrel mechanical behaviour, carried out by professor Katrin Beyer at the Swiss Federal Institute of Technology of Zurich, is described. For each test unit, tests on the components were carried out. The results of those tests are very useful, as it is described in the third chapter, to calibrate the numerical model developed with the finite element software ATENA.

## 1.5 Object of the study, application domain and limitations

Before going further, it is worth outlining the main features of the study carried out in this thesis.

The aim of this work is to study the mechanical behaviour of composite spandrels. The effort is to obtain equations in order to describe the stiffness and shear capacity of them. These relationship could be used, for instance, to calibrate beam elements in an equivalent frame model approach for masonry walls with RC beams or RC floors.

Now the limitations of the study are highlighted:

- The model is developed in two dimensions, so only the in plane behaviour is studied and it is therefore not possible to catch the three dimensional response of a building under a seismic loading.
- The model is for unreinforced masonry.
- Only composite spandrels are studied. The model is therefore applicable only if there is a RC beam or a RC floor underneath the masonry spandrel. A rather regular distribution of the openings is also preferable.
- It is supposed that there is not axial load in the spandrel, or that is negligible.
- The experimental campaign and the numerical models studied the nonlinear behaviour of composite spandrels with pushover analysis, so it is not possible to get dynamic effects.
- No unloading path are defined, the model is therefore not available for cyclic analyses.
- A small part of a masonry wall that did not comprise the node element was studied, so in the model the nodes are considered as stiff.

# Chapter 2

# Experimental background

The starting point of the study is based on experiments on composite spandrels carried out by professor Katrin Beyer at the Swiss Federal Institute of Technology of Zurich in 2009. In this study, only the most relevant aspect that will be useful for the development of the analytical and numerical models are reported. It is possible to find a wider and more detailed description of this experimental campaign in [BD12] and [BAD10], from where all the data of this chapter come from.
In the experiments, five composite spandrels were tested and the test units were labelled as "TU1" through "TU5".
All the specimens had the same geometry and, each of them was constituted by a masonry spandrel with an RC beam underneath and with two masonry piers in both side of the composite spandrel. The words composite spandrel refer to the sum of the masonry spandrel and the RC beam.
With these experiments it was possible to investigate the effects of the loading regime and of the longitudinal reinforcements ratio in spandrels mechanical behaviour. In TU1-TU2 a monotonic loading was applied whereas a cyclic loading was applied in TU3-TU4-TU5. It was possible to see that the loading regime does not influence so much the force-deformation relationship. It will be shown better in the experimental results.
On the contrary of the other test units, TU1 was built with a different type of bricks with a lower tensile strength. This caused a different crack pattern and a different failure modality in the spandrel, but it will not be studied in

this thesis.
TU1-TU2-TU3 had the same longitudinal reinforcement formed by four steel bars with 12mm diameter. The longitudinal reinforcement for others specimens was still formed by four bars but with a diameter of 16mm for TU4 and 10mm for TU5.
For all specimens the shear reinforcement was kept the same: 6mm diameter stirrups each 150mm.
Firstly, in this chapter first the test setup, the instrumentation used and the testing procedure are described. Then all the material tests are shown. In fact those result are fundamental for a good calibration of the numerical model developed with the computational software "Atena".
The chapter ends with a brief description of the experimental results.

## 2.1 Test setup, instrumentation and testing procedures

All the specimens had the same dimensions, with the geometrical characteristics shown in figure 2.1 The piers and the URM spandrel were made of standard hollow clay bricks 29 cm long, 19 cm high and 20 cm thick, with 1 cm bed and head mortar joints. The RC beam had a rectangular cross-section 20 cm wide and 25 cm high with a nominal concrete cover of 1.5 cm. As already said, the shear reinforcement was kept always the same for all experiments. The only change was the longitudinal reinforcements.
In Italian and European codes there are, some minimum limits for the longitudinal reinforcements. For ring beams the Italian code [OPC03] requires a minimum of 8 $cm^2$ that correspond to four bars of 16 mm each (that is the longitudinal reinforcement used in TU4). For the European code ([CEN04b] §9.5.2), instead, it is required a minimum of 2 $cm^2$, that value is closer to the longitudinal reinforcement of TU5.

### 2.1.1 Test setup

The setup of the test units is shown in figure 2.2. The two piers of each specimen laid on two stiff steel beams at which ends there were two servo-

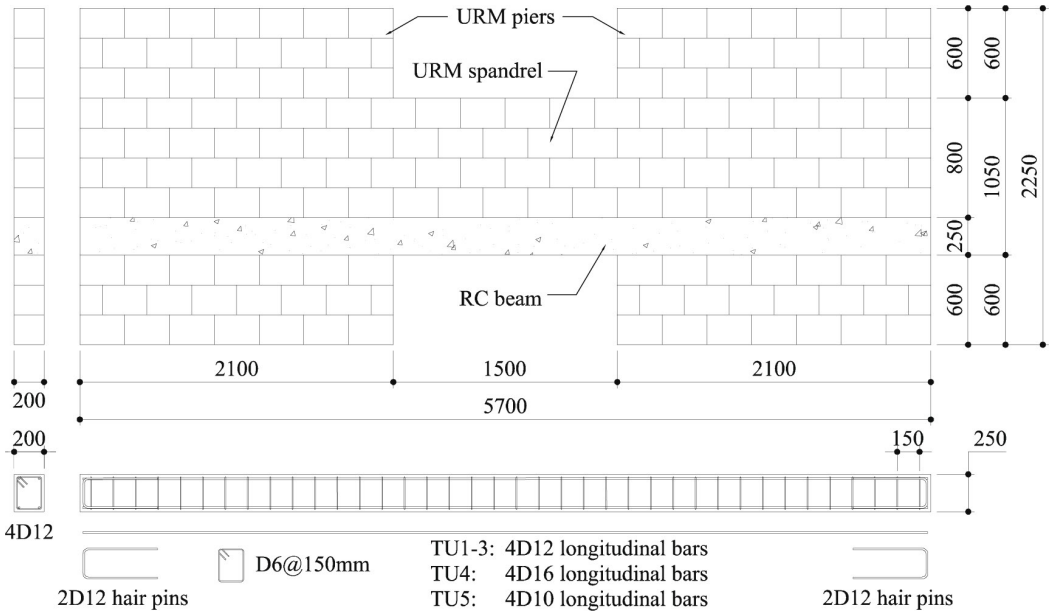


Figure 2.1: Geometry test units and reinforcement layout of the RC beams (from [BD12] p.5)

actuators. These two beams were supported at the centre line of the piers by two hinges. During the experiments the demand on the spandrel was caused by the movement in opposite direction of the two actuators. All the tests, in fact, were carried in displacement control, in order to study also the post-peak behaviour.
Since the support of the South lever beam allowed the sliding, there was therefore not axial restrain in the spandrels.
The two piers were pre-tensioned by four vertical rods each.

The test setup was symmetric, so at each side of the spandrel acted the same shear force equal to the difference of the force acting in the actuators and in the supports, subtracting the half weight. Those forces were recorded with hard-wired instrumentation how it is explained in the next section.
In the graphs of the force-deformation relationship, the drift was calculated as the average of the rotations of the two lever beams.

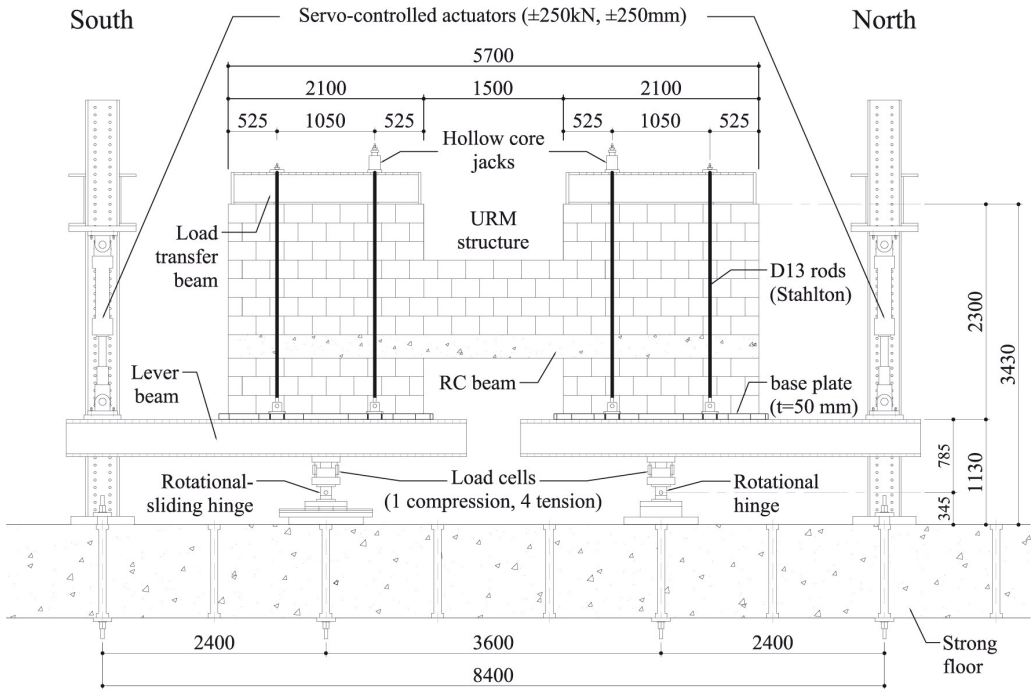


Figure 2.2: Test setup of composite spandrels (from [BAD10] p.5)

### 2.1.2 Instrumentation

Hard-wired instruments and optical measurements were used to measure local and global deformation quantities.
The hard-wired instruments were used to measure the actuator and reaction forces, global deformation quantities (rotation of the lever beam and sliding of the support of the south beam) and local deformation of the RC beam. With the optical measurement system was possible to measure the local deformations of the test units.
With all of these data it has been also possible to carry out local analysis of the numerical model response.
The most important global deformation quantity was the rotation of the piers, which was computed from the LVDTs mounted underneath the lever beams. The final drift was computed as the average rotation of the North and South lever beams [BD12]. In figure 2.3 is described the drift definition and the directions of loading.

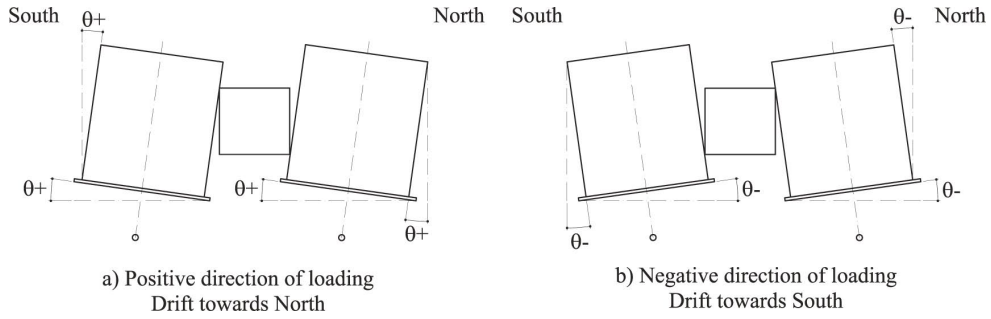


Figure 2.3: Definition of the positive and negative direction of loading (from [BD12] p.13)

### 2.1.3 Testing procedure

All the experimental campaign was carried out with displacements control load steps. A monotonic loading was used for the first two test units, whereas cyclic ones for the other three test units. In the figure 2.4 is possible to see the loading history for the monotonic loading, while in the figure 2.5 is possible to see the loading history for the cyclic loading. In these figures is also possible to see the load steps corresponding to a certain drift value.

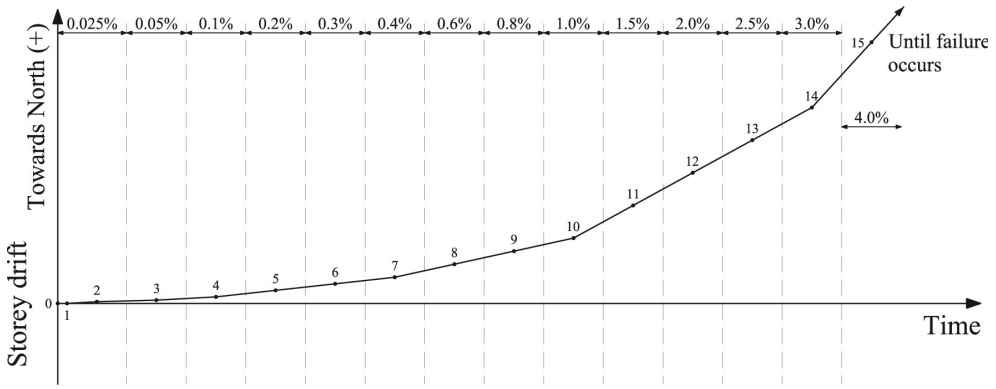


Figure 2.4: Loading history for monotonic loading (from [BAD10] p.45)

The term LS0 (load step zero) refers to the state before any axial load or rotation of the beams is applied. During LS1 the axial load was applied to the piers by four vertical rods for each piers. There were still not applied any rotation in the lever beams. From LS2 the two servo-hydraulic actuators were moved with the same velocity in opposite directions. As a result, the

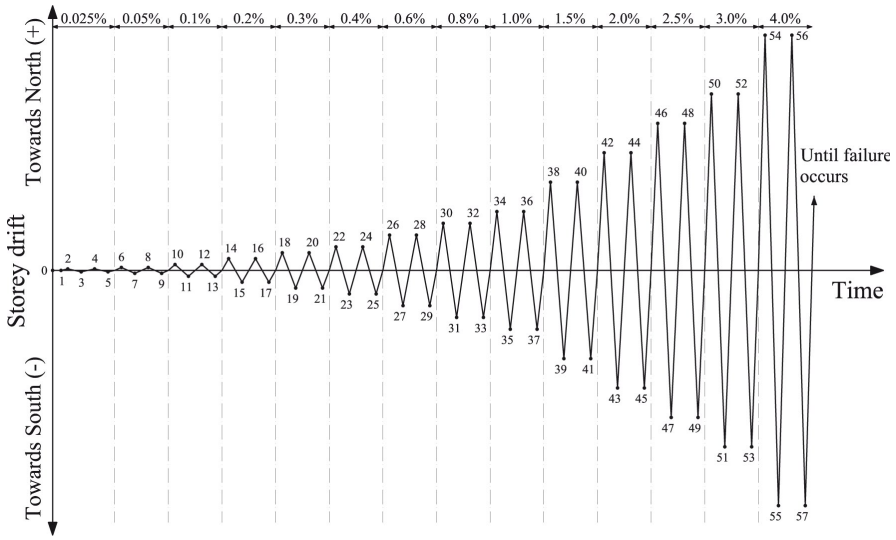


Figure 2.5: Loading history for cyclic loading (from [BAD10] p.45)

two horizontal lever beams rotated and the piers right and left to the spandrel were subjected to the same drifts, which caused the demand on the spandrel. The support of the South lever beam allowed the rotation of the lever beam and also a sliding movement along the longitudinal axis of the beam. Hence, the test stand did not restrain the axial elongation of the spandrel [BD12]. In the following image the load steps schedule and the load speed applied are summarized.

| | Monotonic loading | | Cyclic loading | |
|---|---|---|---|---|
| Storey drift | LS | Loading velocity [mm/min] | LS | Loading velocity [mm/min] |
| 0.025% | 2 | 0.3 | 2-5 | 0.3 |
| 0.05% | 3 | 0.3 | 6-9 | 0.6 |
| 0.1% | 4 | 0.3 | 10-13 | 0.9 |
| 0.2% | 5 | 0.6 | 14-17 | 1.2 |
| 0.3% | 6 | 0.6 | 18-21 | 1.8 |
| 0.4% | 7 | 0.6 | 22-25 | 2.4 |
| 0.6% | 8 | 1.2 | 26-29 | 3.6 |
| 0.8% | 9 | 1.2 | 30-33 | 4.8 |
| 1.0% | 10 | 1.2 | 34-37 | 6.0 |
| 1.5% | 11 | 2.4 | 38-41 | 9.0 |
| 2.0% | 12 | 2.4 | 42-45 | 12.0 |
| 2.5% | 13 | 2.4 | 46-49 | 15.0 |
| 3.0% | 14 | 2.4 | 50-53 | 18.0 |
| 4.0% | 15 | 2.4 | 54-57 | 18.0 |

Figure 2.6: Load steps of monotonic and cyclic loading histories and loading velocity (from [BAD10] p.47)

## 2.2 Material tests

Parallel to the tests on the composite spandrels, material tests on reinforcement bars, concrete, mortar, bricks and masonry were carried out. Those results are fundamental in order to calibrate the numerical model of the spandrels. It will be required, in fact, the knowledge of all mechanical characteristics of all materials of the spandrels.

### 2.2.1 Reinforcement steel

The RC beams of the test units were built with 6, 10, 12 and 16 mm diameter bars. Monotonic tensile strength test in displacement control were carried out in order to evaluate the strength of these reinforcements.
In the following there are the mean values and standard deviations of test results.

| Property | D6 bars | D10 bars | D12 bars | D16 bars |
|---|---|---|---|---|
| # bars | 3 | 6 | 8 | 5 |
| $D_{nom}$ [mm] | 6 | 10 | 12 | 16 |
| $D_{eff}$ [mm] | | $10.1 \pm 0.004$ | $11.8 \pm 0.011$ | $16.0 \pm 0.047$ |
| $E_s$ [GPa] | $215 \pm 15.4$ | $202 \pm 6.7$ | $187 \pm 8.6$ | $206 \pm 13.3$ |
| $f_{y,dyn}$ [MPa] | $586 \pm 14.3$ | $535 \pm 1.9$ | $540 \pm 13.6$ | $505 \pm 2.6$ |
| $f_{t,dyn}$ [MPa] | $634 \pm 13.0$ | $646 \pm 2.3$ | $630 \pm 3.7$ | $616 \pm 2.2$ |
| $f_{t,dyn}/f_{y,dyn}$ | $1.08 \pm 0.01$ | $1.21 \pm 0.01$ | $1.17 \pm 0.02$ | $1.22 \pm 0.01$ |
| $f_{y,stat}$ [MPa] | $563 \pm 13.6$ | $510 \pm 4.4$ | $501 \pm 10.5$ | $485 \pm 6.1$ |
| $f_{t,stat}$ [MPa] | $596 \pm 17.3$ | $618 \pm 2.9$ | $576 \pm 2.9$ | $581 \pm 4.9$ |
| $f_{t,stat}/f_{y,stat}$ | $1.06 \pm 0.01$ | $1.21 \pm 0.02$ | $1.15 \pm 0.02$ | $1.20 \pm 0.02$ |
| $A_{gt}$ [%] | $4.87 \pm 0.36$ | $8.72 \pm 0.59$ | $6.83 \pm 0.69$ | $12.8 \pm 0.58$ |

Figure 2.7: Mechanical properties of reinforcement bars used for the RC beams (from [BAD10] p.51)

Where:

$D_{nom}$ Nominal diameter;

$D_{eff}$ Effective diameter; computed from weight and length of specimen assuming a steel density of $\rho = 7850\ kg/m^3$;

$E_s$ Modulus of elasticity: computed from stress-strain points at 1/3 and 2/3 $f_{y,dyn}$ on the initial loading branch;

$f_{y,dyn}$ Dynamic yield stress: stress at the transition from elastic behaviour to yield plateau (if present) or stress at 0.2% remaining strain (if no yield plateau present);

$f_{y,stat}$ Static yield stress: computed as the dynamic yield stress $f_{y,dyn}$ minus the stress drop measured at $\varepsilon = 0.005$;

$f_{t,dyn}$ Dynamic tensile stress: maximum measured stress;

$f_{t,stat}$ Static tensile stress: computed as the dynamic tensile stress $f_{t,dyn}$ minus the stress drop measured at $\varepsilon = 0.02$ (D6, D10 and D12 bars) or $\varepsilon = 0.04$ (D16 bars);

$A_{gt}$ Percentage total elongation at maximum force.

### 2.2.2 Concrete

The mechanical properties of concrete (as the cube and cylinder strength, the modulus of elasticity, the tensile strength) used to build the RC beams were determined, following the Swiss code, as described in [BAD10].

In the following table there are the mean values and standard deviations of test results.

| Property | TU1+3 | TU2 | TU4 | TU5 |
|---|---|---|---|---|
| Cube strength $f_{c,cube}$ [MPa] | $39.2 \pm 1.55$ | $37.8 \pm 1.13$ | $35.6 \pm 1.05$ | $36.7 \pm 1.35$ |
| Cylinder strength $f_c$ [MPa] | $35.2 \pm 1.59$ | $33.4 \pm 1.62$ | $30.2 \pm 0.75$ | $31.4 \pm 0.53$ |
| Modulus of elasticity $E_{cm}$ [GPa] | $31.0 \pm 1.79$ | $30.0 \pm 0.43$ | $27.8 \pm 0.56$ | $29.1 \pm 1.03$ |
| Tensile strength $f_{ct}$ from double punch test [MPa] | $3.38 \pm 0.32$ | 3.36 | 2.79 | 2.62 |
| Tensile strength $f_{ct}$ from 3-point bending test [MPa] | $6.20 \pm 0.16$ | 6.49 | 5.39 | 7.04 |

Figure 2.8: Mechanical properties of concrete (from [BAD10] p.54)

### 2.2.3 Mortar

Two different kinds of mortar were used for TU1 and for TU2-5. But, as already said, the behaviour of TU1 is not studied. The tensile and the com-

pression strength of the mortar were determined. The three points bending test, on specimens with length of 160mm, was used to determine the tensile strength. For this test a force control loading was applied. With the two halves remained after the bending test, the compressive tests were carried out. These test had also a force control loading.
In the figure 2.9 there are the mean values and standard deviations of the test results, both for the test units and the wallettes (which were used to determine the strength of the masonry).

| Test unit / Wallette | Mortar | # prisms | # cubes | Age [d] | Density [kg/m$^3$] | $f_{ctm}$ [MPa] | $f_{cm}$ [MPa] |
|---|---|---|---|---|---|---|---|
| TU1 | Kelit 110 | 4 | 8 | 211 | $1720 \pm 63.5$ | $4.64 \pm 0.33$ | $16.5 \pm 3.20$ |
| TU2 + 3 | Maxit 920 | 9 | 18 | 68 | $1670 \pm 23.2$ | $2.47 \pm 0.68$ | $11.4 \pm 2.25$ |
| TU4 | Maxit 920 | 6 | 12 | 61 | $1670 \pm 20.9$ | $3.21 \pm 0.28$ | $12.2 \pm 0.88$ |
| TU5 | Maxit 920 | 5 | 12 | 61 | $1660 \pm 31.4$ | $2.86 \pm 0.17$ | $12.1 \pm 0.90$ |
| Wallettes TU1 | Kelit 110 | 2 | 4 | 210 | 1770 | 4.92 | $19.2 \pm 1.87$ |
| Wallettes TU2+3 | Maxit 920 | 3 | 6 | 113 | $1640 \pm 20.8$ | $2.11 \pm 0.50$ | $9.9 \pm 1.41$ |
| Wallettes TU4+5 | Maxit 920 | 6 | 12 | 60 | $1680 \pm 14.5$ | $3.22 \pm 0.45$ | $13.4 \pm 0.89$ |
| Wallettes shear tests | Maxit 920 | 3 | 6 | 82 | $1670 \pm 10.2$ | $2.80 \pm 0.22$ | $10.8 \pm 1.81$ |

Figure 2.9: Mechanical properties of the mortar (from [BAD10] p.56)

### 2.2.4 Bricks

The testing procedure to determine the mechanical properties of the bricks is described in detail in [BAD10]. Two compressive strength were determined, one parallel to the height (x-direction) of the bricks and one perpendicular to it (y-direction). Since it is not codified a test to determine the tensile strength of the bricks, it was determined with a three points bending test. The specimens had to have a sufficient length to carry that test. For this reason three bricks were glued with a particular glue that has a tensile strength much more superior than the bricks. In this way it was certain that the failure was in the bricks.

In the figure 2.10 there are the mean values and standard deviations of test results. The E-modulus and the Poisson's ratio were calculated with Demec measurement as described in [BAD10] .

| Property | Brick Type 1 (TU1) | Brick Type 2 (TU2-5) | Ratio Type 2/ Type 1 |
|---|---|---|---|
| Tests in the $x$-direction | | | |
| Compressive strength $f_{c,bx}$ [MPa] | $24.7 \pm 3.2$ | $30.9 \pm 3.1$ | 1.25 |
| E-Modulus $E_{bx}$ [GPa] | $8.38 \pm 1.16$ | $14.0 \pm 3.80$ | 1.91 |
| Poisson's ratio $\nu_{bx}$ [-] | $0.20 \pm 0.05$ | $0.09 \pm 0.05$ | 0.45 |
| Tests in the $y$-direction | | | |
| Compressive strength $f_{c,by}$ [MPa] | $3.45 \pm 0.24$ | $8.92 \pm 1.23$ | 2.58 |
| E-Modulus $E_{by}$ [GPa] | $2.13 \pm 0.48$ | $6.12 \pm 1.86$ | 2.87 |
| Poisson's ratio $\nu_{by}$ [-] | $0.10 \pm 0.07$ | $0.26 \pm 0.18$ | 2.60 |
| 3-point-bending tests | | | |
| Tensile strength $f_{tb}$ [MPa] | $0.72 \pm 0.03$ | $1.39 \pm 0.29$ | 1.92 |

Figure 2.10: Mechanical properties of the bricks (from [BAD10] p.60)

### 2.2.5 Masonry wallettes

Tests on masonry wallettes are necessary to determine the compression strength in orthogonal and parallel direction to the bed joint and the shear strength at the interface between bricks and masonry. With the shear test, in fact, it is possible to determine the cohesion of the mortar and the friction between mortar and bricks. All of these values are very useful to obtain a good model for the joints.

#### Compression tests

Compression tests were carried out in the two directions, perpendicular and parallel to the bed joints. The test setup, the instrumentation and the testing procedure are described in detail in [BAD10].
The compressive strength of a test unit was defined as the maximum force divided by the nominal area. The mean values and standard deviations of the test results are summarised in the figure 2.11 for the load applied perpendicular to the bed joints and in figure 2.12 for the load applied parallel to the bed joints.

| Property | TU1 (MX1) | TU2+3 (MX2) | TU4+5 (MX3) |
|---|---|---|---|
| Compressive strength $f_{mx}$ [MPa] | 6.64 | $3.96 \pm 0.48$ | $6.38 \pm 0.47$ |
| E-Modulus $E_{mx}$ [GPa] | 8.47 | $5.26 \pm 0.95$ | $7.02 \pm 1.19$ |
| Ratio $E_{mx}/f_{mx}$ [-] | 1270 | $1350 \pm 360$ | $1100 \pm 20$ |
| Poisson's ratio $\nu_{mx}$ [-] | 0.30 | $0.06 \pm 0.02$ | $0.23 \pm 0.04$ |

Figure 2.11: Mechanical properties of the masonry material subjected to compression perpendicular to the bed joints (from [BAD10] p.71)

| Property | TU1 (MY1) | TU2+3 (MY2) | TU4+5 (MY3) |
|---|---|---|---|
| Compressive strength $f_{my}$ [MPa] | $1.25 \pm 0.05$ | $1.27 \pm 0.15$ | $1.37 \pm 0.18$ |
| E-Modulus $E_{my}$ [GPa] | $2.94 \pm 0.29$ | $1.84 \pm 0.56$ | $1.21 \pm 0.39$ |
| Ratio $E_{my}/f_{my}$ [-] | $2350 \pm 150$ | $1450 \pm 450$ | $910 \pm 360$ |
| Ratio $f_{my}/f_{mx}$ [-] | 0.19 | 0.32 | 0.21 |

Figure 2.12: Mechanical properties of the masonry material subjected to compression parallel to the bed joints (from [BAD10] p.71)

Since it was not so simple to determine the Poisson's ratio (in fact the values found are unusual), for the numerical model is used the value of 0.2 as suggested by the codes.

### Shear tests

In order to determine the mechanical properties at the interface between bricks and mortar, tests on masonry wallettes were carried out. Those specimens were formed by three bricks and two mortar joints. The test setup, the instrumentation and the testing procedure are described in detail in [BAD10]. As already discussed in the first chapter, the interface between bricks and mortar is very important, usually, in fact, the failure is recorded there and not in the mortar which after the test is still in good conditions how it is shown in figure 2.13.

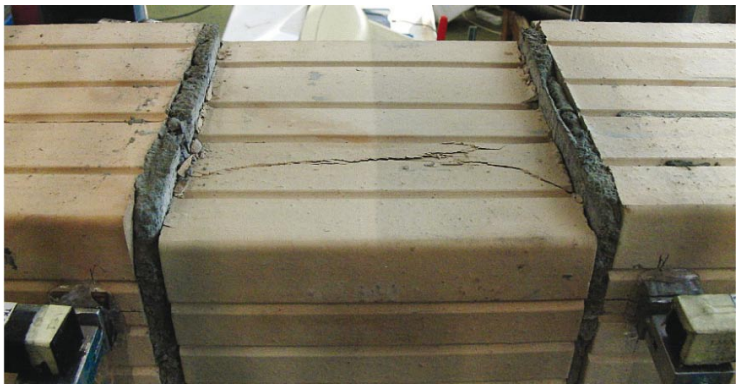

Figure 2.13: Failure of wallettes tested in shear, local brick failure due to shearing off of the mortar pillars (b). (from [BAD10] p.77)

A Mohr-Coulomb relationship has been used to describe the behaviour of the joints. More tests, in fact, were carried out, with normal stress levels from 0.2 MPa to 0.65 MPa. For every value of axial load were therefore determined the corresponding shear stress values.
For all tests the peak and residual shear stress were determined. In [BAD10] is written how those quantities were determined. The peak stress was defined as the shear force divided by the gross cross section area of the two mortar beds. The residual shear stress was defined as the shear stress when the shear displacement reached 10 mm. Although this definition of the residual stress could seem arbitrary, it is explained, always in [BAD10], that once the cracks between mortar and bricks had formed and all mortar pillars within the bricks had sheared off, the shear stress remained in most cases fairly constant.

In the figure 2.14 are summarised the friction coefficient $\mu$, the cohesion c and correlation coefficient $R^2$ for peak and residual shear stress.

| Mohr-Coulomb relationship | $\mu$ [-] | $c$ [MPa] | $R^2$ [-] |
|---|---|---|---|
| Peak stress: $\tau_{max} = \mu_{max} \cdot \sigma + c_{max}$ | 0.71 | 0.25 | 0.78 |
| Residual stress: $\tau_{res} = \mu_{res,1} \cdot \sigma + c_{res}$ | 0.70 | 0.03 | 0.97 |
| Residual stress: $\tau_{res} = \mu_{res,2} \cdot \sigma$ | 0.77 | 0 | 0.96 |

Figure 2.14: Shear tests results (from [BAD10] p.78)

## 2.3 Test results

In this section the test results of the experimental campaign on the composite spandrels are shown.
First TU1 is briefly described, then, for each test unit, the cracks pattern and its evolution, the force distribution and the kind of failures are shown.

### 2.3.1 Test unit 1

TU1 is not described in detail because different bricks than other test units were used. Moreover the Italian code does not allow to use this kind of bricks. It is required, in fact, that the layers parallel to the wall plane are continuous and straight ([NTC08] §7.8.1.2).
In TU1, however, it is possible to see all the main peculiarity of the other test units. It is possible to see the first cracks for a drift of 0.1%. Those cracks are both in the mortar joint of the masonry and in the RC beam. Increasing the load those cracks became wider and two plastic hinges formed at the two side of the RC beam. A very important feature of these plastic hinges is their extension. The plastic hinge in the south side of the specimen was spread out over a significantly larger length than the North plastic hinge. This was probably due to the contribution of the masonry spandrel. Another effect of the masonry spandrel was to modify the shape of cracks in RC beam. In the South plastic hinge, in fact, it was possible to see almost only flexural cracks, while in the north plastic hinge there were shear-flexural cracks. This happened because in the spandrel south side, part of the shear force was probably carried by a compression strut in the masonry spandrel. In the north side, instead, the masonry spandrel was in tension, so it almost supplies nothing to the shear or flexural capacity [BAD10].

### 2.3.2 Test unit 2

As already described in the section of the testing procedure at LS0 the forces in the vertical rods were zero. The vertical load was applied during LS1. Each rod was pre-stressed to a force of approximately 40kN. The aim was to have an axial stress of 0.4 MPa, considering also the self-weight. The first

rotation in the lever beams was applied in LS2.
This was the schedule followed for all test units, with the only exception of TU4, were after a drift of 2% an axial load of 0.6MPa was applied.
The first cracks appeared when a drift of 0.1 % was reached. This value was rather recurrent. Also for the other test unit indeed most of the cracks usually appeared for a drift of 0.1%. For that drift also first cracks in RC beam appeared as it is possible to observe in figure 2.15. Moreover, for that drift demand, already half of the shear capacity of the composite spandrel was already exploited (figure 2.19).
In figure 2.16 is possible to see the crack pattern for a drift of 0.4 %. It is already possible to see the main features of the deformed shape: (i) in the masonry spandrel there are stair-stepped cracks originating close to the top South of the spandrel, (ii) the North and South plastic hinges developed in a different way. The North plastic hinge was relatively small, with few cracks that are however usually bigger than the ones in the South plastic hinge. This plastic hinge was more extended probably due to the effect of the masonry of the spandrel. In the South side of the spandrel indeed, the masonry was compressed, and it was able to carry some load, likely mainly shear forces. Since cracks in bed joints were almost completely developed, (there were also cracks between the masonry spandrel and the RC beam), it is thought that there was no contribution of the masonry in the flexural capacity.
In the figure 2.17 is possible to see the main crack pattern for a drift of 0.8% and it remained however rather stable. The part of the masonry spandrel North of the stair-stepped crack lifted up and was therefore almost stressless. There were likely some shear stresses generated by the clamping stresses that originated from geometrical compatibility requirements [BAD10].
Increasing the drift demand was possible to see the first drops in force due to the crushing of the mortar in the head joint and the opening of more cracks in the masonry part where the strut developed.
Failure in TU2 occurred for a drift of 4% due to rupture of longitudinal bars in the RC beam.

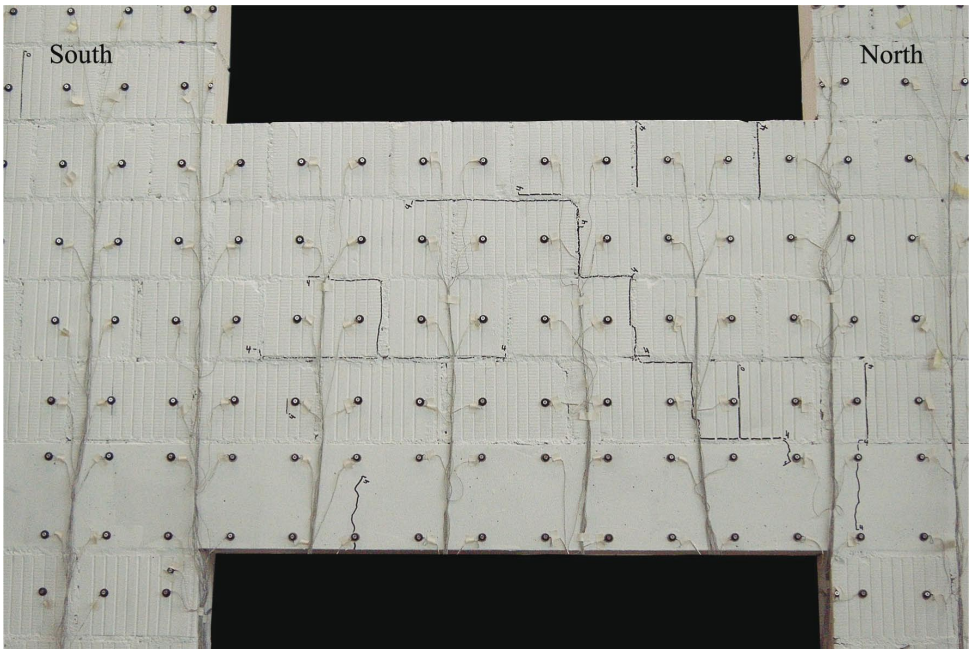


Figure 2.15: TU2 - Drift towards North with $\theta_{nom} = 0.1\%$. (from [BAD10] p.95)

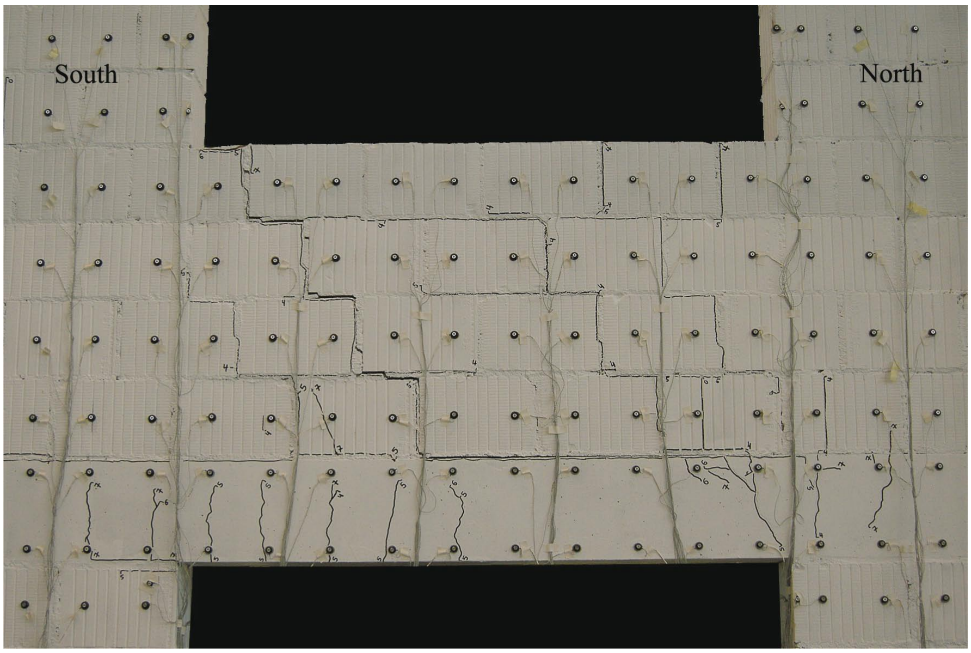


Figure 2.16: TU2 - Drift towards North with $\theta_{nom} = 0.4\%$. (from [BAD10] p.96)

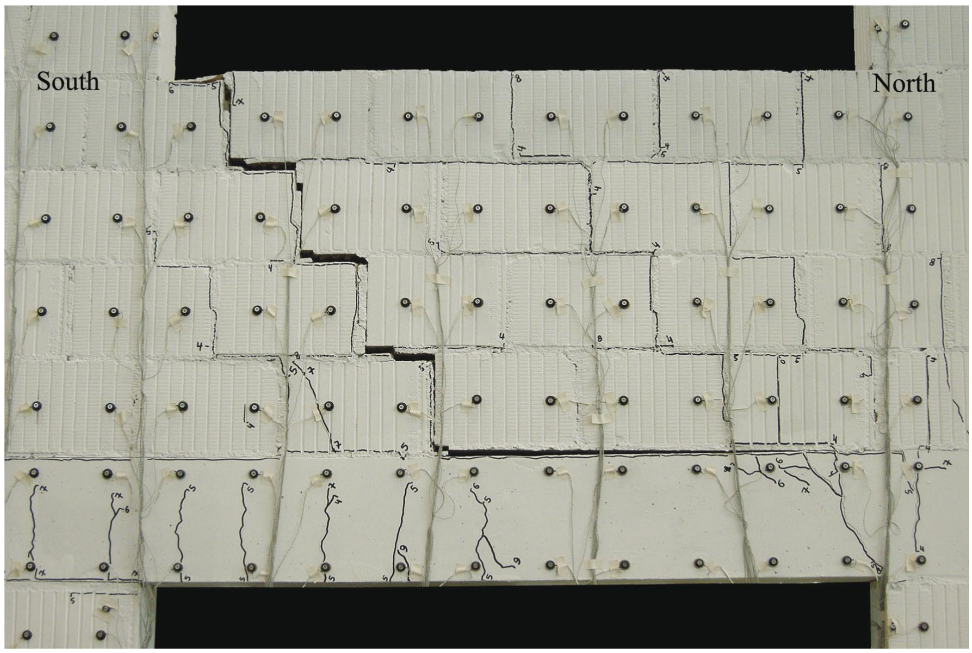


Figure 2.17: TU2 - Drift towards North with $\theta_{nom} = 0.8\%$. (from [BAD10] p.97)

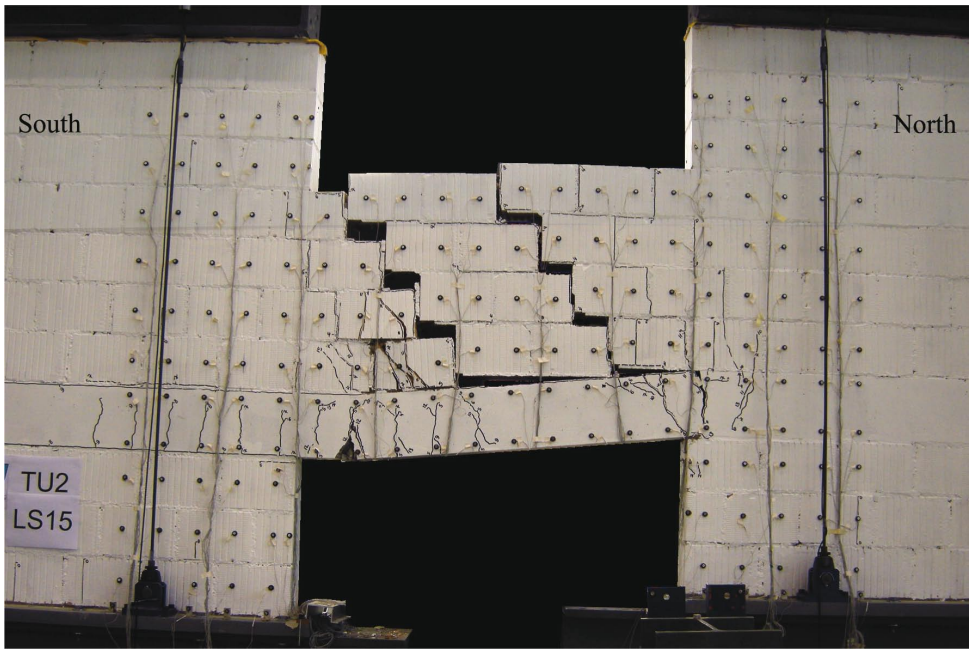


Figure 2.18: TU2 - Drift towards North with $\theta_{nom} = 4\%$, failure of TU2. (from [BAD10] p.98)

**Force-rotation relationship of TU2**

In figure 2.19 is shown the force-rotation relationship of TU2. The drops in shear force for rotations smaller than 0.25% are associated with the formation of diagonal stair-stepped cracks in the spandrel. The final drops in shear force are associated with the rupture of three longitudinal bars [BAD10].

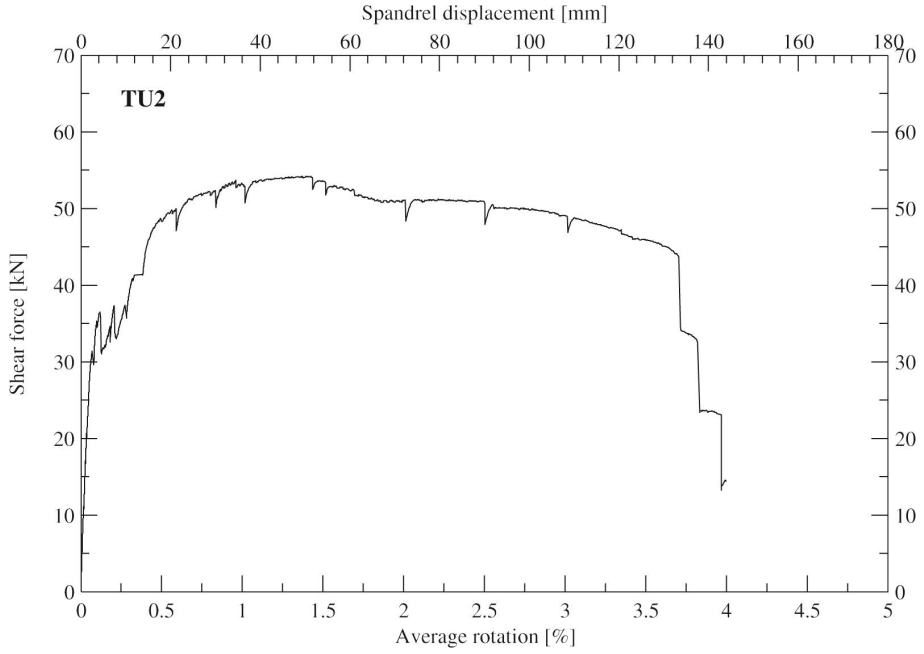


Figure 2.19: TU2 - Force-rotation relationship (from [BAD10] p.99)

### 2.3.3 Test unit 3

Test unit 3 was the first spandrel tested under cyclic loading. It had the same general properties of TU2 as the longitudinal reinforcement and the kind of bricks.

The cracks development was rather close to TU2 one. As in TU2, indeed, the first cracks appeared when a drift of 0.1% was reached and for a drift of 0.4% the crack pattern in the masonry spandrel and in RC beam was almost completely developed.

In figure 2.22 is shown the crack pattern for a drift of 0.8%. It is rather close to TU2 one, it is indeed possible to see a big stair-stepped crack and

no failures in the bricks. It means that the shear capacity was not reached yet. For the negative direction of loading (toward South) there was not a big stair-stepped crack, but the deformation was distributed over two cracks with almost equal crack width [BAD10]. The cyclic loading induced, obviously, some differences in the cracks pattern, due to the fact that the loading was applied in two directions. The cracks, therefore, were more equally distributed over the spandrel. The general behaviour of TU3 was however rather close to TU2 one.
For a drift of 1.5% the first drop in force was reached. This was most likely associated with the formation of a new shear crack in RC beam [BAD10].
When a drift of 2.0% was reached the compression diagonal strut in masonry spandrel failed. Probably also the inner part of the bricks were crushed. In fact, the outer shell of a brick fell off, so for one of them, it was possible to see that the internal part also failed. For a drift of 2.5% the first stirrup fractured and just before reaching the drift of 3% a longitudinal bar in the North side fractured, the experiments was therefore stopped.

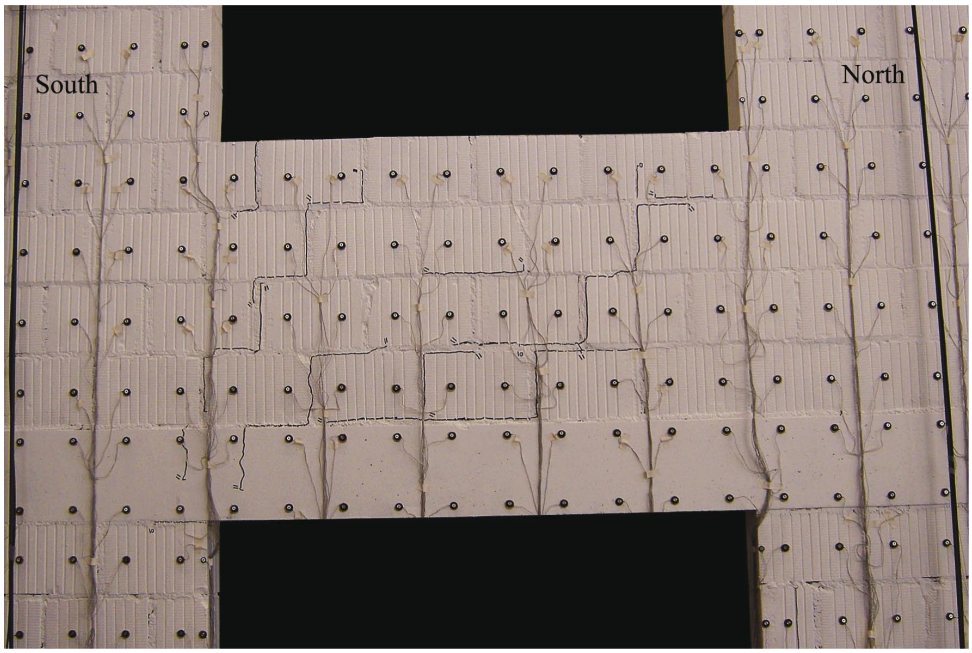


Figure 2.20: TU3 - LS 11, drift towards South with $\theta_{nom}$ = -0.1%. (from [BAD10] p.105)

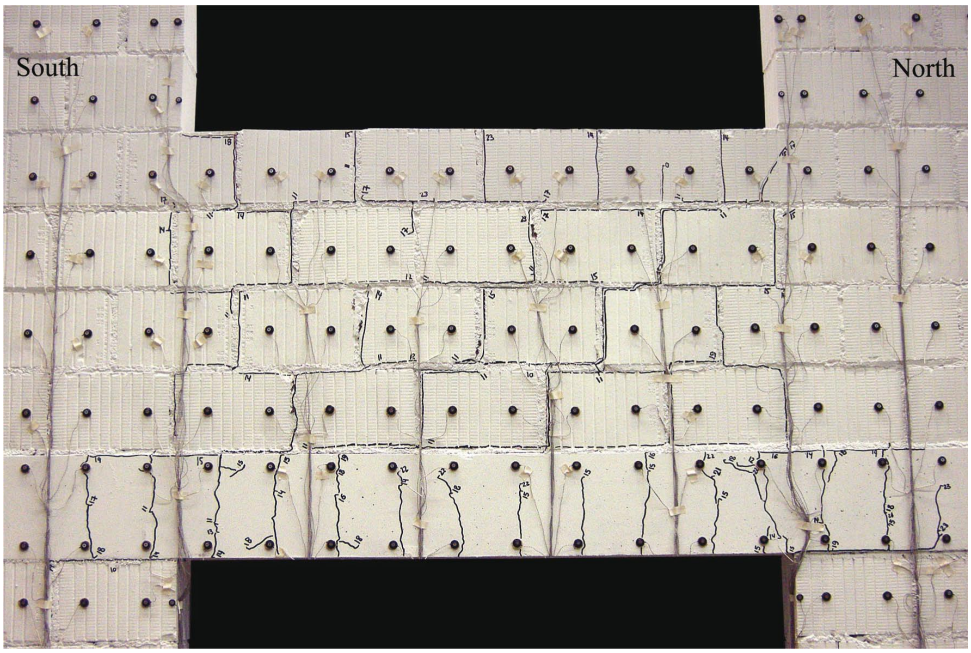


Figure 2.21: TU3 - LS 23, drift towards South with $\theta_{nom}$ = -0.4%. (from [BAD10] p.106)

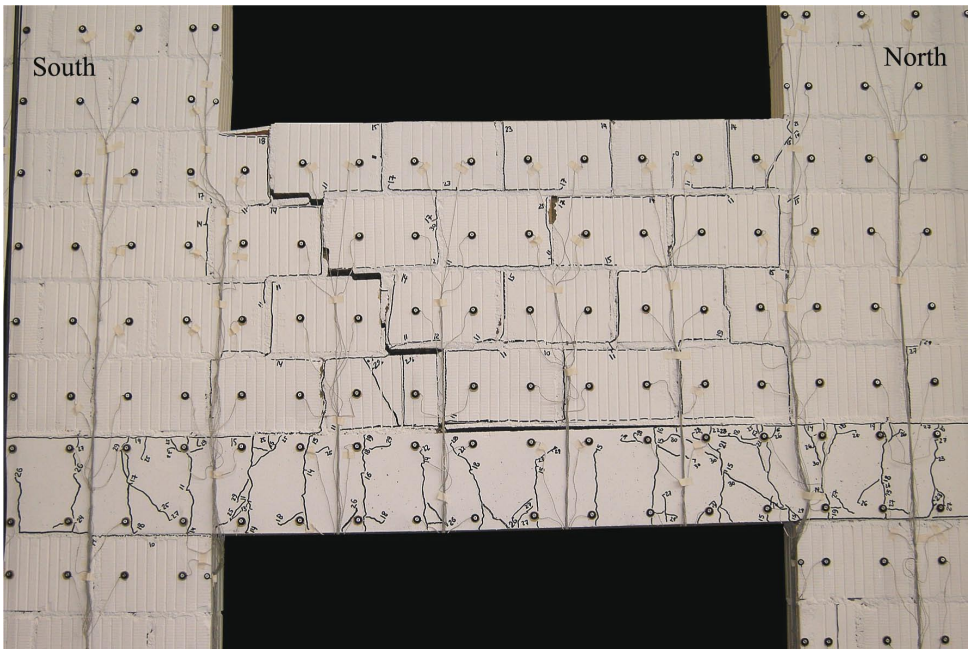


Figure 2.22: TU3 - LS 30, drift towards North with $\theta_{nom}$ = 0.8%. (from [BAD10] p.106)

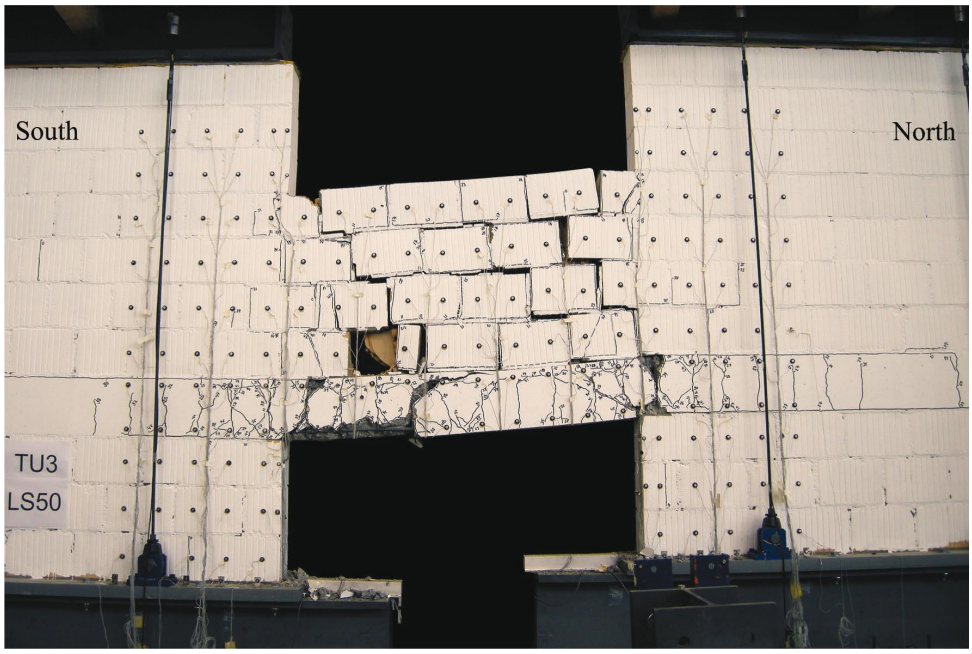


Figure 2.23: TU3 - Drift towards North with $\theta_{nom} = 3\%$, failure of TU3. (from [BAD10] p.108)

**Force-rotation relationship of TU3**

In figure 2.24 the force-rotation relationship of TU3 is shown. This is not so far from TU1 and TU2. This specimen had a shear capacity a bit stronger than the other test units. It probably occurred because they were built in the same days, but TU3 was tested more than two months after than the other two test units. The mortar increased therefore its strength.

### 2.3.4 Test unit 4

The longitudinal reinforcement in the RC beam for TU4 was stronger than TU1-2-3. It had four bars of 16 mm each instead of 12 mm. Some problems occurred when TU4 was bolted on the lever beams. That caused some little cracks, also in the RC beam. The result was an initial asymmetry that disappeared already for a drift of 0.05%. For that drift value, moreover the first cracks appeared. This was earlier than for the previously tested units. A possible reason of this is the larger strength of the RC beam, which might

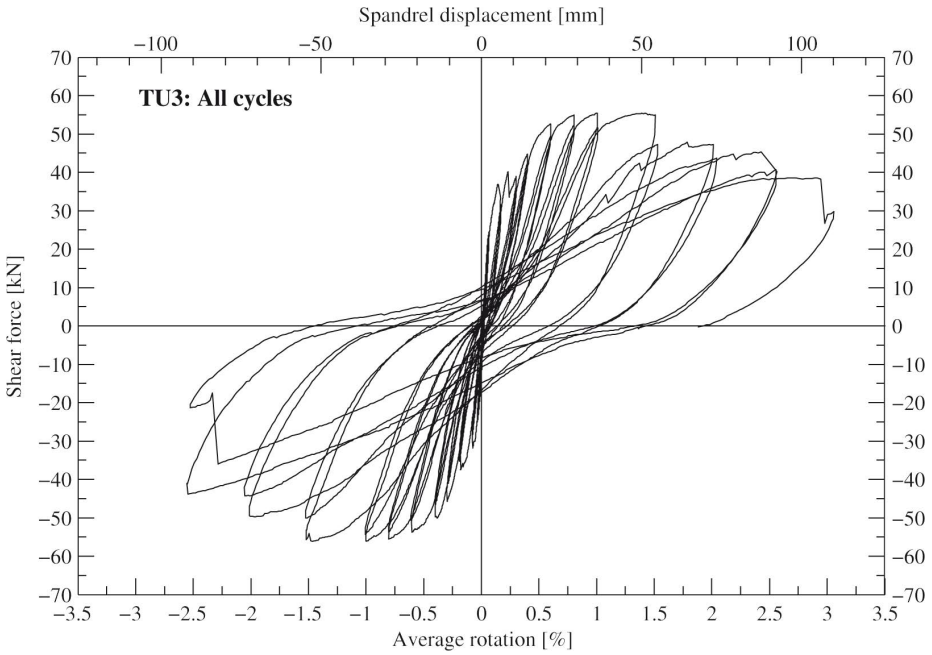


Figure 2.24: TU3 - Force-rotation relationship (from [BAD10] p.109)

have forced the masonry spandrel to deform more [BAD10].
As happened for TU3, when the drift of 0.4% was reached almost all head and bed joints of the masonry spandrel were cracked. It is possible to find, however, some differences. The first is that at this load step there were no bricks with cracks due to the compression strut that developed in the masonry. The RC beam showed moreover signs of shear cracking that there were not in TU3. This is probably because the longitudinal reinforcement changed but not the shear reinforcement ratio [BAD10]. Another important consequence of the stronger longitudinal reinforcement is the rocking underneath the RC beam. In this case, in fact, the RC beam is stronger and stiffer and a long horizontal crack formed between the RC beam and the top part of the pier. This crack extended over about 80% of the pier length.
This aspect influenced a lot the hysteretic behaviour of TU4, in fact, as the drift demand on the spandrel increased, the gap between the bottom of the RC beam, and the top part of the pier became longer and wider. The consequence is that for a drift of 1.5% the largest part of the deformation demand on the spandrel was absorbed by this rocking mechanism.

After the load step 45 the axial load in the piers was doubled, in order to determine the shear capacity of the spandrel. The consequence was a reduction of the rocking movement and a bigger curvature demand in the RC beam. After two more cycles the experiment ended. First the RC beam failed in shear due to fracture of a stirrup and, for a drift of 2.5% the compression diagonal in the masonry crushed.

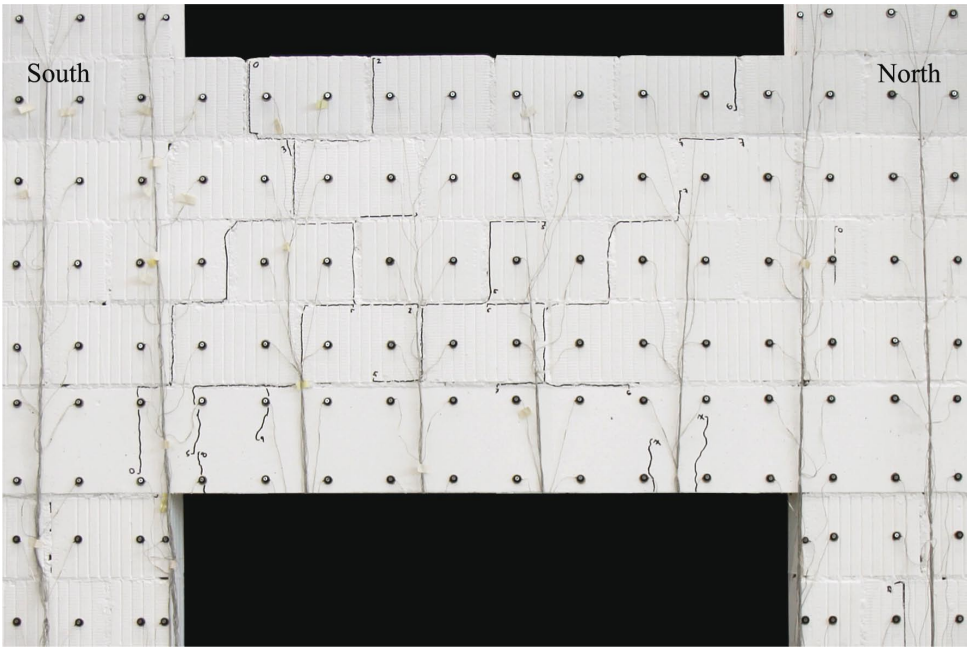


Figure 2.25: TU4 - LS 9, drift towards South with $\theta_{nom}$ = -0.05%. (from [BAD10] p.118)

**Force-rotation relationship of TU4**

In figure 2.29 is shown the force-rotation relationship of TU4 for all cycles. In the figure 2.30 only the cycles with the axial load in the piers of 0.4 MPa are plotted and in the figure 2.31 the last two cycles with the axial load of 0.6MPa.

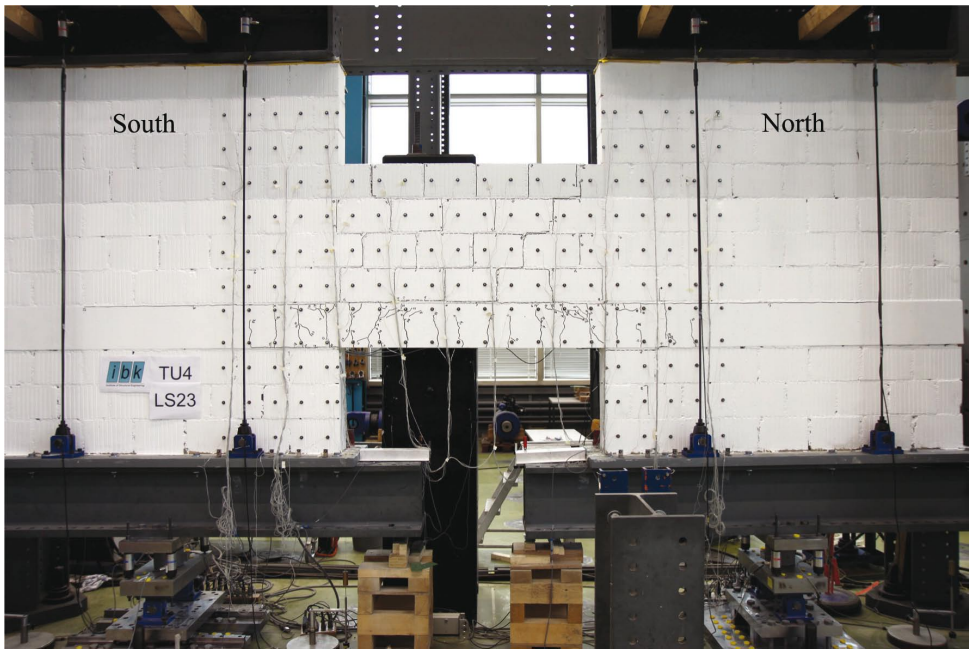


Figure 2.26: TU4 - LS 23, drift towards South with $\theta_{nom}$ = -0.4%. (from [BAD10] p.118)

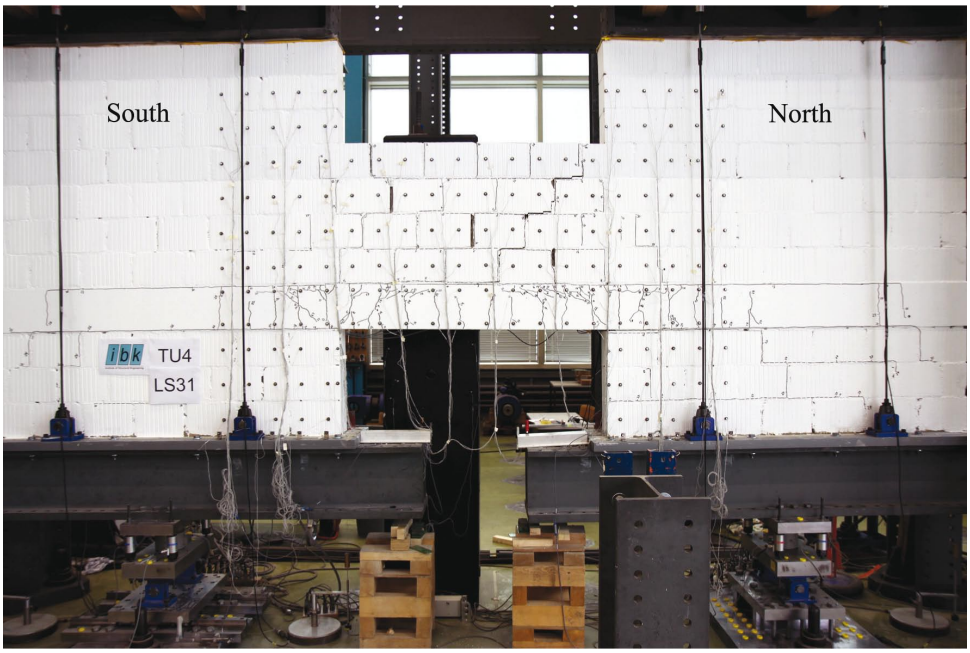


Figure 2.27: TU4 - LS 30, drift towards South with $\theta_{nom}$ = -0.8%. (from [BAD10] p.119)

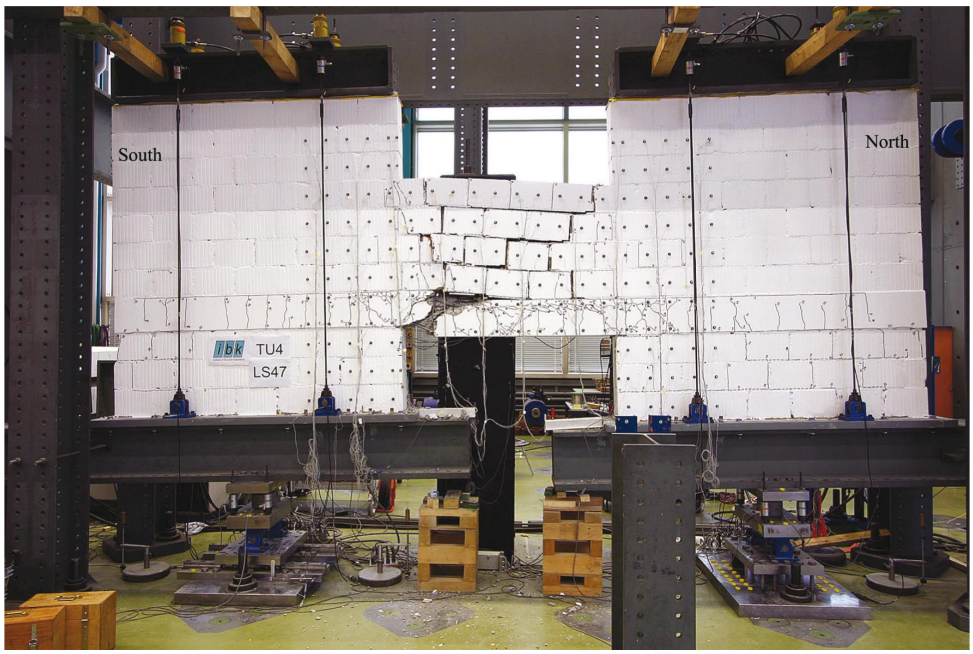


Figure 2.28: TU4 - Drift towards South with $\theta_{nom} = 2.5\%$, failure of TU4. (from [BAD10] p.120)

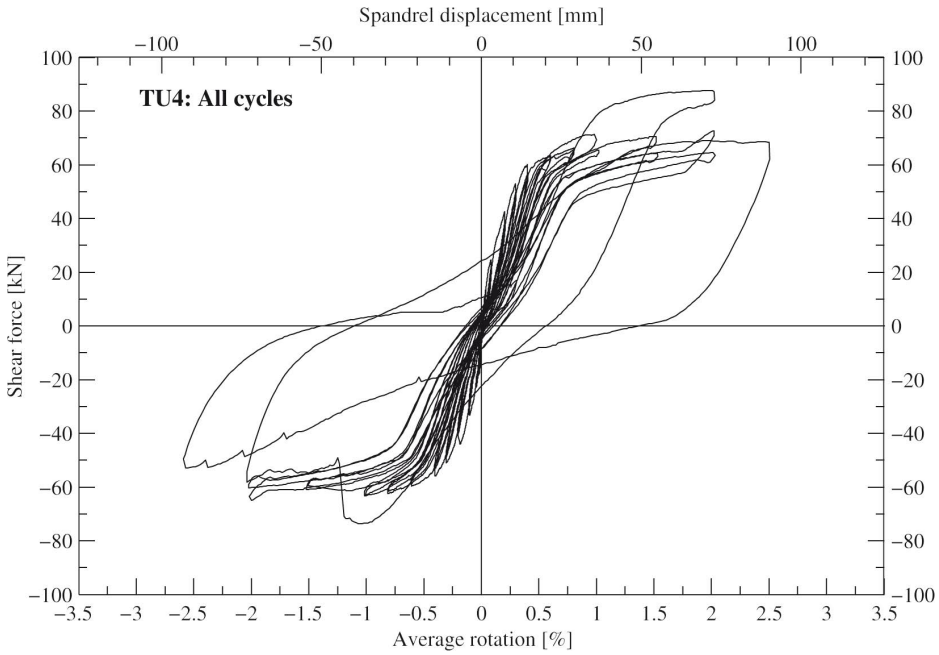


Figure 2.29: TU4 - Force-rotation relationship (from [BAD10] p.122)

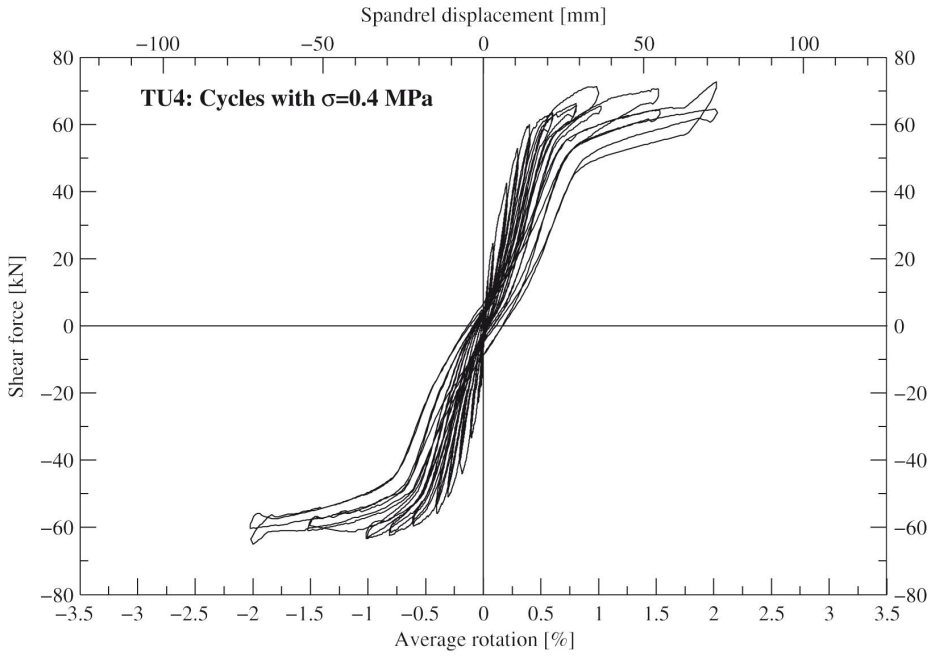


Figure 2.30: TU4 - Force-rotation relationship with axial load in the piers of 0.4MPa (from [BAD10] p.123)

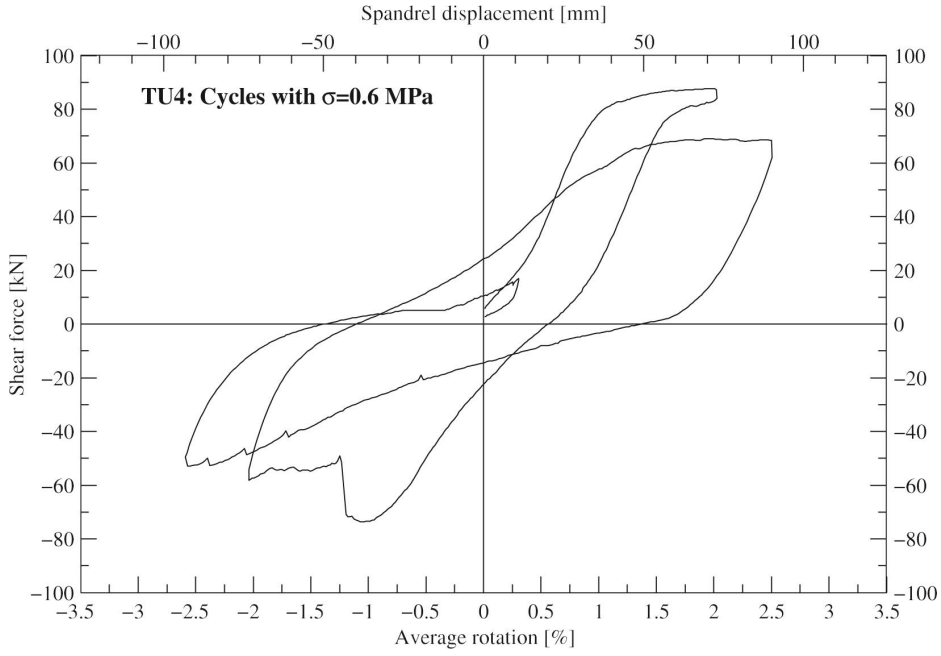


Figure 2.31: TU4 - Force-rotation relationship with axial load in the piers of 0.6MPa (from [BAD10] p.124)

### 2.3.5 Test unit 5

The longitudinal reinforcement in this test units consisted of four bars of 10 mm each. It was therefore weaker than the other test units.
In TU5 the first small cracks appeared for a drift demand lower than 0.1 %, but only for this drift a complete stair-stepped crack opened and the spandrel was fully cracked. Also in this case, when first cracks appeared, already half of the shear capacity of the composite spandrel was exploited.
The RC beam was almost uncracked, only four flexural cracks opened.
In the figure 2.32 is shown the crack pattern for a drift of 0.4%. It is possible to see that all cracks in the RC beam were flexural cracks. On the contrary of TU4, in TU5 only a few shear cracks appeared. It happened because the shear reinforcement ratio for all test units was the same, but, in this test unit the RC beam had a smaller flexural stiffness and strength.
Increasing the drift demand the deformation concentrated in the joints, but the bricks remained, until the failure of the test, without significant cracks.
For a drift of 4% two bottom bars of the South plastic hinge fractured, whereas the bottom bars of the North plastic hinge buckled as it is shown in figure 2.34.

#### Force-rotation relationship of TU5

In figure 2.35 the force-rotation relationship for test unit 5 is shown. Since there is not rocking the hysteresis loop are rather wide. The shear strength is of course less than other test units, due to the lower longitudinal reinforcement ratio.

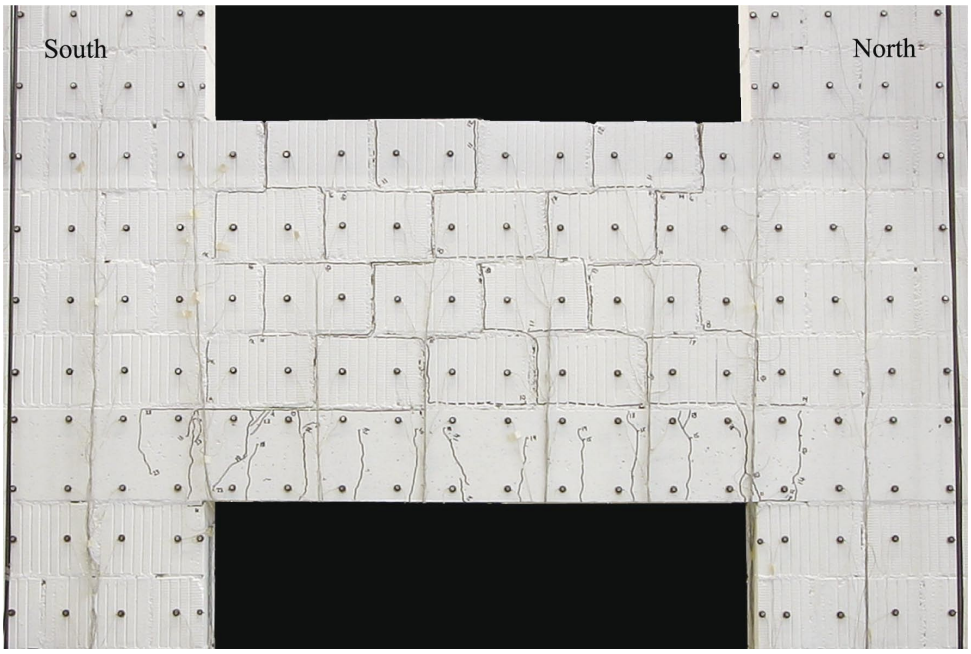


Figure 2.32: TU5 - LS 23, drift towards South with $\theta_{nom}$ = -0.4%. (from [BAD10] p.133)

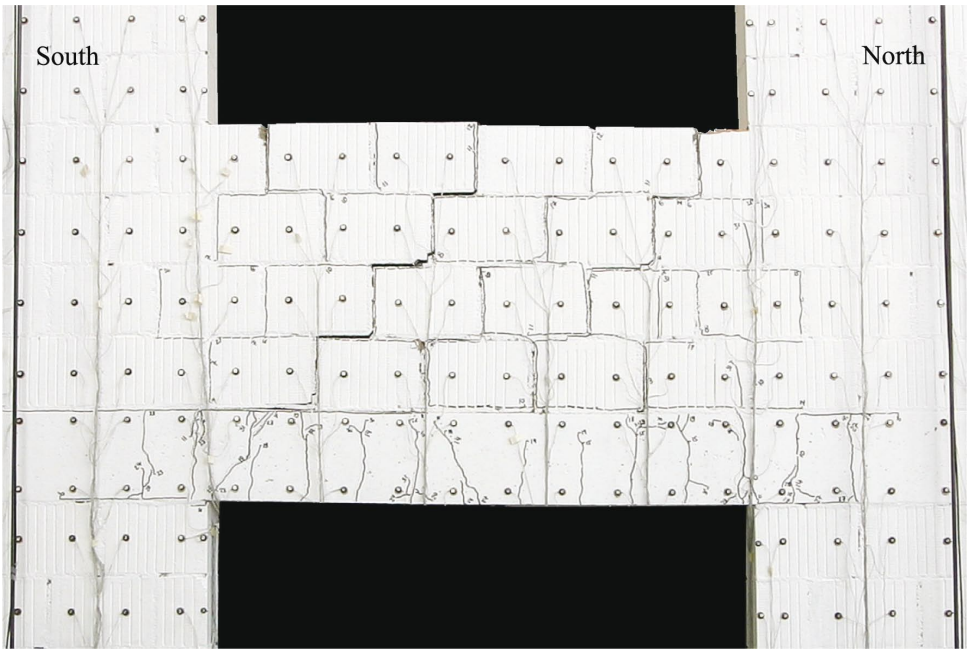


Figure 2.33: TU5 - LS 31, drift towards South with $\theta_{nom}$ = -0.8%. (from [BAD10] p.134)

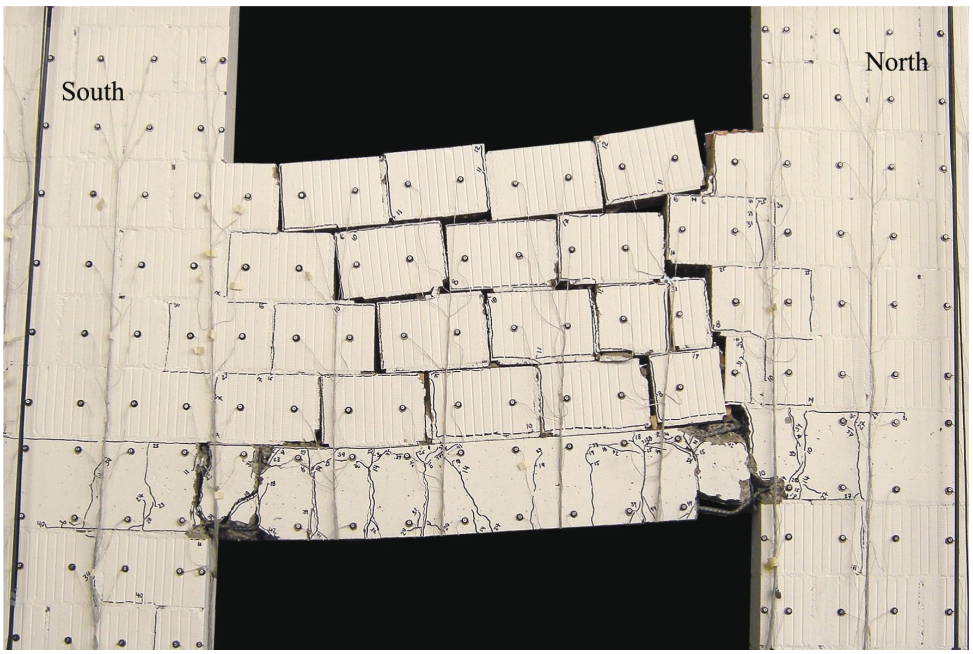


Figure 2.34: TU5 - Drift towards North with $\theta_{nom} = 4\%$, failure of TU5. (from [BAD10] p.135)

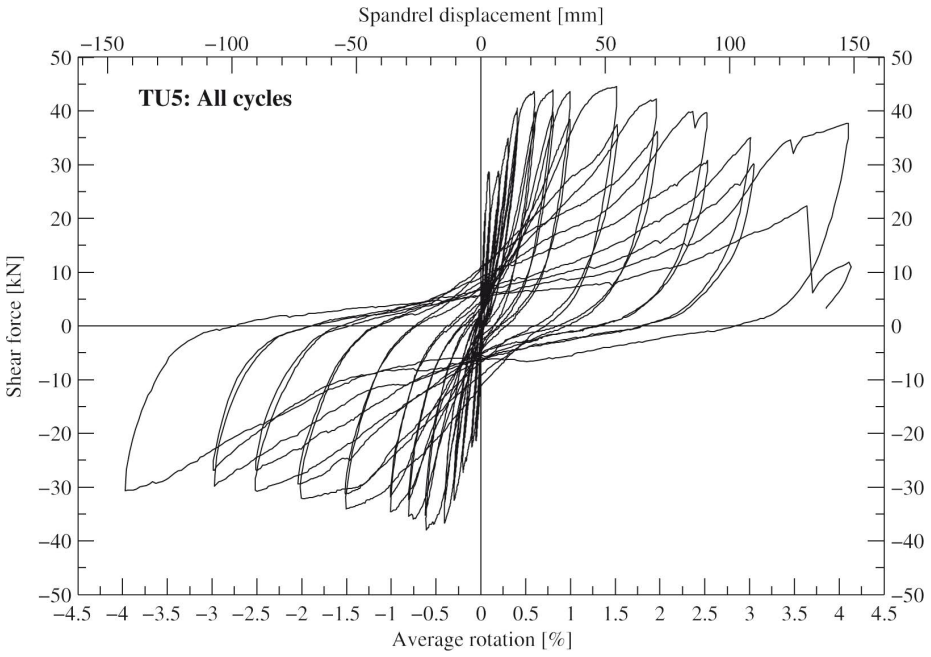


Figure 2.35: TU5 - Force-rotation relationship (from [BAD10] p.136)

## 2.4 Summary of the results

In this section a brief summary of the main results obtained from the experimental campaign is reported.

1. The longitudinal reinforcement ratio of the RC beam influences deeply the mechanical response of the composite spandrel. In figure 2.36 the force-rotation relationships for TU3, TU4 and TU5 are compared (for TU4 only the load steps with an axial stress of 0.4 MPa are considered). The envelopes of these relationships are highlighted with ticker lines. It is possible to see differences in the shear and drift capacity and also in the energy dissipated during the cycles of loading.

2. First cracks usually appeared for drift demands between 0.05 and 0.1 %. Furthermore, for these drift demands, half of the shear capacity of the composite spandrel was already exploited. The consequences of this are:

   - It is possible to distinguish two behaviours of the spandrel until it reaches its peak strength. A first, almost elastic, behaviour till a drift demand corresponding to half of its shear capacity. This part has an its own value of stiffness, then cracks appear and stiffness reduces.
   - Since the masonry spandrel is already cracked for low drift values probably it does not give contribution in the bending capacity., neither in the case of positive bending.

3. The shear and drift capacity are strongly influenced by the failure mechanism. The experiments show, in fact, two main mechanisms: rocking of the RC beam with only the negative plastic hinge or the formation of two hinges and a consequent shear or flexural failure of the RC beam. It has been also shown that the trigger of one mechanism is also influenced by the vertical load acting in the piers.

In the table 2.1 the main results that came out from this experimental campaign are summarized.

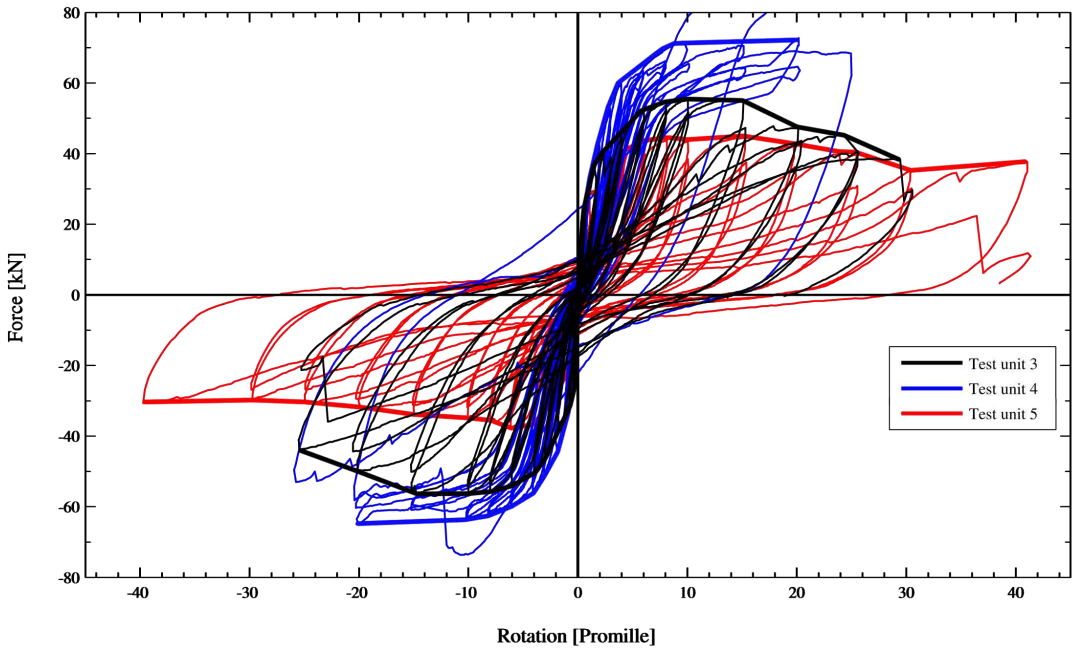


Figure 2.36: Force-Rotation relationships and correspondent envelopes for TU3, TU4 and TU5

| **Test unit** | **Shear capacity** | **Final drift** | **Failure description** |
|---|---|---|---|
| TU2 | 54 kN | 4% | Fracture of longitudinal bars (test unit with monotonic loading). |
| TU3 | 56 kN | 3% | First stirrup fractured for 2.5%. Just before reaching 3% longitudinal bar fractured. |
| TU4 | 73 kN ($\sigma = 0.4$MPa)<br>89 kN ($\sigma = 0.6$MPa) | 2.5% | Rupture of a stirrup.<br>Compression diagonal crushed |
| TU5 | 44 kN | 4% | Rupture of longitudinal reinforcement.<br>Buckling of longitudinal reinforcement. |

Table 2.1: Summary of the test results

# Chapter 3

# Composite spandrel numerical model

In this chapter it is described the numerical model developed in order to study the mechanical behaviour of the composite spandrels. This model has been developed with the numerical software ATENA. First of all, the geometry and the materials used for the model are described. The effort is to reproduce the geometry of the test setup described in the second chapter. Concerning the material properties, the results from the tests carried out on the materials, always described in the second chapter, are used.
The model is subsequently tested with a pushover analysis, in a displacement control. Then, the results obtained are compared with the experimental ones obtained by means of the experiments.

The final goal is to carry on further analyses with this model, by varying one parameter at the time, in order to study their effect on the mechanical response. For this reason, first, it is necessary, a validation of the model, with the comparison of both global and local behaviours.
The parametric analyses (i.e. analyses by varying one parameter at the time) and the results obtained from them are described in the fifth chapter of this thesis.

## 3.1 Description of the model

The numerical model has been developed with the finite element package, ATENA, with a simplified micro-modelling approach (method described in section 1.4). The aim is to replicate the test setup of the experimental campaign, described in the second chapter of this thesis, carried out by professor Katrin Beyer.
A representation of that numerical model is shown in figure 3.1.

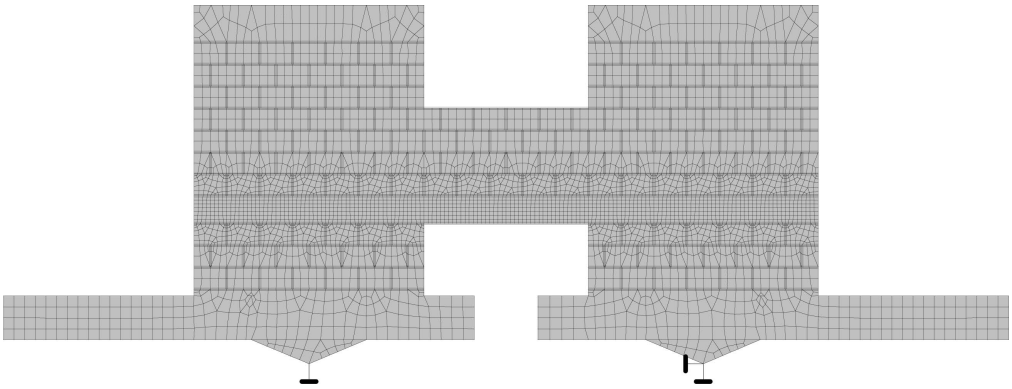

Figure 3.1: Numerical model for composite spandrels, developed with the finite element package, ATENA

### 3.1.1 Geometry of the model

The effort is to replicate the main features of the test setup with the numerical model. This in order to obtain a response as close as possible to the experimental recorded. For this reason element as the steel beams above and underneath the piers are also modelled.
In figure 3.2 the geometry of the model with its dimensions (in mm) is shown. As it is possible to see the aim is to define a model with, as more as possible, the same characteristics of the test units tested. Two triangular elements are modelled underneath the lever beams in order to define at their ends two rotational points. Since a micro-modelling approach is used, bricks dimensions are a little bigger than experimental ones. Bricks used for the experiments were, in fact, 190 mm high and 290 mm long. In this approach, however the

mortar joints and the bricks-mortar interface are lumped in a discontinuous element with zero thickness, for this reason mortar thickness has to be included in bricks geometry. The dimensions of the bricks in the model are therefore 200 mm high and 300 mm long.
A 50 mm high plate lied underneath the piers in the test setup, for this reason, in the model, the elements corresponding to the lever beams are 60 mm thicker than experimental ones.
The analysis in ATENA are carried out, as in the experiments, in a displacement control, the demand in the spandrel is applied imposing a displacement in two different directions in the points highlighted by the arrows in figure 3.2.
As in the test setup, also in the numerical model the horizontal restrain is only in the North support, in this way no axial elongation restrain is applied to the composite spandrel.

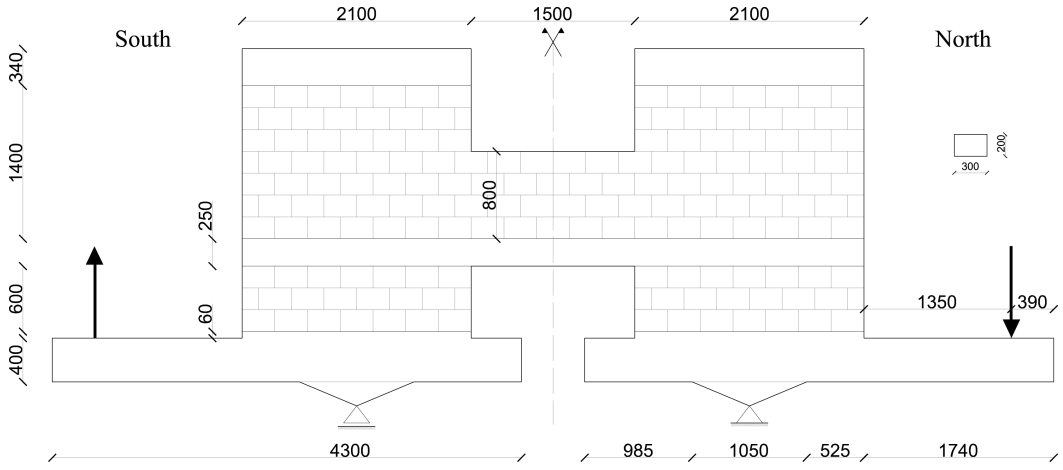


Figure 3.2: Geometry of the numerical model

### 3.1.2 Material properties

The model has been developed in 2-dimension with both elastic and inelastic materials. The bricks and the steel beams are modelled with elastic properties, whereas for the concrete of the RC beam a non-linear material is

used. The material properties are defined from the tests on the elements that formed the test units. Those tests are described in the second chapter and in this section. Several kind of elements, are used, listed herein.

1. Macro-elements. With this kind of element, the bricks, the concrete and the steel beams were modelled. Two kind of materials were used, an elastic isotropic one for the bricks and the steel beams, and an inelastic one for the concrete.
   The description of each material is in the next sub-sections:

   - Plane stress elastic isotropic, used for the bricks and the steel beams;
   - SBeta material, used for the concrete.

2. Interface element. With this element, described in detail next, it is possible to define with some parameters the behaviour of the whole joints and the interface between joints and bricks. This element has no thickness, for this reason the bricks in the model are bigger than the experimental ones.

3. Reinforcements. In ATENA the reinforcement can be modelled in two distinct forms: discrete and smeared [CJ12a]. The discrete form is suitable for the reinforcing bars elements, that form is modelled by truss elements. The smeared element is used to model shear reinforcement, in this case there are not single elements, but the reinforcement is "diffuse" in the concrete. In both cases the state of uniaxial stress is assumed [CJ12a].

**Materials for the macro-elements.**

Four kind of materials are used for the macro-elements, one for the steel beam, two for the bricks and one for the concrete (figure 3.3).

The colours in figure 3.3 refer to the following materials:

- Blue: Steel beams, modelled with a plane stress elastic isotropic material;

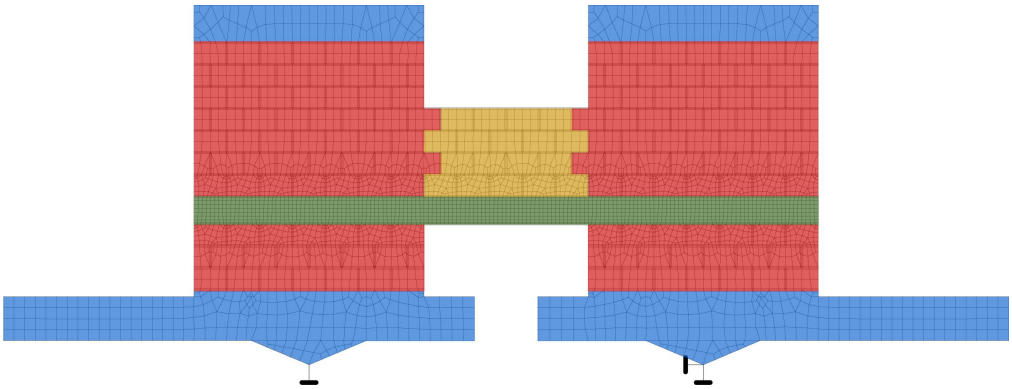

Figure 3.3: Numerical model for composite spandrels, materials analysis of the macro-elements

- Red: Bricks in the piers, modelled with a plane stress elastic isotropic material;
- Yellow: Bricks in the spandrel, modelled with a plane stress elastic isotropic material;
- Green: Concrete, modelled with a non-linear material.

**Steel beams.** These elements are modelled with a linear elastic material for 2D-plane stress state. In ATENA those materials require as input data the elastic modulus and the Poisson's ratio. For the analyses the values in table 3.1 are used.

| | |
|---|---|
| E | 210000 MPa |
| $\nu$ | 0.3 |

Table 3.1: Mechanical properties used for the steel in the numerical analyses

Also other properties as the specific material weight and the coefficient of thermal expansion can be defined, but they are not useful. Neither the specific material weight because no gravity is applied during the analysis.

**Bricks.** Two kinds of elements are used to model the bricks. In fact, bricks, as it is also shown in the second chapter, have two different modulus of

elasticity in the two direction: vertical and horizontal. In ATENA, however, it is not possible to define a non-isotropic material, therefore it is not possible to define two E-modules. For this reason two kind of bricks are used. Both are modelled with a plane stress elastic isotropic material, but, for the bricks in the piers the E-modulus in the vertical direction is used, whereas the horizontal E-modulus is used for the bricks in the spandrel. This is because piers are loaded mainly in the vertical direction, whereas the spandrel not.
There is also another possible way to consider the anisotropy of the masonry, described in section 3.2.3. That method, however, was not preferred because it is subjected to more convergence problems. As already described in the first chapter, a simplified micro-modelling approach is used, this implies that joints are not modelled and also accuracy is lost. For these reasons, the elastic modulus of the bricks are not used, but the E-modulus of the masonry instead. In fact, the sum of bricks and mortar joints is less stiff than only bricks.
The bricks are modelled as elastic, so, as for the steel beam, only the elastic modulus and the Poisson's ratio are used as input data, as shown in table 3.2. The values of the E-modules come from the experimental results described in the second chapter, whereas for the Poisson's ratio an average value of 0.2 was used. During the experiments, in fact, it was not always possible to evaluate it properly.
Since bricks are modelled as elastic it is not possible to catch their cracks pattern and the subsequently failure. Therefore, it is neither possible to study the post-peak behaviour of the composite spandrel.
However, there were no alternatives to this choice. To define a non-linear material, in fact, it is necessary to define the compressive ($f_c$) and the tensile ($f_t$) strength. In ATENA (for numerical reasons) it is not possible to define non-linear materials with ratio $f_c/f_t < 10$, that is the case of masonry.

| | |
|---|---|
| $E_{piers}$ | 5960 MPa |
| $E_{spandrel}$ | 1840 MPa |
| $\nu$ | 0.2 |

Table 3.2: Mechanical properties used for the bricks in the numerical analyses

**Concrete.** In order to model the concrete of the RC beam a SBeta material is used. A detailed description of the mechanical behaviour of the material is given in [CJ12a], here the main features are reported. In that material, developed for ATENA, the formulation of constitutive relations is considered in the plane stress state. The name SBETA comes from the former program, in which this material model was first used. It is the abbreviation for the analysis of reinforced concrete in German language - StahlBETonAnalyse. [CJ12a].
The non-linear behaviour of concrete in the biaxial stress state is described by means of the so called effective stress $\sigma_c^{ef}$, and the equivalent uniaxial strain $\varepsilon^{ef}$. The equivalent uniaxial strain can be considered as the strain that would be produced by the stress $\sigma_{ci}$ in a uniaxial test with modulus $E_{ci}$ associated with the direction i [CJ12a]. In figure 3.4 it is represented the stress-strain law of the material and it is also shown an unloading path that is a linear function to the origin.

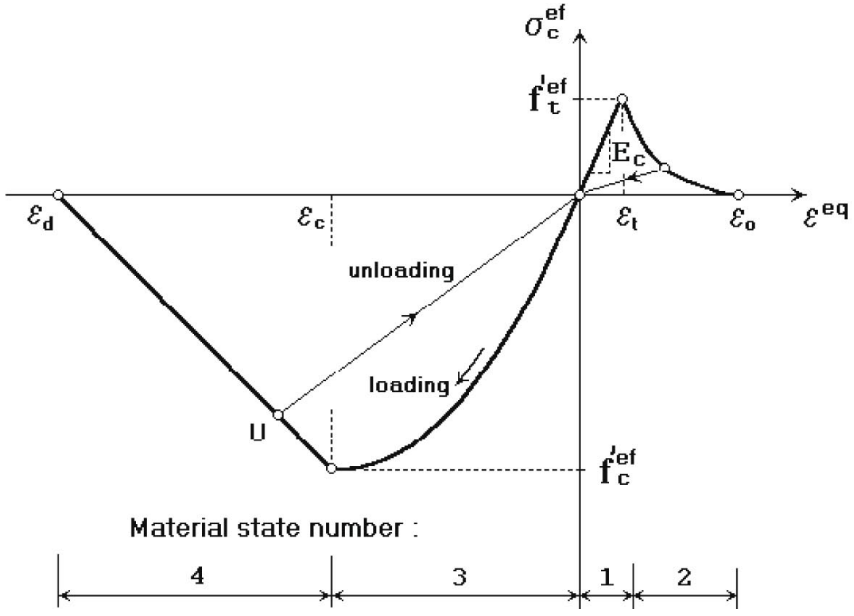


Figure 3.4: Uniaxial stress-strain law for concrete (from [CJ12a] p.27)

The behaviour is of course different in tension and in compression. The behaviour of concrete in tension without cracks is linear elastic. After cracking five possible softening laws are defined. Since no experimental data of

the post peak behaviour are available, the standard formulation, with an exponential crack opening law, is used.
In compression a parabolic path is defined up to the peak stress, whereas the softening law in compression is linearly descending.
To model the concrete were used the values shown in table 3.3, whereas, as already said, the default values for the compressive, tensile and shear after-peak behaviours were used.

| | |
|---|---|
| $E_c$ | 31000 MPa |
| $\nu$ | 0.2 |
| $f_t$ | 3.4 MPa |
| $f_c$ | -35.2 MPa |

Table 3.3: Mechanical properties used for the concrete in the numerical analysis

### Interface elements

Interface material describes the physical properties of contact between two surfaces. The interface material is based on Mohr-Coulomb criterion with tension cut off. The initial failure surface corresponds to a Mohr-Coulomb condition [CJ12a] with ellipsoid in tension regime. After stresses violate this condition, this surface collapses to a residual surface which corresponds to dry friction, that means c=0 and $f_t$=0. In figure 3.5 both surfaces are shown.

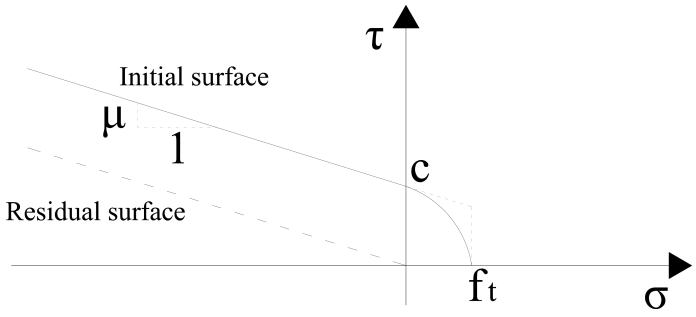


Figure 3.5: Initial and residual surfaces for interface elements in ATENA

where:

| | |
|---|---|
| c | interface element cohesion |
| $f_t$ | interface element tensile strength |
| $\mu$ | interface element friction |

As stated in [CJ12a], the parameters for the interface model cannot be defined arbitrarily. Defining the interface parameters, the following rules should be observed:

$$f_t < \frac{c}{\mu}; f_t < c$$

and

$$c > 0; f_t > 0; \mu > 0$$

The tensile strength of the mortar recorded in the test is much bigger than the limits above written. For this reason it was not used the tensile strength of the mortar, but the value $f_t$ = - $\frac{c}{\mu}$. This also probably reflects that the tensile strength of the interface joint-brick is weaker than a specimen only formed by mortar.

There is also a second set of parameters to define, the so called stiffness coefficients, which serve purely for numerical purposes [CJ12b]. There are two stiffness coefficients, $K_{nn}$ (normal), $K_{tt}$ (shear) and each has two values: basic and minimal. In the same manual is stated that the basic stiffness should be very high in order to represent well the rigid body, whereas the minimum stiffness should be near zero in order to represent the open contact. At the same time it is recommended not to use extremely high values as this may result in numerical instabilities. In [CJ12a] the following formulas are proposed to evaluate them:

$$K_{nn} = \frac{E}{t}; K_{tt} = \frac{G}{t}$$

where E and G is minimal elastic modulus and shear modulus respectively of the surrounding material, t is the width of the interface zone. To determine these values only the shear modulus corresponding to the bricks in the spandrel was used. That is because in this way the stiffness of the model is practically the same, but less convergence problems, during the analysis, occurred.

The minimal stiffness, instead, are used only for numerical purposes, after the failure of the element, in order to preserve the positive definiteness of the global system of equations [CJ12a]. These values are required since theoretically, after the interface failure, the interface stiffness should be zero, which would mean that the global stiffness will become indefinite.
As suggested in the same manual aforesaid, these minimal stiffness should be about 0.001 times of the initial ones.

Two kinds of interface elements were modelled, one for the bed-joints and another for the head-joints. The difference between the two elements is that it is supposed that the head-joints are weaker than the bed-joints. For this reason it is supposed that the cohesion and the tensile strength are a fifth of the ones in the bed-joints. They are not zero because in the manual it is recommended that the parameters c, $f_t$ and $\mu$ should be always greater than zero. In cases when no cohesion or no tensile strength is required, some very small values should be prescribed.

| | |
|---|---|
| $K_{nn}$ | $7360 \cdot 10^4$ MN/$m^3$ |
| $K_{tt}$ | $7360 \cdot 10^4$ MN/$m^3$ |
| $f_t$ | 0.35 MPa |
| $c$ | 0.25 MPa |
| $\mu$ | 0.71 |

Table 3.4: Mechanical properties used for the bed-joints in the numerical analyses

In ATENA it is also possible to define evolution laws for tensile as well as shear softening. Those laws were not defined in the model since there are no experimental data on the fracture energy of the joints.

| | |
|---|---|
| $K_{nn}$ | $7360 \cdot 10^4$ MN/$m^3$ |
| $K_{tt}$ | $7360 \cdot 10^4$ MN/$m^3$ |
| $f_t$ | 0.07 MPa |
| $c$ | 0.05 MPa |
| $\mu$ | 0.71 |

Table 3.5: Mechanical properties used for the head-joints in the numerical analyses

**Reinforcement**

Reinforcement can be modelled in two distinct forms: discrete and smeared. Discrete reinforcement is in form of reinforcing bars and is modelled by truss elements, whereas the smeared is a sort of layer with the aim to model the shear reinforcement. In both cases the state of uniaxial stress is assumed [CJ12a].
The software allows to choose between four types of stress-strain laws. For both longitudinal and shear reinforcement bilinear stress-strain laws with hardening were used, with the values reported in tables 3.6 and 3.7.

| | |
|---|---|
| $E$ | 206000 MPa |
| $\sigma_y$ | 505 MPa |
| $\sigma_t$ | 616 MPa |
| $\varepsilon_{lim}$ | 0.12 |

Table 3.6: Mechanical properties used for the longitudinal reinforcement in the numerical analyses

For the shear reinforcement its ratio has also to be defined.
In figure 3.6, $d_s$ is the distance between two stirrups and t the thickness of the RC beam. The ratio is therefore defined as:

$$ratio = \frac{A_c}{A_{reinf}} = \frac{d_s \cdot t}{2D6} = \frac{150mm \cdot 200mm}{56mm^2} = 0.00188$$

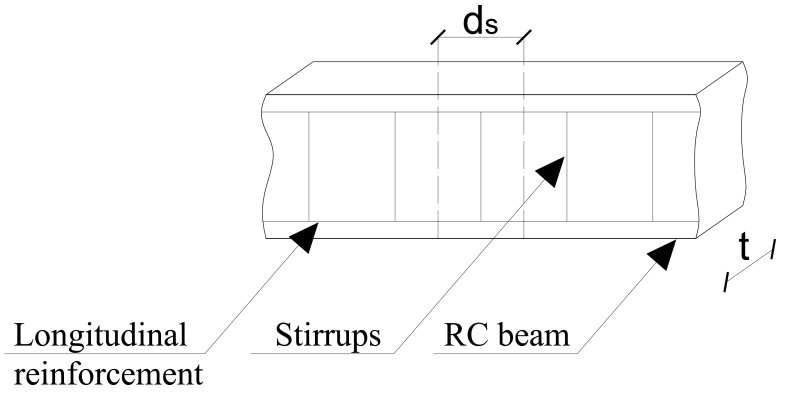


Figure 3.6: Shear reinforcement ratio

In table 3.7 the mechanical properties used for the shear reinforcement are shown.

| | |
|---|---|
| $E$ | 210000 MPa |
| $\sigma_y$ | 586 MPa |
| $\sigma_t$ | 634 MPa |
| $\varepsilon_{lim}$ | 0.05 |
| ratio | 0.00188 |

Table 3.7: Mechanical properties used for the shear reinforcement in the numerical analyses

### 3.1.3 Mesh properties

In this section the mesh properties of the numerical model are described. It is known, in fact, that the reliability of the results in numerical analysis is heavily influenced both by the dimension of the mesh and the type of elements used.
As described in the previous section the bricks were modelled with elastic properties, the concrete of the RC beam with an inelastic material instead. For this reason a more dense mesh for the inelastic elements is used. For the concrete and for the two rows of bricks above and underneath the RC beam a mesh with a element size of 0.05 m was used, whereas for the other

macro-elements a 0.1 m mesh size is used. This is shown in figure 3.2 where the elements with a 0.05 m size are drawn in red.

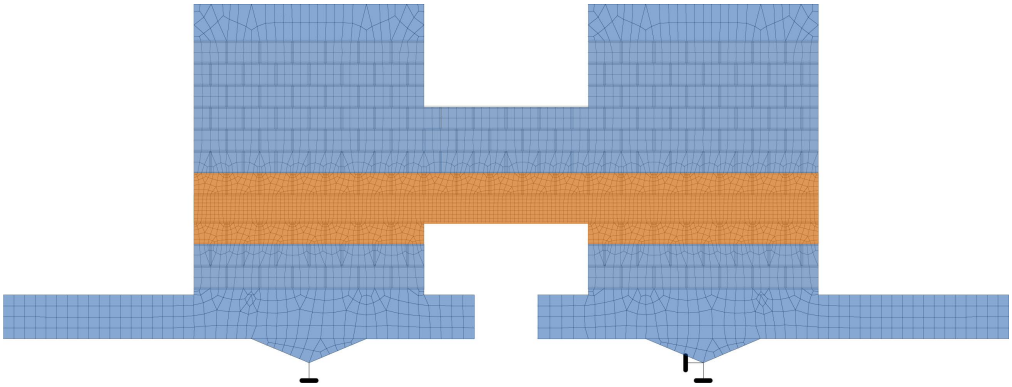

Figure 3.7: Elements size in the numerical model

For the model four node elements are used. It is also important that those elements are rather regular and for this reason some rules should be followed.

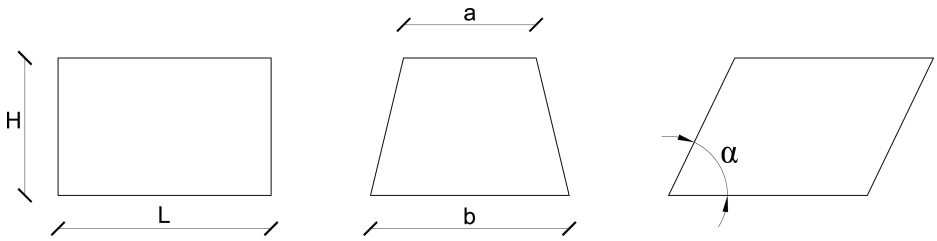


Figure 3.8: Distorsion in 2D elements

With the notations in figure 3.8, where it is required to know the stresses, for rectangular elements, the aspect ratio (relation of width to height) should not be greater than 2. When the elements are distorted the ratio a/b should be more than 4 and there should not be internal angles smaller than 45° [Gug02].
Also for this reason two rows of bricks were modelled with a smaller mesh dimension, in this way, in fact, these limitations were respected rather well.

Furthermore, as recommended [CJ12c] in 2D plane stress element needs at least 4 elements through the thickness to obtain reliable results. However

with more elements the solution is more accurate. The RC beam, was modelled splitting the 150 mm width and 250 mm height elements in four elements in the horizontal direction and in seven elements in the vertical. In this way almost square elements are obtained.

A particular four node element was used to carry on the analysis, the CCQ10Sbeta element. This element is a variation of the CCQ10 element. Both elements are described in detail in [CJ12a].
The CCQ10 quadrilateral finite element is composed from two 4-node triangular elements, as shown in figure 3.9. The triangular element is derived from the 6-node triangle by imposing kinematic constraints on two mid-side nodes [CJ12a].

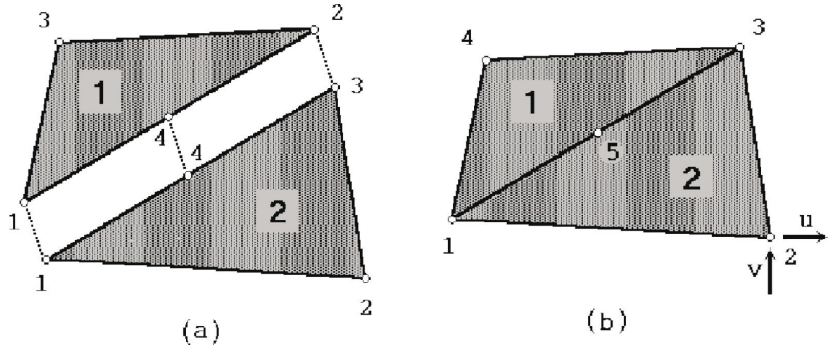


Figure 3.9: Quadrilateral element (b) composed from two triangular elements (a) (from [CJ12a] p. 124)

For the given displacement field, the strains and stresses are evaluated in the centre of the quadrilateral element. The stresses at this point are obtained from material laws as functions of strains .
In the CCQ10SBeta element the material law is evaluated only at the element centroid. Based on the current state of damage a secant constitutive matrix is calculated and it is used to determine the integration point stresses and the resulting resisting forces [CJ12a].

### 3.1.4 Load cases and analysis steps

In this section the actions applied in the model are described. The aim of the numerical analysis is to simulate as close as possible the experimental setup of the experiments described in the second chapter.
To carry on the analyses, the supports, the vertical load in the piers and the rotation of the beams underneath the specimen have to be defined.
As the experimental ones, a support that did not allow the sliding was used in the South side, whereas in the North one the sliding was impeded.

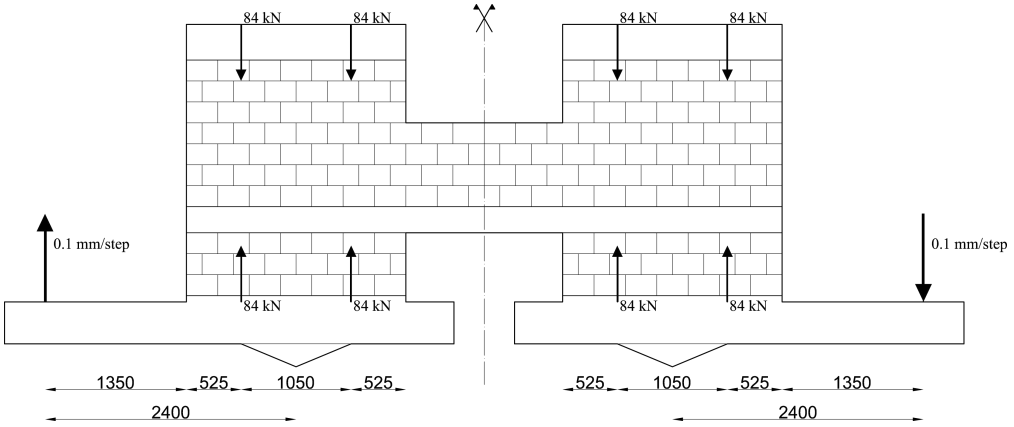


Figure 3.10: Actions applied in the numerical model

#### Axial load in the piers

Apart for TU4, for all experiments the axial stress in the piers was kept as more as possible at the constant value of 0.40 MPa. For this reason, not considering the self weight (no gravity is applied in the numerical model), for each pier a force of 168 kN is applied. This axial load corresponds to a mean compressive stress of 0.40 MPa. This load is the sum of two forces applied above the steel beam on the piers and other two forces underneath the piers, as shown in figure 3.10.

**Drift demand in the composite spandrel**

The analysis are carried on with a static non-linear method (pushover analysis), the actions therefore increased monotonically until it is possible to reach convergence. The drift demand in the composite spandrel is applied by the rotation of the "lever beam", as defined in the second chapter. For each step two displacements of 0.1 mm in opposite directions are applied at the two steel beams as shown in figure 3.10. In this way, for instance, there is a drift demand of 1% in the composite spandrel, when a displacement of 24 mm is reached, corresponding to load step 242 (in fact, the first displacement is imposed in the third load step).

### 3.1.5 Solution parameters

The analyses are carried on with a modified Newton-Raphson method. The standard method was used only for the first load step, when the axial load is applied. In this method is used a tangent stiffness that is update at each iteration, and maximum 40 iterations are done.
In table 3.8 are shown the errors tolerance. Is is possible to read a detailed description of the meaning of each error in [CJ12a].

| | |
|---|---|
| Displacement error tolerance | 0.010000 |
| Residual error tolerance | 0.010000 |
| Absolute error tolerance | 0.010000 |
| Energy error tolerance | 0.000100 |

Table 3.8: Standard Newton-Raphson method, characteristics

ATENA does not automatically end an analysis if the convergence limits are not met when the maximum number of iterations are reached. It can be stopped at any time or at the end of the iterations. It depends if the error is bigger than the tolerance times a fixed multiple. Those values, for the standard Newton-Raphson method are shown in table 3.9.

| | Break immediately | Break after step |
|---|---|---|
| Displacement error tolerance | 10000 | 10000 |
| Residual error tolerance | 10000 | 10000 |
| Absolute error tolerance | 10000 | 10000 |
| Energy error tolerance | 1000000 | 1000000 |

Table 3.9: Standard Newton-Raphson method, break criteria

For the analyses, however, the parameters of this method were modified. It is preferred to update the stiffness matrix at each step (in this way the analyses are faster) but to increase the number of iterations to 250. In fact, as just said, ATENA does not automatically end an analysis if the convergence limits are not met when the maximum number of iterations are reached, but with only 40 or 100 iterations often a rather big error (however less than the maximum accepted) occurred. There were used also different errors tolerance and the break criteria as shown in tables 3.10 and 3.11.

| | |
|---|---|
| Displacement error tolerance | 0.005000 |
| Residual error tolerance | 0.005000 |
| Absolute error tolerance | 10.00000 |
| Energy error tolerance | 0.000001 |

Table 3.10: Newton-Raphson method used, characteristics

| | Break immediately | Break after step |
|---|---|---|
| Displacement error tolerance | 2000.0 | 200.00 |
| Residual error tolerance | 2000.0 | 200.00 |
| Absolute error tolerance | 10000 | 1000.0 |
| Energy error tolerance | 100000000 | 1000000 |

Table 3.11: Newton-Raphson method used, break criteria

In this way the errors tolerance as well as the break criteria were reduced.

## 3.2 Validation of the numerical model

The final aim of the analyses with the numerical model is to study further configurations that were not possible to study in the experimental campaign. For this reason it is required a comparison of the global and local results among the numerical model and the experimental tests.

### 3.2.1 Comparison of the global characteristics

The main characteristic which is studied in order to validate the model is the force-deformation relationship of the composite spandrel. By means of it, it is possible, in fact, to study features such as the stiffness and the shear strength. However, also other characteristic have been studied, as the deformed shape, the global cracks pattern and the shear-resistance mechanism triggered.
This comparison has been done from TU2 to TU5.

#### Test Unit 2

In figure 3.11 the comparison of force-deformation curves obtained from experimental test and the numerical simulations for TU2 is shown. In figure 3.12 it is plotted the force-deformation relationship up to a drift demand of 1%.
As it is possible to observe in those graphs, the numerical model capture rather well the mechanical behaviour recorded till a drift demand of about 1%. This characteristic will recur also for the other test units. In fact, bricks in the experimental tests started cracking usually for drift demand bigger than 1%. In the model, however, as said, bricks were modelled with elastic properties, so it was not possible to catch their failure and the consequent reduction in strength of the spandrel.
It is therefore possible to say that for drift values bigger than 1-1.5% the numerical model is not able to predict the shear capacity properly. As shown in figure 3.11, after those values, since no failure in bricks occur, the shear capacity seems that constantly increases, this effect is due to the strengthen of longitudinal reinforcement after the yield.
In figure 3.13 the deformed shapes comparison of the experimental test and

the numerical model is shown. In the numerical model, cracks in the RC beam and in the mortar joints appeared for very low drift demands, lower than what it was possible to record in the specimen of TU2. This is depicted in figure 3.13a, where the deformed shape corresponding to a drift of 0.1% is shown. In the numerical model the deformed shape has a magnification factor of 10, but the cracked joints have been however highlighted because the deformations were rather small. For that drift value the cracks pattern of the numerical model is rather different from the experimental one, but it is already possible to see the stair-stepped cracks originating to the top South of the spandrel, as the one in the specimen of TU2, described in the second chapter of this thesis. The cracks pattern in masonry, however, become closer to the experimental one as more as the drift demand increases as it is possible to see in figures 3.13b and 3.13c.

As just said, also for the RC beam, in the numerical model the first cracks appeared first than in the experimental specimen. In fact, for a drift of 0.1% in the specimen only two cracks formed, whereas in ATENA model there are already a few. Also in this case, however, increasing the drift demand the cracks pattern became closer, and there is a rather well correspondence between the models. In TU2 specimen, in fact, the two plastic hinges in the north side and in the south side developed in a different way. In the North side a rather narrow negative plastic hinge developed, whereas in the South side the cracks were spread. Same behaviour is shown by the numerical model in ATENA, as depicted in the figures above mentioned.

The deformed shape of the whole specimen is shown in figures 3.14 and 3.15. All the observations just discussed are still valid and it is therefore possible to see two cracks, above and under the RC beam, that spread through the length of the South pier. The crack underneath the RC beam in the Atena model is however rather big and a “gap” forms between the bottom side of the RC beam and the piers underneath. This gap was noticed also in TU2 specimen, but in that case was not so wide.

We could say that this numerical model is ruled mainly by a rocking behaviour, whereas in TU2 also a shear mechanism in the RC beam triggered.

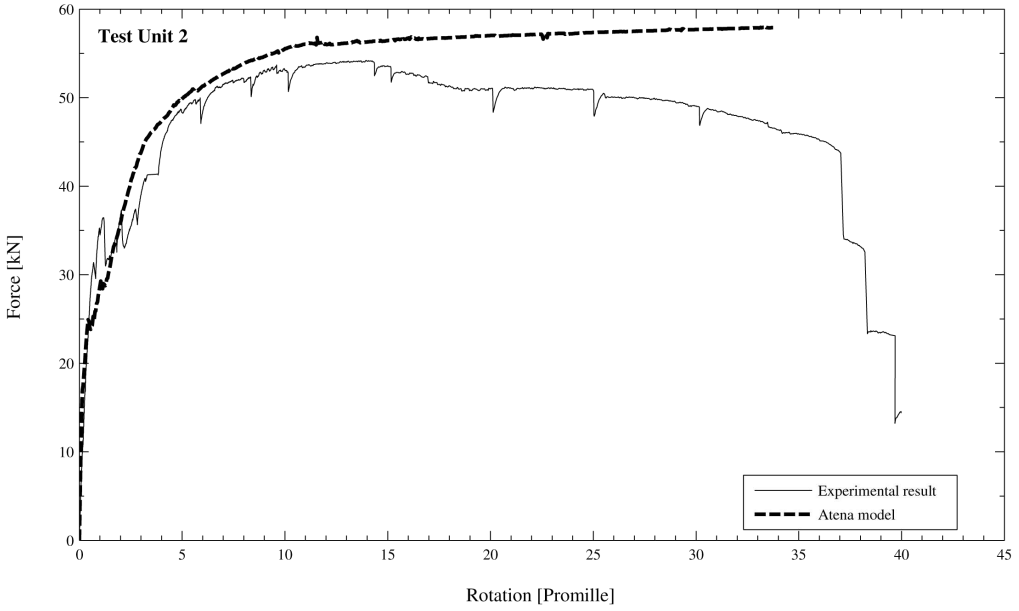


Figure 3.11: TU2 - Comparison of force-deformation curves obtained from experiments and numerical simulations.

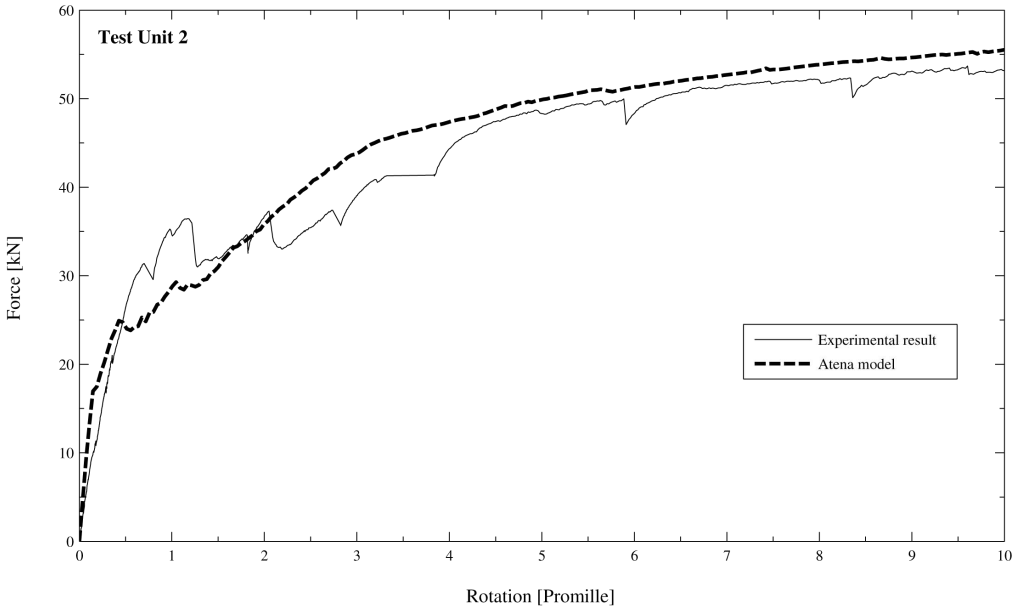


Figure 3.12: TU2 - Comparison of force-deformation curves obtained from experiments and numerical simulations up to a maximum drift of 1%.

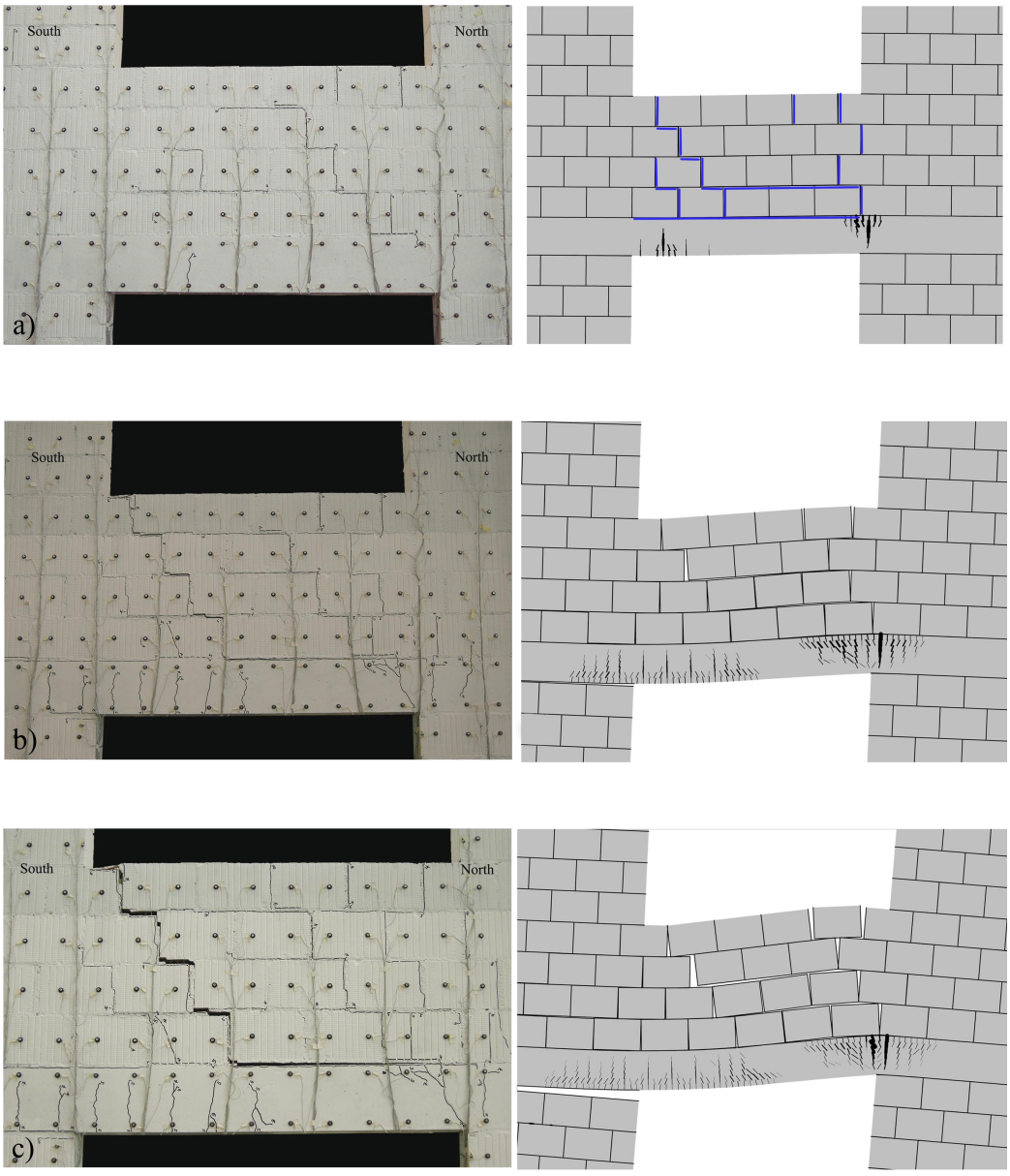


Figure 3.13: TU2 - Deformed shape comparison at a drift of a.0.1%, b.0.4%, c.0.8%. Numerical model in Atena magnification factor of 10

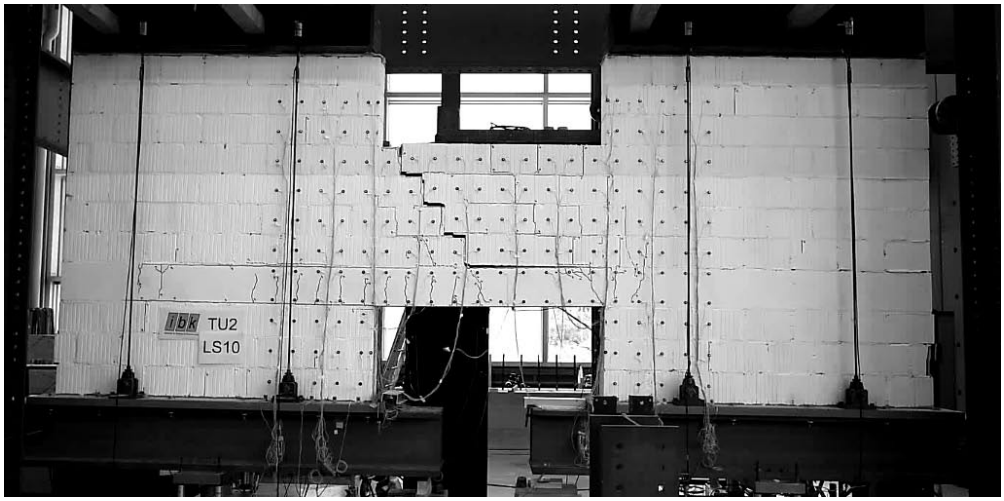


Figure 3.14: TU2 - Crack pattern of the concrete spandrel at LS 10. Drift towards North of 1%

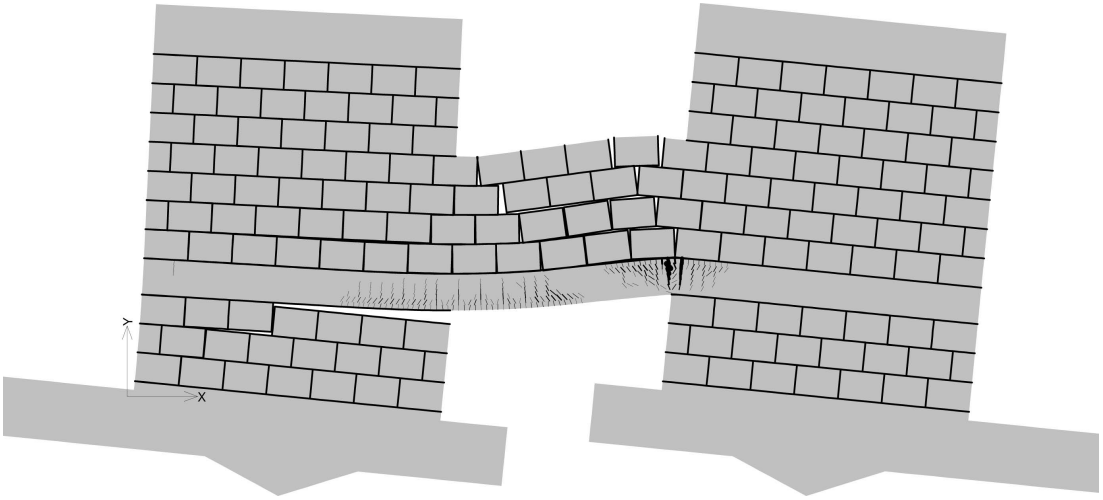


Figure 3.15: TU2 - Numerical model deformed shape for a drift of 1%

**Test Unit 3**

As described in the second chapter, TU3 had the same properties of TU2, but it was loaded with a cyclic action. In ATENA no cyclic actions were imposed, so for TU2 and TU3 the same model was used.
As already done for TU2, in figure 3.16 the comparison of force-deformation curves obtained from experimental test and the numerical simulations is shown. In figure 3.17 it is plotted the force-deformation relationship up to a drift demand of 1%. Since in ATENA only a monotonic loading is applied, the same force-deformation relationship is used to compare spandrel reaction when it went towards north or towards south.

Although TU2 and TU3 had the same properties, TU3 resulted quite stronger than TU2. This was probably due to the fact that they were built the same day, but the test in TU3 was carried out more than two months after the one in TU2. Therefore the mortar probably increased in strength.
However, as for TU2, until masonry in the specimen did not lose its load bearing capacity the numerical model is able to predict the mechanical behaviour rather well. After LS41 (corresponding to a drift of 1.5%) several cracks opened in the masonry, therefore the shear capacity of the spandrel decreased.

Concerning the cracks pattern, also comparing the numerical model with TU3, for very low drift values (drift demand minor than 0.1%) the specimen was fairly uncracked, whereas Atena model it is not. First cracks in the mortar joints appears indeed for a drift value of 0.1%, and also for that demand the RC is almost totally uncracked, as shown in figure 3.18.
Since this specimen was loaded with a cyclic action it is not clearly possible to see a narrow negative plastic hinge and a spread positive one as in TU2, but cracks spread in both directions. It is however still possible to see the main characteristic of the deformed shape, as the stair-stepped crack in the masonry and that, the positive plastic hinge did not form at the end of the RC beam, but in a certain distance from the piers.

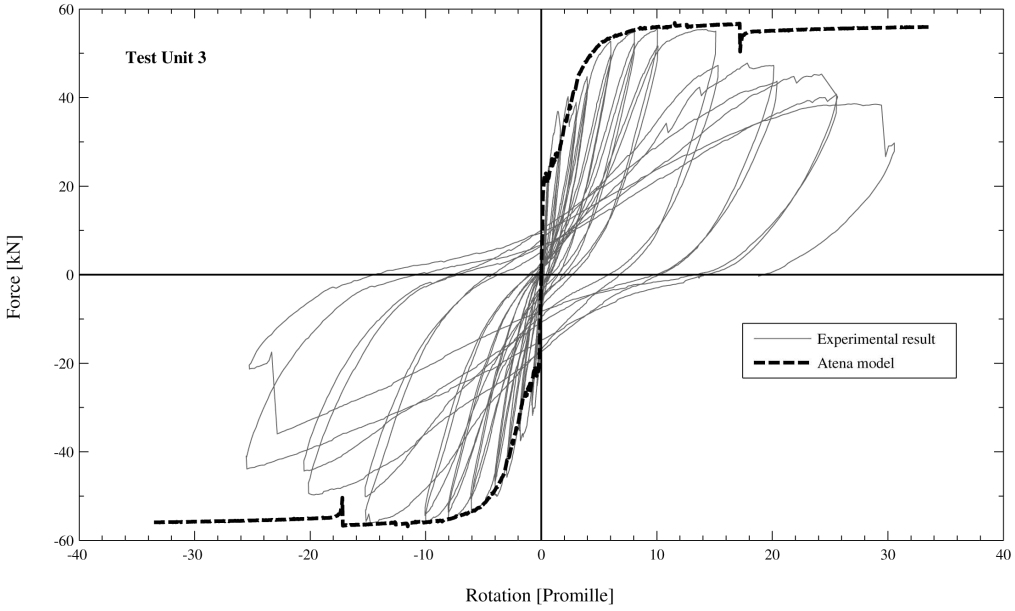


Figure 3.16: TU3 - Comparison of force-deformation curves obtained from experiments and numerical simulations.

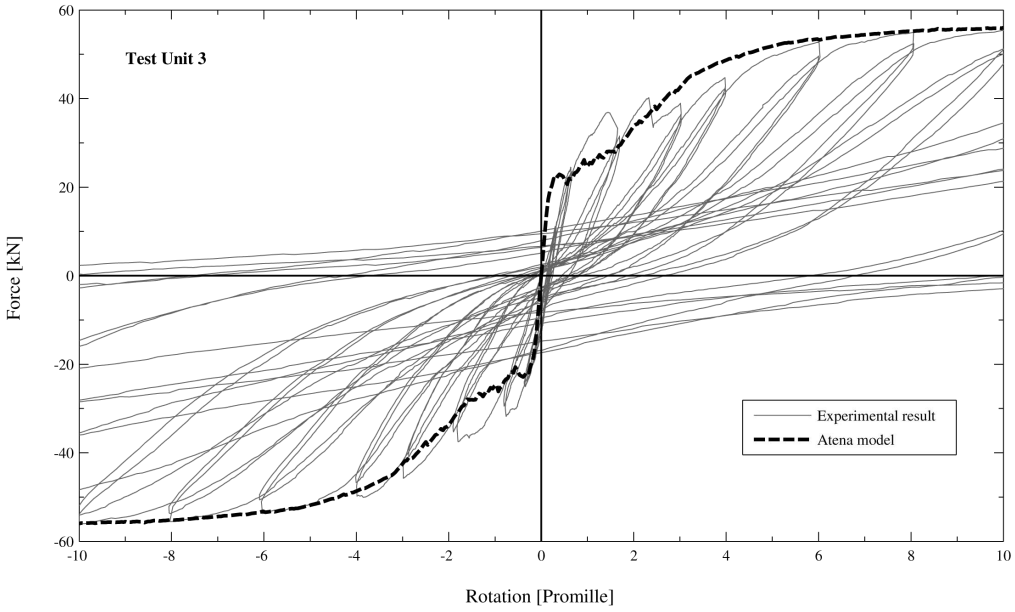


Figure 3.17: TU3 - Comparison of force-deformation curves obtained from experiments and numerical simulations up to a maximum drift of 1%.

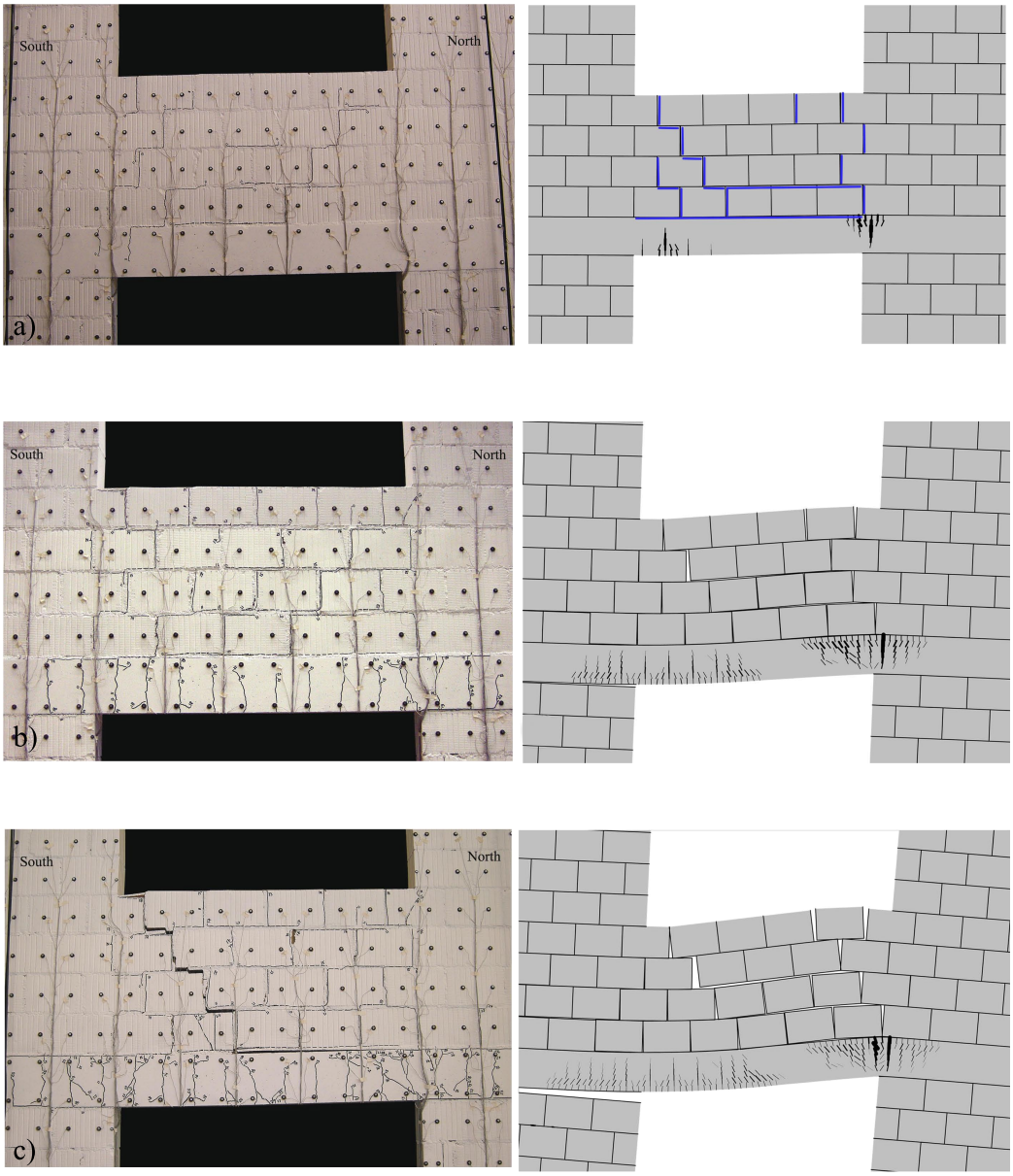


Figure 3.18: TU3 - Deformed shape comparison at a drift of a.0.1% (cracks patter in masonry highlighted in blu), b.0.4%, c.0.8%. Numerical model in Atena magnification factor of 10

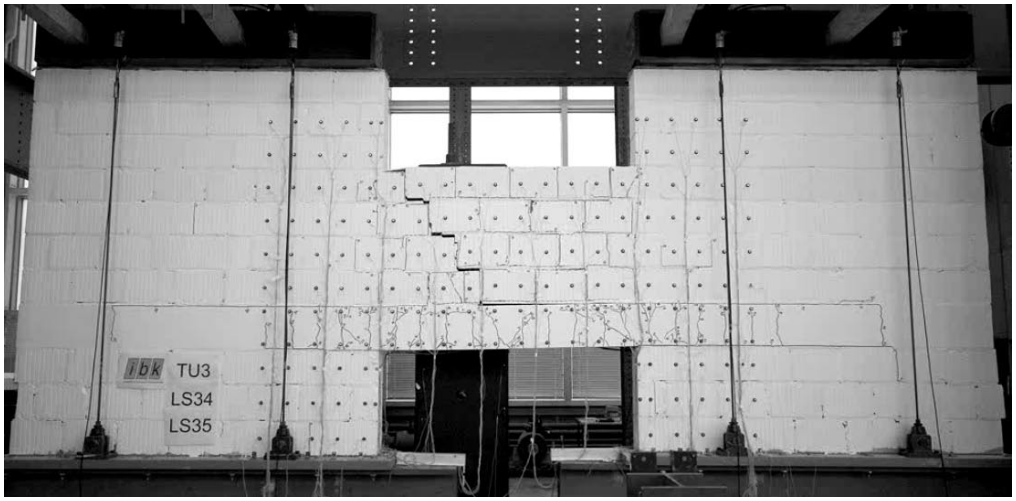


Figure 3.19: TU3 - Crack pattern of the concrete spandrel at LS 34. Drift towards North of 1%

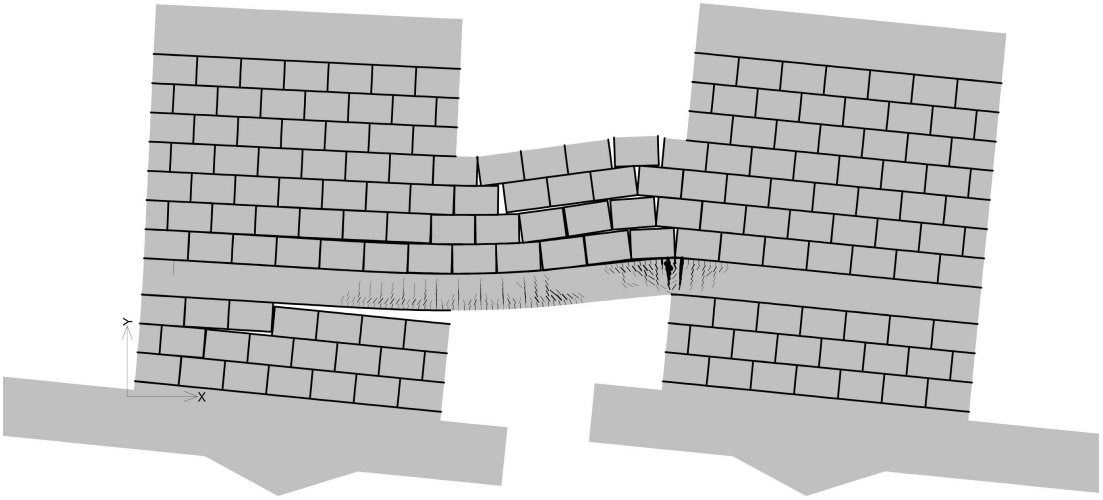


Figure 3.20: TU3 - Numerical model deformed shape for a drift of 1%

**Test Unit 4**

The specimen of TU4 had a stronger longitudinal reinforcement than TU3, but both had the same geometry and were subjected to a cyclic loading. Since it had a stronger reinforcement the RC beam resulted stiffer and stronger than RC beam of other test units. The consequences were that the shear capacity of the composite spandrel obviously increased and it was possible to see a clear rocking effect between the RC beam and the piers underneath. For this reason during the experiment the axial load in the piers was increased from 0.4 Mpa to 0.6 Mpa, in fact, as it will be shown in the parametric analysis in the fifth chapter, the axial load in the piers influences heavily the load bearing mechanism in the composite spandrels. It is possible to say, in fact, roughly, that if the axial load in the piers is relatively low there is a higher possibility to have a rocking mechanism instead of having a shear failure in the RC beam, and vice versa.

In figure 3.21 there is the comparison of the experimental force-deformation relationship with the numerical one. All experimental cycles are plotted, both those with an axial load in piers of 0.4 Mpa and 0.6 MPa. The last loops correspond to the axial load of 0.6 MPa.
As it is possible to see, since for an axial load of 0.4 MPa the response of the composite spandrel was governed mainly by a rocking mechanism and the bricks remained fairly undamaged, the numerical model (with elastic bricks) manages to predict the mechanical behaviour of the spandrel also for drift demands more than 1%.
In this case, however, the numerical model predicts a lower shear capacity than the experimental one, that is probably due to the fact that during the experiment the axial load had not always the constant value of 0.4 MPa, but, sometimes it was more. More information about this are in [BAD10].

In the numerical models the axial load is not changed during the test, as done for TU4 but two analyses are carried out, one with an axial load of 0.4 MPa and another with 0.6 MPa.

The aim of this last analysis is to predict the new shear capacity of the composite spandrel changing the axial load in the piers.

In figure 3.22 it is plotted the force-deformation relationship up to a drift demand of 1%.
The different stiffness of TU4 RC beam than others test units influenced also the deformed shapes of the spandrel, see figure 3.23. In this experiments, in fact, the first cracks opened for a drift of only 0.05%. Then, the more strength of RC beam, at least in the numerical model, does not allow the development of a positive plastic hinge. The negative plastic hinge, instead, clearly develops with several flexural and also shear cracks. Finally, the gap between the RC beam and the pier underneath results much bigger than the one of other test units, but this feature was found also in the experiment.

Increasing the axial load in the piers, in the numerical model, the gap dimension decreases and a shear mechanism triggers in the RC beam, as happened in the experimental test when the axial load was changed from 0.4 Mpa to 0.6 MPa, see figures 3.25 and 3.26.

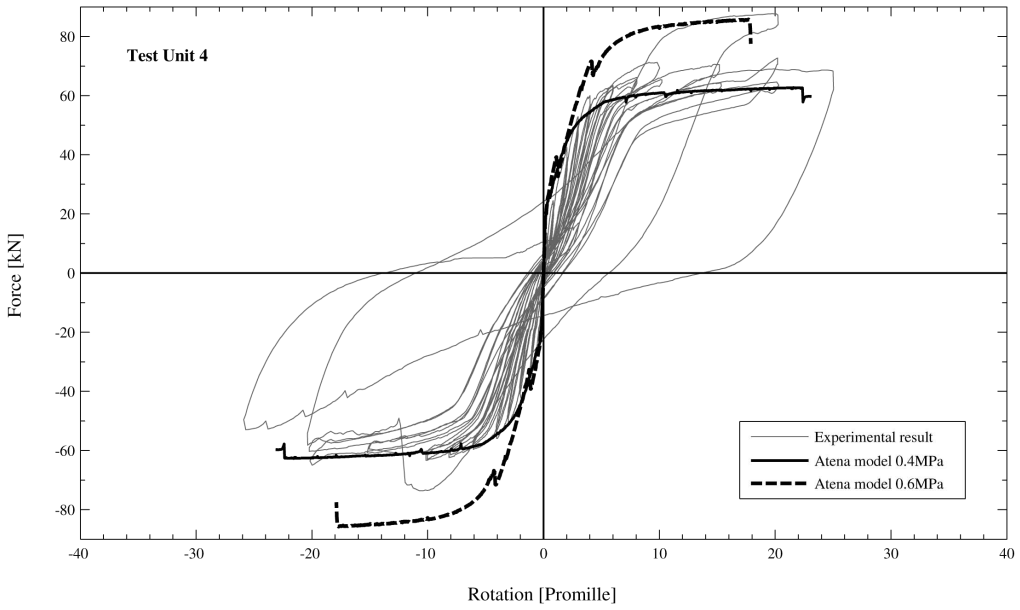


Figure 3.21: TU4 - Comparison of force-deformation curves obtained from experiments and numerical simulations.

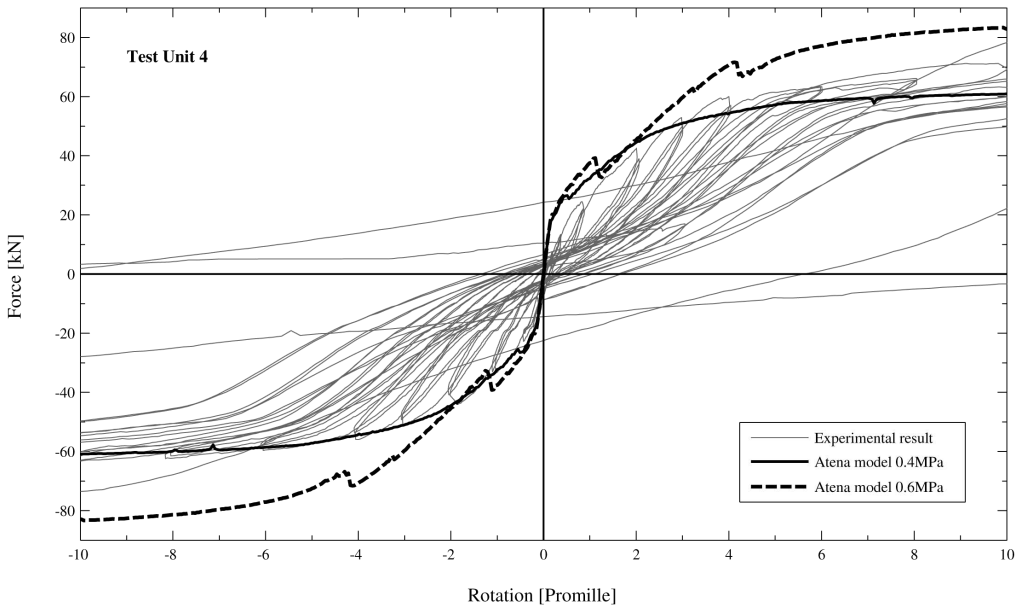


Figure 3.22: TU4 - Comparison of force-deformation curves obtained from experiments and numerical simulations up to a maximum drift of 1%.

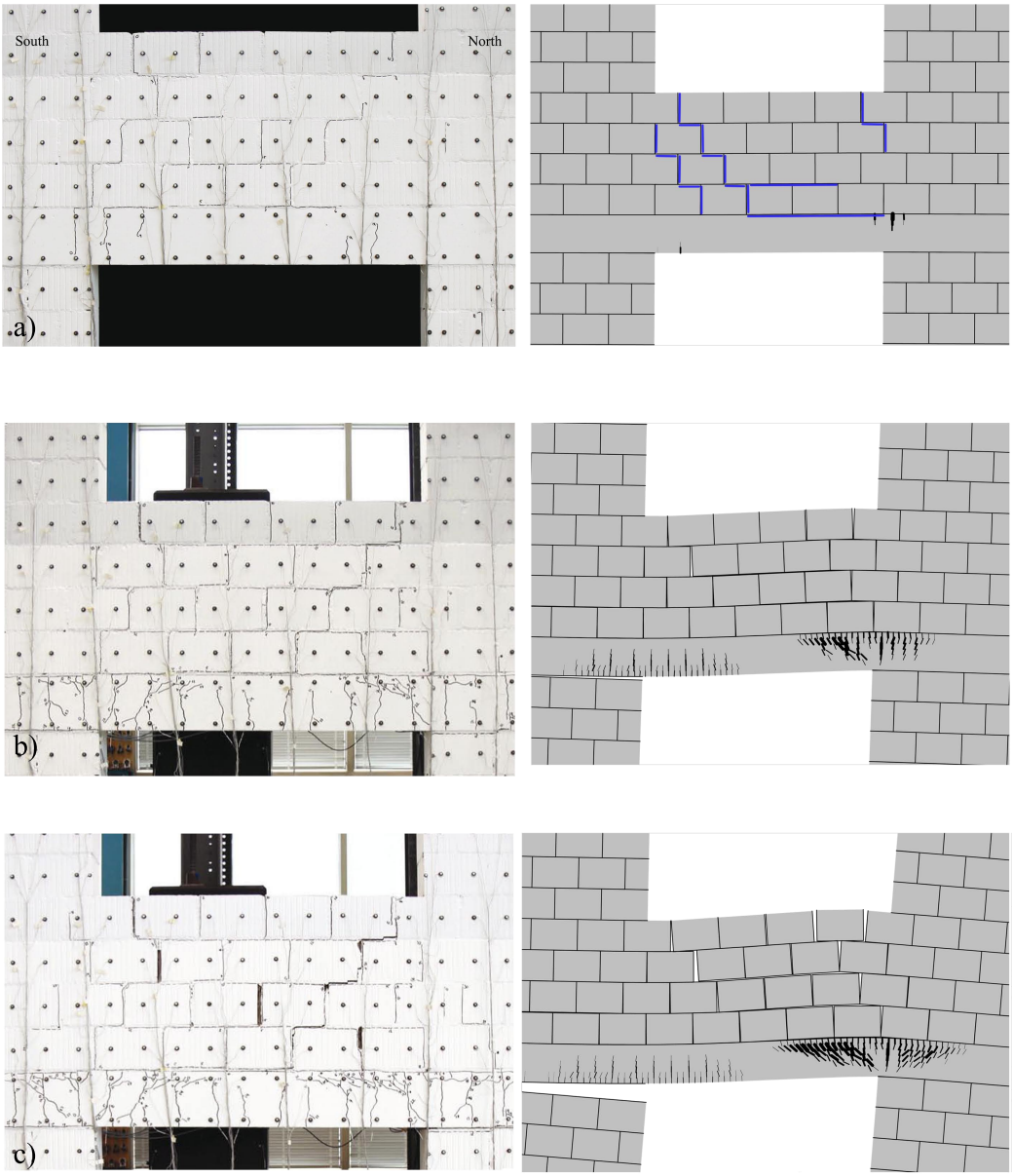


Figure 3.23: TU4 - Deformed shape comparison at a drift of a.0.05% (cracks patter in masonry highlighted in blu), b.0.4%, c.0.8%. Axial load in the piers 0.4 MPa. Numerical model in Atena magnification factor of 10

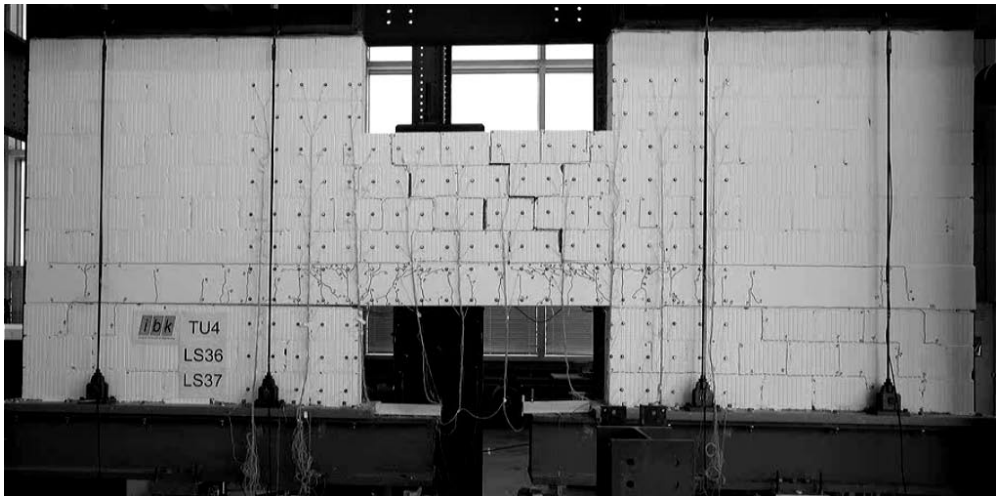


Figure 3.24: TU4 - Crack pattern of the concrete spandrel at LS 36. Drift towards North of 1%

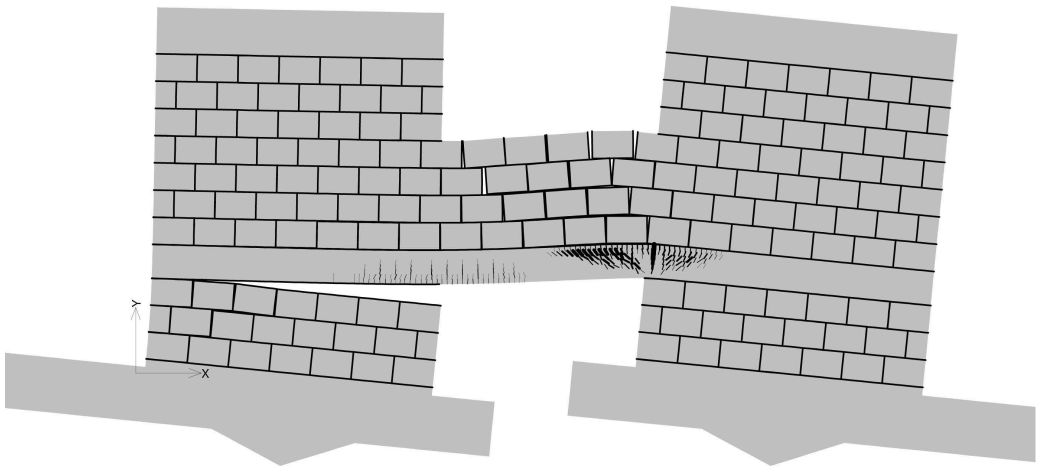


Figure 3.25: TU4 - Numerical model deformed shape for a drift of 1%. Axial load in the piers 0.4 MPa.

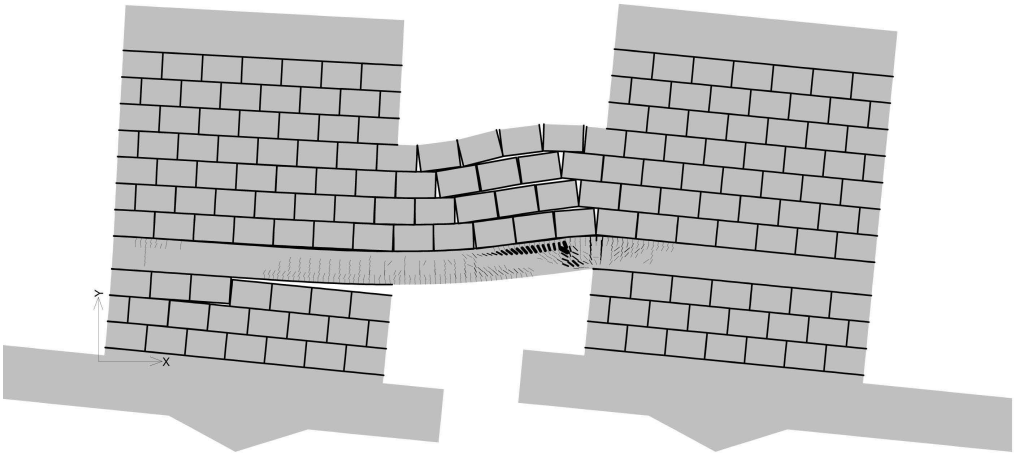


Figure 3.26: TU4 - Numerical model deformed shape for a drift of 1%. Axial load in the piers 0.6 MPa.

**Test Unit 5**

The specimen of TU5 had the weakest longitudinal reinforcement of all test units. Its RC beam resulted therefore weaker and less stiff than the other ones. Consequently, also the shear capacity of the spandrel resulted lower, and no rocking mechanism were noted.
These aspects are fairly reported both in force deformation relationship and in the deformed shapes. For instance, no gap formed underneath the RC beam, neither in the experimental specimen nor in the numerical model.
As it is shown in figure 3.27, it seems that the numerical model manages to predict the mechanical behaviour till a drift of almost 2%. A possible explanation of the better correspondence of these results could be that since the RC beam is less stiff, it keeps the majority of the deformations and the bricks therefore result with less cracks. However, after a drift of 1%, many convergence problems occur that undermine the reliability of those results. Also for this reason it is possible to see spikes in the curve after that value of drift.

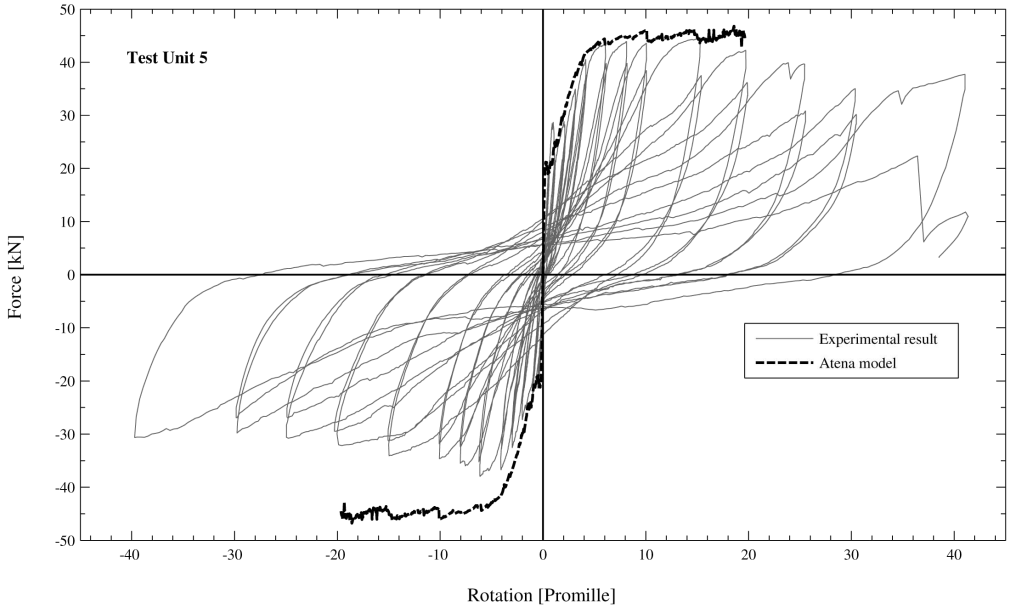


Figure 3.27: TU5 - Comparison of force-deformation curves obtained from experiments and numerical simulations.

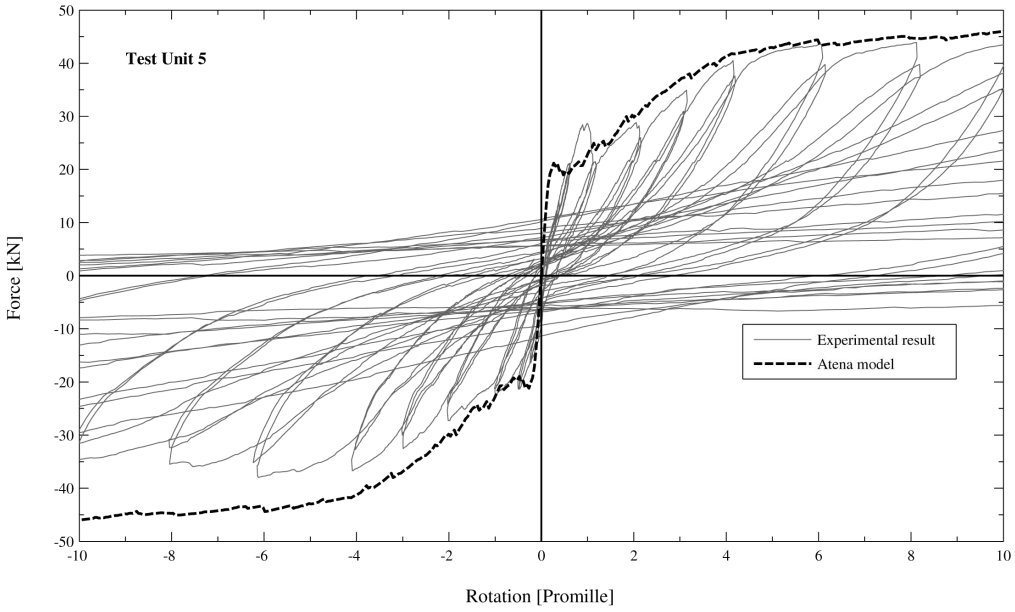


Figure 3.28: TU5 - Comparison of force-deformation curves obtained from experiments and numerical simulations up to a maximum drift of 1%.

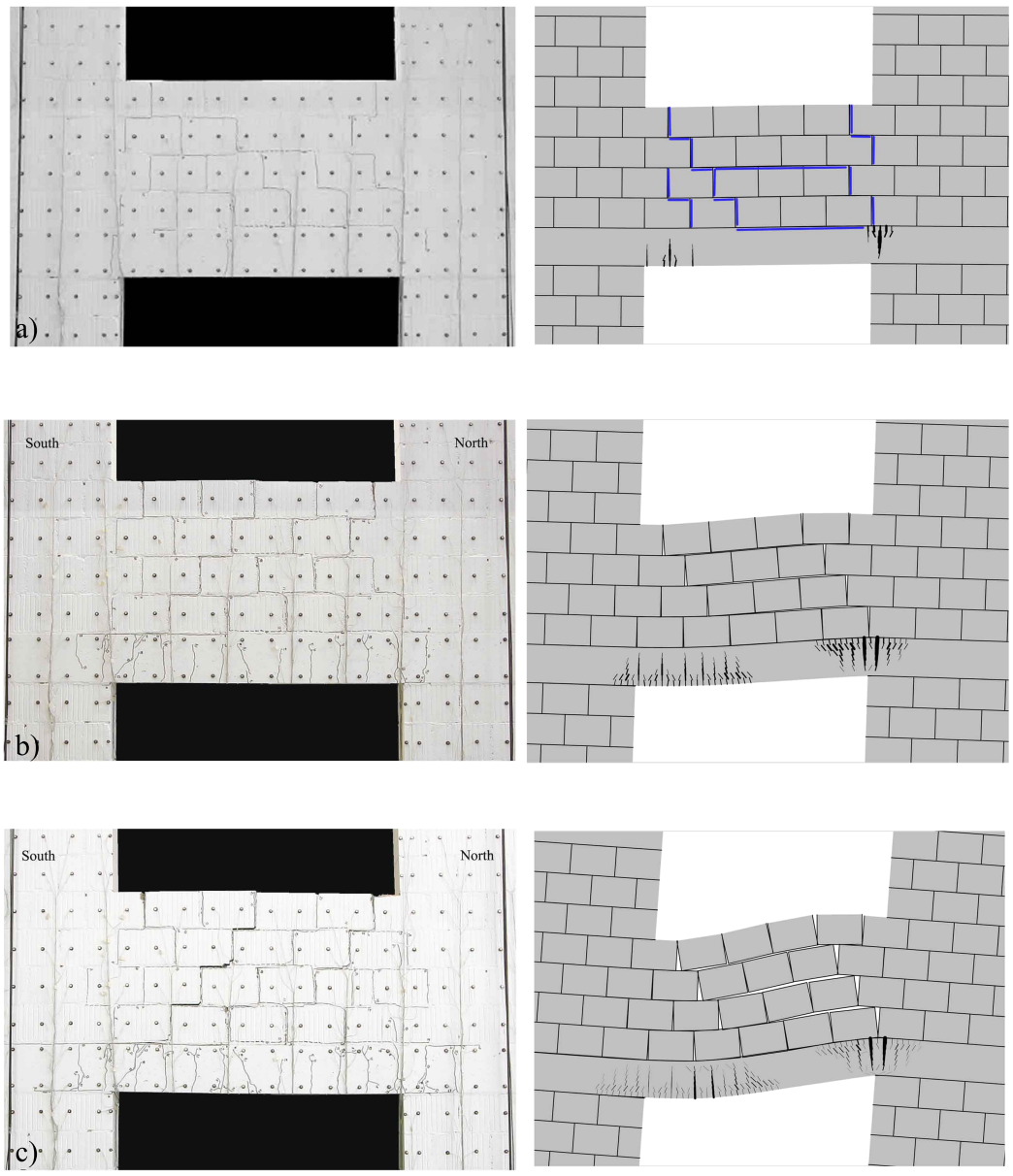


Figure 3.29: TU5 - Deformed shape comparison at a drift of a.0.1% (cracks patter in masonry highlighted in blu), b.0.4%, c.0.8%. Numerical model in Atena magnification factor of 10

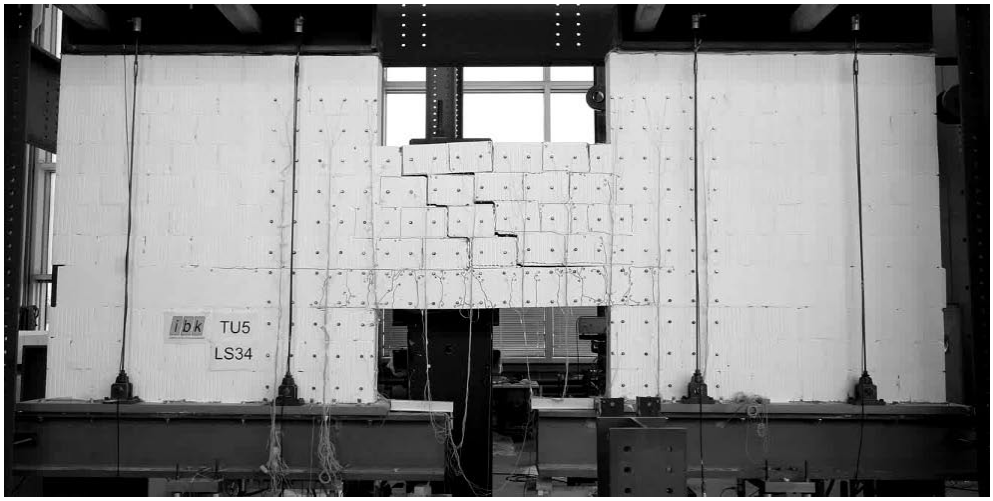


Figure 3.30: TU5 - Crack pattern of the concrete spandrel at LS 34. Drift towards North of 1%

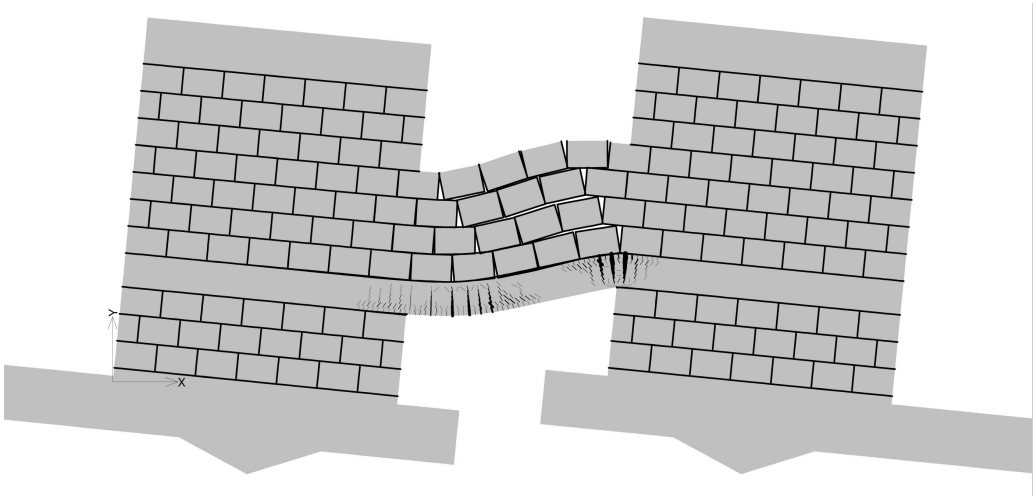

Figure 3.31: TU5 - Numerical model deformed shape for a drift of 1%.

### 3.2.2 Comparison of the local characteristics

In the previous section the global characteristics of the composite spandrel were studied. In this section, instead, the focus is on the local characteristics of the RC beam as its curvature and the width of the cracks that opened in the concrete. Those characteristics of the numerical model are compared with the one of TU2. The other test units are not compared because they were subjected to a cyclic loading, that influences characteristics as the cracks width, and also because for cyclic loading it is more difficulty to point out those local features from the experimental raw data.

#### Curvature of the RC beam

In order to compare the curvature in the experimental and numerical model local analysis were carried out.
This comparison has been done in correspondence of the two plastic hinges. The curvature has been evaluated considering the strains of the top and bottom four-node elements that form the RC beam, considering the following relationship:

$$\phi = \frac{\varepsilon_{sup} - \varepsilon_{inf}}{h_{RC} - h_{element}} \tag{3.1}$$

where:

$\varepsilon_{sup}$ Strain in horizontal direction of the top four-node element of RC beam;

$\varepsilon_{inf}$ Strain in horizontal direction of the bottom four-node element of RC beam;

$h_{RC}$ RC beam height;

$h_{element}$ four-node element height;

Strains, in fact, are evaluated in the centre of each four-node element, therefore it is necessary to not consider half height of each element, as shown in figure 3.32.

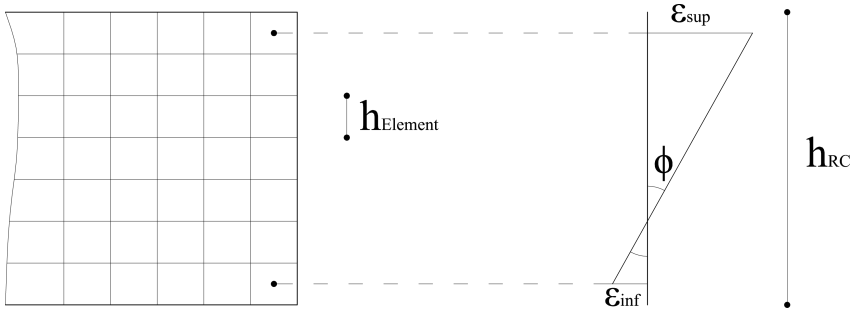


Figure 3.32: Curvature of the RC beam.

Where $h_{element} = h_{RC}/7$, therefore ($h_{RC}$-$h_{element}$) = 0.214 m.

In figures 3.33 and 3.34 the mesh patterns of the numerical model, where, in experimental test setup, the plastic hinges formed, are depicted. In blue are highlighted the elements with the biggest tensile strain, whereas in red the ones with the biggest compressive strain.
In the following tables the strain values in correspondence of those elements for drift values of 0.4%, 0.8% and 1.0% are summarized. With the average strain, the curvature values are then calculated. Those values are summarized in tables 3.15 and 3.19.


Figure 3.33: Mesh pattern in correspondence of negative plastic hinge.

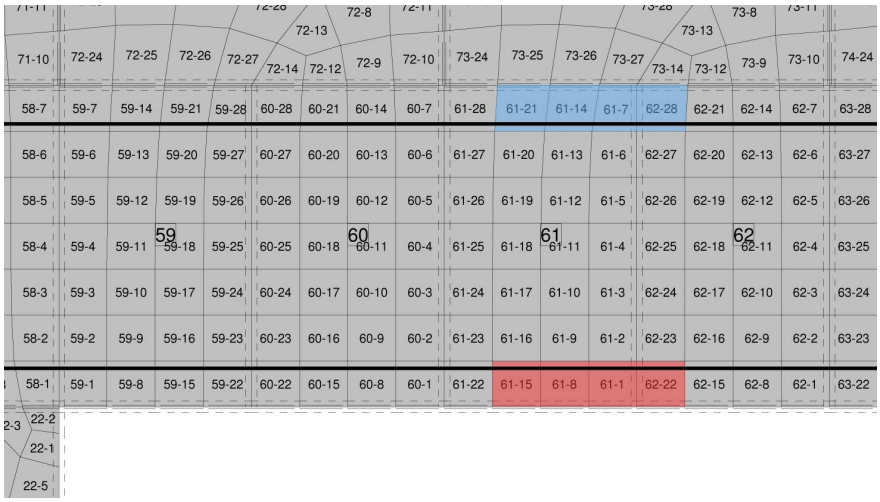


Figure 3.34: Mesh pattern in correspondence of positive plastic hinge.

**Negative Plastic hinge**

In tables 3.12, 3.13 and 3.14 the strain values of four node elements in correspondence of negative plastic hinge are summarised (for drift values of 0.4, 0.8 and 1%).

| Top Elements | Strain [-] | Bottom Elements | Strain [-] |
|---|---|---|---|
| 197-21 | 0.0026 | 197-15 | -0.0003 |
| 197-14 | 0.0027 | 197-8 | -0.0004 |
| 197-7 | 0.0025 | 197-1 | -0.0005 |
| 198-28 | 0.0028 | 198-22 | -0.0004 |
| Average strain | 0.0027 | Average strain | -0.0004 |

Table 3.12: Strains in correspondence of negative plastic hinge for a drift value of 0.4%

**Positive Plastic hinge**

In tables 3.16, 3.17 and 3.18 the strain values of four node elements in correspondence of negative plastic hinge are summarised (for drift values of 0.4, 0.8 and 1%).

| Top Elements | Strain [-] | Bottom Elements | Strain [-] |
|---|---|---|---|
| 197-21 | 0.0029 | 197-15 | -0.0004 |
| 197-14 | 0.0092 | 197-8 | -0.0005 |
| 197-7 | 0.0150 | 197-1 | -0.0007 |
| 198-28 | 0.0077 | 198-22 | -0.0005 |
| Average strain | 0.0087 | Average strain | -0.0005 |

Table 3.13: Strains in correspondence of negative plastic hinge for a drift value of 0.8%

| Top Elements | Strain [-] | Bottom Elements | Strain [-] |
|---|---|---|---|
| 197-21 | 0.0040 | 197-15 | -0.0004 |
| 197-14 | 0.0136 | 197-8 | -0.0006 |
| 197-7 | 0.0218 | 197-1 | -0.0008 |
| 198-28 | 0.0117 | 198-22 | -0.0005 |
| Average strain | 0.0128 | Average strain | -0.0006 |

Table 3.14: Strains in correspondence of negative plastic hinge for a drift value of 1%

| Drift | Curvature |
|---|---|
| 0.4% | 0.0145 $m^{-1}$ |
| 0.8% | 0.0430 $m^{-1}$ |
| 1% | 0.0626 $m^{-1}$ |

Table 3.15: Curvature values in correspondence of negative plastic hinge

| Top Elements | Strain [-] | Bottom Elements | Strain [-] |
|---|---|---|---|
| 61-21 | -0.0002 | 61-15 | 0.0016 |
| 61-14 | -0.0002 | 61-8 | 0.0018 |
| 61-7 | -0.0002 | 61-1 | 0.0018 |
| 62-28 | -0.0002 | 62-22 | 0.0018 |
| Average strain | -0.0002 | Average strain | 0.0018 |

Table 3.16: Strains in correspondence of positive plastic hinge for a drift value of 0.4%

| Top Elements | Strain [-] | Bottom Elements | Strain [-] |
|---|---|---|---|
| 61-21 | -0.0003 | 61-15 | 0.0020 |
| 61-14 | -0.0003 | 61-8 | 0.0023 |
| 61-7 | -0.0002 | 61-1 | 0.0024 |
| 62-28 | -0.0003 | 62-22 | 0.0025 |
| Average strain | -0.0003 | Average strain | 0.0023 |

Table 3.17: Strains in correspondence of positive plastic hinge for a drift value of 0.8%

| Top Elements | Strain [-] | Bottom Elements | Strain [-] |
|---|---|---|---|
| 61-21 | -0.0003 | 61-15 | 0.0021 |
| 61-14 | -0.0003 | 61-8 | 0.0024 |
| 61-7 | -0.0003 | 61-1 | 0.0025 |
| 62-28 | -0.0003 | 62-22 | 0.0026 |
| Average strain | -0.0003 | Average strain | 0.0024 |

Table 3.18: Strains in correspondence of positive plastic hinge for a drift value of 1%

| Drift | Curvature |
|---|---|
| 0.4% | 0.0093 $m^{-1}$ |
| 0.8% | 0.0121 $m^{-1}$ |
| 1% | 0.0127 $m^{-1}$ |

Table 3.19: Curvature values in correspondence of negative plastic hinge

In figure 3.35 the experimental curvature development of the RC beam through its length is depicted. In this graph, the dots represent the results obtained with the numerical model. It is possible to see that the development of the negative plastic hinge is well predicted, whereas the positive one not. The numerical model developed for TU2, in fact, shows a rocking behaviour (in the experiment it was possible to notice a mixed flexural/rocking behaviour). As a consequence the longitudinal reinforcements in correspondence of the positive plastic hinge are not yielded, and hence the curvature is strongly underestimated.
No comparison for a drift value of 2% has been done because after a drift value of 1%, in the experiment, bricks started to crush. Hence, since the bricks are modelled with an elastic behaviour, both global and local responses of the numerical models are probably not reliable.

### Cracks width in the RC beam

Local analysis are carried out in order to compare the cracks pattern developed in RC beam during the experiment and in the numerical models.

In table 3.20 the dimension of the widest crack for the most significant drift values is reported. As already said, after drift values of 1% the model is probably not able to predict well the behaviour of the structure, for this reason no comparison are done after that drift demand.

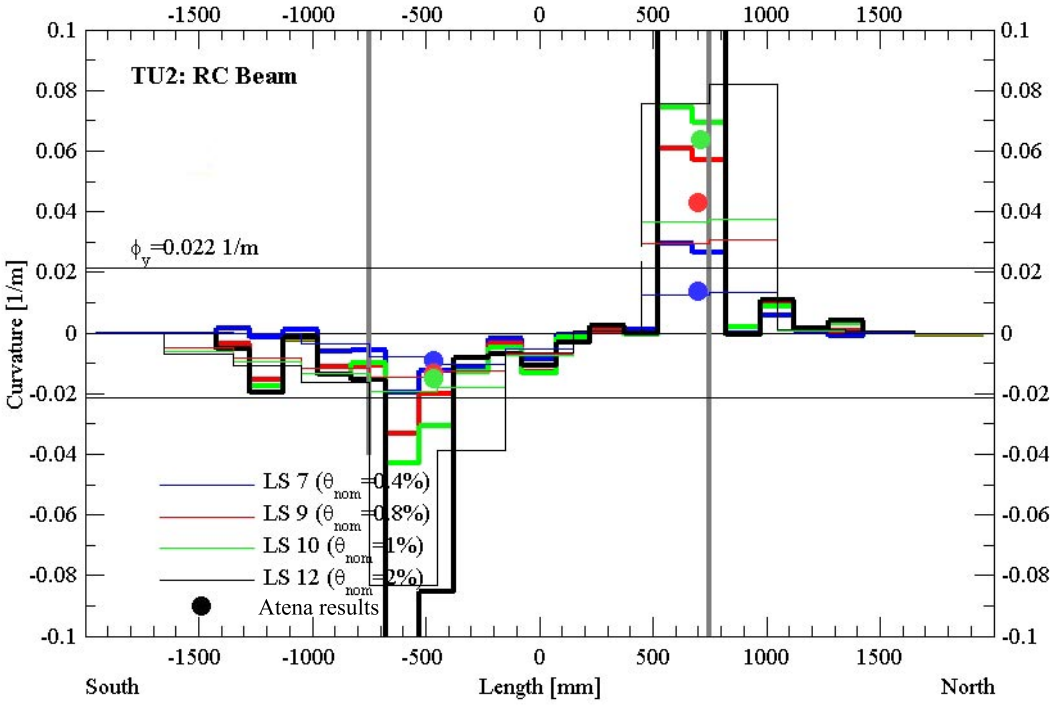


Figure 3.35: TU2: Curvature of the RC beam.

| Drift | Max crack width |
|---|---|
| 0.2% | 0.169 mm |
| 0.3% | 0.281 mm |
| 0.4% | 0.546 mm |
| 0.6% | 0.994 mm |
| 0.8% | 1.101 mm |
| 1.0% | 1.448 mm |

Table 3.20: Maximum crack width for different drift values

In figure 3.36 the dimension of the widest cracks, for different drift values, are plotted.
The purple dots represent the results obtained with the numerical model developed in ATENA for TU2. In order to evaluate the width of the cracks different techniques were used. The cracks width, in fact, was measured both with the LVDTs and the optical instrument described in the second chapter. Moreover, also manual measurement were carried out. These last measurements are probably the most reliable, because with the electronic tools it is necessary to define an average number of cracks per length. By means of manual measurements, instead, the width of the single cracks is measured.

In this case the numerical model was able to predict rather well what happened in the experiment. This is probably due to that the widest crack is located in the negative plastic hinge that is better described, in the numerical model, than the positive one.

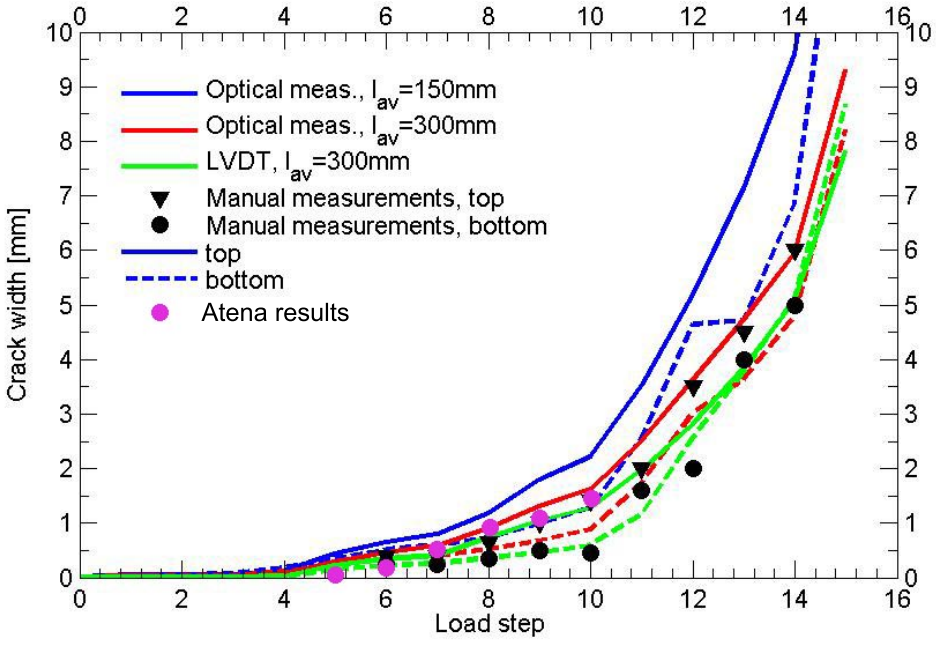


Figure 3.36: TU2: max cracks width in RC beam

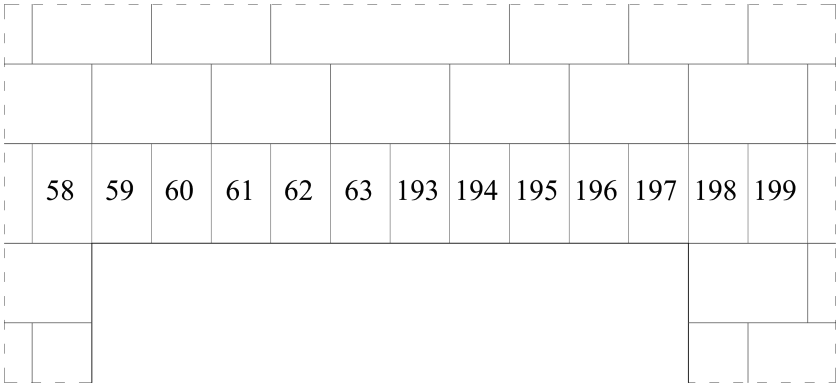


Figure 3.37: Atena model, numbers of the elements of the RC beam

| Element | Max crack width |
|---|---|
| 58 | 0.177 mm |
| 59 | 0.167 mm |
| 60 | 0.192 mm |
| 61 | 0.195 mm |
| 62 | 0.250 mm |
| 63 | 0.311 mm |
| 193 | 0.247 mm |
| 194 | — |
| 195 | 0.247 mm |
| 196 | 0.337 mm |
| 197 | 1.448 mm |
| 198 | 1.021 mm |
| 199 | 0.168 mm |

Table 3.21: Max crack width for each element that constitute the RC beam

In table 3.21 the widest crack for each element that constitutes the RC beam is reported. Those values refer to a drift of 1% that correspond of LS 10 of TU2.
In figure 3.21 the comparison between the measurement recorded during the test on TU2 and the result from ATENA model is shown.
As already said in the section where the curvature was compared, also in this case the numerical model predicts better the mechanical behaviour of the composite spandrel in correspondence of the negative plastic hinge. The positive plastic hinge does not form in the numerical model, therefore the cracks in the concrete resulted smaller and with a more uniform distribution.

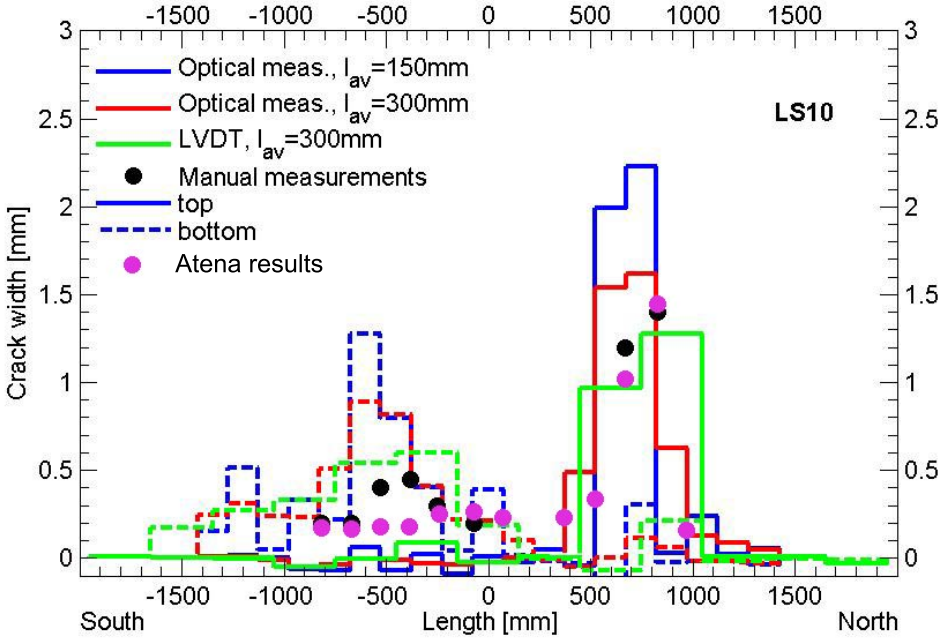


Figure 3.38: TU2: Cracks width in RC beam at LS 10

### 3.2.3 Model with smeared reinforcement in masonry

As already discussed in section 3.1.2, in ATENA it is not possible to define not-isotropic materials. This is not an insignificant problem. Masonry, in fact, has different behaviours in horizontal and vertical directions. In the model proposed in this thesis, two different materials are used, one for the bricks in the piers and one for the bricks that lie on the RC beam (section 3.1.2).
In the consulting forum of Cervenka web-site (http://www.cervenka.cz/), however, another way of modelling is also proposed. In this method it is first defined the E-modulus of weaker direction. Then it is added a smeared reinforcement layer in the stronger direction to represent the additional stiffness.

Therefore, in order to use this method, the values in table 3.22 are used. For all bricks in the model the E-modulus of masonry in the horizontal direction is applied. To represent the additional stiffness in vertical direction a smeared reinforcement with a linear behaviour is applied. The ratio of that reinforcement is rather low because the stiffness of it is very bigger than masonry one.

| | |
|---|---|
| $E_{masonry}$ | 1840 MPa |
| $E_{reinforcement}$ | 200000 MPa |
| ratio | 0.0173 |

Table 3.22: Mechanical properties used for the smeared reinforcement in the masonry

The positive aspect of this method is that there is not a clear (and rather arbitrary) differentiation in the mechanical behaviour of bricks in the piers and in the spandrel.
In figure 3.39 it is shown the comparison between the two models proposed. The blue line represents the model where two different materials are used to define the bricks. One for the bricks in the piers and one for the bricks of the spandrel. The red line represent the model with added the smeared reinforcement layer to the masonry.

As it is possible to observe there are not very relevant differences in the global behaviour. The model with the smeared reinforcement layer, however, shows more convergence problems, also for rather low drift demands. They are highlighted by the spikes of the curve.
For this reason, although there are rather arbitrary assumptions, the model with two different materials is used in this thesis.

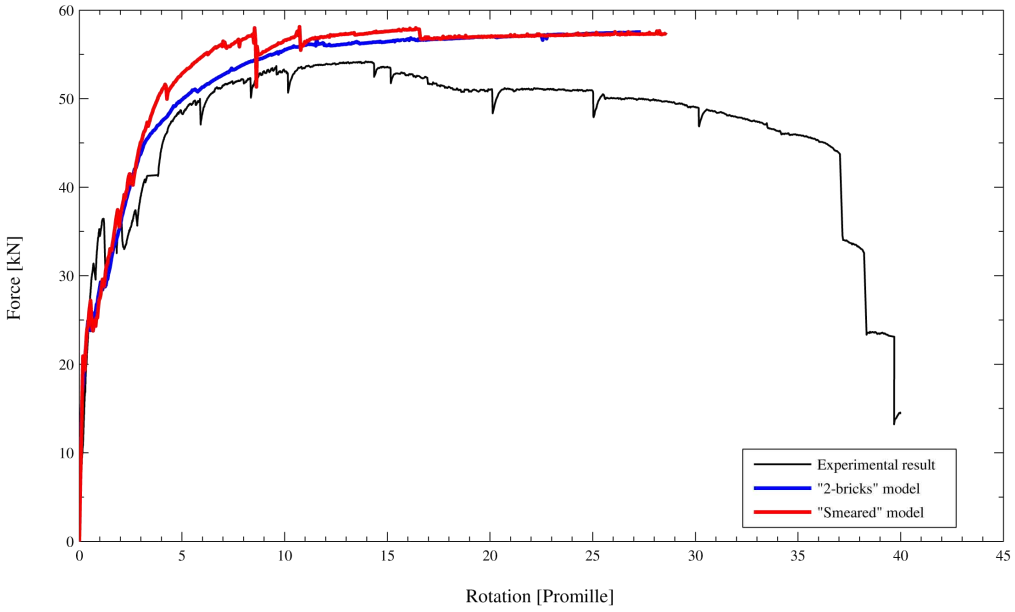


Figure 3.39: TU2 - Comparison of force-deformation curves obtained using two different types of bricks and with a smeared reinforcement layer in the masonry.

## 3.3 Composite spandrel numerical model: main features

In this section the main characteristics of the numerical model developed in ATENA are summarized.

The aim of that model is to reproduce as more faithfully as possible the test setup and the experiments carried out by professor Katrin Beyer at Swiss Federal Institute of Technology in Zurich.
However, this model has some limitations that do not allow a complete study of the mechanical behaviour of the composite spandrels. These limitations are here listed:

1. In Atena it is not possible to introduce not-isotropic elements. Masonry however, behave differently if loaded in vertical (as for piers) or horizontal (as for spandrels) direction. Therefore, in order to take into account this aspect:
    - For the bricks in the piers the vertical modulus of elasticity of masonry is used.
    - For the bricks in the spandrels the horizontal modulus of elasticity of masonry is used.
2. The bricks are modelled as elastic (the reasons are explained in section 3.1.2). As consequence of this:
    - The non-linearities are present only in the concrete of the RC beam and in the mortar joints (also the reinforcements have inelastic properties but they do not have an important influence in the general response).
    - With this model it is possible to approximate rather well:
        - the stiffness of the spandrel;
        - the shear capacity of the spandrel;
        - the deformed shape;

– the cracks pattern in the RC beam.

Yet, since it is not possible to detect the cracks and the subsequent failure of the bricks, it is not possible to evaluate post-peak response.

# Chapter 4

# Stiffness and shear strength of composite spandrels

In this chapter equations to evaluate the stiffness and the shear capacity of composite spandrel are proposed.

First of all, there is a brief overview of what it is proposed, in literature and by the codes, to evaluate the shear capacity of masonry coupling beams. Then, the main failure mechanisms recorded in the experimental campaign which are described in the second chapter are studied. It was shown that in the experiments, two main mechanism developed: the flexural and the rocking mechanism. For each failure mechanism, equations to evaluate the shear capacity are proposed.
Subsequently, the focus is pointed at the stiffness of composite spandrels. Two kinds of stiffness are studied. A first stiffness for very low drift demands, when cracks are not still open, and the composite spandrel has an almost elastic and linear behaviour. Then, it is studied the stiffness when cracks start to open and the first consequence is a reduction of spandrel stiffness.

The chapter ends with the comparison between the experimental results and the trilinear approximation obtained with the equations proposed.

## 4.1 Spandrel shear strength

The European code [CEN04b] provides that, in the structural model, masonry spandrels may be taken into account as coupling beams between two wall elements if: they are regularly bonded to the adjoining walls and connected both to the floor tie beam and to the lintel below. However, no equations to evaluate spandrels shear capacity are supplied.
In the Italian code [NTC08] (see section 7.8.2.2.4), there are some prescriptions in order to evaluate the shear capacity of masonry coupling elements, that are shown in next section. These equations, however, as already demonstrated in [DB11] and further confirmed by the analyses described in the fifth chapter of this thesis, do not reflect well the failure mechanism or the force capacity of composite spandrels elements. This may be due to that they are more oriented to masonry spandrel analysis, instead of composite spandrels. In those formulations, for instance, there are not any particular prescriptions to take into account the effect of an RC beam.

Concerning the composite spandrels, in [PCK07] is recommended, for the design of URM buildings, not to consider the contribution of masonry to increase the coupling between different walls. Hence it is suggested to consider the shear capacity only in function of RC beam flexural strength, as shown in equation 4.1.

$$V_{SP} = \frac{2M_{RC}}{L_{SP}} \tag{4.1}$$

The shear capacity supplied by equation 4.1 refers to the failure mechanism represented in figure 4.1, that, as said, does not consider the contribution of masonry in composite spandrel strength.

### 4.1.1 Masonry coupling beams shear strength in the Italian code NTC2008

The Italian code [NTC08] prescribes different procedures if there is axial load in the spandrel or not. If it is known the axial force in the spandrel, strength

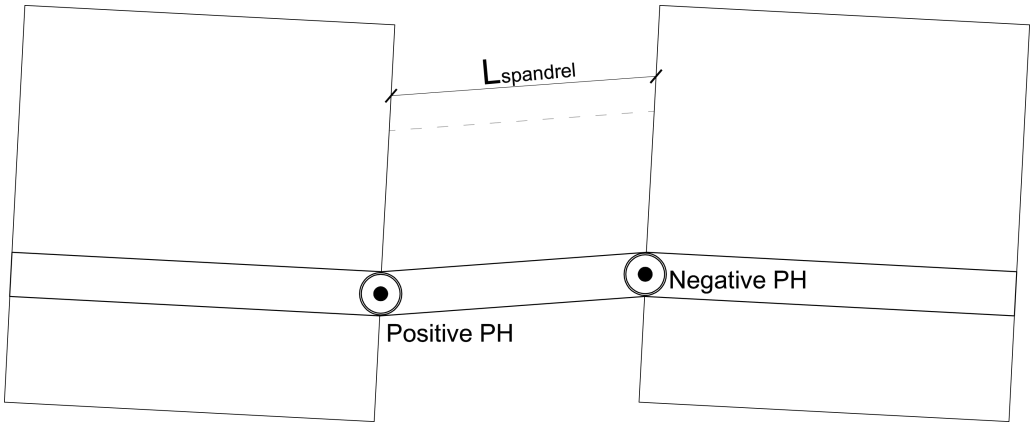


Figure 4.1: Flexural mechanism neglecting contribution of masonry spandrel

checks are required with the same equations used for the piers. If the axial force is not known, it is necessary to evaluate the spandrel shear and flexural strength. The code supplies the following equations that are possible to use if there is the presence of elements with also a tensile capacity (as tie or RC beam).

### Shear failure

The shear strength of coupling beams, considering a shear failure, can be assumed as:

$$V_s = h_{cp} t f_{vd0} \tag{4.2}$$

Where:

| | |
|---|---|
| $h_{cp}$ | spandrel height (it is not specified if consider or not the RC beam height); |
| $t$ | thickness of the coupling beam; |
| $f_{vd0}$ | shear design strength in absence of compression stress. |

### Flexural failure

The flexural capacity of a spandrel is defined in [NTC08] by next equation.

$$M_{u,cp} = H_p \frac{h}{2} [1 - \frac{H_p}{0.85 f_{hd} h t}] \tag{4.3}$$

Where:

| | |
|---|---|
| $M_{u,cp}$ | Coupling beam flexural strength |
| $H_p$ | minimum between beam tensile capacity and $0.4 f_{hd} ht$ |
| $f_{hd}$ | Masonry design compression strength in horizontal direction |

The shear strength associated to this failure mechanism is equal to:

$$V_f = \frac{2M_{u,cp}}{L_{SP}} \tag{4.4}$$

### 4.1.2 Composite spandrel failure mechanisms and equations proposed

The two equations proposed by the Italian code [NTC08] are related to spandrels failure modality. In fact, whereas it is possible to determine three failure mechanisms for piers, spandrels collapse typically occurs following two mechanisms: rocking and diagonal cracking. Sliding failure, in fact, cannot occur due to the interlocking phenomena originated at the interface between the end-sections of spandrels and the adjacent piers; crushing cannot occur given the very low axial forces acting [SR11].

In the experimental campaign described in the second chapter of this thesis, in the five composite spandrels there were both rocking and shear failures. It mainly depended by the stiffness and strength of the RC beam. In fact if the RC beam is very stiff and strong it deforms a little and a gap between it and the piers underneath forms. In figure 4.2 it is highlighted the gap that formed in TU4, in that test unit in fact the RC beam had a stronger longitudinal reinforcement than other ones.
In the red circle in figure 4.3, instead, the shear failure that occurred in the RC beam of TU3 is shown. The red arrow indicates the direction of the compressive strut developed in masonry. The red stair splits the part of masonry where this strut developed and the other part that resulted almost stressless.

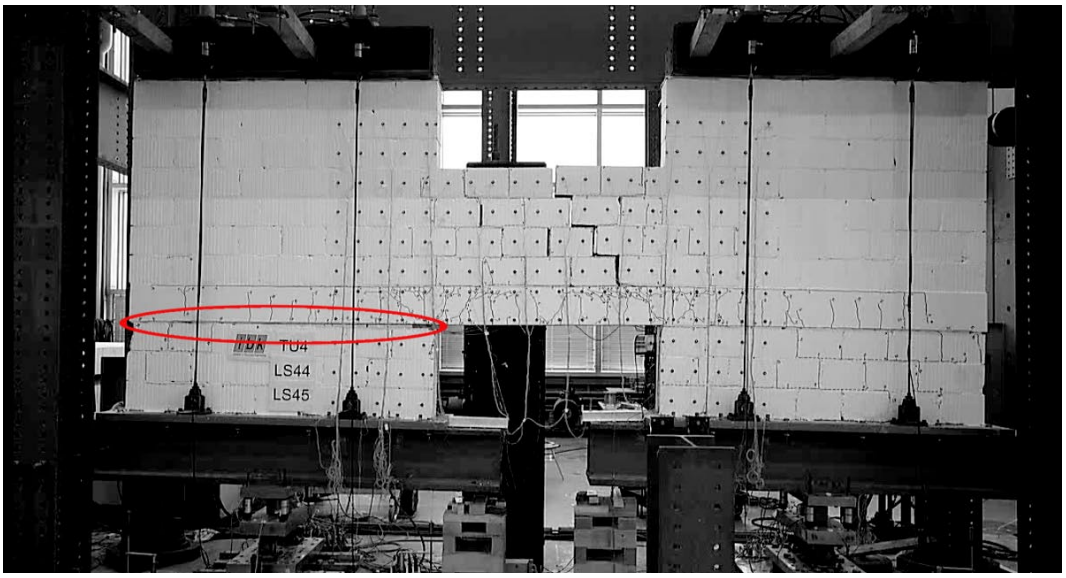


Figure 4.2: Rocking in TU4 (video frame)

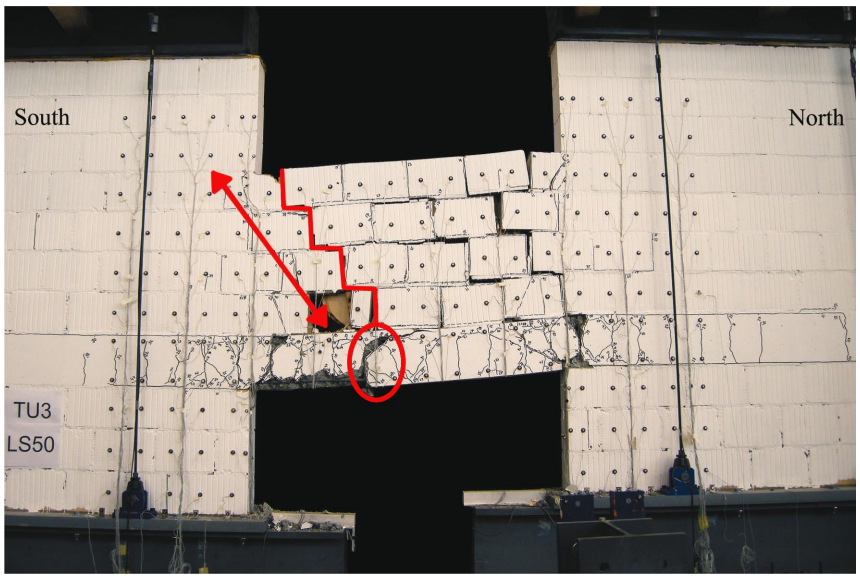


Figure 4.3: RC beam shear failure in TU3 (from [BAD10] p.106)

These two mechanisms trigger in different ways. If there is a rocking mechanism, usually only one plastic hinge forms and it is possible to determine the shear strength from a condition of equilibrium, while the shear failure is more related to the geometry of the spandrel and also of its bricks. These two different mechanisms were already studied in [DB11], where the following models for the prediction of the force capacity of composite spandrels were proposed.

$$V_{SP} = \frac{M_{pos} + M_{neg}}{L_{SP} - \frac{L_{bricks} h_{sp}}{2 h_{bricks}}} \tag{4.5}$$

Where:

| | |
|---|---|
| $M_{neg}$ | Nominal moment capacity for a negative bending |
| $M_{pos}$ | Nominal moment capacity for a positive bending |
| $L_{SP}$ | Spandrel length |
| $h_{SP}$ | Height of the masonry of composite spandrel |
| $L_{bricks}$ | Bricks length |
| $h_{bricks}$ | Bricks height |

$$V_{SP} = \frac{\frac{N_{pier} L_{pier}}{2} + M_{neg}}{L_{SP} + L_{pier}} \tag{4.6}$$

Where:

| | |
|---|---|
| $M_{neg}$ | Nominal moment capacity for a negative bending |
| $N_{pier}$ | Axial force in the piers |
| $L_{pier}$ | Piers length |
| $L_{SP}$ | Spandrel length |

In the following sub-sections the demonstrations of these formulations are shown and it is also shown a possible variation in the rocking mechanism formulation.

**Flexural mechanism**

If the RC beam is not enough stiff or strong two plastic hinges (a positive and a negative one) form in it. As already described in the previous section, the shear capacity of a coupling beam, due to a flexural failure can be evaluated with the equation 4.1 here reported:

$$V_f = \frac{2M_{RC}}{L_{SP}}$$

In this formulation the shear capacity is related to the formation of two plastic hinges, and that value is divided by the length of the spandrel. It is therefore neglected the contribution of the masonry, a scheme of this behaviour is described in figure 4.1. In the experiments, instead, it was possible to observe that the positive plastic hinge was not at the beginning of the spandrel but it shifted inside the free span of the spandrel, as shown in figure 4.4.

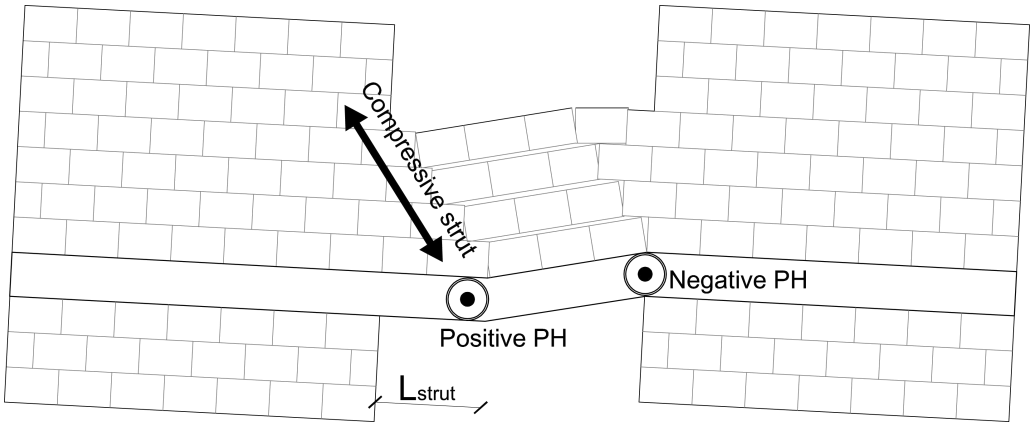


Figure 4.4: Flexural-shear mechanism

Considering the masonry contribution, the equation 4.4 can be re-written as:

$$V_f = \frac{2M_u}{L_{SP} - L_{strut}}$$

Where $L_{strut}$ is the distance of the positive plastic hinge from the edge of the

pier. Since in the masonry the joints are usually weaker than the bricks, it is supposed failure occurs in them. For this reason the distance between the plastic hinge and the pier is function of the bricks geometry (following the idea that the cracks follow the joints). So, if the compressive strut in the masonry starts in the top corner between the spandrel and the piers, since the bricks are staggered the cracks in the joints are stair-stepped, so it is possible to write:

$$L_{strut} = \frac{L_{bricks} n_{bricks}}{2}$$

Where $n_{bricks}$ is the number of bricks in the spandrel, and it is possible to write:

$$n_{bricks} = \frac{h_{spandrel}}{h_{bricks}}$$

Substituting all of these values in equation 4.7, it is possible to evaluate the shear capacity in a composite spandrel in case of flexural-shear failure.

$$V_{SP} = \frac{M_{pos} + M_{neg}}{L_{SP} - \frac{L_{bricks} h_{sp}}{2 h_{bricks}}} \tag{4.7}$$

Where:

| | |
|---|---|
| $M_{neg}$ | Nominal moment capacity for a negative bending |
| $M_{pos}$ | Nominal moment capacity for a positive bending |
| $L_{SP}$ | Spandrel length |
| $h_{SP}$ | Spandrel height |
| $L_{bricks}$ | Bricks length |
| $h_{bricks}$ | Bricks height |

### Rocking mechanism

Equation 4.6 refers to composite spandrel shear capacity if a rocking mechanism, as shown in figure 4.5, develops.

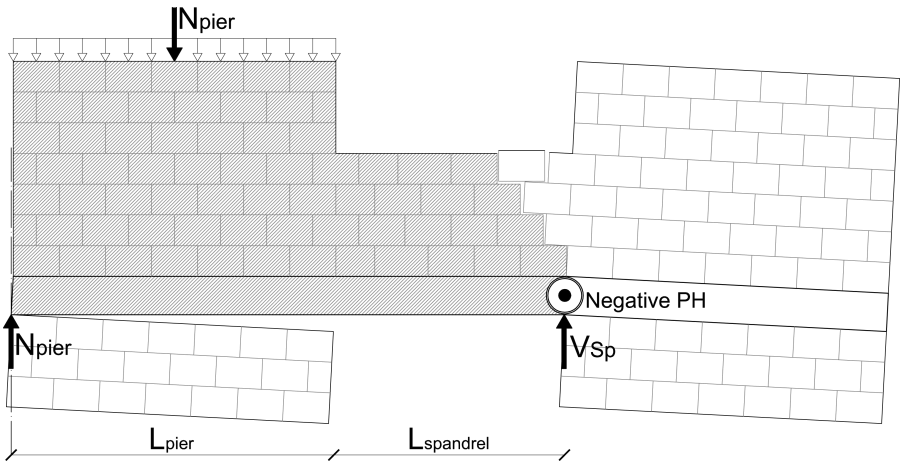


Figure 4.5: Rocking mechanism

To obtain the shear capacity of the composite spandrel it is necessary to impose balance of forces around the dash-dot axis. In the negative plastic hinge the nominal flexural capacity (see section 4.5) of the RC beam, in case of negative bending, develops. Therefore, the equation of equilibrium is:

$$V_{SP} \cdot (L_{pier} + L_{SP}) = N_{pier} \cdot L_{pier}/2 + M_{neg}$$

Dividing both terms by the quantity $(L_{pier} + L_{SP})$ it obtains equation 4.6.

In the mechanism above described, however, it is thought that the force produced by the pier underneath the RC beam is a punctual force. In other words, the pier is in contact with the RC beam in a single point. Physically this could not be possible, because it would mean that the stress in that point is infinite. Therefore a variation of the equation for the rocking mechanism is proposed herein.

As it was possible to see during the experimental campaign on the composite spandrel, a long crack often opened underneath the RC beam. That developed in a gap if a rocking mechanism triggered. That gap, of course, did not open thorough whole piers length, but it had its own extension. Hence, the total axial force in the piers went through the part without cracks underneath the RC beam. In figure 4.6 this mechanism is depicted.

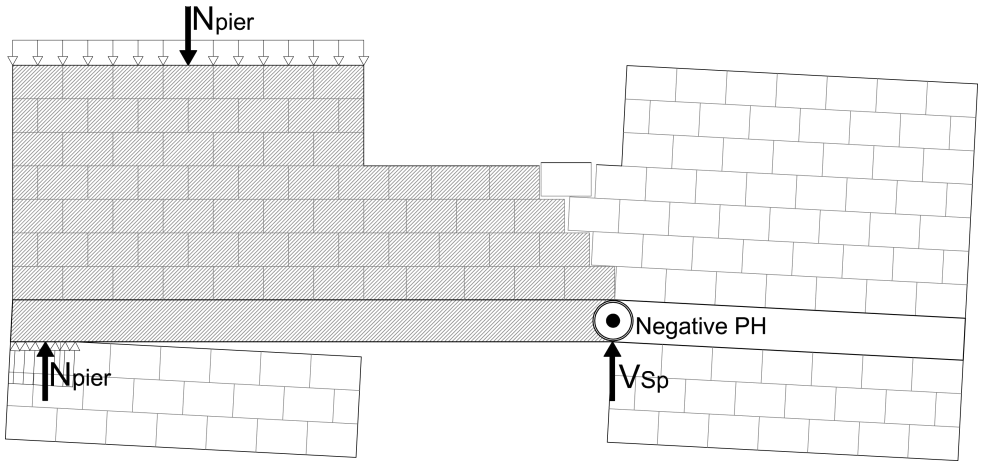


Figure 4.6: Rocking mechanism with a stress block distribution of tension

Also in that case, to evaluate the shear capacity it is necessary to impose the balance to the rotation considering the grey part of the spandrel in figure 4.6. All those forces go through the piers till the RC beam. In figure 4.7 is shown the rotation equilibrium of the forces around the dash-dot line. Solving the equation of equilibrium it is possible to determine the shear capacity in case of a rocking mechanism.

$$V_{SP} = \frac{\frac{N_{pier} L_{gap}}{2} + M_{neg}}{L_{SP} + \frac{L_{pier}}{2} + \frac{L_{gap}}{2}} \tag{4.8}$$

Where:

| | |
|---|---|
| $M_{neg}$ | Nominal moment capacity for a negative bending |
| $N_{pier}$ | Axial force in the piers |
| $L_{gap}$ | Length of the gap between the RC beam and the pier underneath |
| $L_{pier}$ | Piers length |
| $L_{SP}$ | Spandrel length |

For the sake of clarity all the passages to get equation 4.8 are here detailed.

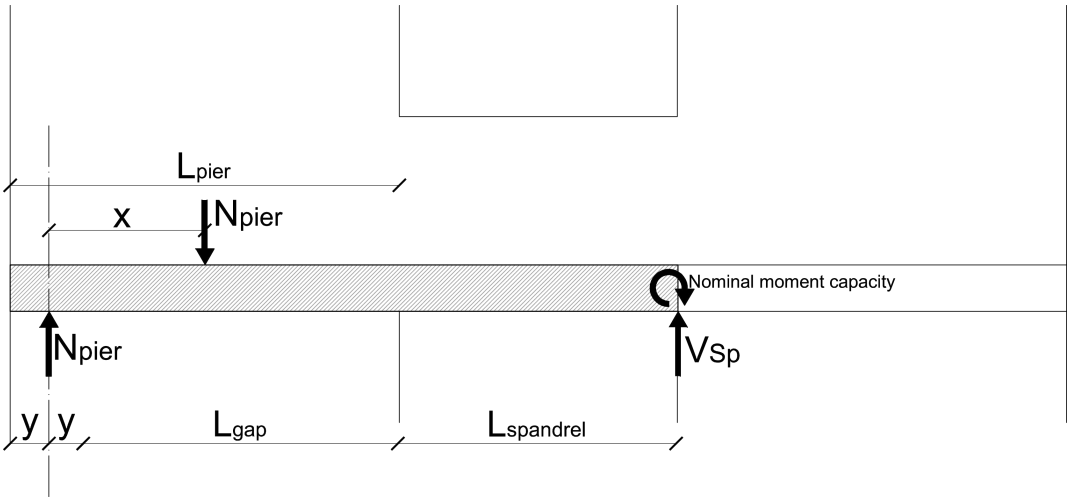


Figure 4.7: Forces equilibrium in case of stress block distribution of tension

The equation of equilibrium is:

$$V_{SP} \cdot (L_{SP} + L_{pier} - y) = N_{pier} \cdot x + M_{neg} \tag{4.9}$$

In figure 4.7 the quantities x and y are defined as:

$$2y = L_{pier} - L_{gap}$$

$$x = \frac{L_{pier}}{2} - y = \frac{L_{pier}}{2} - \frac{L_{pier}}{2} + \frac{L_{gap}}{2} = \frac{L_{gap}}{2}$$

Substituting those quantities in equation 4.9:

$$V_{SP} \cdot (L_{SP} + L_{pier} - \frac{L_{pier} - L_{gap}}{2}) = N_{pier} \frac{L_{gap}}{2} + M_{neg} \tag{4.10}$$

Dividing both terms by the quantity $(L_{SP} + L_{pier}/2 + L_{gap}/2)$ it obtains equation 4.8.

Since there are not experimental data to study the extension of this gap, here this is determined with equilibrium considerations (figure 4.8).

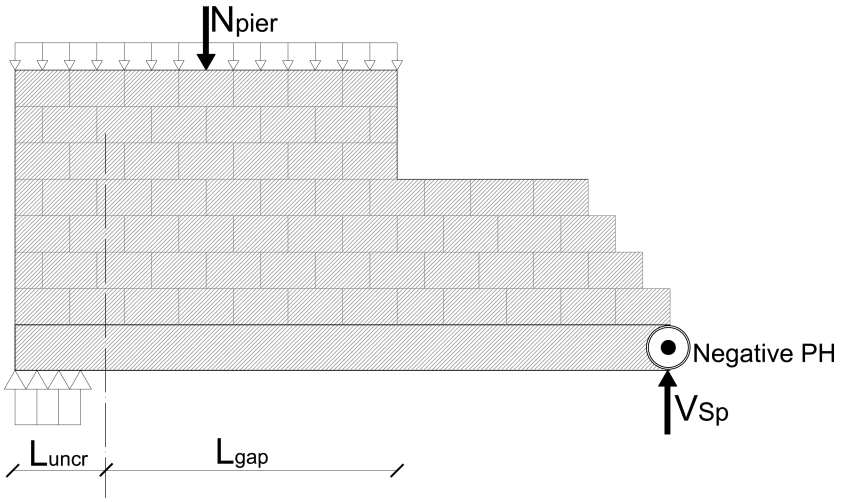


Figure 4.8: Extension of the gap underneath the RC beam

A stress block distribution of tension it is thought that acts underneath the RC beam. Under this hypothesis the tensions act for a length of 0.8 times the part uncracked ($L_{uncr}$):

$$L_{uncr} = \frac{1}{0.8} \frac{\sigma_{pier}}{f_{mx}} L_{pier}$$

Therefore the length of the gap is:

$$L_{gap} = L_{pier} - L_{uncr} = L_{pier}(1 - \frac{\sigma_{pier}}{0.8 f_{mx}})$$

Where $\sigma_{pier}$ is the axial stress in the pier and $f_{mx}$ is the compressive strength of the masonry in vertical direction.

## 4.2 Elastic stiffness of beams deformable for shear and bending

Using an equivalent frame model approach for the design/assessment of masonry walls, piers and spandrels are modelled as equivalent mono-dimensional elements (i.e. beams). Therefore it is necessary to find some equations which allow to determine the stiffness of the spandrels, considering them as beams. It has been noticed that for very loft drift demands the spandrels has an almost elastic and linear behaviour. Hence, in this section, it is reported what is present in literature on the stiffness of a beam that behaves in the elastic field.

The general definition of stiffness is the force required to obtain in a certain section a movement (rotation or displacement) equal to one [Poz72].
These movements are caused by the deformations due to the presence of forces acting in the beam. If a beam has an in-plane behaviour the forces that acts in it are three: axial force, shear and bending moment. In the spandrels, usually, there is not a relevant axial load, therefore the axial deformations are negligible. Furthermore, RC or steel beams are rather slender, and a consequence of this is that the deformation due to the presence of shear are negligible respect the flexural ones. However, spandrels are squat elements, therefore the shear deformations are not negligible, and it is hence necessary to calculate the deformations due to the bending moment and shear.
Since for each deformation there is a consequent movement, it is possible to define a flexural and a shear stiffness. The total stiffness of a beam element deformable for shear and bending depends from both stiffness as shown in next sections.

### 4.2.1 Elastic field: effect of the bending moment

In this section the elastic flexural stiffness of composite spandrels is studied. Made the assumption of equal rotation of the two piers [BD12], there is not relative rotation between the two end sections of the spandrels, as it is shown in figure 4.9.

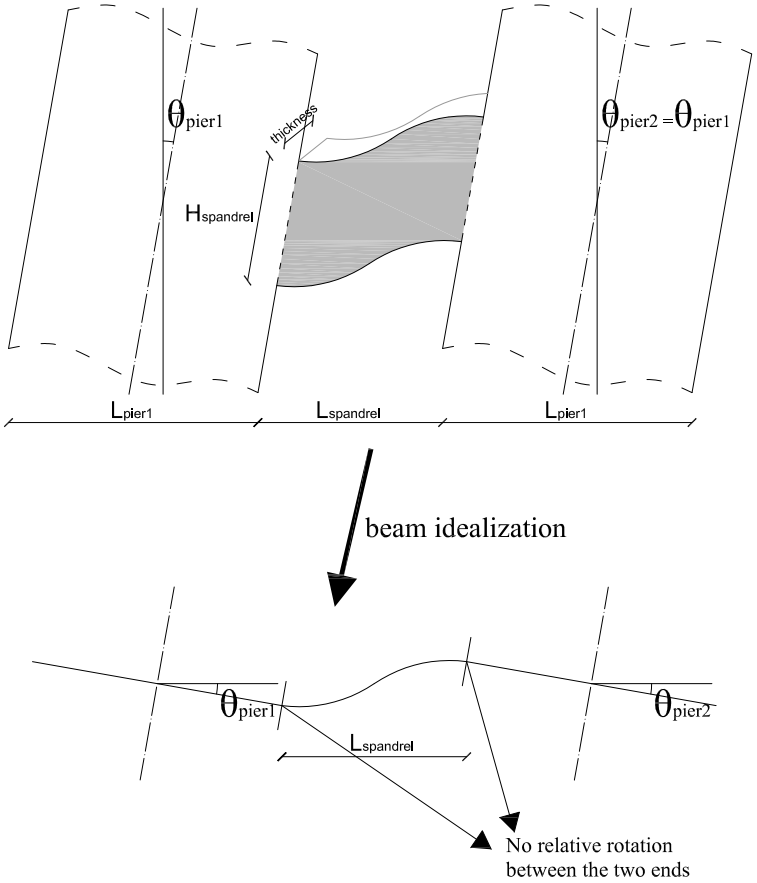


Figure 4.9: Piers rotation

With this assumption the spandrel can be studied like a double fixed beam:

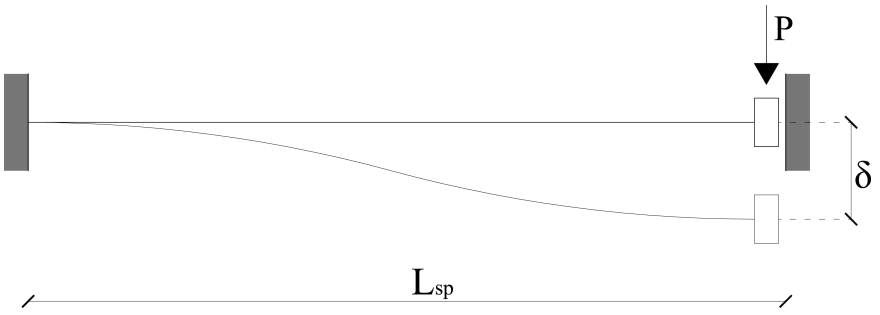


Figure 4.10: Deformed shape of a double fixed beam

The displacement caused by the load P is known and it is equal to:

$$\delta = \frac{PL_{sp}^3}{12EI} \tag{4.11}$$

Where E is the modulus of the elasticity of the material of the beam, I the moment of inertia of the cross section of the beam.

### 4.2.2 Elastic field: effect of the shear

In figure 4.11 the deformed shape of a "shear beam" is shown. The words "shear beam" refer to a beam enough squat for which the flexural deformations are small in comparison with the shear ones. For a shear beam subjected to a load P, the probably most important feature is the average drift $\theta$. The drift indicates the ratio between the displacement of the top of the beam and its height. The average drift of a squat beam, in the elastic field, is known [Vio92b], and it is equal to:

$$\theta = \chi \frac{P}{GA} \tag{4.12}$$

Where G is the shear modulus of the material, A the area of the gross cross

section of the beam and $\chi$ is the shear factor ($\chi$=1.2 for a rectangular section). As said, the displacement of a point at the top of the beam is equal to the drift times spandrels length:

$$\delta = \theta L_{sp} = \frac{PL_{sp}}{GA'} \tag{4.13}$$

Where $A'$ is the spandrels area including the shear factor ($A'$=A/$\chi$)

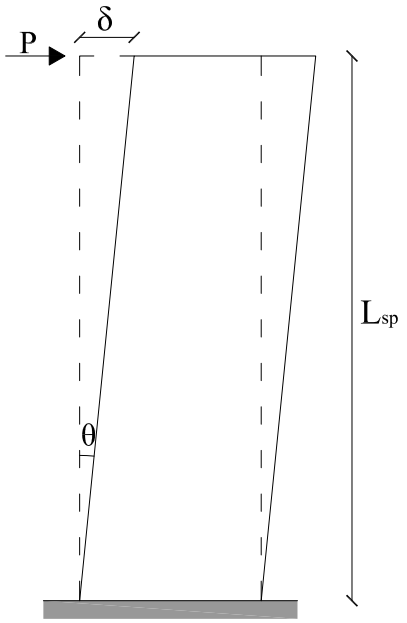


Figure 4.11: Shear deformation

### 4.2.3 Total elastic stiffness

As it is shown in previous sections for a beam with length $L_{sp}$ it is possible to write:

$$\delta = \frac{PL_{sp}^3}{12EI} + \frac{PL_{sp}}{GA'} \tag{4.14}$$

To find the stiffness value it is necessary to match the expression 4.14 equal to one:

$$P = K_{tot} = \frac{1}{\frac{L_{sp}^3}{12EI} + \frac{L_{sp}}{GA'}} \tag{4.15}$$

The two terms in the denominator are the inverse of the flexural ($K_f$) and shear ($K_s$) stiffness for a beam. Those quantities, in fact, are known from the literature. For a beam with length L, modulus of elasticity E, shear modulus G and area of the cross section A they are defined as:

$$K_f = \frac{12EI}{L^3}; K_s = \frac{GA'}{L}$$

Therefore it is possible to write equation 4.15 as:

$$K_{tot} = \frac{1}{K_f^{-1} + K_s^{-1}} = (K_f^{-1} + K_s^{-1})^{-1} \tag{4.16}$$

The equation 4.16 allows to obtain the stiffness of a beam from the values of the flexural stiffness $K_f$ and the shear stiffness $K_s$. In this way it is possible to consider beam shear and flexural capacity.

## 4.3 Displacement demand of composite spandrels

The "spandrel displacement" is the quantity bounded by blue arrows in figure 4.12. This is the equivalent of the displacement $\delta$ of the beam in figures 4.10 and 4.11. This is an useful parameter in order to carry on pushover analyses. In fact, they are usually based on relationships between the force and the consequent displacement of the load bearing elements. A definition of the spandrel displacement was already given in [BD12].

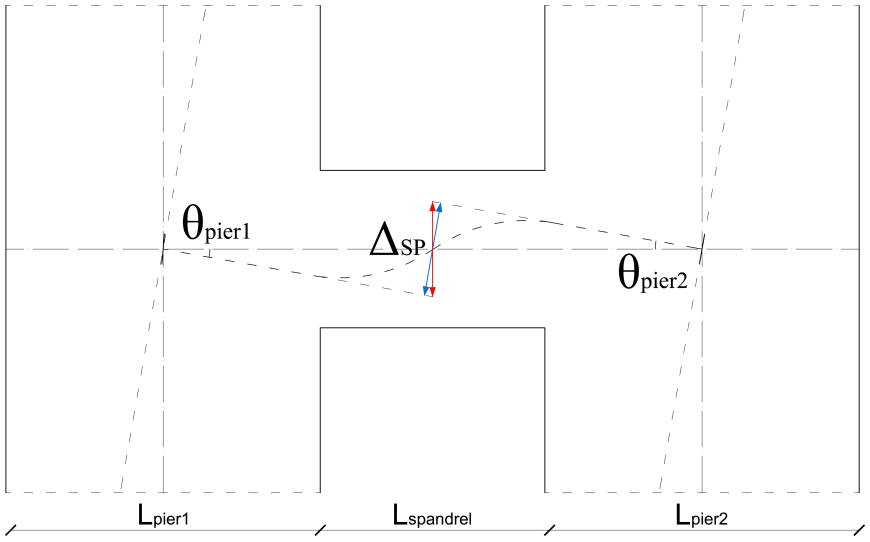


Figure 4.12: Displacement demand in the composite spandrel

Under the hypothesis of little displacements, the quantity described by the blue arrows is practically the same of the one described by the red arrows. This last quantity is equal to:

$$\Delta_{SP} = \theta_{pier,1}\frac{L_{SP} + L_{pier,1}}{2} + \theta_{pier,2}\frac{L_{SP} + L_{pier,2}}{2} \tag{4.17}$$

If the two piers have same length and present same rotation, equation 4.17 could be reduced to:

$$\Delta_{SP} = \theta_{pier}(L_{SP} + L_{pier}) \tag{4.18}$$

## 4.4 Composite spandrels initial stiffness

In this thesis, a first elastic stiffness and a cracked stiffness are studied. The reason of this choice is explained herein. In the experiments described in the second chapter it is possible to point out that first cracks appear between drift values of 0.05% and 0.1%. Hence, up to that drift value the mechanical behaviour of the composite spandrel is approximately elastic and linear. Furthermore, when first cracks appeared, half of the shear capacity was already exploited.
For this reason, it is thought to consider two kinds of stiffness. A first "initial stiffness" up to half of the shear capacity of the composite spandrel and a "cracked stiffness" until the peak strength is reached.
In section 4.2 it is detailed the general procedure to evaluate the elastic stiffness of a beam. Here, when the composite spandrel works in an elastic field, the flexural and the shear stiffness are evaluated as described in that section.
To calculate the flexural stiffness only the contribution of the RC beam is considered, whereas it is thought that only the masonry gives contribution to the shear stiffness. The equation 4.19 define the initial shear stiffness of the composite spandrel:

$$K_{s,in} = \frac{G_{m,hor} A_m}{1.2 L_{SP}} \tag{4.19}$$

where:

| | |
|---|---|
| $K_{s,in}$ | Initial shear stiffness of the composite spandrel |
| $G_{m,hor}$ | Shear modulus of the masonry in horizontal direction |
| $A_m$ | Area of the gross section of the masonry |
| $L_{SP}$ | Length of the spandrel |

The shear modulus of the masonry is considered as 0.4 the modulus of elasticity, as foreseen by the Italian code. The modulus of elasticity could be determined experimentally or by means of the compression strength of masonry [NTC08]. It has been thought to use the shear modulus in the horizontal

direction because, as already said, the bricks in the spandrel are subjected to a force that is oriented in a different direction respect to the piers.
Equation 4.20 defines the initial flexural stiffness of a composite spandrel:

$$K_{f,in} = \frac{12 E_c I_c}{L_{SP}^3} \tag{4.20}$$

where:

| | |
|---|---|
| $K_{f,in}$ | Initial flexural stiffness of the composite spandrel |
| $E_c$ | Modulus of elasticity of the concrete |
| $I_c$ | Inertia modulus of the gross section of the RC beam |
| $L_{SP}$ | Length of the spandrel |

In order to evaluate the flexural stiffness, it has been thought to consider only the contribution of the RC beam for a number of reasons herein reported.
In figure 4.13 the force-displacement relationship of TU2 and the corresponding Atena model, up to a displacement demand of 2 mm, is shown.
As it is possible to see, up to a displacement demand of 0.5 mm (that correspond to a very low drift demand, little more than 1 promille) the stiffness obtained from the numerical model is higher than the experimental one. After that displacement, instead, stiffness starts to decrease and it is also lower than what recorded in the experiment.
The reason of this behaviour can be explained with figures 4.14 and 4.15.

Figure 4.14 shows the distribution of strains in horizontal direction, for the sixth load step in Atena model. As it is possible to see, this distribution is as it is expected for a composite beam subjected to a bending moment. In the part of the spandrel subjected to a positive bending, the elements at the top of the masonry are compressed and the elements at the bottom of the RC beam are in tension. Vice versa for the case of negative bending. Already for the eighth load step (figure 4.15), instead, it does not seem that the composite spandrel work as a composite beam anymore. In fact, there is not a linear distribution of strains but through the height of the spandrel it is possible to see both compressed and tense elements.

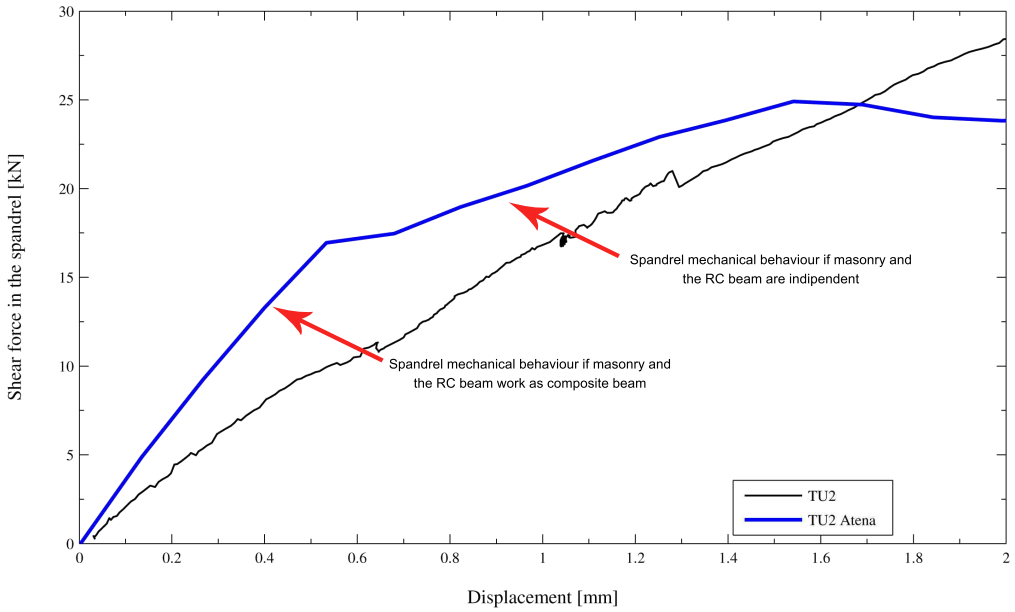


Figure 4.13: TU2: Force - displacement relationship up to a displacement demand of 2 mm

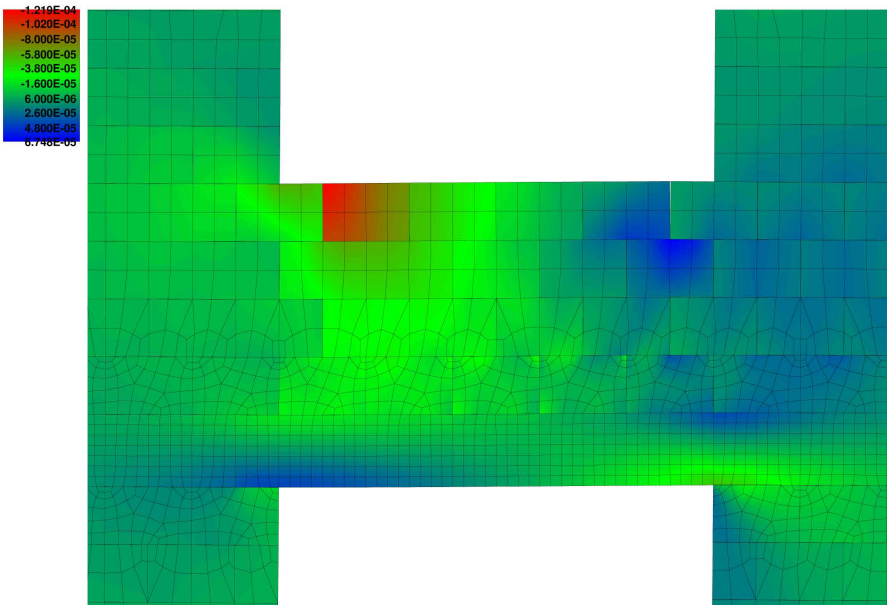


Figure 4.14: Strains in horizontal direction corresponding to the load step 6 of the numerical analysis. Deformed shape magnification factor of 10.

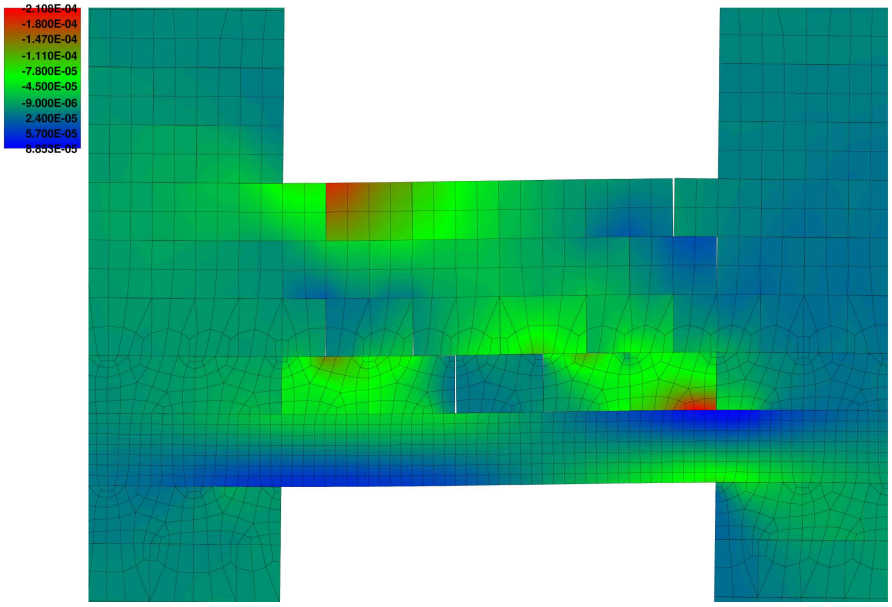


Figure 4.15: Strains in horizontal direction corresponding to the load step 8 of the numerical analysis. Deformed shape magnification factor of 10.

In the experiment, instead, it seems that up to a displacement demand of 2 mm there are not significant drops in spandrel stiffness, and maybe it means that the spandrel, in that range, works as a composite beam (in fact no cracks were located in the mortar joints yet). The experimental stiffness, however, is lower than the initial one recorded with Atena model.
This may be due to several reasons. First, the spandrel behaviour is not likely as a perfect double fixed beam, but there are some relative rotations between the two ends of it. Then, in the specimen, there could some deformations not taken into account in the numerical model. These deformation could be for instance in the mortar joints (that in the numerical model are rather stiff) or there could also be shear deformations in the piers. The reason of those shear deformation is explained hereinafter.

For all the reasons above listed, it was preferred to consider the flexural contribution of the RC beam only.

As just said, it is possible to do a consideration on the elements subjected to shear deformations. In equation 4.19, only the spandrel is considered subjected to shear deformations, in fact the shear stiffness is considered function of the length of the spandrel. This follows the idea that the nodes between piers and spandrels (grey zones in figure 4.16) are rigid and stiff. However, it is likely that also the nodes are subjected to shear deformations. In that case, in the equation 4.21, it is necessary to consider the length of the piers subjected to shear deformations.
In this equation $L_{Pier,sd}$ is the length of the pier, in the node between pier and spandrel, that is subjected to shear deformations.

$$K_{s,el} = \frac{G_{m,hor} A_m}{1.2(L_{SP} + L_{Pier,sd})} \tag{4.21}$$

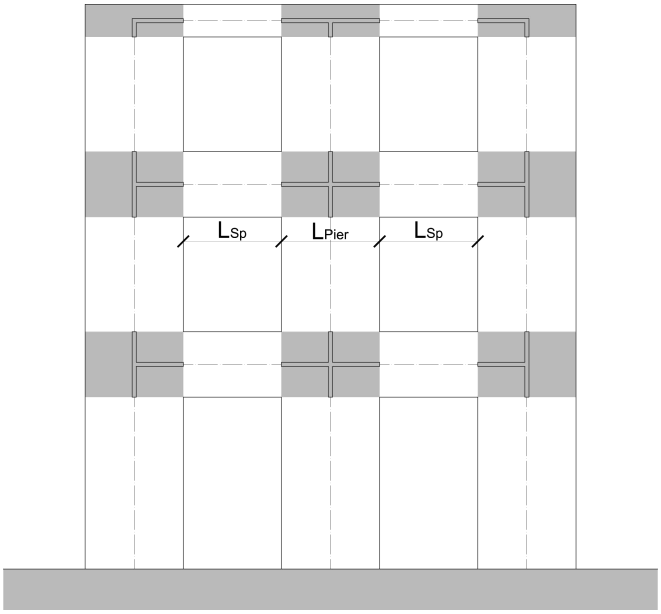


Figure 4.16: Equivalent frame idealization of a masonry wall and node zones.

In figure 4.17 the force-displacement relationship up to a displacement of 1.8 mm (that corresponds to a drift demand of 0.05%) is plotted. In that figure, it is possible to see the differences in stiffness considering the three different values of $L_{Pier,sd}$.

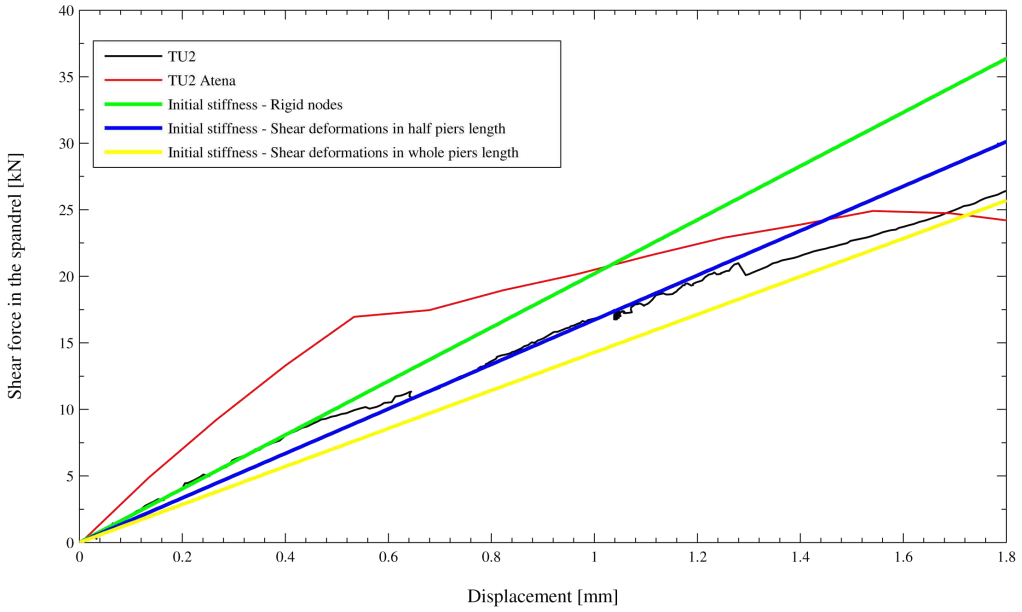


Figure 4.17: Composite spandrel initial stiffness: effect of the shear deformation of the nodes in the force-deformation relationship

The green line represents the case of rigid node, the presence of shear deformations in only half the length of the pier, instead, is represented by the blue line. Finally, the yellow line represent the case where the whole node between pier and spandrel is subjected to shear deformations. As it is possible to observe, there are not very relevant differences. The case that is probably the closest to the very initial stiffness of the composite spandrel is the first, whereas the third seems that, in the average, approximates better the experimental behaviour.
However, since no experimental data are available on this argument, in this thesis, it is preferred not to choose arbitrarily the length of the nodes that is subjected to the shear deformations. Therefore, the nodes are still considered as stiff.

## 4.5 Cracked stiffness of RC beams and masonry piers

When cracks start to open in the concrete or in the mortar joints the stiffness starts to decrease. This is because only part of the gross section of the elements that constitute the spandrel is still load bearing.
Both in Italian and European codes there are prescription to consider the effect of cracks. In particular, in [CEN04b] is defined that in the absence of an accurate evaluation of the stiffness properties, substantiated by rational analyses, the cracked bending and shear stiffness may be taken as one half of the gross section uncracked elastic stiffness.
This reduction of the fifty per cent, however, may give problems of accuracy, in fact it does not take into account the effective part of the section that is cracked and neither the influence of flexural reinforcement ratio. In next section a more detailed method, proposed by researchers, to evaluate the stiffness of RC beams is described.

A study of the effect of the presence of cracks in masonry piers is in [FMMC09] and it is discussed in section 4.5.2.

### 4.5.1 Cracked stiffness of an RC beam

A procedure to determine the stiffness of a RC beam taking into account the cracks in the concrete and the flexural reinforcement ratio is detailed in [Pri03] and in [PCK07], here the main features are briefly reported.
The starting point of this procedure is the moment-curvature relationship. The link between the bending moment M and the curvature $\phi$, in a beam, is known, as described by the equation:

$$EI = \frac{M}{\phi} \tag{4.22}$$

Figure 4.18 shows a typical moment-curvature relationship for an RC beam and a bilinear approximation. Hence, the stiffness of an RC beam is considered as the slope of the first part of the bilinear approximation. It has become accepted by the research community that the most appropriate

linearization of moment-curvature relationships is by an initial elastic segment passing through "first yield", and extrapolated to the nominal flexural strength, $M_N$, and a postyield segment connected to the ultimate strength and curvature [Pri03].

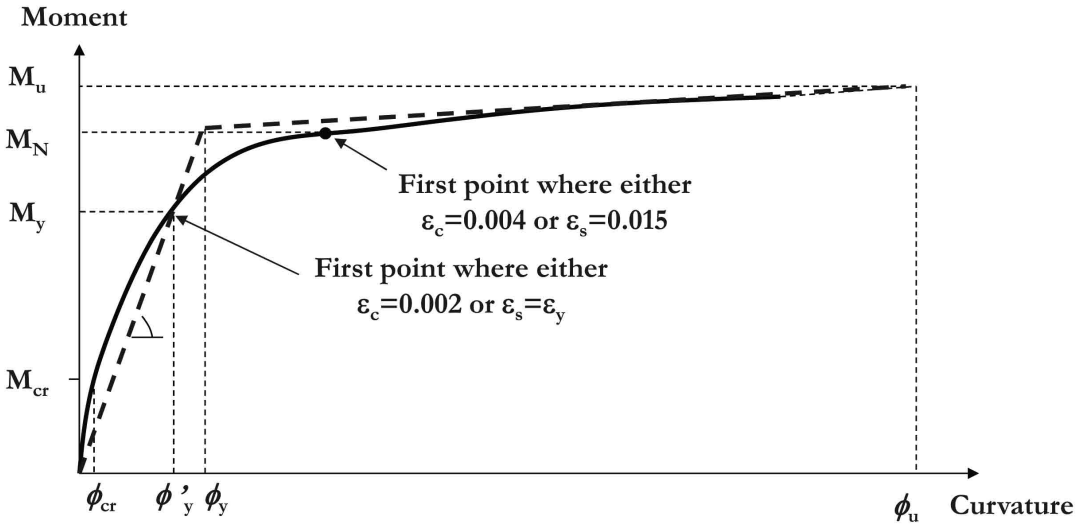


Figure 4.18: Moment-Curvature relationship and bilinear approximation for a RC beam (from [Sul13])

In [Pri03] the definitions of first yield and the nominal flexural strength are also given. The first yield of a section is defined as the moment, My and curvature $\phi'_y$ when the section first attains the reinforcement tensile yield strain of $\varepsilon_s = f_y/E_s$ , or the concrete extreme compression fibre attains a strain of 0.002, whichever occurs first.
The nominal flexural strength $M_N$ develops when the extreme compression fibre strain reaches 0.004, or the reinforcement tension strain reaches 0.015, whichever occurs first.
Therefore, the equation to determine the stiffness of a RC beam is:

$$(EI)_{cr} = \frac{M_N}{\phi_y} \tag{4.23}$$

In [Pri03] this stiffness is still defined as elastic stiffness. However, since this relationship takes into account the effect of the cracks, here it is preferred to name this as cracked stiffness, in order to distinguish it clearly from the

initial stiffness discussed in section 4.4.
In conclusion, to determine the stiffness of an RC beam taking into account the presence of cracks it is necessary first to calculate the nominal flexural strength for the two cases: (i) when in the cross section the extreme compression fibre reaches the strain of 0.004, (ii) when the reinforcement tension strain reaches 0.015. For each of the two cases, the strain profile (assumed to be linear) is known, because it is necessary to ensure a balance to the rotation of the cross section. The yielding curvature will be the lowest of the two cases.

### 4.5.2 Cracked stiffness of a masonry pier

During the experimental campaign it was possible to observe that after a drift demand of 0.05% or not more than 0.1% the mortar joints in the masonry of the spandrel were already cracked. The presence of cracks clearly influences also the stiffness of the masonry and it is not possible to consider the stiffness of the gross section anymore. A in depth study of this problem is in [FMMC09], where numerous experiments on masonry piers specimen are considered and studied in detail. This study allows to get a better evaluation, for the effective cracked stiffness, at least for the piers.
One of the results of this study is that the cracked stiffness of a masonry pier is approximately the forty per cent of the stiffness considering the gross section.
In that report no spandrel specimens were studied. In this thesis, however, is still used the reduction coefficient of 0.4 to consider the effect of cracks in the masonry. This because there is not the availability of experimental data or specific study on the spandrels. It is worth to remind, however, that there are deep differences between spandrel and piers as the absence of a relevant axial load in the spandrel and the different orientation of the bed-joints respect to the direction of the shear load; furthermore in the composite spandrel there is also the presence of an RC beam.

## 4.6 Composite spandrels cracked stiffness

In this section the equations proposed to determine the cracked stiffness of the composite spandrel are reported. As already discussed for the initial stiffness, for the flexural stiffness only the contribution of the RC beam has been considered, whereas it is thought that only the masonry has influence on the shear stiffness. Knowing the flexural and shear cracked stiffness, the total cracked stiffness is obtained with an equation analogous at 4.16.

### 4.6.1 RC beam cracked flexural stiffness

In order to determine the cracked flexural stiffness of the RC beam of a composite spandrel (i.e. taking into account the effect of the cracks) the procedure described in previous section has been used.
It is an iterative procedure, because there are two equations available to solve the problem (the equilibrium to the translation and to the rotation) but three are the unknown quantities: the strain of the concrete (or of the longitudinal reinforcement, it depends which of the two cases described in 4.5.1 is being studied), the position of the neutral axis and the nominal flexural strength.
Hence, here the iterative procedure, for the case of strain of the longitudinal of 1.5%, is described:

- it is fixed a position of the neutral axis as first attempt;
- knowing the position of the neutral axis and the strain of the longitudinal reinforcement, with the hypothesis of a linear strain distribution in the cross beam section, it is possible to determine the strain of the concrete;
- using the equation of the equilibrium at the translation it is possible to obtain the position of the neutral axis that provides the equilibrium;
- with the new position of the neutral axis the new strain profile is calculated and the equilibrium at the translation is imposed again;
- this procedure is repeated until the new position of the neutral axis is rather close to the previous one.

Same procedure for the case of concrete strain of 0.04, in that case the strain of the longitudinal reinforcement is unknown. In Annexe A the Matlab script used to calculate the cracked stiffness is detailed.

### 4.6.2 Cracked shear stiffness of the masonry in the spandrel

The equation used in order to determine the shear cracked stiffness of the masonry is:

$$K_{s,cr} = 0.4\frac{G_{m,hor}A_m}{1.2L_{SP}} \tag{4.24}$$

The reason of the coefficient 0.4 is outlined in section 4.5.2.

## 4.7 Stiffness of the composite spandrels, comparison with the experimental results

In this section, the equations proposed to evaluate the stiffness and the shear strength of composite spandrels are used in order to develop a trilinear approximation of the force-displacement relationship.
For each spandrel, first, the shear capacity is calculated with the equations proposed in section 4.1. After that, the bilinear approximation for the stiffness is calculated. The composite spandrels work with the initial stiffness up to half of the shear capacity. Then their stiffness decreases to the cracked one, until the shear capacity is reached. In figures 4.19 and 4.20 the comparison among the equations proposed and the experimental and numerical results for TU2 is shown. The comparison for TU4 is shown in figures 4.21 and 4.22. Finally, in figures 4.23 and 4.24 there is the comparison for TU5.
To complete the force-displacement relationship it is necessary to know also the post peak behaviour (the dash lines indicate it is not yet known when strength starts to decrease). This aspect and a summary of the results obtained are discussed in the conclusion of this thesis.

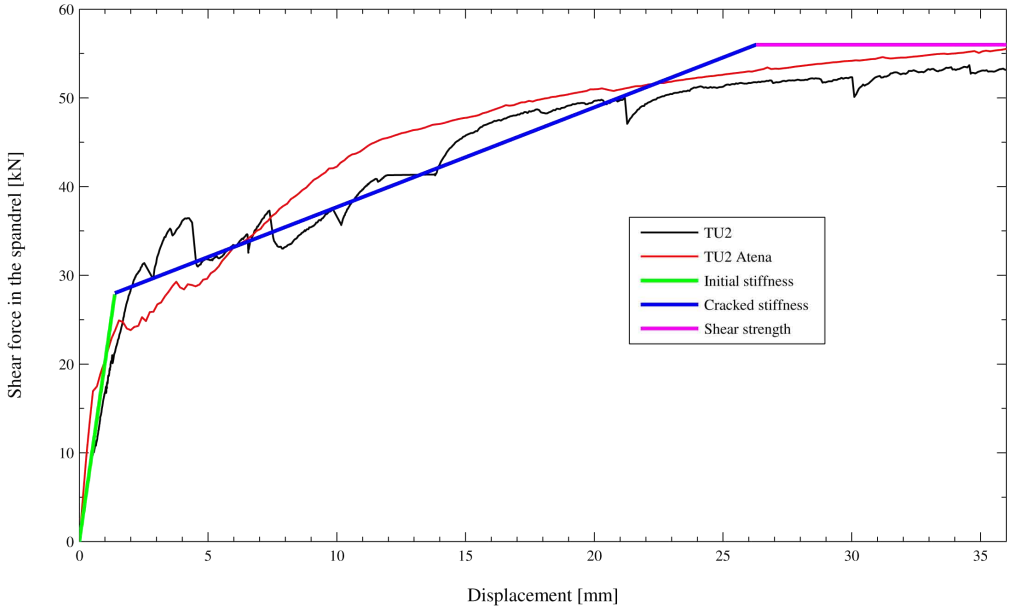


Figure 4.19: TU2: experimental and analytical results and comparison with the trilinear approximation. Up to a drift demand of 1%

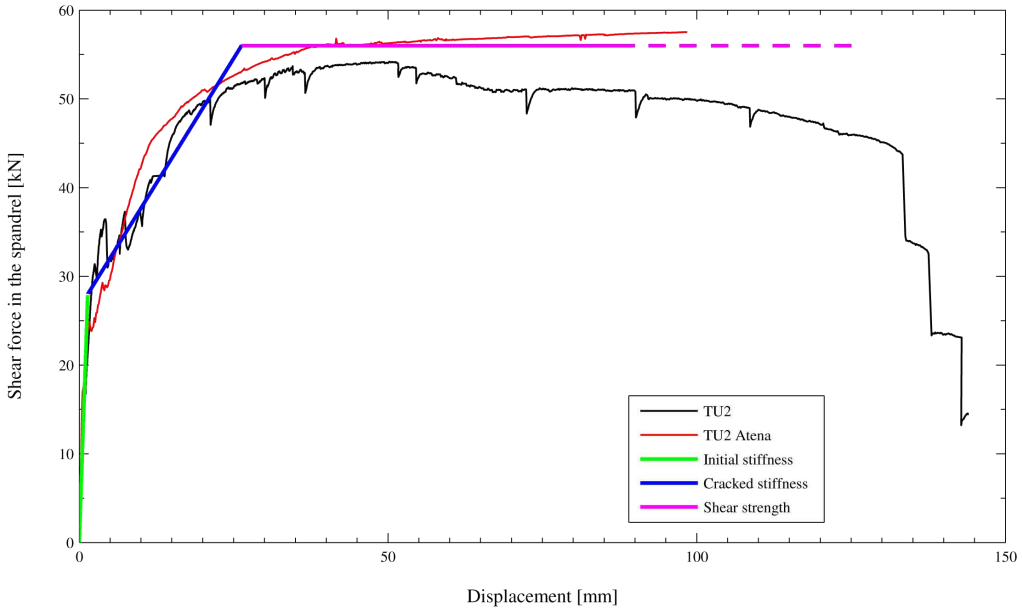


Figure 4.20: TU2: experimental and analytical results and comparison with the trilinear approximation.

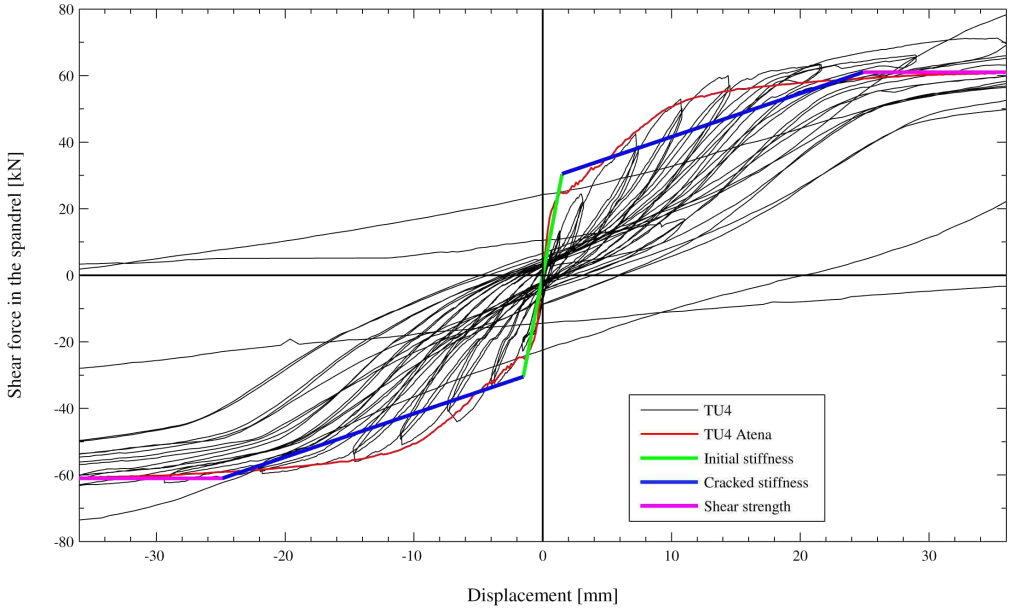


Figure 4.21: TU4: experimental and analytical results and comparison with the trilinear approximation. Up to a drift demand of 1%

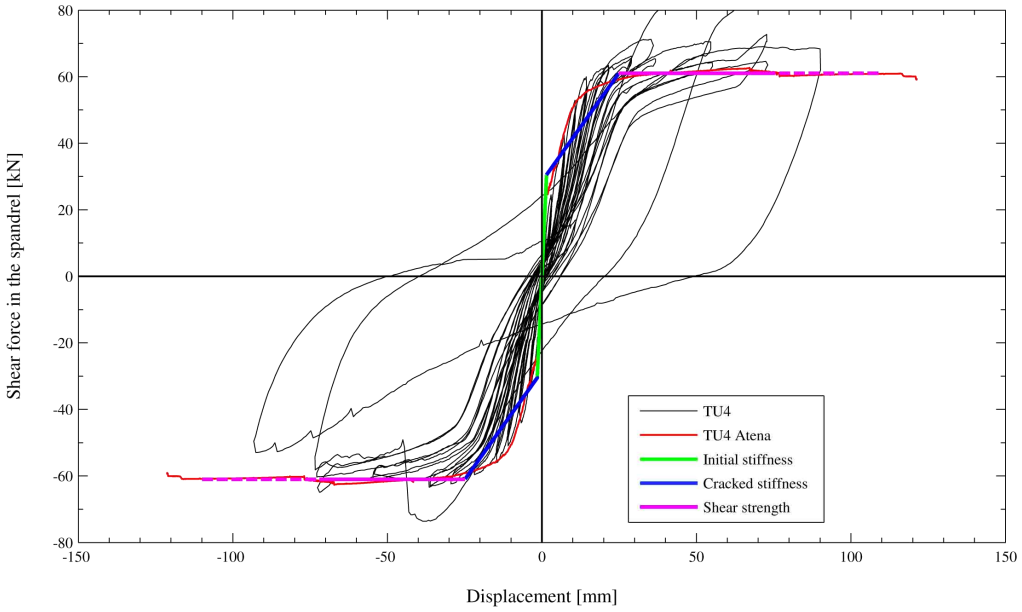


Figure 4.22: TU4: experimental and analytical results and comparison with the trilinear approximation.

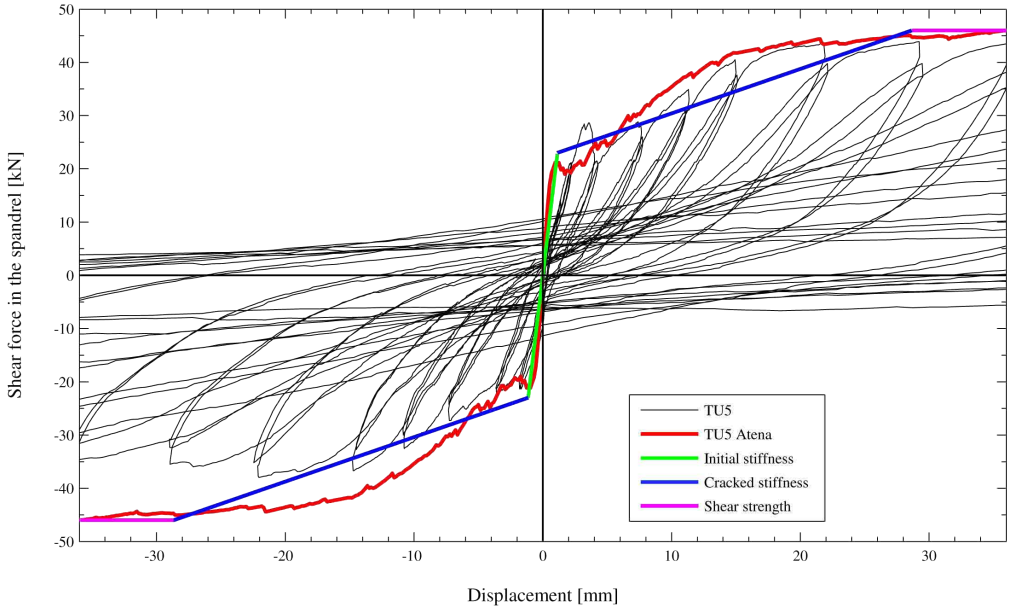


Figure 4.23: TU5: experimental and analytical results and comparison with the trilinear approximation.

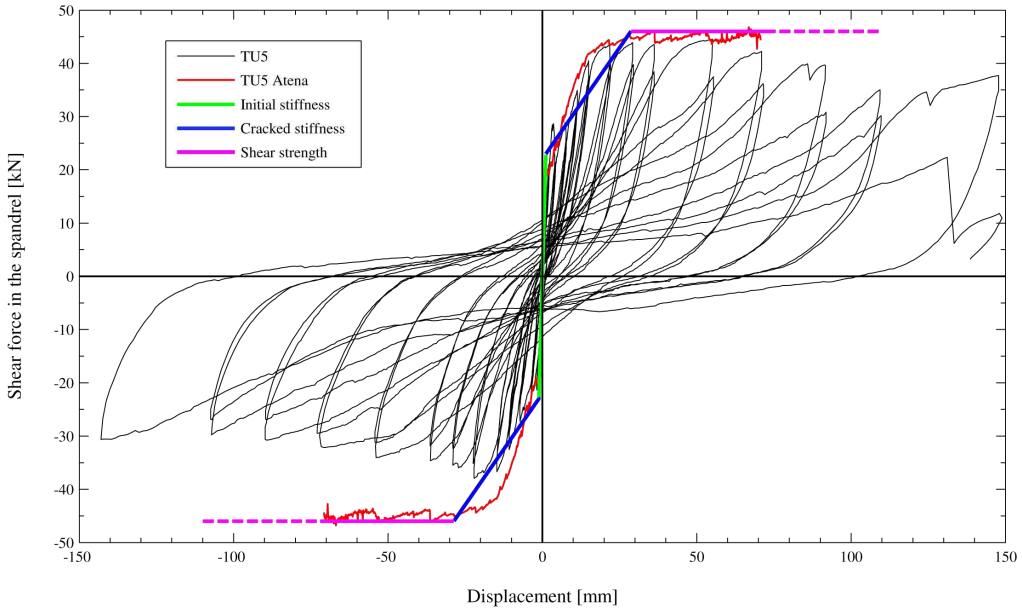


Figure 4.24: TU5: experimental and analytical results and comparison with the trilinear approximation. Up to a drift demand of 1%

# Chapter 5

# Parametric analyses

In this chapter the parametric analyses carried out with the numerical model developed in Atena are described in detail.
The aim of these analyses is to study how some specific parameters influence the mechanical behaviour of composite spandrels. For this reason, further analyses were carried out by varying one parameter at the time from the numerical model, used for the experimental calibration.

The parameters studied are:

1. the axial load in the piers,
2. the height of the RC beam,
3. the length of the spandrel,
4. the height of the spandrel,
5. the geometry of the bricks.

For each analysis, characteristics as the force-rotation relationship and the failure mechanism are studied. Subsequently those result are compared with the equations proposed to evaluate the shear capacity of the composite spandrels.

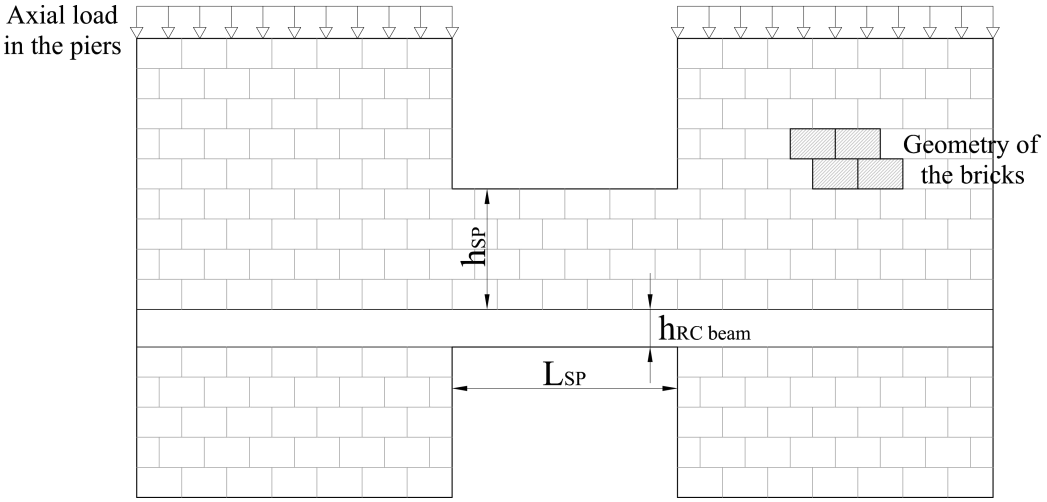


Figure 5.1: Parametric analyses: characteristics studied

## 5.1 The effect of axial load in the piers

During the experiment on TU4, it was fairly noticed that the axial load in the piers had great influence in the mechanical behaviour of composite spandrels. That test unit, in fact, showed a rocking behaviour for an axial stress of 0.4 MPa, whereas, when it was increased to 0.6 MPa, a shear behaviour triggered.
However, as it is discussed in section 5.1.1 it is not important the axial stress itself, but the total vertical load that weighs on the piers.
Therefore, in order to investigate how the axial load influences the mechanical behaviour of composite spandrels, analyses were carried out with different values of vertical loads. Those load were applied always in the same two points for each piers (as discussed in section 3.1.4). TU2 and TU4 were analysed and, by keeping constant all other characteristics, the axial stress on the pier is varied, from the 0.2 to 0.7 MPa for TU2 and from 0.2 to 0.8 for TU4.
In figure 5.2 the force-deformation relationship for TU2 is plotted. For axial stress values of 0.2, 0.3 and also 0.4 MPa the spandrel shows a rocking behaviour. This is probably the biggest difference in the mechanical response between the numerical model and the experimental results. In fact, for that axial stress, in the experiment, the reinforcements for positive bending were

already yielded.
For an axial stress of 0.45 MPa it is possible to notice a mixed flexural/rocking behaviour. Still there is a rather wide gap underneath the RC beam, but also a plastic hinge for the positive bending formed. Increasing the axial stress the gap becomes always smaller and a shear behaviour with two plastic hinges clearly developed.
However, two aspect has to be taken into account: (i) since the bricks are modelled as elastic no reduction in shear capacity were recorded increasing the drift demand (ii) as more a flexural behaviour developed as more convergence problems occurred. For instance no solution were found for drift demands superior than 1.3% when flexural behaviour developed.
In figure 5.3 the effect of the axial stress in the piers in the force-deformation relationship for TU2 up to a drift demand of 1% is shown.

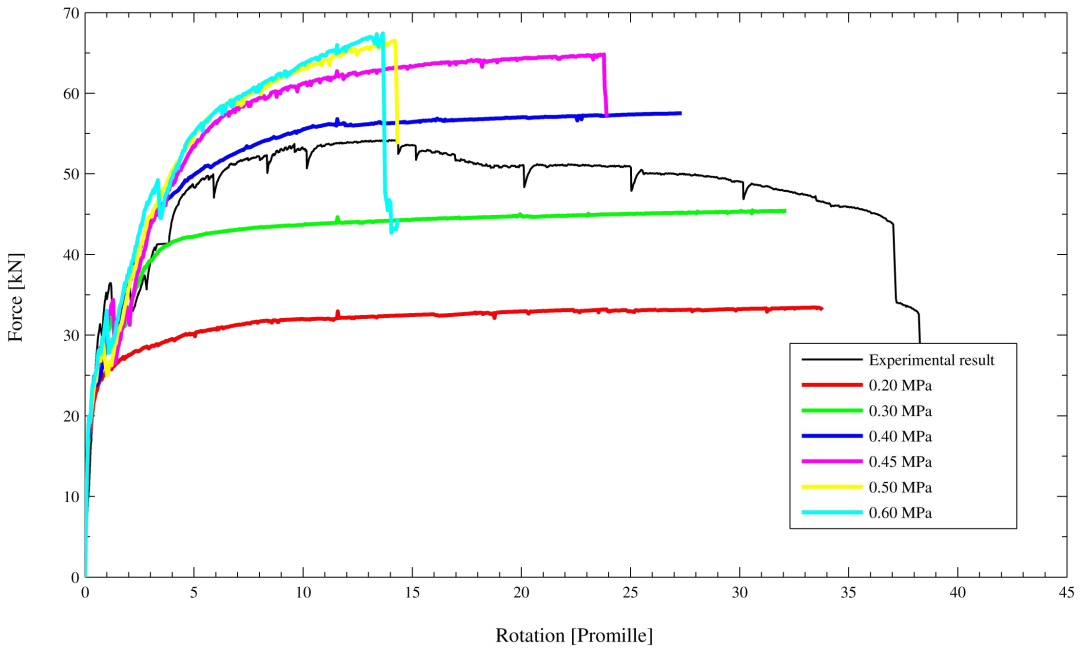


Figure 5.2: TU2. Effect of the axial stress in the piers in the force-rotation relationship

In figure 5.4 the force-deformation relationship for TU4 is plotted.
In this case a rocking behaviour developed up to an axial stress in the piers of 0.6 MPa, although for this last value it was expected a more flexural

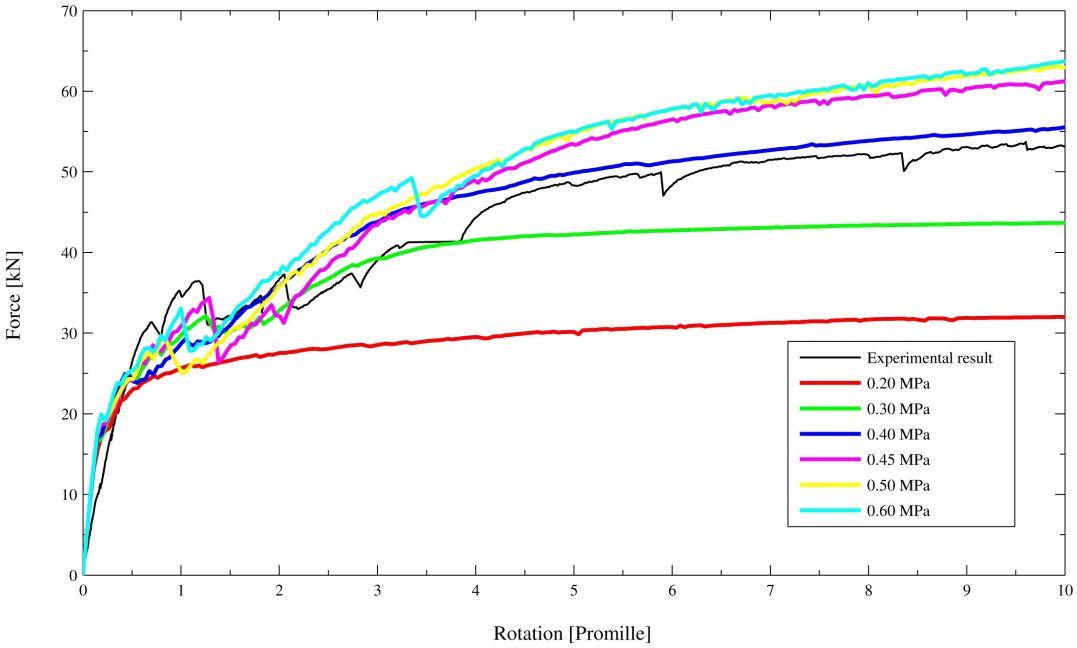


Figure 5.3: TU2 - Effect of the axial stress in the piers in the force-rotation relationship, up to a drift of 1%

behaviour. For an axial stress of 0.7 MPa convergence problems occurred so that the drift demand of 1% was not reached. For an axial load of 0.8 MPa positive plastic hinges, and therefore a flexural behaviour, developed. Also in this case, however, many convergence problems undermine the reliability of the results.
In figure 5.5 the effect of the axial stress in the piers in the force-deformation relationship for TU4, up to a drift demand of 1%, is shown.

### 5.1.1 The effect of the length of the piers

It was created a model with piers half the length. The aim of it was to understand if the rocking mechanism is actually dependent on the vertical load instead of axial stress. That model was created by moving roughly half of the bricks that constituted the original model (as shown in figure 5.6).

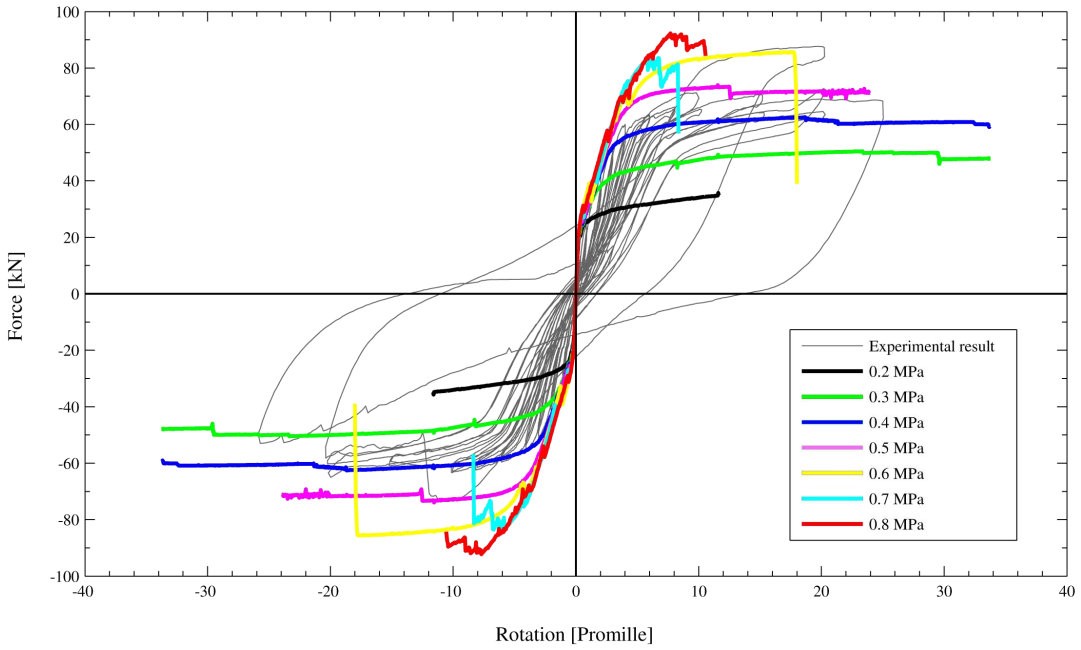


Figure 5.4: TU4 - Effect of the axial stress in the piers in the force-rotation relationship

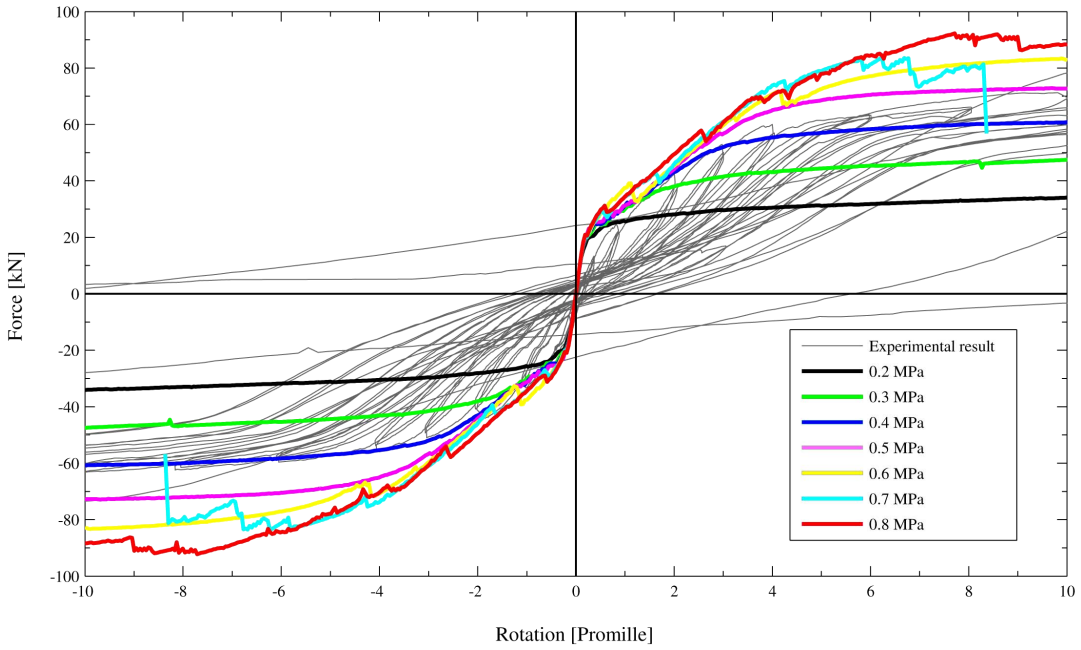


Figure 5.5: TU4 - Effect of the axial stress in the piers in the force-rotation relationship, up to a drift of 1%

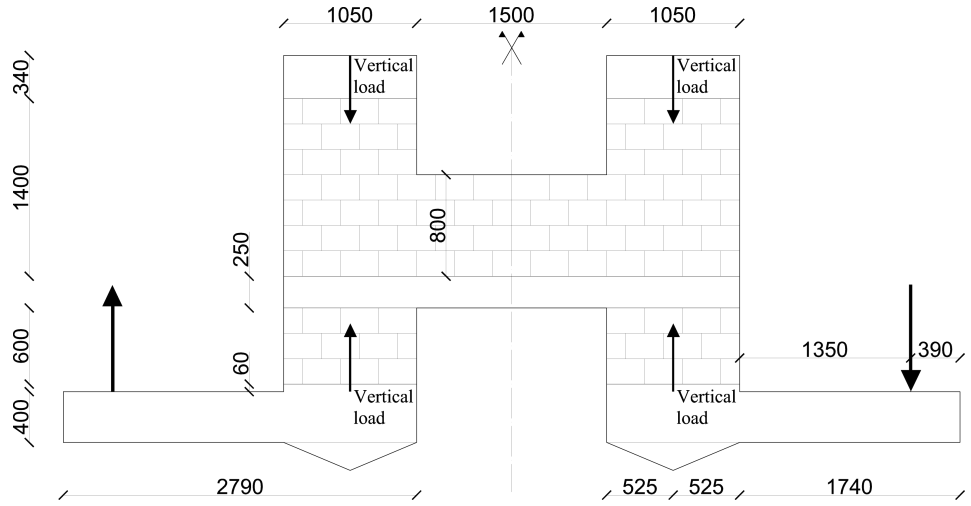


Figure 5.6: Geometry of the model with piers half the length

Those results are shown in figure 5.7. In that figure the green line shows the force-deformation relationship of the model with piers half the length of the original one. That curve is rather close to the one obtained in the original model with an axial load of 0.2 MPa. It is possible to find bigger differences in blue and violet curves. The last one represent the force-deformation relationship of the model with piers half the length of the original one and an axial load of 0.8 MPa. The blue one represent the force-rotation relationship of the original model with an axial stress of 0.4 MPa. Those results are however as expected. The rocking behaviour, in fact, is function of both vertical loads and the distance between these forces. Therefore, increasing the forces acting in the elements the effect given by their distance is more influential. Using the formulation proposed for the rocking mechanism, the values of shear capacity of composite spandrels for the two models are reported herein. As it is possible to see, they are rather close to the numerical model results for a drift demand of 1%.

| | |
|---|---|
| Half piers length - 0.4 MPa | 28.0 kN |
| Half piers length - 0.8 MPa | 45.3 kN |

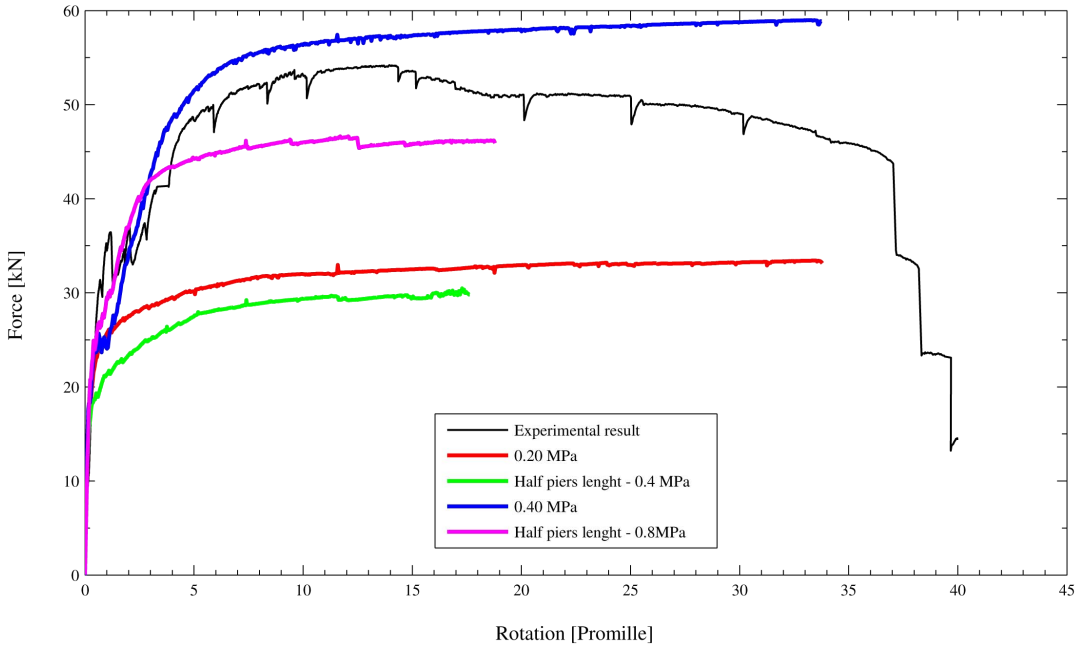


Figure 5.7: Effects of the piers length in the rocking mechanism

### 5.1.2 Analysis of the results

In this section the main results obtained are summarized and they are compared with the analytical equations proposed.

#### Stiffness

The axial load in the piers has not influence in composite spandrel stiffness, neither for the initial stiffness. In this case, the trigger of a rocking or a flexural mechanism is not due to changes of the stiffness of RC beam, but it depends on the forces acting in it. The flexural mechanism triggers if with the action of those forces the longitudinal reinforcements yield.

#### Shear strength

As already discussed in the third chapter of this thesis, the bricks in the numerical model have an elastic behaviour, therefore, reductions of shear capacity in the force-rotation relationship are not expected.
For this reason, the shear capacity is considered as the shear force acting in

composite spandrel when a drift demand of 1% is reached. Therefore, this shear force is considered, in this thesis, as the result, in term of shear capacity from the numerical analysis. This drift value has been chosen, because, for this demand bricks, in the experimental specimens, started to crack, and hence to lose their load bearing capacity.
In figures 5.8 and 5.9 the results from the numerical model and a comparison with the equations discussed in the fourth chapter are depicted.
In those graphs, in black, there are the rocking and shear failure equations proposed in the fourth chapter. The continuous grey line represents the composite spandrel shear strength obtained neglecting masonry contribution, as suggested in [PCK07] (see equation 4.1).
The shear capacity proposed in the Italian code is defined with the dashed grey line. As already discussed in section 4.1.1, in that code two equations are proposed, one for a shear failure and a second for the flexural failure. The corresponding shear strength is the lowest of these two values, here reported:

| | |
|---|---|
| Shear failure | **40 kN** |
| Flexural failure | 41 kN |

In figures 5.8 and 5.9 the blue dots represent a rocking mechanism in the numerical model, a shear mechanism the red ones and with purple the mixed mechanisms are represented.

As it is possible to see, an important drawback of both equations proposed by the Italian code or in [PCK07] is not to consider the influence of axial load, hence, a constant value of shear strength is obtained.
However, as it has already said several times, the axial load is rather influential to determine the failure mechanism in composite spandrels. Moreover, if a rocking mechanism triggers, the shear capacity of composite spandrel is function of axial load in the piers, whereas it has no influence in flexural mechanism.
Another disadvantage of the equations proposed in the Italian code is that it does not consider the longitudinal reinforcement ratio in the RC beam. In the equation for the flexural mechanism, in fact, it is required to take

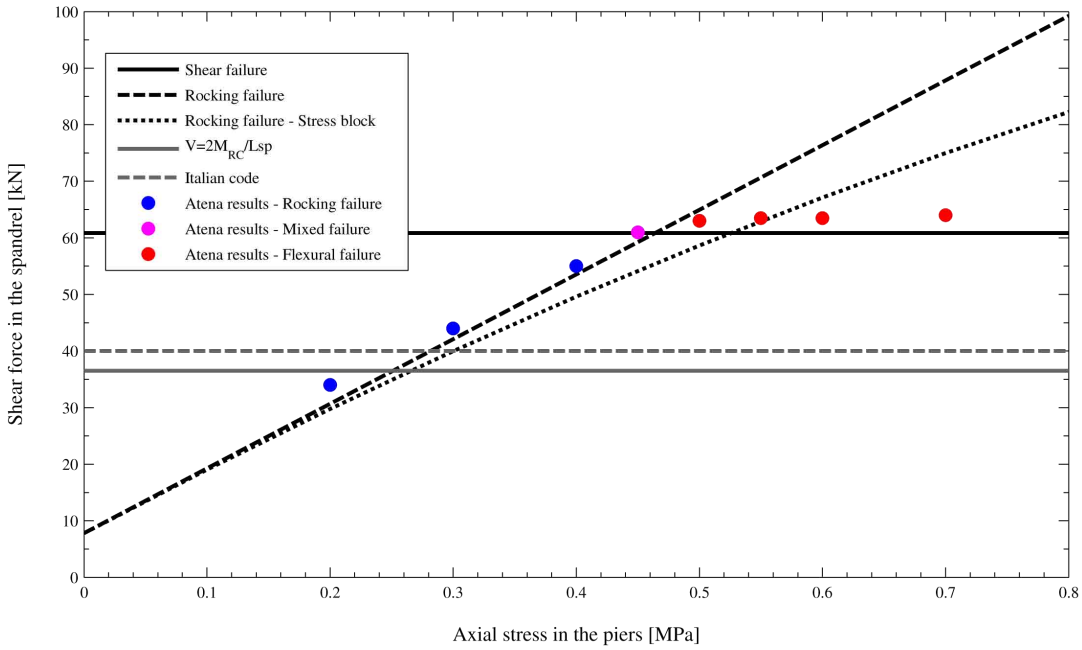


Figure 5.8: TU2 - Effect of axial load in composite spandrel shear capacity - Analytical and numerical models comparison.

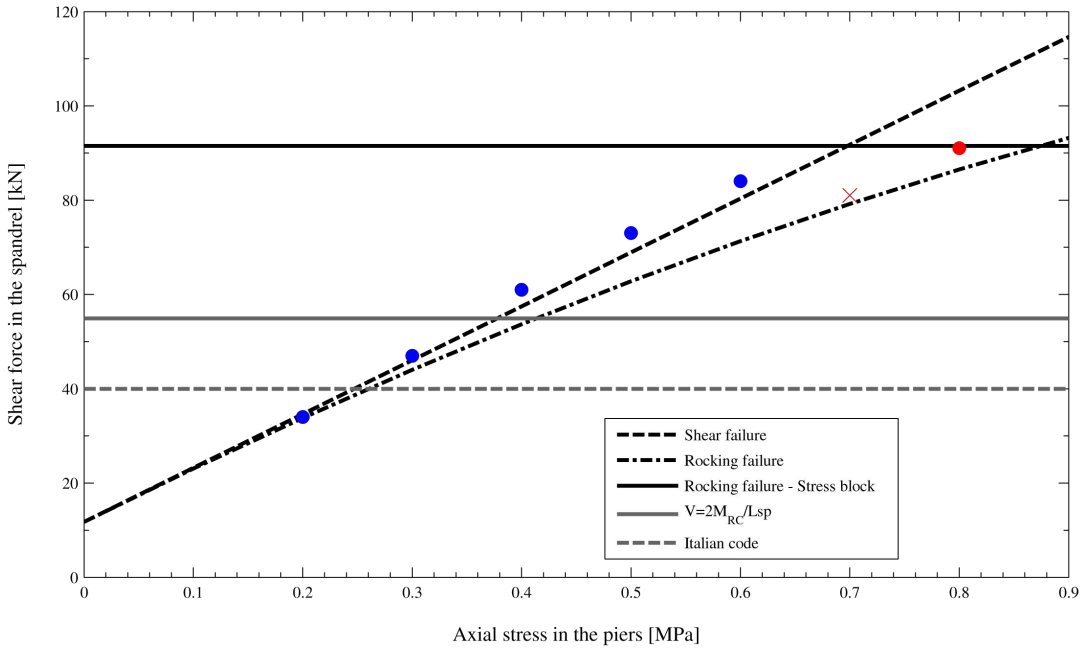


Figure 5.9: TU4 - Effect of axial load in composite spandrel shear capacity - Analytical and numerical models comparison.

into account the minimum force between the tensile strength of RC beam (namely the tensile strength of its longitudinal reinforcement) and the compressive strength of masonry in horizontal direction. For both TU2 and TU4 elements, the strength of masonry is lower than the strength of the longitudinal reinforcement, therefore both test units are evaluated with the same shear capacity.
As said, in the analysis carried out with TU4 longitudinal reinforcement, many convergence problems occurred when a shear mechanism triggered. Those problems were rather influential for an axial load in the piers of 0.7 MPa, for this reason, in figure 5.9 that shear strength value is represented with a red cross.

## 5.2 The effect of the height of the RC beam

The five different configurations of the RC beam analysed, in order to study the effect of its height, are shown in figure 5.10. The reinforcement ratio used has the constant value of 4D12, that is the one of TU2 and TU3.

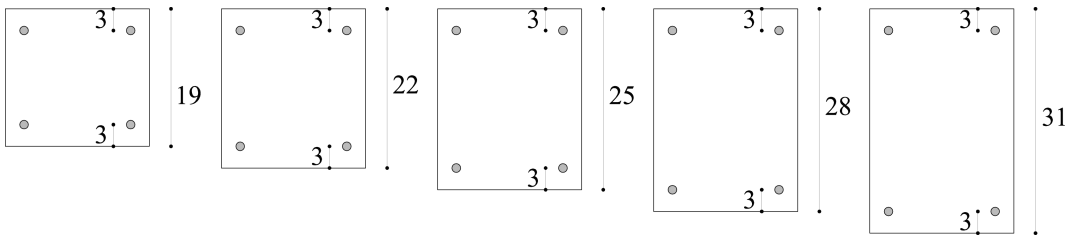


Figure 5.10: Heights of the RC beam studied

In figure 5.11 the whole force-deformation relationship is depicted, and in figure 5.12 the same relationship, up to 1% is shown. The height of RC beam directly influences its flexural strength and stiffness. Therefore, since the failure mechanism is related to the flexural strength of the spandrel, increasing the height of the RC beam, always a more rocking mechanism developed. For heights of 19 and 22 cm, instead, it was noticed a shear behaviour. Differently from the axial load in the piers, variations in the height of RC beam influence the shear capacity for both rocking and shear mechanism. The last mechanism is, besides, the one more influenced by variations in RC beam height. In fact, the difference in shear capacity are bigger between 19 and 22 cm (where a shear mechanism triggered) than 25, 28 and 31 cm (where there is a rocking behaviour).

### 5.2.1 Analysis of the results

#### Stiffness

The height of the RC beam has not an important influence in the stiffness of the composite spandrel. It is more evident for the cracked stiffness but for the initial stiffness has almost not importance.

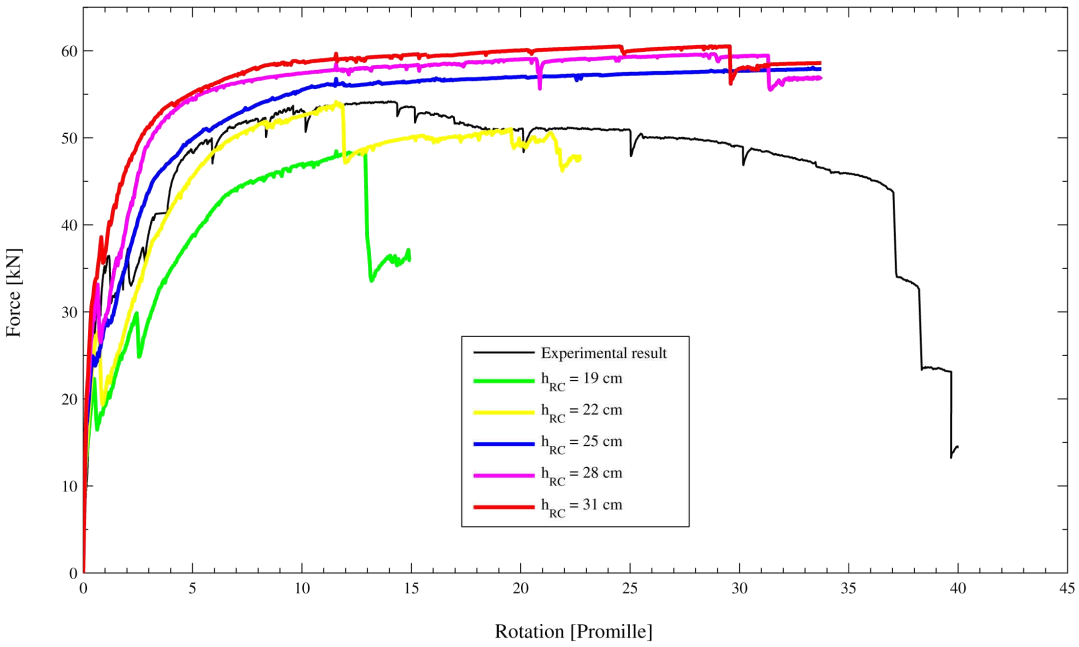


Figure 5.11: Effect of the height of the RC beam in the force-rotation relationship

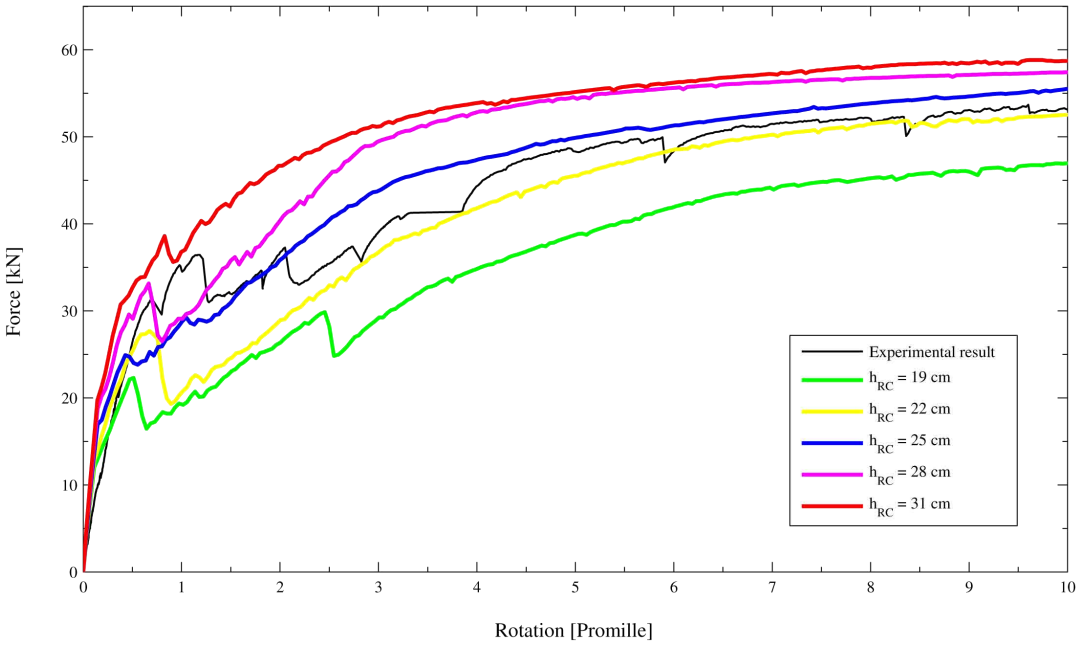


Figure 5.12: Effect of the height of the RC beam in the force-rotation relationship, up to a drift of 1%

### Shear strength

In figure 5.13 the comparison between the numerical model results and the analytical model is depicted. As already said, for both analytical and numerical models variations in RC beam height have bigger influence to the shear capacity if a shear/flexural mechanism triggers.

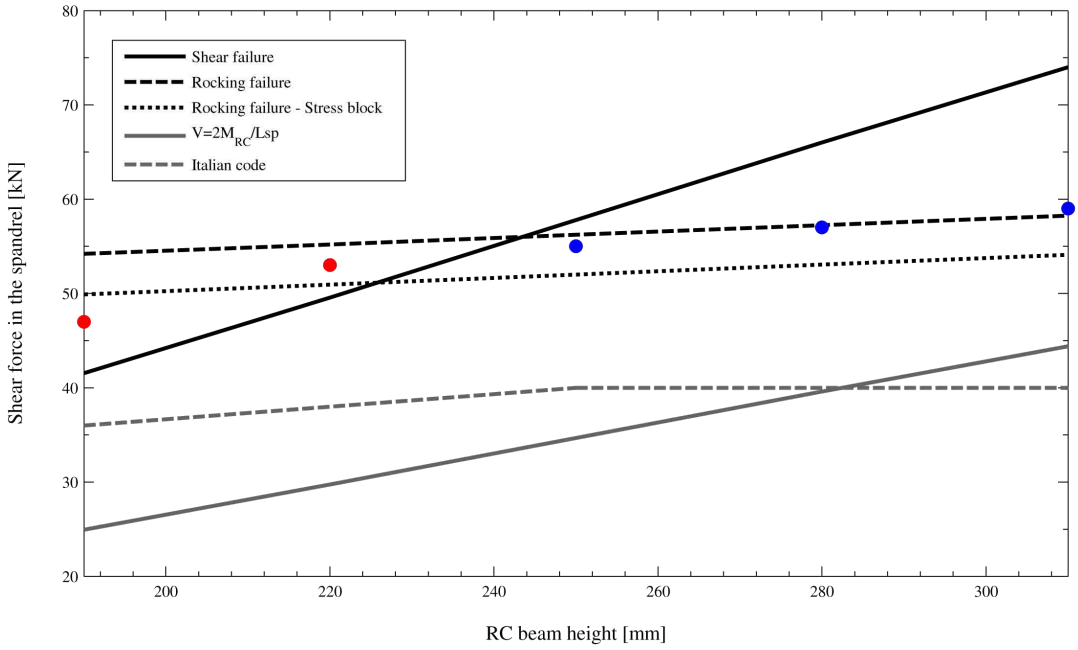


Figure 5.13: Effect of the height of RC beam in composite spandrel shear capacity - Analytical and numerical models comparison.

As it could be expected, the shear capacity increases with the spandrel height. In fact an increase of RC beam height cause an increase of its stiffness and strength.
As already seen in the section about the effect of the axial load, not considering the presence of masonry underestimates the shear capacity of composite spandrel. In the following table the values of the shear capacity obtained according to Italian code formulation are shown.

| | |
|---|---|
| RC beam 19 cm | 36 kN (flexural formulation) |
| RC beam 22 cm | 38 kN (flexural formulation) |
| RC beam 25 cm | 40 kN (shear formulation) |
| RC beam 28 cm | 40 kN (shear formulation) |
| RC beam 31 cm | 40 kN (shear formulation) |

Table 5.1: Effect of the height of RC beam: composite spandrel strength according with the Italian code formulations

## 5.3 The effect of length of the spandrel

In order to study the effect of the spandrel length to its mechanical behaviour five different configurations were studied. The length of the spandrel was considered from 0.9 m to 2.1 m with steps of 30 cm. It has been used a step of 30 cm because the geometry of the element that constitute the bricks is 30 cm long. Also, it was decided to do not introduce in this analysis the further variable on the geometry of the bricks. It was preferred, in fact, to study the effects of the bricks geometry separately in others analyses.

The result of those analysis are shown in figures 5.14 and 5.15. Up to the length of 1.5 m the model shows a rocking behaviour, whereas, for length of 1.8 and 2.1 m a flexural one.
The same analyses were carried out with the model that has the longitudinal reinforcement ratio of TU4. The results of these analyses are shown in figure 5.16. For all of these model a rocking behaviour developed.

### 5.3.1 Analysis of the results

#### Stiffness

As it could be expected, the length of the spandrel has a strong influence in its stiffness. If the length increases the stiffness decreases. In the numerical model, this is observed also in the initial stiffness (figure 5.15).

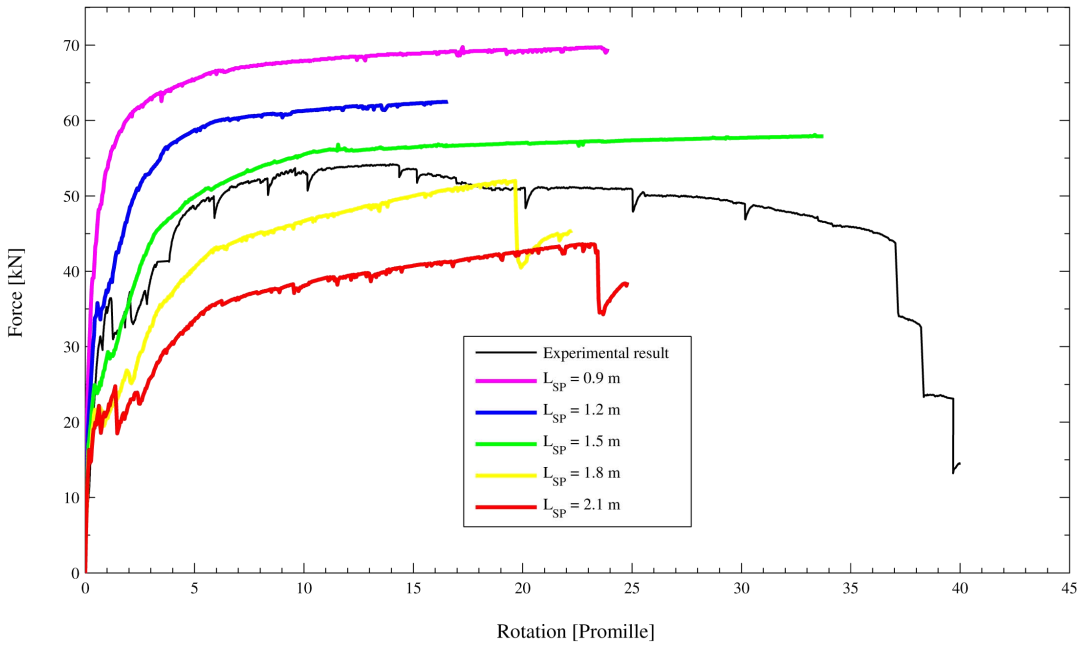


Figure 5.14: TU2 - Effect of the length of the spandrel in the force-rotation relationship

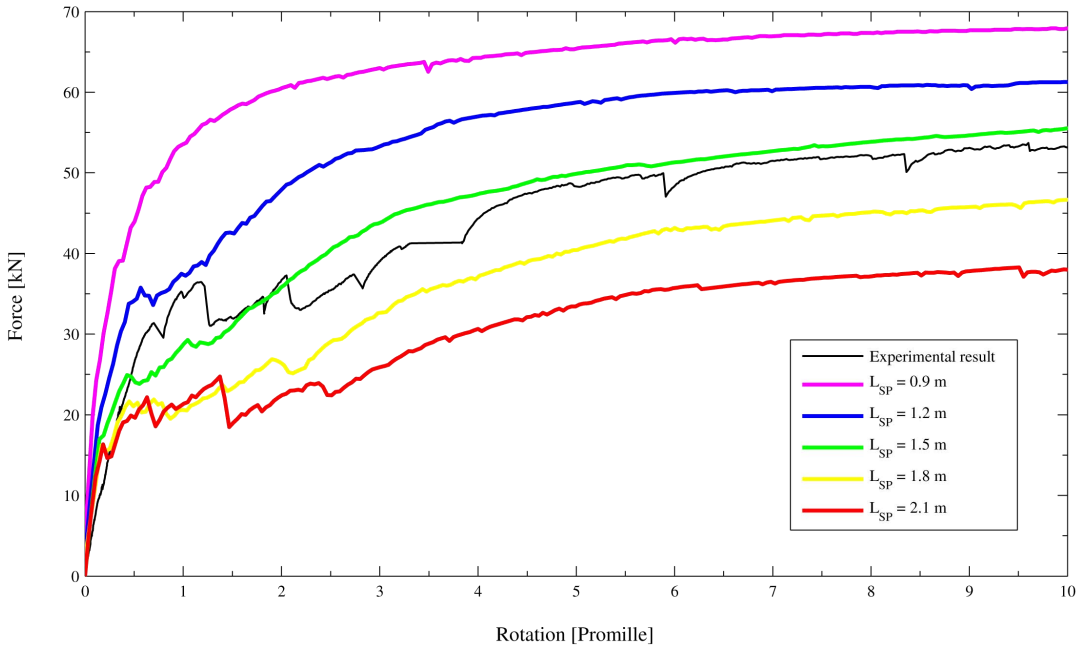


Figure 5.15: TU2 - Effect of the length of the spandrel in the force-rotation relationship, up to a drift of 1%

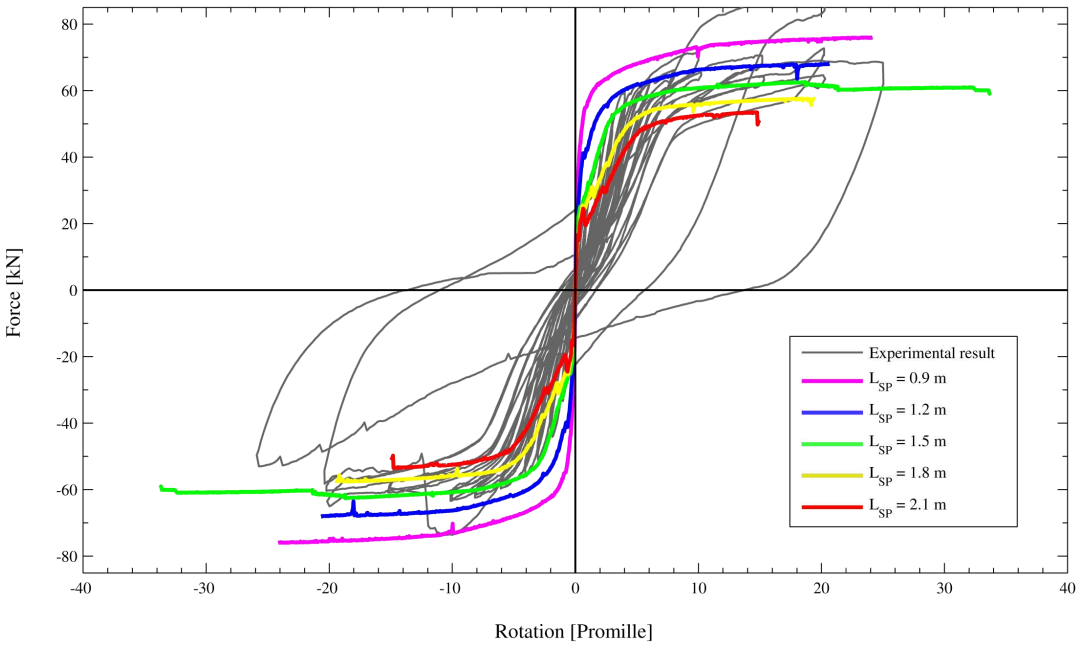


Figure 5.16: TU4 - Effect of the length of the spandrel in the force-rotation relationship

### Shear strength

The length of the spandrel influences deeply its mechanical behaviour. The shear capacity for both rocking and flexural mechanisms decrease if the length of the spandrel increases. This reduction is linear for the rocking mechanism, whereas it is very strong for the flexural behaviour, where it is neither linear, but it has a sort of hyperbolic decrease.
For TU2 longitudinal reinforcements ratio, if the composite spandrel is rather short (up to 1.5 m) it is enough stiff to trigger a rocking mechanism. For superior lengths, a flexural mechanism develops. In the models with the longitudinal reinforcement ratio of TU4 triggers always a rocking behaviour.
The shear strength capacity for each spandrel length, according to the Italian code, are summarized herein. They are valid for both TU2 and TU4 RC beam longitudinal reinforcement. This is because, for the flexural mechanism, it is required to obtain the shear capacity from the lowest compressive force due to the compression of masonry and the tensile strength of the longitudinal reinforcements. For both TU2 and TU4 the force due to masonry

compression is weaker than the reinforcements tensile one. Therefore, with the Italian code formulation is not possible to catch the difference in shear capacity due to different longitudinal reinforcements ratio.

| | |
|---|---|
| SP length 0.9 m | 40 kN (shear formulation) |
| SP length 1.2 m | 40 kN (shear formulation) |
| SP length 1.5 m | 40 kN (shear formulation) |
| SP length 1.8 m | 34 kN (flexural formulation) |
| SP length 2.1 m | 29 kN (flexural formulation) |

Table 5.2: Effect of the length of the spandrel: composite spandrel strength according with the Italian code formulations

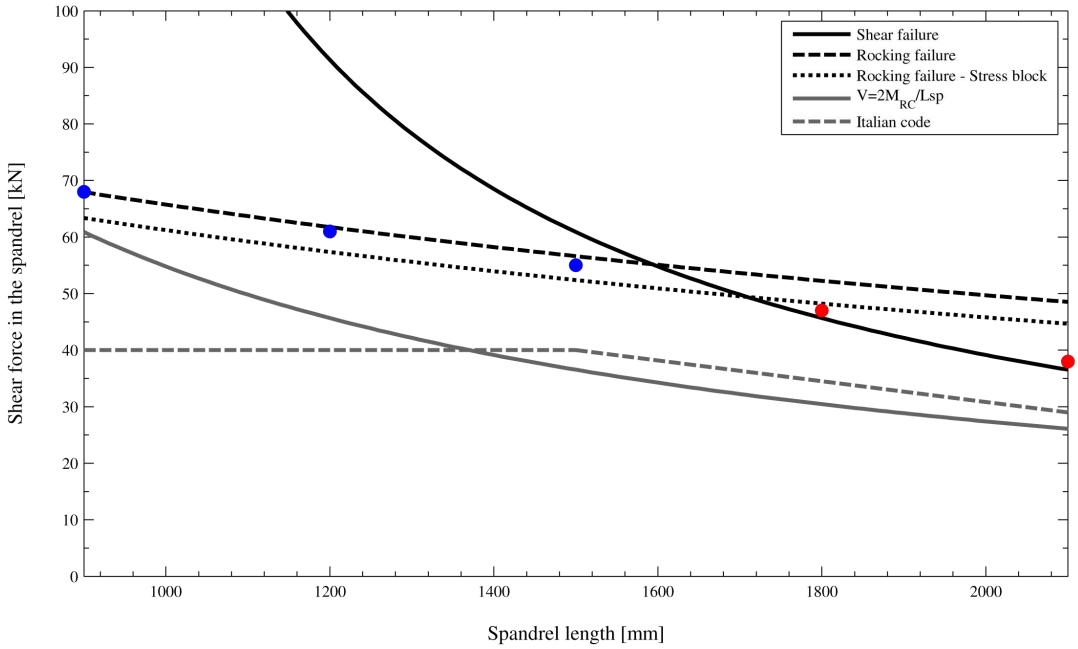


Figure 5.17: TU2 - Effect of the length of RC beam in composite spandrel shear capacity - Analytical and numerical models comparison.

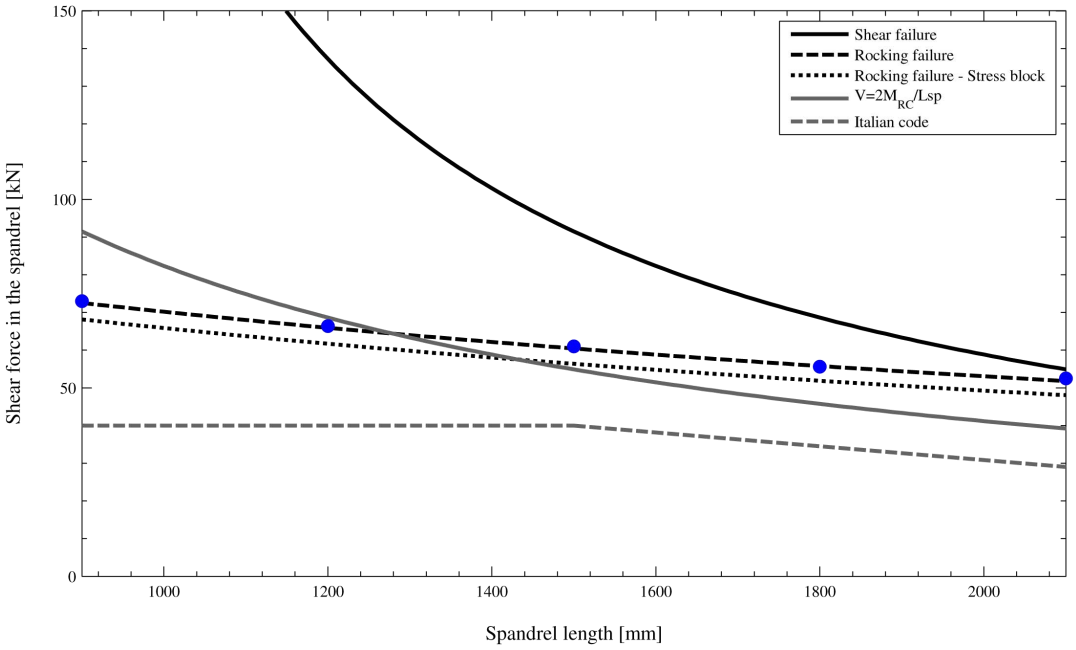


Figure 5.18: TU4 - Effect of the length of RC beam in composite spandrel shear capacity - Analytical and numerical models comparison.

## 5.4 The effect of the height of the spandrel

Several analysis were carried out in order to study how the height of the spandrel influences its mechanical behaviour. For this reason different models with height of the spandrel of 0.6 m, 1.0 m and 1.2 m were created. As for the analysis on the length of the spandrel, no models with height of the spandrel in-between were created. This because it was preferred not to change the geometry of the bricks. In the initial models, in fact, the bricks have an height of 20 cm, therefore, no other models were created because, it is not common to find spandrels with an height of 0.4m or 1.4m or more.
In these model were applied both reinforcement ratio of TU2 and TU5. The reasons why are applied these reinforcement ratio are explained hereafter. In figure 5.19, the force-deformation relationship of the analysis carried out for the model with the reinforcement ratio of TU2 is depicted. As it observed, there are differences in the stiffness but not in the shear capacity. This is due to the fact that all models show a rocking behaviour that is not influenced

by the height of the spandrel. Thus, it is not possible to get considerable differences in composite spandrels shear capacity.
For this reason the same model were analysed with the reinforcement ratio of TU5. The results of these analysis are shown in figure 5.21.
In this case it is possible to notice differences in the mechanical behaviour changing the height of the spandrel. In fact, for height of the spandrel of 0.6 and 0.8 m a flexural mechanism triggered, for heights of 1.0 and 1.2 m, instead, the behaviour is closer to a rocking one. Unfortunately, also in this case, many convergence problems occurred in the models that showed a flexural mechanism, that could partially undermine the reliability of their results.
No analysis were carried out with the reinforcement ratio of TU4, since in these models always a rocking mechanism developed for which the height of the spandrel has no interest.
Finally, analysis in the model with TU2 reinforcement ratio, and with an axial stress in the piers of 0.6 MPa, were carried out. This because, as said above, in the models which RC beam has the reinforcement ratio of TU2 always a rocking mechanism triggered. Therefore, the axial stress in the piers was increased in order to force the development of flexural mechanism in the spandrel.
The results of these analysis are shown in figures 5.22 and 5.23. For all these models flexural mechanism developed, consequently an increasing of the height of the spandrel is followed by an increasing of its shear capacity.

### 5.4.1 Analysis of the results

#### Stiffness

As for the length of the spandrel, its height has influence on the stiffness too. If the height increases, the stiffness also increases. However, it has a less relevant importance than the length of the spandrel. In fact, in this case there are variations in the initial stiffness, but with a lesser extent.

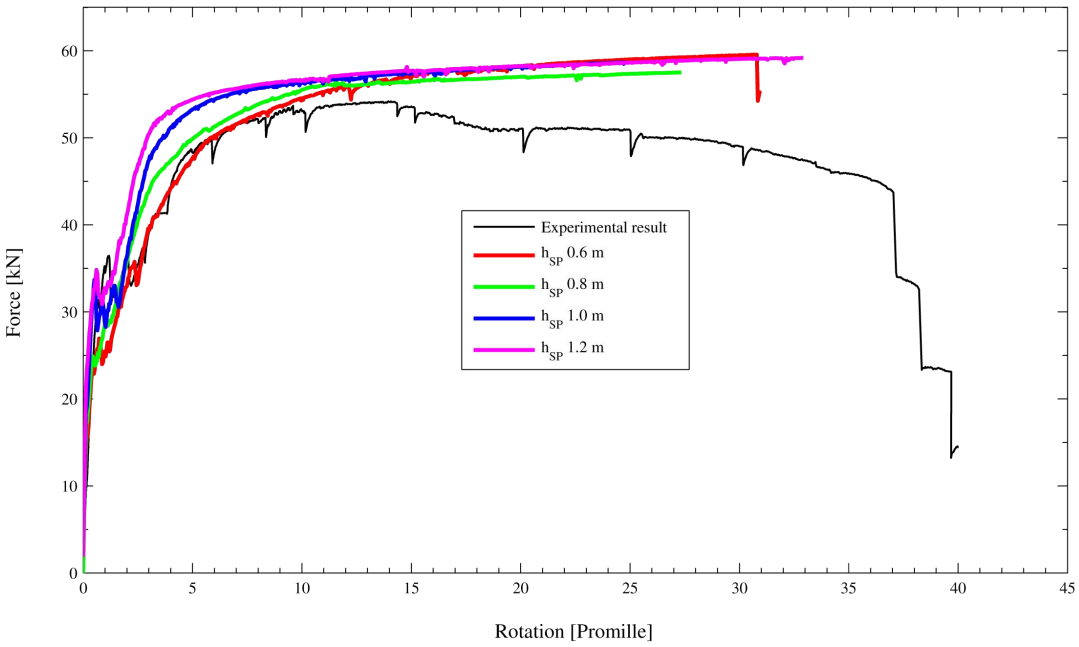


Figure 5.19: TU2 - Effect of the height of the spandrel in the force-rotation relationship

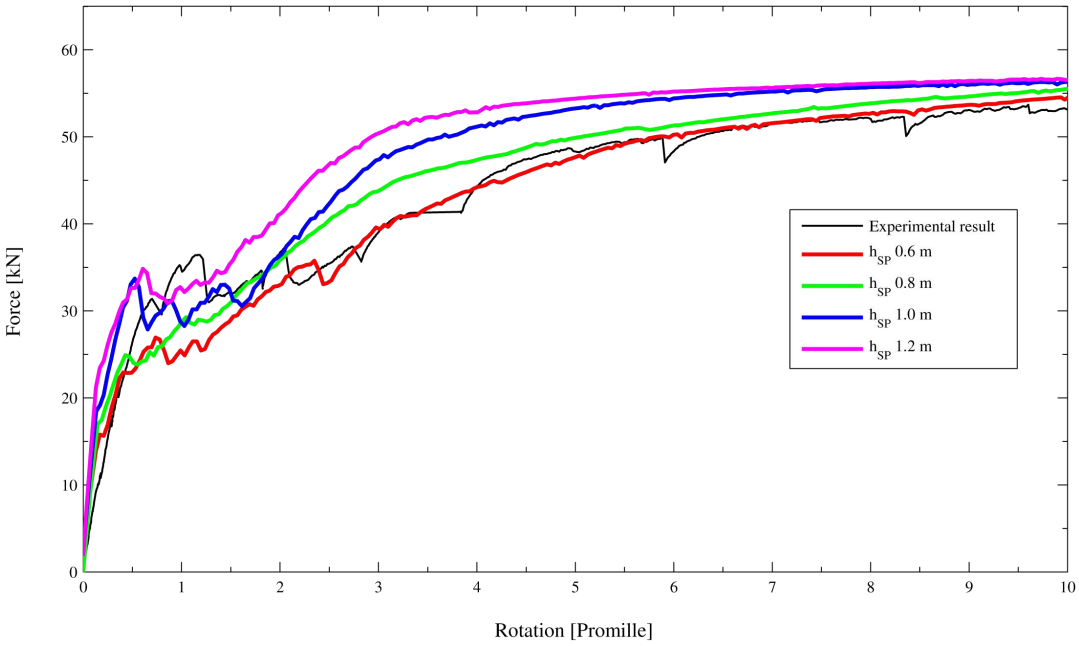


Figure 5.20: TU2 - Effect of the height of the spandrel in the force-rotation relationship, up to a drift of 1%

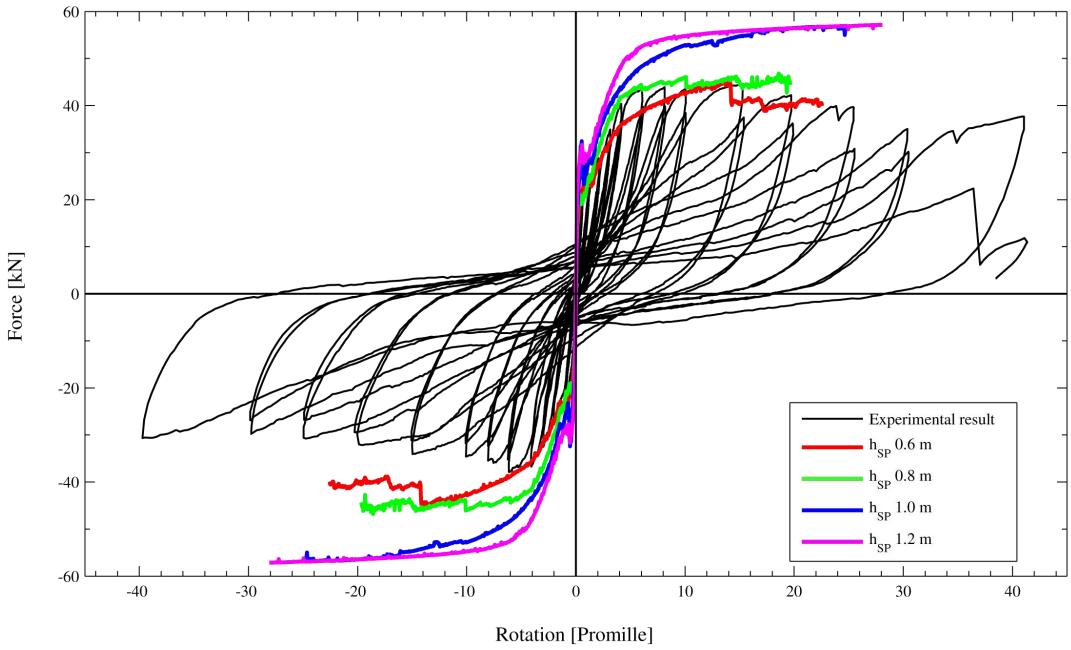


Figure 5.21: TU5 - Effect of the height of the spandrel in the force-rotation relationship

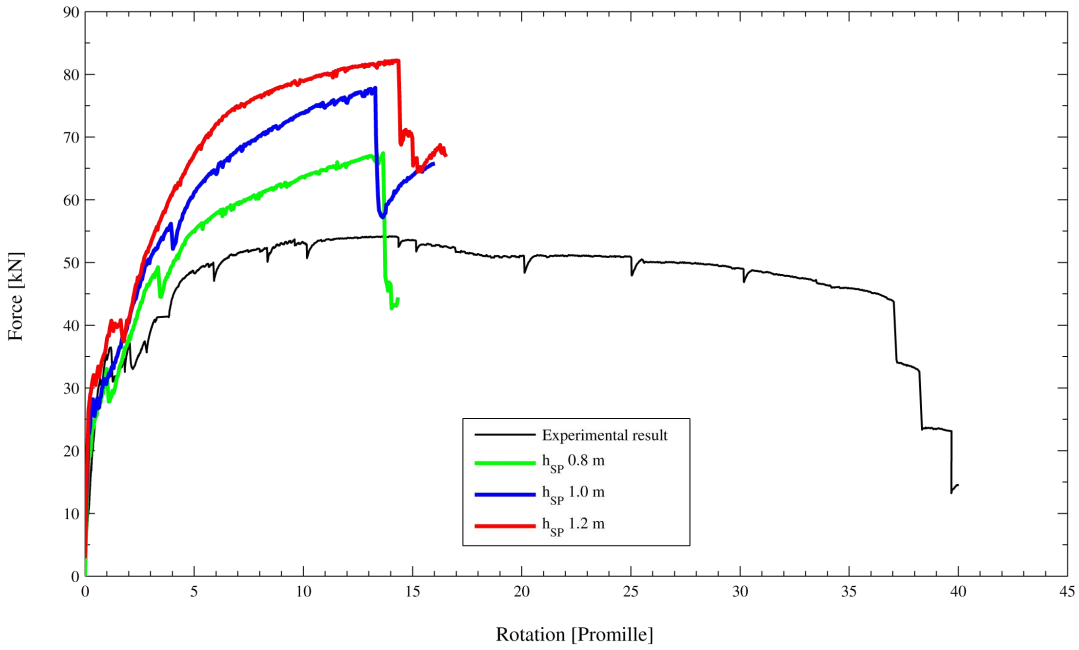


Figure 5.22: TU2, axial stress of 0.6 Mpa - Effect of the height of the spandrel in the force-rotation relationship

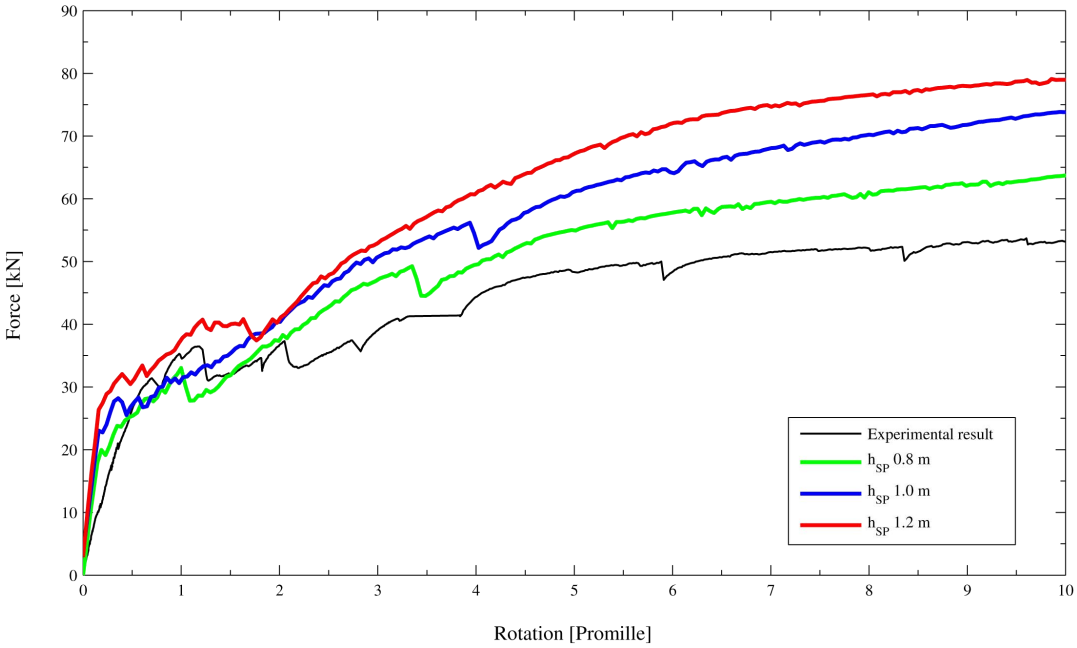


Figure 5.23: TU2, axial stress of 0.6 Mpa - Effect of the height of the spandrel in the force-rotation relationship, up to a drift of 1%

### Shear strength

The global behaviour of the models analysed has been already described in the previous section. The result of those analysis are reported in figures 5.24, 5.26 and 5.25. The numerical model with height of the spandrel of 1.2 m and an axial load of 0.6 MPa had some convergence problems, hence its results are maybe not entirely credible.
As for others analysis, the blue dots represent a rocking failure, the red ones a flexural failure and the purple ones mixed failures.
The shear capacity values for each spandrel height, as defined by Italian code, are reported herein. As for the others models already described, they are the same for TU2 and TU5 longitudinal reinforcement, as well as for the model with variations in axial load stress.

| | |
|---|---|
| SP height 0.6 m | 27 kN (flexural formulation) |
| SP height 0.8 m | 40 kN (shear formulation) |
| SP height 1.0 m | 50 kN (shear formulation) |
| SP height 1.2 m | 60 kN (shear formulation) |

Table 5.3: Effect of the height of the spandrel: composite spandrel strength according with the Italian code formulations

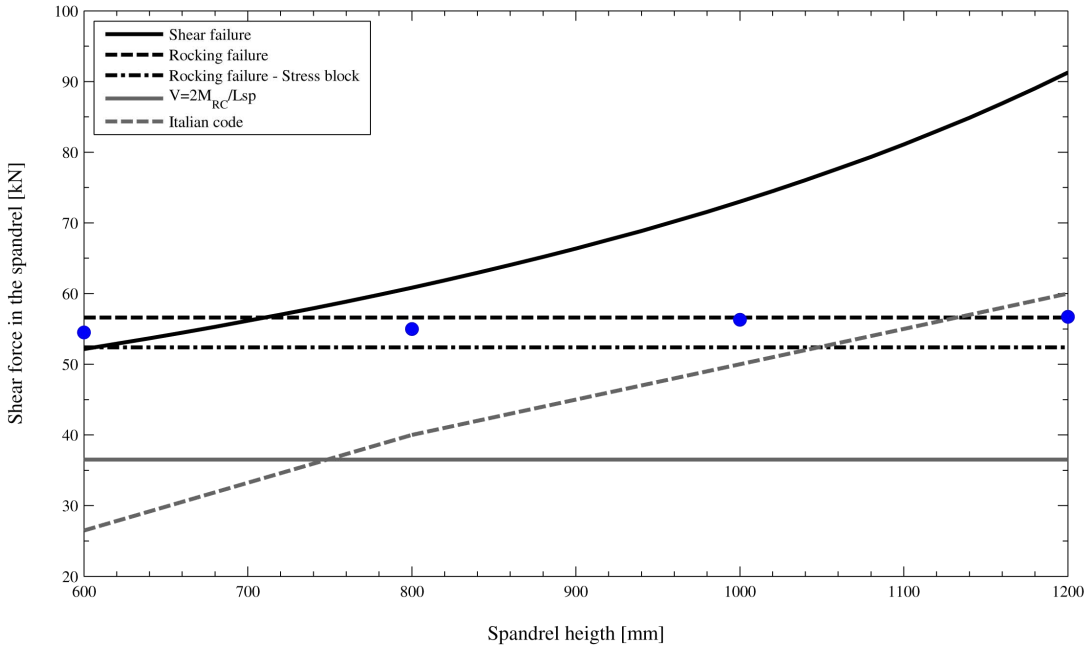


Figure 5.24: TU2 - Effect of the height of spandrel in its shear capacity - Analytical and numerical models comparison.

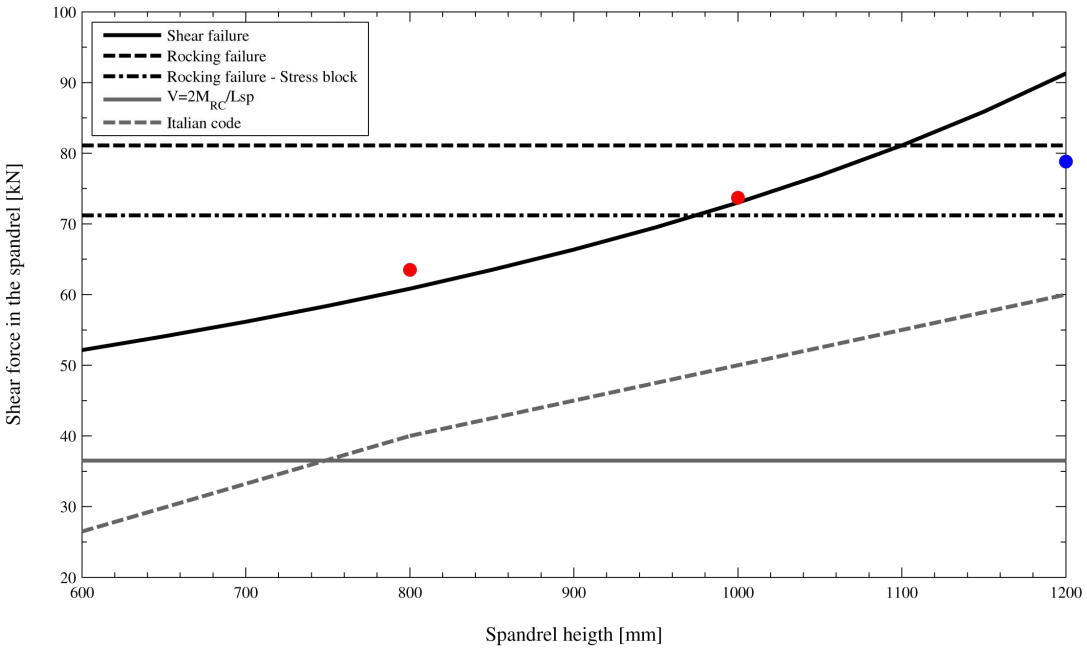


Figure 5.25: TU2, axial stress of 0.6 MPa - Effect of the height of spandrel in its shear capacity - Analytical and numerical models comparison.

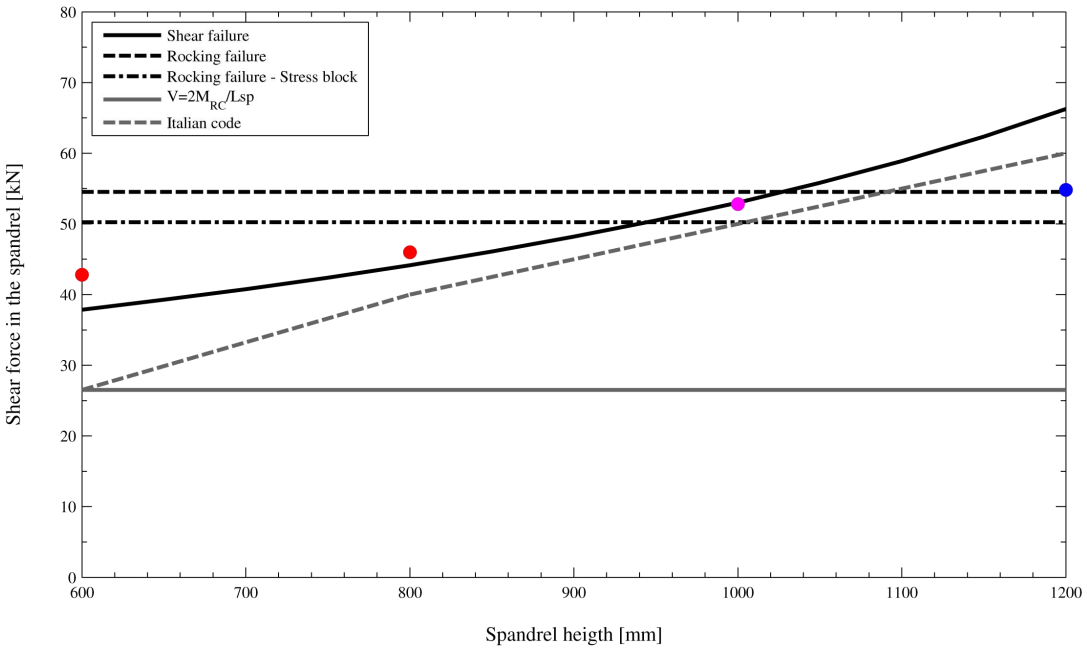


Figure 5.26: TU5 - Effect of the height of spandrel in its shear capacity - Analytical and numerical models comparison.

## 5.5 The effect of the geometry of the bricks

In this last series of analysis the effect of the geometry of the bricks is studied. Three different kinds of brick geometries were considered: 26x26 cm, 50x20 cm and 50x26 cm.
These measures were chosen because they are similar to those of the bricks available in the construction market.
However, it is worth to remind, that these dimensions refer to the sum of the dimensions of bricks and mortar joints, in the spirit of the simplified micro-modeling, as already explained in section 1.4 of this thesis. The aim of these analysis is to study only the effect of the bricks geometry, therefore the idea is not to change other geometrical characteristics. However, changing the dimension of the bricks, it was not possible to keep exactly the same geometry of the model. For this reason, it was preferred to keep as more constant as possible the length of the spandrel and to introduce, instead, little changes in the length of the piers.

The result of these analysis are shown in figure 5.27. Except the model with bricks geometry of 26x26 cm, all the models show a rocking mechanism, which is not dependent by bricks dimensions. For this reason, in order to carry on a deeper study of this characteristic, further analysis were carried out changing the axial load in the piers (with the aim to obtain a flexural failure mechanisms).
These analysis, and the geometry of the model used, are detailed in next sections.

It is worth to underline that in the equations proposed in the Italian code there are no references to the geometry of the bricks. Therefore, neglecting the little difference in spandrel height (2 cm) of the models with bricks geometry of 26x26 cm and 50x26 cm, for all models the same shear capacity is expected.
In these equations, moreover, as already said in section 5.1, the effect of the axial load in the piers it is considered. Hence, for all models a shear capacity of 40 kN is expected.

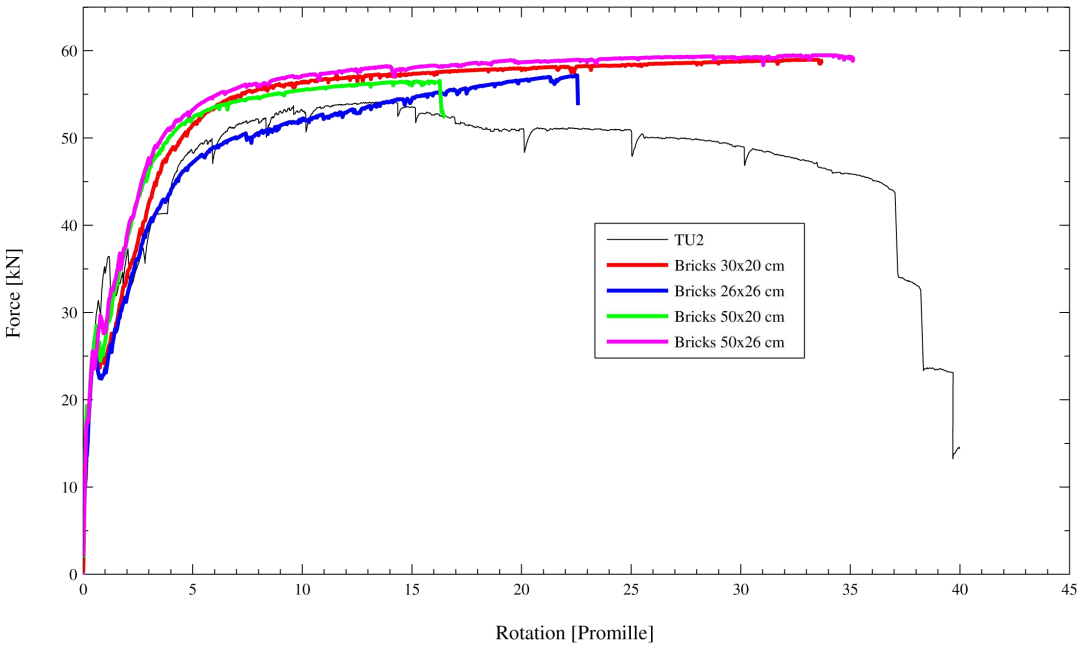


Figure 5.27: Effect of the bricks geometry in composite spandrel shear capacity

### 5.5.1 Bricks 26x26 cm

#### Description of the model

In figure 5.28 the geometry of the numerical model used to carry on analysis with bricks of 26x26 cm is depicted. With this kind of geometry it was not possible to keep constant the length and the height of the spandrel with the values of 1.5 and 0.8 m. Furthermore, in this model, the spandrel is formed only by three rows of bricks, because a fourth row would increase its height to 94 cm, rather different from the initial of 80 cm. For the same reason above-mentioned, it was also necessary to introduce a little modification in piers length.

#### Effect of the axial load

The force-deformation relationship of these analysis are shown in figures 5.29 and 5.30. Observing this figure, differently from the models with the original

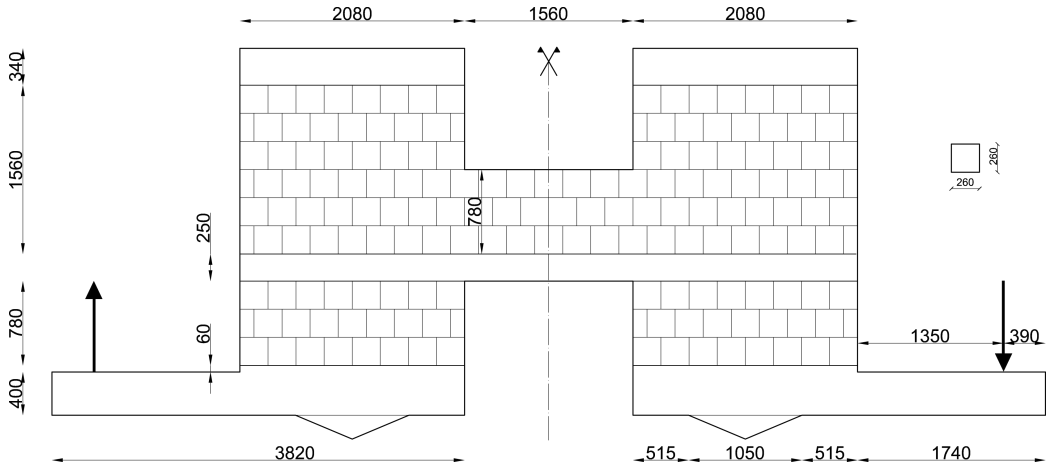


Figure 5.28: Bricks 26x26 cm: model geometry

bricks geometry, a flexural mechanism develops already for an axial stress of 0.4 MPa. However, no increase in shear capacity are recorded for axial stress superior of 0.5 MPa.

### Analysis of the results

The comparison between the numerical results and the analytical equations proposed is in figure 5.31. As it is possible to see, the rocking mechanism is well captured, whereas the shear capacity is little underestimated by flexural failure mechanism proposed.

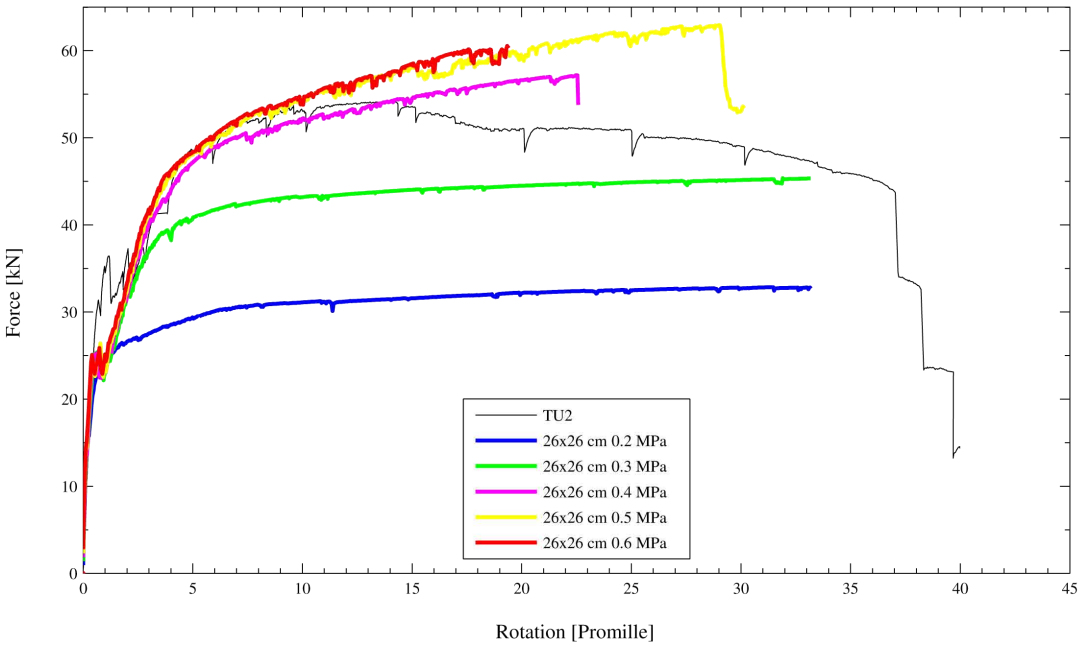


Figure 5.29: Force-deformation relationship of the spandrel made of bricks 26x26 cm

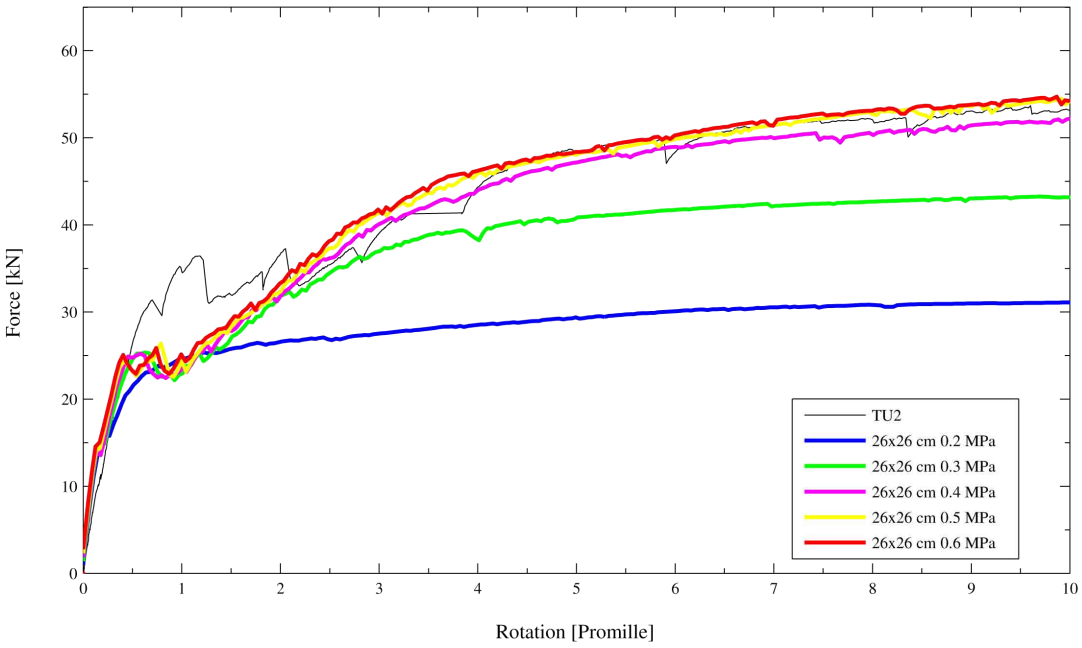


Figure 5.30: Force-deformation relationship of the spandrel made of bricks 26x26 cm, up to a drift of 1%

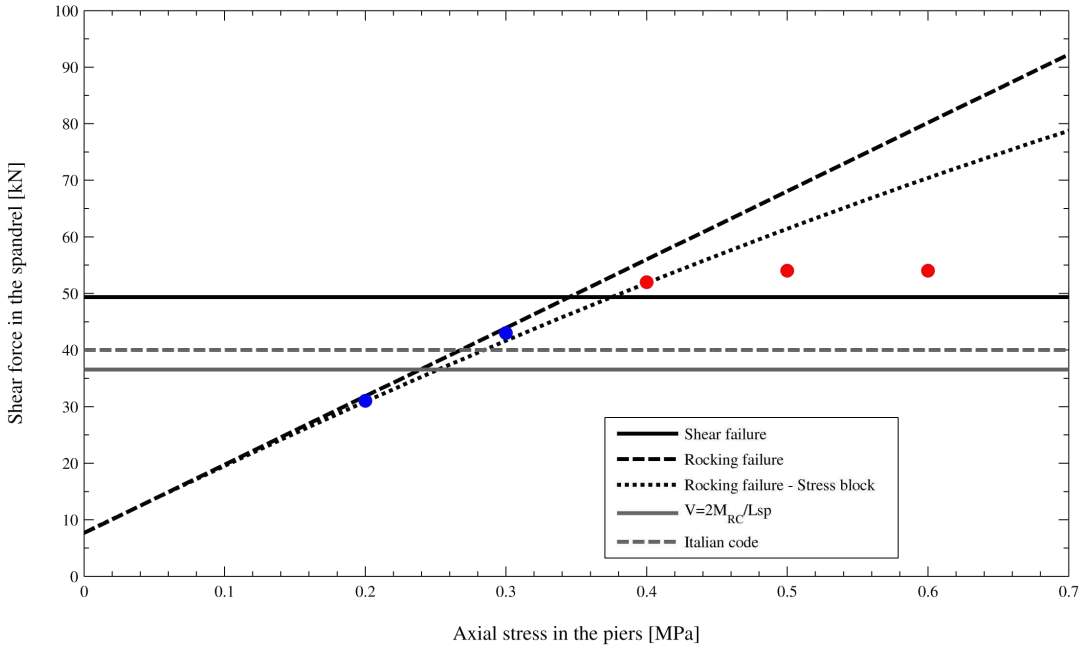


Figure 5.31: Bricks 26x26 cm: Effect of axial load in composite spandrel shear capacity - Analytical and numerical models comparison.

### 5.5.2 Bricks 50x20 cm

#### Description of the model

In figure 5.32 the geometry of the numerical model used to carry on analysis with bricks of 50x20 cm is shown. With this kind of geometry was possible to keep the length of the spandrel at 1.5 m, but the piers are a little shorter, they are, in fact, 2.0 m long. In this case, differently from the 26x26 cm model, it was possible to keep constant the height of the spandrel at the value of 0.8 m which was formed by four rows of bricks.

#### Effect of the axial load

In these models rocking behaviours develop up to axial stress of 0.5 MPa. Only for an axial stress of 0.6 MPa a flexural mechanisms starts to trigger. As for the other models, many convergence problems occurred in presence of flexural mechanisms. However, in this case the convergence was not found before that a drift value of 1% was reached, therefore it is not possible to

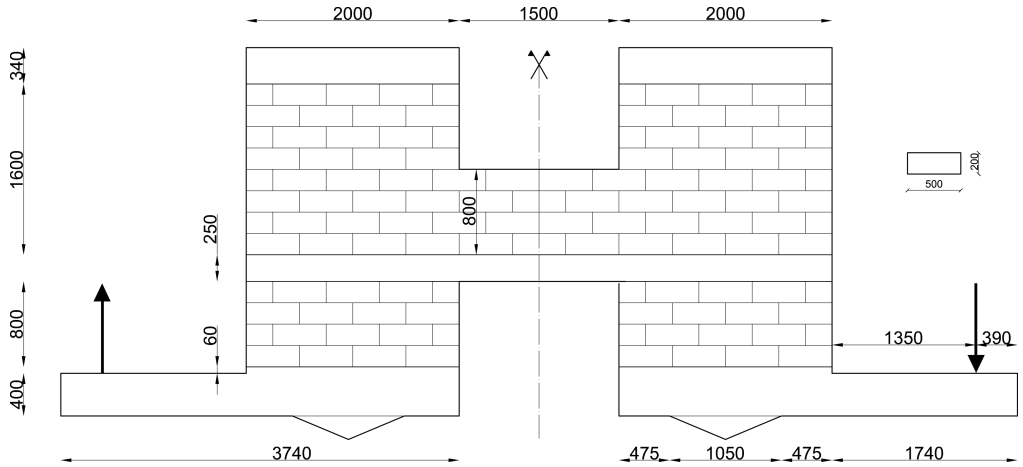


Figure 5.32: Bricks 50x20 cm: model geometry

determine a shear capacity as for the previous models.
Still, for an axial stress of 0.6 MPa, the result obtained is reliable, but the one for an axial stress 0.7 MPa is not.

### Analysis of the results

The comparison between the numerical results and the analytical equations proposed is in figure 5.35. It is observed that the rocking mechanism is rather well predicted, whereas, the equation for the flexural mechanism strongly overestimates the numerical results. Although, as said, when a shear mechanism developed many convergence problems occurred, the result obtained with the analytical model is maybe not reliable. This is probably due to the fact that, with this geometry, three bricks are enough (instead of the five required in the original model) to cover thoroughly the spandrel span. Therefore, if it is used equation 4.7 the slope of compressive strut in masonry would be really low, and it would almost pass through the whole length of the spandrel. This probably does not occur in reality. Therefore it would be more convenient to consider a certain limit in the reduction of the span of composite spandrel due to the presence of masonry. Studying all other analysis carried out it would be possible to say that, as first attempt, it could be possible to fix a maximum reduction of one half of spandrel length. However,

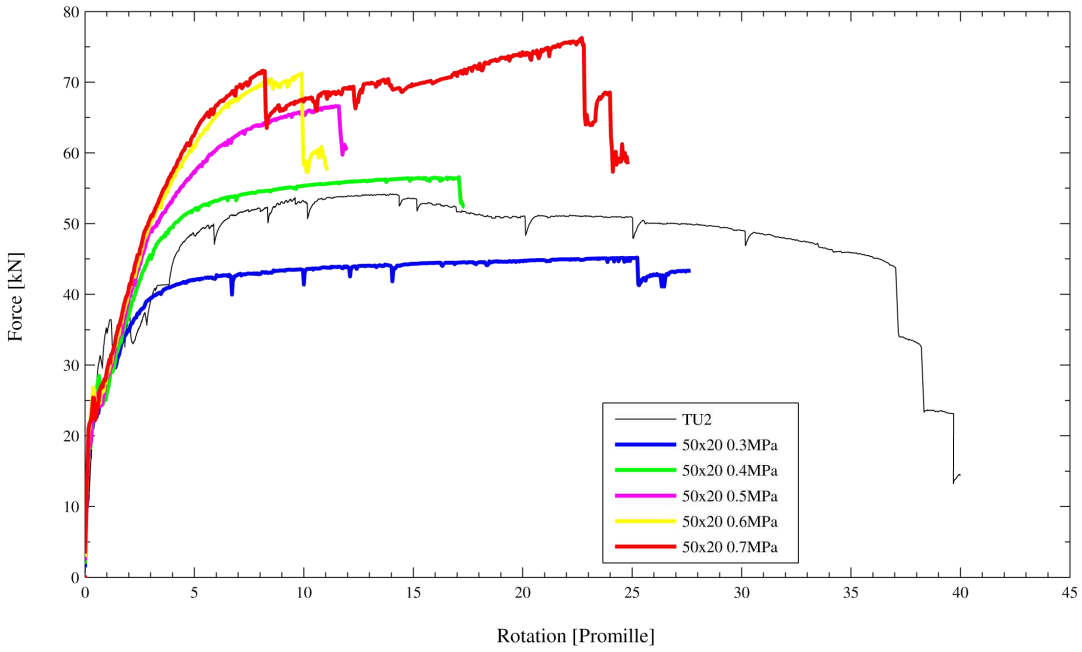


Figure 5.33: Force-deformation relationship of the spandrel made of bricks with length of 50 cm and height of 20 cm

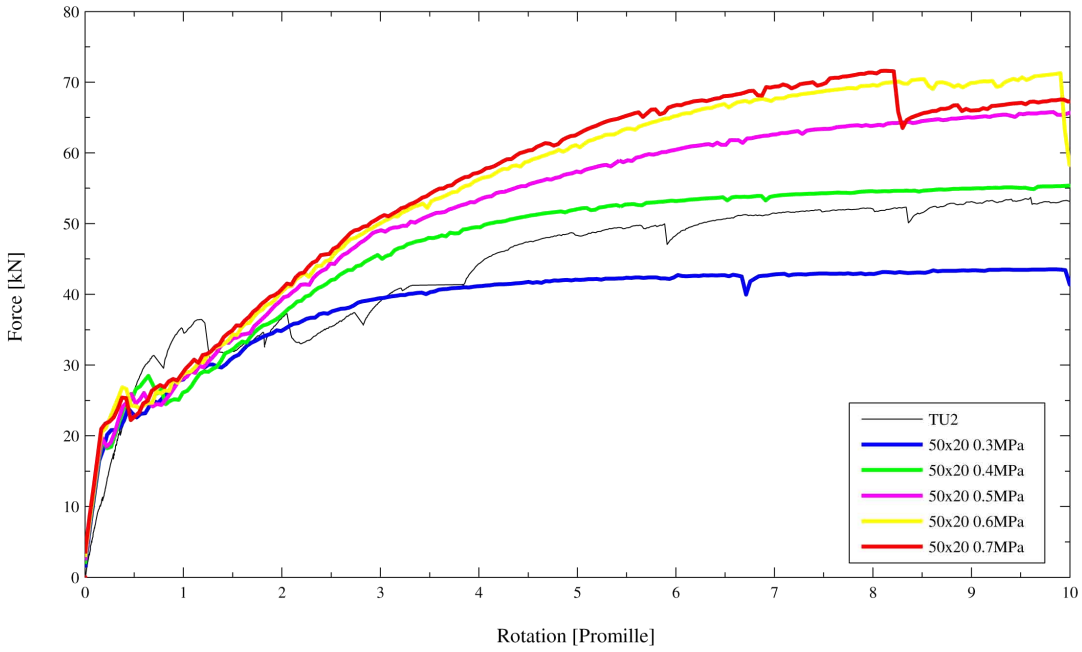


Figure 5.34: Force-deformation relationship of the spandrel made of bricks with length of 50 cm and height of 20 cm, up to a drift of 1%

not enough data are available to study this limit properly. Therefore, for the moment, it is possible to say that care must be taken if the bricks are rather long in comparison with spandrel length.

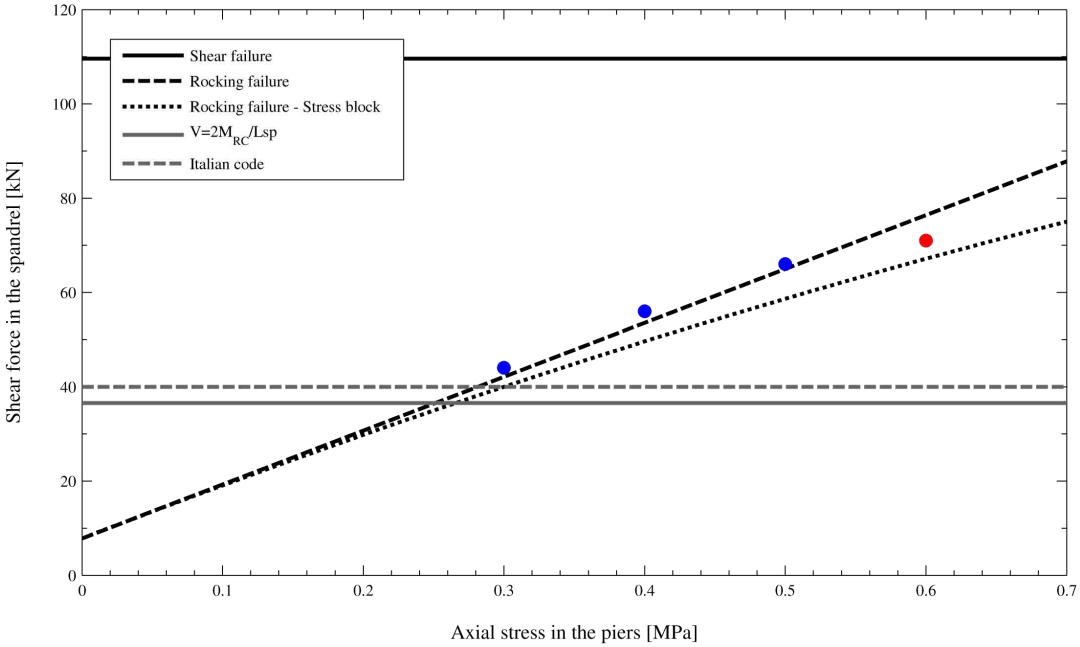


Figure 5.35: Bricks 50x20 cm: Effect of axial load in composite spandrel shear capacity - Analytical and numerical models comparison.

### 5.5.3 Bricks 50x26 cm

#### Description of the model

As for the model with bricks geometry of 50x20, also in this case it was possible to keep the spandrel length of 1.5 m, but it was not possible to keep the height of 0.8 m. In this model, in fact, the spandrel is formed by three rows of bricks and its height is 0.78 m. Differently from the previous model, in this case the piers are longer, having a length of 2.25 m. All the geometric characteristics of the model are shown in figure 5.36.

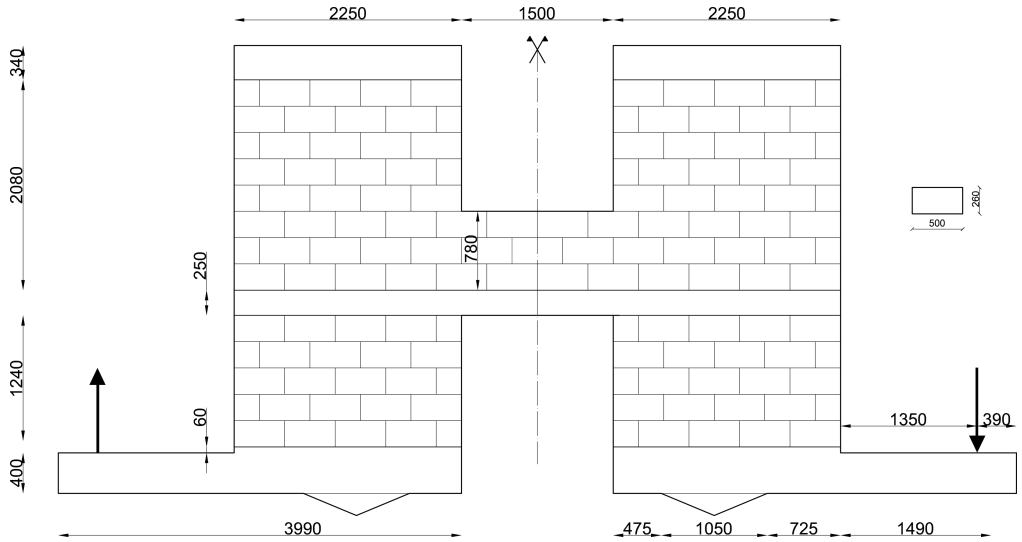


Figure 5.36: Bricks 50x26 cm: model geometry

#### Effect of the axial load

As for the models with 50x20 cm bricks, these models show rocking behaviours up to axial stress of 0.5 MPa. For axial stresses of 0.6 and 0.7 MPa, instead, flexural behaviour develop.

#### Analysis of the results

The comparison between the numerical results and the analytical equations proposed is in figure 5.39. In this case the rocking mechanism is better pre-

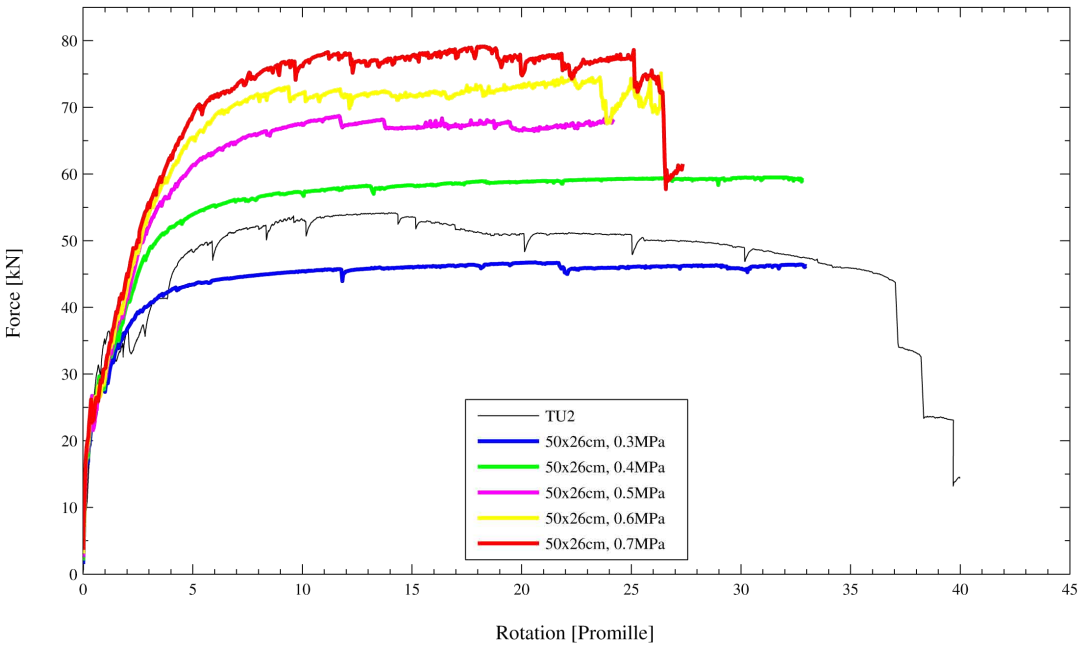


Figure 5.37: Force-deformation relationship of the spandrel made of bricks with length of 50 cm and height of 26 cm

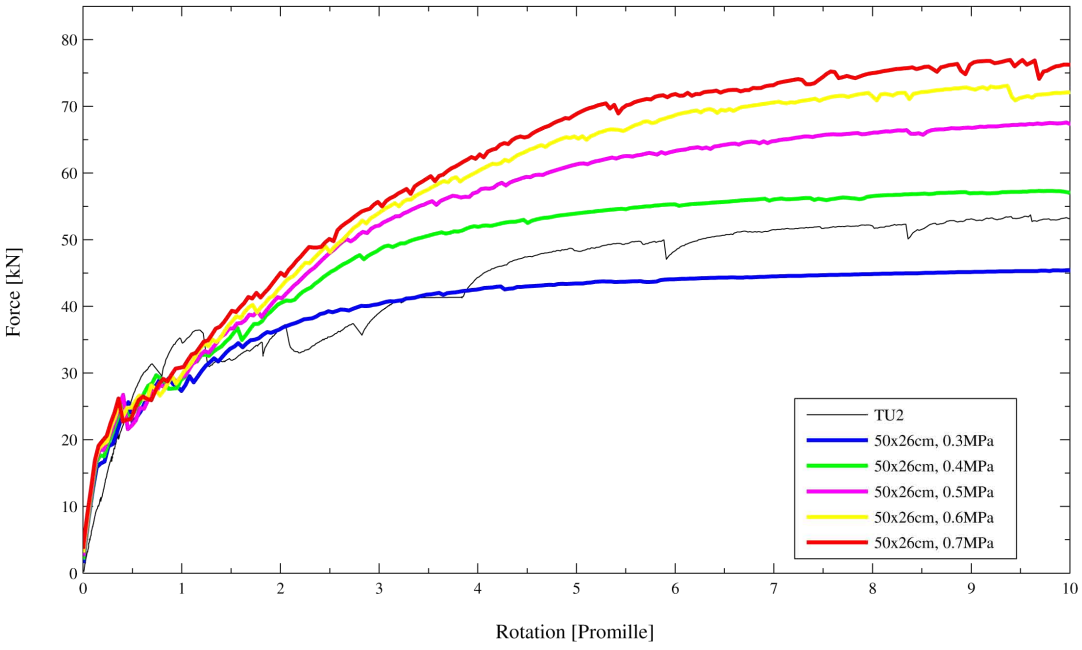


Figure 5.38: Force-deformation relationship of the spandrel made of bricks with length of 50 cm and height of 26 cm, up to a drift of 1%

dicted by the formulation that consider a stress block distribution underneath the RC beam. On the contrary of the models with geometry of the bricks of 50x20 cm, even if the bricks are long, the flexural failure is rather well predicted. This is probably due to the fact that, in this case the spandrel is formed by only three rows of bricks. Hence, the span of the spandrel is not strongly reduced due to the presence of masonry, as it happens for the model with bricks geometry of 50x20 cm (where there are four rows of bricks).

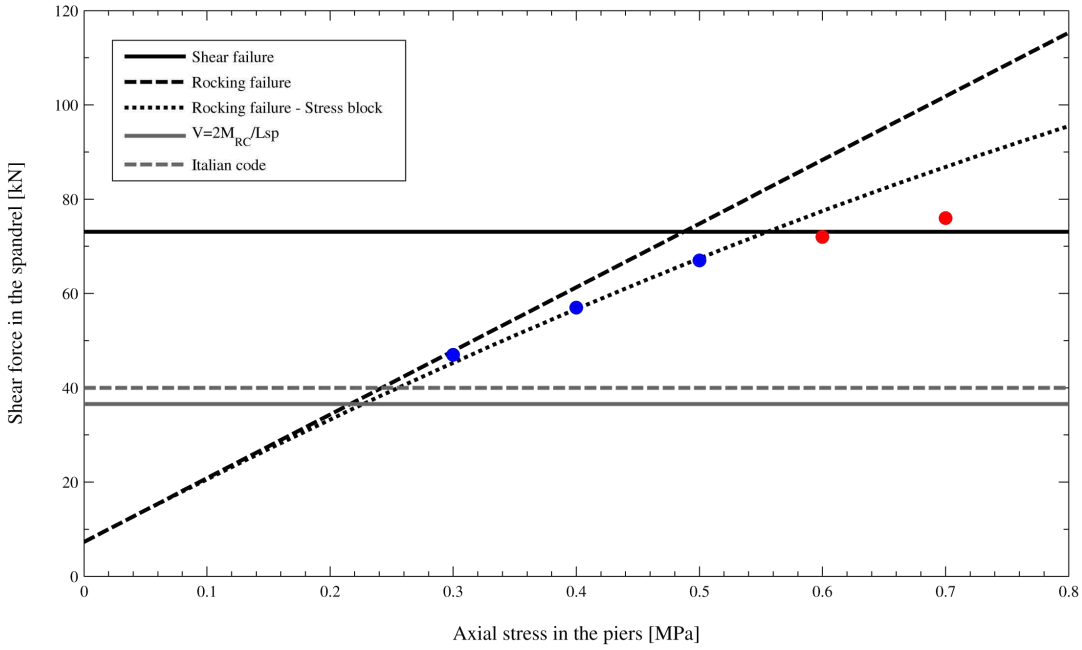


Figure 5.39: Bricks 50x26 cm: Effect of axial load in composite spandrel shear capacity - Analytical and numerical models comparison.

## 5.6 Summary of the results

The purpose of these analyses were to verify if there are correspondences in the results between the analytical and the numerical models.
As already explained in the third chapter, in the numerical model bricks have an elastic behaviour. Therefore, it is not possible to determine when the shear capacity of the composite spandrel reduces due to the presence of cracks in the masonry.
For this reason, as result of the numerical model, it has been chosen the shear acting in the composite spandrel for a drift demand of 1%. For this drift demand, in the experimental campaign, the specimens had already reached the peak strength. After this drift, in fact, the shear acting in the spandrel kept constant or started to decrease.

For each parameter studied the results obtained from the numerical model are compared with the equations proposed by the codes and in literature and with the equations discussed in the fourth chapter of this thesis.
As it has been shown, not to consider the presence of masonry underestimates the capacity of the composite spandrel.
Concerning the formulations proposed by the Italian code, features as the axial load in the piers and the height of the RC beam are not taken into account. Also the longitudinal reinforcement ratio has often not a relevant importance in those equations.
It has been proved, instead, that those parameters are rather important and influence deeply the force-deformation relationship and also the failure modalities.

In all parametric analysis carried out, there was a rather good correspondence between the numerical and analytical results. The widest differences among the two model appeared when the geometry of the bricks changed. However, this is only for the flexural mechanism. In fact, for the rocking one, even if the geometry of the bricks changes, the analytical and the numerical models show close results.

# Conclusions and outlook

As often underlined in this thesis, the mechanical behaviour of composite spandrels is still largely unknown. A great effort in this field has been made by the research of professor Katrin Beyer. In her research, experiments on masonry and composite spandrels were carried out. The experiments on composite spandrels were briefly described in the second chapter of this thesis. As said, a wider and more complete description of these experiments is in [BAD10].
From the results of that experimental campaign other articles were written, as [BD12] and [Bey12]. The last article is focused on masonry spandrels.
A first study on shear strength of composite spandrels and on their failure modalities is in [DB11].
This thesis would be included in this wider work of research. The aim of this thesis was to make a little contribution to this work, focusing on the stiffness and the shear capacity of composite spandrels.
For this reason, both numerical and analytical models were used. The analytical models consist in the equations proposed in the fourth chapter. The numerical model described in the third chapter had the aim to give a first validation of the equations proposed.
For this reason several parametric analysis were carried out. These analyses were described in the fifth chapter of this thesis. In the same chapter the results obtained from the numerical models were compared with equations proposed. In the next section there is a summary of those equations.
Concerning the shear strength two failure modalities (rocking and flexural-shear) were studied and also two kind of stiffness. An initial stiffness for very low drift demands and a cracked stiffness, valid up to the peak strength is reached.

## Composite spandrels stiffness and strength

In this thesis, equations were proposed in order to determine the shear capacity and the stiffness of composite spandrels. In figure 5 the idealized non-linear behaviour of a composite spandrel is depicted. As it has already explained in the fourth chapter, two kinds of stiffness were studied, the aim was to reproduce better the mechanical behaviour of composite spandrels. In fact, it was observed that until cracks are not open, the spandrel is rather stiff, and, for very low drift demands, half of the shear capacity is already exploited. When cracks start to open, both in the mortar joint and in the concrete of the RC beam, the stiffness clearly reduces. For this reason it has been named cracked stiffness.
The composite spandrel "works" with the cracked stiffness up to the peak strength is reached.

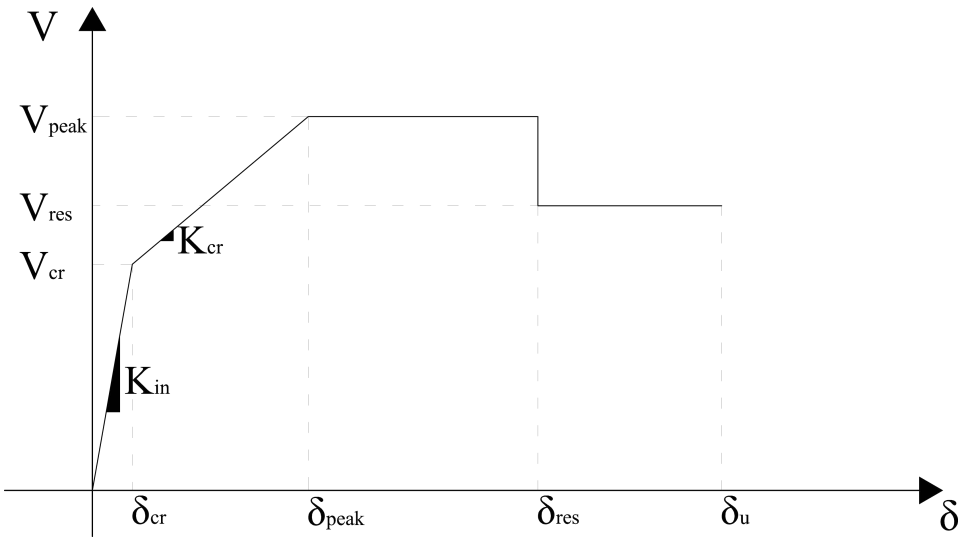


Figure 5: Idealized non-linear behaviour of composite spandrels.

During the experiments two main failure modalities were recorded. A rocking and a flexural-shear failure (the two modalities were detailed in the fourth chapter). The equations that allow to determine the shear capacity are summarized in table 1. The shear capacity corresponds to the lowest value of the mechanism proposed.

| | |
|---|---|
| Flexural failure | $V_{SP} = \dfrac{M_{pos} + M_{neg}}{L_{SP} - \frac{L_{bricks} h_{sp}}{2 h_{bricks}}}$ |
| Rocking failure | $V_{SP} = \dfrac{\frac{N_{pier} L_{pier}}{2} + M_{neg}}{L_{SP} + L_{pier}}$ |
| Rocking failure (stress block) | $V_{SP} = \dfrac{\frac{N_{pier} L_{gap}}{2} + M_{neg}}{L_{SP} + \frac{L_{pier}}{2} + \frac{L_{gap}}{2}}$ |

Table 1: Equations proposed to determine the shear capacity of composite spandrels

Where:

| | |
|---|---|
| $h_{bricks}$ | Height of the bricks; |
| $h_{SP}$ | Height of the spandrel; |
| $L_{bricks}$ | Length of the bricks; |
| $L_{gap}$ | Length of the gap between the RC beam and the pier underneath; |
| $L_{pier}$ | Length of the piers; |
| $L_{SP}$ | Length of the spandrel; |
| $M_{neg}$ | Nominal moment capacity for a negative bending; |
| $M_{pos}$ | Nominal moment capacity for a positive bending; |
| $N_{pier}$ | Axial force in the piers. |

The value $V_{peak}$ of the graph in figure 5 corresponds to the lowest value that come out from the equations proposed for the failure mechanisms. The value $V_{cr}$ is equal to $V_{peak}/2$. This because, in the experiments, when cracks started to open, already half of the shear capacity were exploited.

Those equations predict well the shear capacity recorded both in the experiments and in the numerical simulations. Rather wide differences, however, were recorded in the analyses where the geometry of the bricks were changed.

This was noticed for the flexural mechanism, as it is possible to see in figure 5.35. The basic idea of the flexural mechanism equation is that the masonry above RC beam reduces its effective span. However, it has to be fixed a maximum limit of this reduction. In fact, for long bricks, it could bring to unreliable results. There is not the availability of experimental data to determine the limit of this reduction. From the data obtained from the numerical analysis, as first attempt, it could be fixed a maximum reduction of the span of 1/2 of the initial length. This value, however, need to be subjected to further research.

The equations proposed to calculate the stiffness of composite spandrels are summarized in table 2.

| | | |
|---|---|---|
| Initial stiffness | $K_{s,in} = \frac{G_{m,hor} A_m}{1.2 L_{SP}}$ | $K_{f,in} = \frac{12 E_c I_c}{L_{SP}^3}$ |
| Cracked stiffness | $K_{s,cr} = 0.4 \frac{G_{m,hor} A_m}{1.2 L_{SP}}$ | $K_{f,cr} = \frac{12 (EI)_{cr}}{L_{SP}^3}$ |

Table 2: Equations proposed to determine the stiffness of composite spandrels

Where:

| | |
|---|---|
| $A_m$ | Area of the gross section of the masonry; |
| $E_c$ | Modulus of elasticity of the concrete; |
| $(EI)_{cr}$ | Cracked flexural stiffness of a RC beam cross section; |
| $G_{m,hor}$ | Shear modulus of the masonry in horizontal direction; |
| $I_c$ | Inertia modulus of the gross section of the RC beam; |
| $K_{f,in}$ | Initial flexural stiffness of the composite spandrel; |
| $K_{f,cr}$ | Cracked flexural stiffness of the composite spandrel; |
| $K_{s,in}$ | Initial shear stiffness of the composite spandrel; |
| $K_{s,cr}$ | Cracked shear stiffness of the composite spandrel. |

In order to determine $(EI)_{cr}$, the procedure suggested in [PCK07] is followed. There, it is suggested to calculate the stiffness from the nominal flexural capacity of the RC beam and the yielding curvature, as shown in next equation.

$$(EI)_{cr} = \frac{M_N}{\phi_y}$$

It is an iterative procedure and in the Annexe A the Matlab script used to calculate that stiffness is shown.

Since these relationship are linear, it is simple to determine the displacement $\delta_{cr}$ as:

$$\delta_{cr} = \frac{V_{cr}}{K_{in}}$$

where

$$K_{in} = (K_{f,in}^{-1} + K_{s,in}^{-1})^{-1}$$

The displacement $\delta_{peak}$, therefore, would have value:

$$\delta_{peak} = \delta_{cr} + \frac{V_{peak} - V_{cr}}{K_{cr}} = \delta_{cr} + \frac{V_{peak}}{2K_{cr}}$$

And, similarly to the initial stiffness, the cracked stiffness has value:

$$K_{cr} = (K_{f,cr}^{-1} + K_{s,cr}^{-1})^{-1}$$

# Further research

The bricks in the model behaved in the elastic field, therefore it was not possible to study the post-peak behaviour of the composite spandrel. It would have great interest to develop a model with bricks that present an inelastic behaviour in order to study:

- The value of the displacement when the shear strength starts to decrease ($\delta_{res}$). Namely, it could be when bricks crack and the major part of the shear is carried by the RC beam alone.
- The ultimate drift of composite spandrels ($\delta_u$).

Once completed the study on the force-deformation relationship that model could be implemented in an equivalent frame model approach (section 1.3.1).

In order to validate that model, the first analysis could be carried out comparing those results with the results obtained with the numerical model, developed in ATENA, of a whole masonry wall, by professor Katrin Beyer. That model is depicted in figure 6a) and it is described in detail in [BD08]. In figure 6b) the pushover curves for the cases of coupled and uncoupled piers are plotted. As expected, considering the coupling effect supplied by spandrels, both stiffness and shear strength increase.
This is another confirmation that spandrels coupling effect should not be neglected.
However, to carry out analyses with this numerical model it is required a huge amount of time, even days. Therefore, this approach is not suitable for engineering applications.

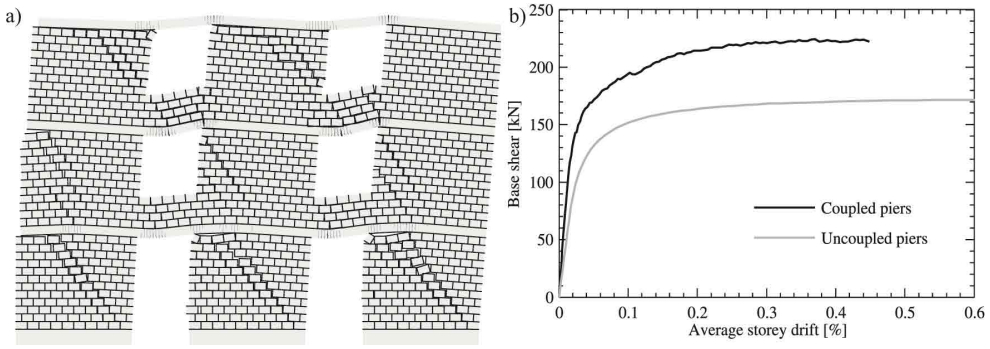


Figure 6: Deformed shape of the URM wall at an average storey drift of $\theta = 0.4\%$ (a, displacements are magnified by a factor of 20) and pushover curve of the URM wall in comparison to the pushover curve of uncoupled piers (b) (from [BAD10] p.4).

In this context the study of masonry and composite spandrel is inserted. In fact, once completed the study on their mechanical behaviour it would be possible to develop an equivalent frame model for masonry walls that takes into account the peculiarities of the spandrels. This approach, on the contrary of complex FEM models is more suitable for engineering purposes.

# Annexe A

## Iterative procedure to calculate the cracked flexural stiffness of an RC beam

Here the Matlab script used to calculate the cracked flexural stiffness of an RC beam cross section $(EI)_{cr}$ is reported. The values used are valid for TU2 reinforcement.

Geometry

```
Hc = 250;       % RC beam Height [mm]
d = Hc - 30;    % RC beam Height - concrete cover [mm]
dcompr = 30;    % Top cover [mm]
Bc = 200;       % RC beam thickness [mm]\\
Ac = Hc*Bc;     % RC beam area [mm^2]
Bm = 200;       % Masonry thickness [mm]
Hm = 800;       % Masonry Height [mm]
Am = Hm*Bm;     % Masonry area [mm^2]
```

Concrete and masonry mechanical properties

```
Ec = 31000;     % Concrete E-modulus [MPa]
fc = 30;        % Concrete compressive strength [MPa]
Emhor = 1840;   % Masonry horizontal E-modulus [MPa]
ni = 0.2;       % Masonry Poisson ratio [-]
Gm = Emhor/(2*(1+ni)); % Masonry shear modulus [MPa]
```

*ANNEXE A*

Reinforcement mechanical properties

```
As = 226;      % reinforcement area [mm^2]
Asc = 226;     % compressed - reinforcement area [mm^2]
fy = 540;      % Reinforcement tensile strength [MPa]
Es = 206000;   % Reinforcement E-modulus [MPa]
```

**PROCEDURE TO CALCULATE THE CRACKED STIFFNESS**

**Case 1 Reinforcement strain = 1.5%**

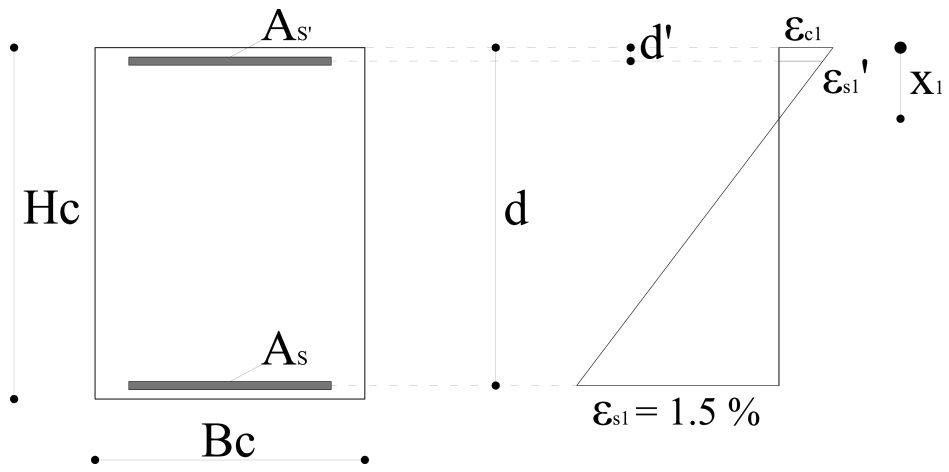


Figure 7: Case 1: Tensile reinforcement strain = 1.5%

With the assumption of plane deformed cross section it is possible to write:

$$\varepsilon_{c1} = \varepsilon_{s1}\frac{x_1}{d - x_1}; \varepsilon_{s'1} = \varepsilon_{s1}\frac{x_1 - d'}{x_1}$$

Matlab script.

```
delta1=100;
x1=d/4;   % Starting value for the neutral axis [mm]
```

```
while delta1 > 0.1

eps_reinf_1 = 0.015; % Case 1) reinforcement strain is fixed
= 1.5% [-]
esp_c1 = eps_reinf_1*x1/(d-x1); % concrete strain [-]
eps_reinf_compr1 = esp_c1*(x1-dcompr)/x1;  % compressed
reinforcement strain [-]

Sst1 = As*fy; % Reinforcement tensile force [N]
Ssc1 = eps_reinf_compr1*Es*Asc;   % Reinforcement compressive
force [N]

x1eq = (Sst1-Ssc1)/(0.8*Bc*fc); % Neutral axis position after
equilibrium condition [mm]

delta1 = abs(x1eq-x1);  % Difference between first value and
equilibrium result [mm]

memo1 = x1;
x1 = x1eq;

end

x1 = memo1;

if x1/d < 0.05;     % To check if x/d value is correct
disp('Error!!! x/d < 0.05!!!')
   end

Mu1 = (0.8*Bc*x1eq*fc)*(d-0.4*x1eq)+((eps_reinf_compr1*Es*Asc*(d-dcompr)));
%Nominal moment capacity for a reinforcement strain of 1.5% [N*mm]
curv1 = (eps_reinf_1+esp_c1)/d;   %Curvature [1/mm]
```

**Case 2 Concrete strain = 0.4%**

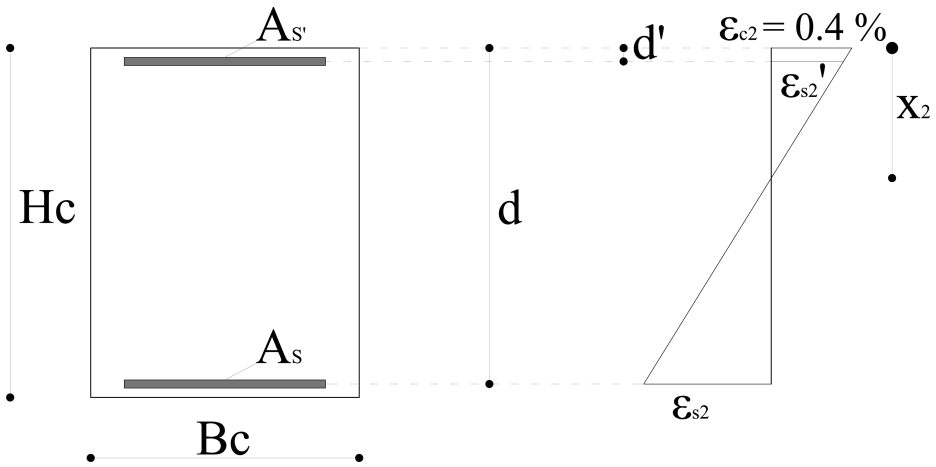


Figure 8: Case 2: Concrete strain = 0.4%

With the assumption of plane deformed cross section it is possible to write:

$$\varepsilon_{s2} = \varepsilon_{c1}\frac{x_2}{d - x_2}; \varepsilon_{s'2} = \varepsilon_{c1}\frac{x_2 - d'}{d - x_2}$$

Matlab script.

```
delta2=100;
x2=1;          % Starting value for the neutral axis [mm]

while delta2 > 0.1

esp_c2 = 0.004; % Case 2) concrete strain is fixed = 0.4% [-]
eps_reinf_2 = esp_c2*(d-x2)/x2;  % reinforcement strain [-]
eps_reinf_compr2 = esp_c2*(x2-dcompr)/x2; % compressed
reinforcement strain [-]

Sst2 = As*fy;  % Reinforcement tensile force [N]
Ssc2 = eps_reinf_compr2*Es*Asc; % Reinforcement compressive
```

```
force [N]

x2eq = (Sst2-Ssc2)/(0.8*Bc*fc);  % Neutral axis position
after equilibrium condition [mm]

delta2 = abs(x2eq-x2);  % Difference between first value
and equilibrium result [mm]

x2 = x2+0.1;

end

x2 = x2-0.1;   % Neutral axis position [mm]

if x2/d < 0.05;
disp('Error!!! x/d < 0.05!!!')
    end

Mu2 = (0.8*Bc*x2eq*fc)*(d-0.4*x2eq)+((eps_reinf_compr2*
Es*Asc*(d-dcompr)));  %Nominal moment capacity for a
reinforcement strain of 1.5% [N*mm]
curv2 = (eps_reinf_2+esp_c2)/d;    %Curvature [1/mm]

if abs(x1eq-x2eq)>50    %It is a check of the position
of the neutral axis with the two methods
disp ('Warning! The difference in the position of the neutral
axis with the two method is more than 50mm, check if their
positions are as expected!')

   end
```

*ANNEXE A*

RC beam cracked stiffness (Priestley's formulation)

```
if curv1 < curv2;
    EIcr = Mu1/curv1;
else
     EIcr = Mu2/curv2;
end
```

# Bibliography


[And05] T. L. Anderson. *Fracture Mechanics - Fundamentals and applications*. Taylor and Francis group, New York, USA, 2005.

[BAD10] K. Beyer, A. AboElEzz, and A. Dazio. Quasi-static cyclic tests on different types of masonry spandrels. Technical report, Swiss Federal Institute of Technology, Zurich, Switzerland, 2010.

[BD08] K. Beyer and A. Dazio. Analysis of coupled masonry walls. Technical report, Swiss Federal Institute of Technology, Zurich, Switzerland, 2008.

[BD11] K. Beyer and A. Dazio. Modelling of spandrels elements in URM structures with slabs or ring beams. In *Proceedings of the 11th North American Masonry Conference*, Minneapolis, Minnesota, USA, 2011.

[BD12] K. Beyer and A. Dazio. Quasi-static monotonic and cyclic tests on composite spandrels. *Earthquake Spectra, vol. 28, num. 3, p. 885-906*, 2012.

[Bel41] O. Belluzzi. *Scienza delle Costruzioni - Volume Primo*. Zanichelli, Bologna, Italy, 1941.

[Bey12] K. Beyer. Peak and residual strenghts of brick masonry spandrels. *Engineering structures, vol. 41, p. 533-547*, 2012.

[BGL98] A. Brencich, L. Gambarotta, and S. Lagomarsino. A macroelement approach to the three-dimensional seismic analysis of ma-

sonry buildings. In *Proceedings of the Eleventh European Conference on Earthquake Engineering*, Paris, France, 1998.

[BP09] L. Boscotrecase and F. Piccaretta. *Edifici in muratura in zona sismica*. Dario Flaccovio Editore, Palermo, Italy, 2009.

[CEN04a] *CEN, "Eurocode 6 - Design of concrete structures - Part 1-1: General rules and rules for buildings"*. Brussels, Belgium, 2004.

[CEN04b] *CEN, "Eurocode 8: Design of structures for earthquake resistance, Part 1: General rules, seismic actions and rules for buildings"*. Brussels, Belgium, 2004.

[CEN05] *CEN, "Eurocode 2 - Design of concrete structures - Part 1-1: General rules for reinforced and unreinforced masonry structures"*. Brussels, Belgium, 2005.

[CJ12a] V. Cervenka and L. Jendele. *Atena – Computer Program for Nonlinear Finite Element Analysis of Reinforced Concrete Structrues - Program documentation, Part 1 - Theory*. Cervenka Consulting Ltd., Prague, Czech Republic, 2012.

[CJ12b] V. Cervenka and L. Jendele. *Atena – Computer Program for Nonlinear Finite Element Analysis of Reinforced Concrete Structrues - Program documentation, Part 2-1 - User's Manual for ATENA 2D*. Cervenka Consulting Ltd., Prague, Czech Republic, 2012.

[CJ12c] V. Cervenka and L. Jendele. *Atena – Computer Program for Nonlinear Finite Element Analysis of Reinforced Concrete Structrues - Program documentation, Part 3-1 - Example manual ATENA Engineering*. Cervenka Consulting Ltd., Prague, Czech Republic, 2012.

[CJ12d] V. Cervenka and L. Jendele. *Atena – Computer Program for Nonlinear Finite Element Analysis of Reinforced Concrete Structrues - Program documentation, Part 6 - ATENA Input File Format*. Cervenka Consulting Ltd., Prague, Czech Republic, 2012.

[DB11] A. Dazio and K. Beyer. Experimental investigation of the effect of the longitudinal reinforcement content of ring beams on the cyclic behavior of masonry spandrels. In *Proceedings of the 11th North American Masonry Conference*, Minneapolis, Minnesota, USA, 2011.

[DM:81] *Decreto Ministero dei Lavori Pubblici 2 luglio 1981, "Normativa per le riparazioni ed il rafforzamento degli edifici danneggiati dal sisma nelle regioni Basilicata, Campania e Puglia".* Rome, Italy, 1981.

[FMMC09] S. Frumento, G. Magenes, P. Morandi, and G.M. Calvi. *Interpretation of experimental shear tests on clay brick masonry walls and evaluation of q-factors for seismic design.* IUSS Press, Pavia, Italy, 2009.

[Fre98] S. A. Freeman. Development and use of capacity spectrum method. In *Proceedings of the 6th US NCEE Conference on Earthquake Engineering*, Seattle, Washington, USA, 1998.

[Gug02] A. Gugliotta. *Elementi finiti.* Otto editore, Politecnico di Torino, Italy, 2002.

[Lan02] K. Lang. Seismic vulnerability of existing buidings. Technical report, Swiss Federal Institute of Technology, Zurich, Switzerland, 2002.

[Lou94] P. B. Lourenço. Analysis of masonry structures with interface elements. Technical report, Delft University of Technology, Delft, 1994.

[Lou96] P. B. Lourenço. Computational strategies for masonry structures. Technical report, Delft University of Technology, Delft, 1996.

[Mag00] G. Magenes. A method for pushover analysis in seismic assessment of masonry buildings. In *Proceedings of the 12th Word*

*Conference on Earthquake Engineering*, Auckland, New Zealand, 2000.

[Mag06] G. Magenes. Masonry building design in seismic areas: recent experiences and prospects form a european standpoint. In *Proceedings of the First European Conference on Earthquake Engineering and Seismology*, Geneva, Switzerland, 2006.

[Man12] S. Mangalathu. Force-deformation characteristics masonry spandrels with shallow arches. Master's thesis, Pavia, Italy, 2012.

[MBD09] G. Milani, K. Beyer, and A. Dazio. Upper bound limit analysis of meso-mechanical spandrel models for the pushover analysis of 2d masonry frames. *Engineering structures, vol.31, p.2696-2710*, 2009.

[MC97] G. Magenes and G. M. Calvi. In-plane seismic response of brick masonry walls. *Earthquake Engineering and Structural Dynamics, vol.26, p.1091-1112*, 1997.

[NTC08] *NTC, "Norme tecniche delle costruzioni"*. Rome, Italy, 2008.

[OPC03] *OPCM 3274, "Primi elementi in materia di criteri generali per la classificazione sismica del territorio nazionale e di normative tecniche per le costruzioni in zona sismica, allegato 2: Norme tecniche per il progetto, la valutazione e l'adeguamento sismico degli edifici".* Rome, Italy, 2003.

[PCK07] M.J.N. Priestley, G.M. Calvi, and M.J. Kowalsky. *Displacement-Based Seismic Design of Structures*. IUSS Press, Pavia, Italy, 2007.

[Poz72] P. Pozzati. *Teoria e Tecnica delle Strutture - Preliminari e Fondamenti*. Unione Tipografico-Editrice Torinese, Torino, Italy, 1972.

[PP92] T. Paulay and M.J.N. Priestley. *Seismic design of reinforced concrete and masonry structures*. John Wiley and sons, New York, USA, 1992.

[Pri03] M.J. N. Priestly. *Myths and Fallacies in Earthquake Engineering.* DIUSS Press, Pavia, Italy, 2003.

[SR11] R. Sabatino and G. Rizzano. A simplified approach for the seismic analysis of masonry structures. *The Open Construction and Building Technology Journal, vol. 5, (Suppl 1-M7) p. 97-104*, 2011.

[Sul13] T. Sullivan. Numerical models for non-linear behavior of structures, 2013. Bologna University, Master Course in Civil Engineering , Earthquake Engineering seminar.

[Tim56] S. Timoshenko. *Strenght of Materials.* D.Van Nostrand Company, Princeton, New Jersey, USA, 1956.

[Tom99] M. Tomaževič. *Earthquake-Resistant Design of Masonry Buildings.* Imperial college press, London, UK, 1999.

[Vio92a] E. Viola. *Scienza delle Costruzioni - Teoria dell'Elasticità.* Pitagora editrice, Bologna, Italy, 1992.

[Vio92b] E. Viola. *Scienza delle Costruzioni 3 - Teoria della Trave.* Pitagora editrice, Bologna, Italy, 1992.

[Vio93] E. Viola. *Esercitazioni di Scienza delle Costruzioni 1 - Strutture isostatiche e geometria delle masse.* Pitagora editrice, Bologna, Italy, 1993.

# List of symbols and acronyms

| Symbol | Units | Description |
|---|---|---|
| $A'$ | $[m^2]$ | Area of a cross section of a beam including the shear factor |
| $A_c$ | $[m^2]$ | Area of the RC beam cross section |
| $A_{gt}$ | [-] | Percentage total elongation at maximum force |
| $A_m$ | $[m^2]$ | Area of the gross section of the masonry of composite spandrel |
| $A_{reinf}$ | $[m^2]$ | Area of reinforcement in a RC beam cross section |
| $A_s$ | $[m^2]$ | Area of the bottom longitudinal reinforcement of a RC beam |
| $A'_s$ | $[m^2]$ | Area of the top longitudinal reinforcement of a RC beam |
| $B_c$ | $[m]$ | Width of a RC beam |
| c | [MPa] | Cohesion of the mortar |
| $D*$ | [m] | Reinforcement bar with diameter of * mm |
| $d$ | [m] | Effective depth of a RC beam |
| $d'$ | [m] | Top longitudinal reinforcement - Top side of a RC beam distance |
| $d_{eff}$ | [m] | Effective diameter of the reinforcement bars |
| $d_{eff}$ | [m] | Effective diameter of the reinforcement bars |
| $d_{nom}$ | [m] | Nominal diameter of the reinforcement bars |
| $d_s$ | [m] | Distance between two stirrups |
| $E$ | [MPa] | Modulus of elasticity |
| $E_{bx}$ | [MPa] | Modulus of elasticity of the bricks in x-direction |
| $E_{by}$ | [MPa] | Modulus of elasticity of the bricks in y-direction |
| $E_c$ | [MPa] | Modulus of elasticity of the concrete |

| | | |
|---|---|---|
| $E_{mx}$ | [MPa] | Modulus of elasticity of the masonry in x-direction |
| $E_{my}$ | [MPa] | Modulus of elasticity of the masonry in y-direction |
| $E_{piers}$ | [MPa] | Modulus of elasticity of the elements that constitute the piers |
| $E_s$ | [MPa] | Modulus of elasticity of the reinforcement bars |
| $f_c$ | [MPa] | Compressive strength |
| $f_{cm}$ | [MPa] | Compressive strength of the mortar |
| $f_{ctm}$ | [MPa] | Tensile strength of the mortar |
| $f_{c,bx}$ | [MPa] | Compressive strength of the bricks in x-direction |
| $f_{c,by}$ | [MPa] | Compressive strength of the bricks in y-direction |
| $f_{c,cube}$ | [MPa] | Cube strength of the concrete |
| $f_{c,t}$ | [MPa] | Tensile strength of the concrete |
| $f_{hd}$ | [MPa] | Masonry design compression strength in horizontal direction |
| $f_{mx}$ | [MPa] | Compressive strength of the masonry in x-direction |
| $f_{my}$ | [MPa] | Compressive strength of the masonry in y-direction |
| $f_t$ | [MPa] | Tensile strength |
| $f_{t,dyn}$ | [MPa] | Dynamic tensile stress of the reinforcement bars |
| $f_{t,stat}$ | [MPa] | Static tensile stress of the reinforcement bars |
| $f_{tb}$ | [MPa] | Tensile strength of the bricks |
| $f_{vd0}$ | [MPa] | Shear design strength in absence of compression stress |
| $f_y$ | [MPa] | Yielding stress |
| $f_{y,dyn}$ | [MPa] | Dynamic yield stress of the reinforcement bars |
| $f_{y,stat}$ | [MPa] | Static yield stress of the reinforcement bars |
| $G$ | [MPa] | Shear modulus |
| $G_{m,hor}$ | [MPa] | Shear modulus of the masonry in horizontal direction |
| $h_{bricks}$ | [m] | Height of the bricks |
| $H_c$ | [m] | Height of a RC beam |
| $h_{cp}$ | [m] | Coupling beam height |
| $H_{el}$ | [m] | Height of a single four-node element |
| $H_{mas}$ | [m] | Height of the masonry of the composite spandrels |
| $H_p$ | [N] | Coupling beam tensile strength |
| $H_{RC}$ | [m] | Height of the RC beam of the composite spandrels |
| $H_{SP}$ | [m] | Height of the composite spandrels |

| | | |
|---|---|---|
| $h_{SP}$ | [m] | Height of the masonry of composite spandrel |
| $I$ | [$m^4$] | Moment of inertia of a beam cross section |
| $I_c$ | [$m^4$] | Moment of inertia of RC beam gross section |
| $K_f$ | [N/m] | Flexural stiffness of a beam |
| $K_{f,cr}$ | [N/m] | Cracked flexural stiffness of composite spandrel |
| $K_{f,in}$ | [N/m] | Initial flexural stiffness of composite spandrel |
| $K_{nn}$ | [N/$m^3$] | Atena model: normal stiffness of the interface element |
| $K_s$ | [N/m] | Shear stiffness of a beam |
| $K_{s,cr}$ | [N/m] | Cracked shear stiffness of composite spandrel |
| $K_{s,in}$ | [N/m] | Initial shear stiffness of composite spandrel |
| $K_{tot}$ | [N/m] | Total stiffness of a beam |
| $K_{tt}$ | [N/$m^3$] | Atena model: tangent stiffness of the interface element |
| $L_{bricks}$ | [m] | Length of the bricks |
| $L_{gap}$ | [m] | Length of the gap between the RC beam and the pier underneath |
| $L_{pier}$ | [m] | Length of the pier |
| $L_{pier,sd}$ | [m] | Length of the pier subjected to shear deformations |
| $L_{SP}$ | [m] | Length of the composite spandrels |
| $L_{Strut}$ | [m] | Distance of the positive plastic hinge from the pier |
| $L_{uncr}$ | [m] | Length of the pier underneath the RC beam without horizontal cracks |
| $M$ | [N·m] | Bending moment |
| $M_N$ | [N·m] | Nominal flexural capacity |
| $M_{neg}$ | [N·m] | Spandrel flexural strength for negative bending |
| $M_{pos}$ | [N·m] | Spandrel flexural strength for positive bending |
| $M_{RC}$ | [N·m] | RC beam flexural strength |
| $M_y$ | [N·m] | First yield bending moment |
| $M_{u,cp}$ | [N·m] | Coupling beam flexural strength |
| $N_{pier}$ | [N] | Axial load in the pier |
| $P$ | [N] | External load |
| $t$ | [m] | Thickness |
| $V_{cr}$ | [N] | Shear in the composite spandrel when $\delta_{cr}$ is reached |
| $V_f$ | [N] | Composite spandrel strength in case of flexural failure |
| $V_{peak}$ | [N] | Composite spandrel peak strength |

| | | |
|---|---|---|
| $V_s$ | [N] | Composite spandrel strength in case of shear failure |
| $V_{SP}$ | [N] | Composite spandrel shear strength |
| $V_{res}$ | [N] | Composite spandrel residual strength |
| $x$ | [m] | Position of the neutral axis |
| $x_1$ | [m] | Position of the neutral axis for the case of $\varepsilon_s = 1.5\%$ |
| $x_2$ | [m] | Position of the neutral axis for the case of $\varepsilon_c = 0.4\%$ |
| | | |
| $\delta$ | [m] | Displacement |
| $\delta_{cr}$ | [m] | Displacement of the composite spandrel when cracks open in the mortar joints |
| $\delta_{peak}$ | [m] | Displacement of the composite spandrel when the peak strength is reached |
| $\delta_{res}$ | [m] | Displacement of the composite spandrel when masonry crushes |
| $\delta_u$ | [m] | Ultimate displacement of the composite spandrel |
| $\varepsilon$ | [-] | Strain |
| $\varepsilon_c$ | [-] | Concrete strain |
| $\varepsilon_{inf}$ | [-] | Strain at the bottom of an element |
| $\varepsilon_{lim}$ | [-] | Strain limit |
| $\varepsilon_s$ | [-] | Strain of longitudinal reinforcements |
| $\varepsilon_s$ | [-] | Strain of the bottom longitudinal reinforcement of an RC beam |
| $\varepsilon_{s'}$ | [-] | Strain of the top longitudinal reinforcement of an RC beam |
| $\varepsilon_{sup}$ | [-] | Strain at the top of an element |
| $\theta$ | [-] | Average drift of the lever beams |
| $\theta_{pier*}$ | [-] | Drift of the pier * |
| $\nu$ | [-] | Poisson's ratio |
| $\nu_{bx}$ | [-] | Poisson's ratio of the bricks in x-direction |
| $\mu$ | [-] | Friction coefficient at the interface bricks - mortar |
| $\nu_{by}$ | [-] | Poisson's ratio of the bricks in y-direction |
| $\nu_{mx}$ | [-] | Poisson's ratio of the masonry in x-direction |
| $\sigma$ | [MPa] | Normal stress |
| $\sigma_{pier}$ | [MPa] | Normal stress in the pier |
| $\sigma_t$ | [MPa] | Rupture stress |

| | | |
|---|---|---|
| $\sigma_y$ | [MPa] | Yielding stress |
| $\tau_{max}$ | [MPa] | Peak shear stress at the interface bricks - mortar |
| $\tau_{res}$ | [MPa] | Residual shear stress at the interface bricks - mortar |
| $\phi$ | $[m^{-1}]$ | Curvature |
| $\phi'_y$ | $[m^{-1}]$ | Curvature at first yield |
| $\phi_y$ | $[m^{-1}]$ | Yielding curvature |
| $\chi$ | [-] | Shear factor |
| $\Delta_{SP}$ | [m] | Spandrel displacement |

## Acronyms

| | |
|---|---|
| EC* | Eurocode number * |
| ELF | Equivalent lateral force |
| FEM | Finite elements model |
| LS* | Load step number * |
| LVDT | Linear variable differential transformer |
| MRS | Modal analysis with response spectrum |
| NLTH | Non-Linear Time History analysis |
| RC | Reinforced concrete |
| SAM | Simplified Analysis of Masonry building |
| TU* | Test unit number * |
| URM | Unreinforced masonry |

# List of Figures

# List of Tables

# Acknowledgements

First of all, I would like to thank professor Katrin Beyer, without her this thesis would not exist. I strongly thank her for the time she spent with me, and for have given me the opportunity to participate to her researches and for the support she gave me also after my return to Bologna.
Thanks also to professors Diotallevi and Landi, for what they taught me and for have given me the possibility to develop my master thesis abroad. This experience has greatly enriched me.

Now I have a huge amount of people to thank. I hope you will excuse me for the extreme synthesis.

Thanks to all the guys of EESD and IBETON laboratories, you made me feel as in a big family. A special thank to Alessandro, for his advices and all the help he gave me. Thank also to Marie-Madeleine and all technicians of the Laboratory of Structural Engineering, for their courtesy and availability. Thank to all the people I had the chance to know in Lausanne. In particular, thanks to Robin, my first travelling comrade, and to Florian, I really don't know how I would managed without your help in my last weeks in Lausanne.

In the city with the "hips a little soft" I really have too much people to thank.

Thanks to Valeria, you know why. Thanks also to the former room-mates of the apartment $21^{st}$ of Ghigi. Every time I went to your apartment you made me feel as I was at home.

Thanks to all my colleagues, you are wonderful!
Thanks to Ube, arrived almost at the end of the path, but he enriched it with his experience.
Thanks to Lollo, and its ability to don't be always serious.
Thanks to Elena, for her straightforwardness. Sometimes it may seem a bit exaggerate, but I think it is a rare gift.
Thanks to Davide, for your kindness and for all nice talks had together. Hoping there will be many others.
Thanks to Charli, you know I'm looking forward the next "cigarette-break".
Thanks to Margherita, without you this thesis would not have this aspect!
Thanks to Marco, my favourite mechanician, to La Gio, La Fra, Andre, Fra and Tommi. It was a great group, now, at least for me, a bit less, but who knows what life will bring to us. Thanks also for the contrasts that happened. Also with them it is possible to grow.
Thanks to Chiara and Susi, to Ervis for his "size", to the Captain for its sympathy, to Giacomino and Minu for the laughs had together. Thanks also to all Candy Mountain group. I don't know if you believe it, but I think we are a great group, and it is hard to create something similar.
Thank to all the room-mate I had the pleasure to know, from Turati to Calori street passing through $21^{st}$ April street. Most of them I still have the fortune to have next to me. So thanks to Angelo and Adelina, also thanks to you I now feel at home.
Thanks to all "canicattinesi-bolognesi" (it is untranslatable!). You brought the warmth of our land in the north not always so hospitable. A special thank, of course, to Giovanni. He, as few people, knows the troubles we had in these years. I wish you a big good luck.

And, thanks to Bologna, of course!

Thanks to my colleagues from Catania University, where this adventure started. Thanks for the beautiful year I passed in that city. It was a great pleasure to know you.

Thanks to my closest friends, KingBobo, Alberto and Vicio. Well, you have been suffering me for more than ten years!
Thanks to Marco, Dino and all my friends of my home town. Thanks to all my fighting comrades, in particular to Gigi and my "brother" Diego. You were a datum point in these last years full of doubts.

Thanks to all people that, everyone with his manner, had gone along with me in these 25 years.

and at the end the most important thank to my family, for their unconditional support and for the awareness that, even if divided by the distance, they would have been. Always.

*Thank you. I mean it.*

# Ringraziamenti

Il primo ringraziamento vorrei dedicarlo alla professoressa Katrin Beyer, senza la quale questa tesi non sarebbe potuta esistere. La ringrazio vivamente per il tempo dedicatomi, per avermi permesso di partecipare alle sue ricerche e anche per tutto il supporto datomi a "distanza" dopo il mio ritorno a Bologna.
Grazie anche ai proff. Diotallevi e Landi per ciò che mi hanno insegnato, e per avermi dato la possibilità d'intraprendere un'esperienza all'estero che mi ha molto arricchito sia professionalmente che umanamente.

Ho adesso tantissimi ringraziamenti da fare, impossibili da riassumere in poche righe. Mi perdonerete quindi per l'estrema sintesi.

Grazie a tutti ragazzi dei laboratori EESD e IBETON, mi avete fatto sentire come in una grande famiglia. Un ringraziamento particolare ad Alessandro, grazie per i consigli e tutto l'aiuto che mi hai dato. Grazie anche a Marie-Madeleine e a tutti i tecnici del laboratorio d'Ingegneria strutturale del Politecnico di Losanna, per la loro cordialità e disponibilità. Grazie a tutte le persone che ho avuto la fortuna di conoscere a Losanna e in particolare a Robin, primo compagno di viaggio, e a Florian, non so come avrei potuto fare senza il tuo aiuto nel mio ultimo periodo losannese.

Nella città "dai fianchi un pò molli" ho veramente troppe persone da ringraziare.

Grazie a Valeria, sai perchè. Grazie anche all'ex appartemento 21 del Ghigi, ogni volta che venivo da voi mi avete fatto sentire come fossi a casa.

Grazie a tutti i miei compagni di facoltà, siete splendidi!
Grazie ad Ube, arrivato quasi alla fine del percorso, ma che lo ha arricchito con la sua esperienza.
Grazie a Lollo e il suo saper non prendersi sempre sul serio.
Grazie ad Elena, per la sua schiettezza, anche se certe volte può apparire esagerata credo sia comunque un dono raro.
Grazie a Davide, per la sua gentilezza, e per i tanti bei discorsi fatti in questi anni, sperando ce ne possano essere ancora altri.
Grazie a Charli, sai che non vedo l'ora di fare la prossima "pausa sigaretta".
Grazie a Margherita, senza di te la tesi non avrebbe questo aspetto!
Grazie a Marco, il mio meccanico di fiducia, alla Gio, alla Fra, ad Andre, a Fra e a Tommi. Un tempo grande gruppo, adesso, almeno per me, un pò meno, ma chissà cosa ci riserva la vita. Grazie anche per i contrasti che ci sono stati, perchè anche grazie ad essi si cresce.
Grazie a Chiara e a Susi, grazie ad Ervis, per la sua grossezza, al Capitano per la sua simpatia, a Giacomino e a Minu per tutte le risate fatte insieme.
E grazie a tutto il gruppo di Candy Mountain, non so se lo credete anche voi, ma io penso che siamo una cosa grandiosa ed è difficile riuscire a creare un tale affiatamento.
Grazie a tutti i numerosi coiquilini che ho avuto la fortuna di conoscere, da via Turati a via Calori passando per via XXI aprile, molti dei quali ho la fortuna di avere ancora accanto a me. Grazie quindi ad Angelo ed Adelina, anche grazie a voi mi sento veramente a casa.
Grazie a tutti i "canicattinesi-bolognesi", che avete portato il calore della nostra terra nel nord non sempre accogliente. Un ringraziamento particolare va, ovviamente, a Giovanni, lui, come pochi, sa le difficoltà che ho/abbiamo passato in questi anni. A te auguro un grande in bocca al lupo.

E, grazie a Bologna chiaramente!

Grazie ai miei colleghi di Catania, dove questa avventura è iniziata, per il meraviglioso anno che mi avete fatto passare nella città etnea, è stato un piacere conoscervi.

Grazie ai miei amici di sempre, a KingBobo, ad Alberto e a Vicio. Beh, siete degli stoici, ormai la vostra sopportazione nei miei confronti supera il decennio! Grazie a Marco e Dino e tutti gli amici che ho la fortuna di rincontrare ogni volta che torno a Canicattì. Grazie a tutti i miei compagni di lotta, in particolare Gigi e il mio "fratello" Diego, siete stati un punto di riferimento in questi ultimi anni pieni di dubbi.

Grazie a tutte le persone che, ognuna a modo suo, mi hanno accompagnato, più o meno a lungo, in questi 25 anni.

ed infine il ringraziamento più importante alla mia famiglia, per il loro supporto incondizionato e per la consapevolezza che, anche se divisi dalla distanza, loro ci sarebbero stati. Sempre.

*grazie, veramente.*